



MONASH University

**Investigation of the pathophysiology of granulosa
cell tumours of the ovary**

*Tan Hung (Dilys) LEUNG
BPsychSci*

A thesis submitted for the degree of *Doctor of Philosophy* at
Monash University in 2017

*Hudson Institute of Medical Research and
Department of Molecular and Translational Science,
Monash University*

Table of Contents

Copyright notice	i
Thesis including Published Works Declaration	ii
Acknowledgements	iv
Publications during Enrolment	vi
Abstracts for Scientific Meetings	viii
Abbreviations	xi
Abstract	xiv
List of Figures	xvi
List of Tables	xviii
Chapter 1 Literature Review	1
1.1 The ovary	2
1.1.1 Anatomy and physiology	2
1.1.1.1 Follicle and folliculogenesis	2
1.1.1.2 Granulosa cells (GC)	6
1.2 Ovarian cancer	8
1.2.1 Granulosa cell tumours (GCT)	9
1.2.1.1 FOXL2 C134W mutation.....	10
1.2.1.2 Prognostic factors	12
1.2.1.3 Aetiology and risk factors.....	12
1.2.1.4 Current therapeutic strategies for GCT.....	14
1.2.2 Signal transduction in GC and GCT.....	15
1.2.2.1 Follicular-stimulating hormone (FSH) and luteinising hormone (LH) .	15
1.2.2.2 Estrogen receptor (ER)	17
1.2.2.3 Peroxisome proliferator-activated receptor-gamma (PPAR γ)	18
1.2.2.4 Nuclear factor-kappa B (NF- κ B)	24
1.2.2.5 X-linked inhibitor of apoptosis protein (XIAP)	27
1.2.2.6 Mitogen-activated protein (MAP) kinase pathway.....	36
1.2.2.7 Activator protein-1 (AP-1)	36
1.2.2.8 Transforming growth factor- β -activated kinase (TAK) 1	37
1.2.3 Apoptosis	40
1.2.4 GCT-derived cell lines	42

1.2.5 Hypotheses and aims	45
Chapter 2 General Methods	46
2.1 Tissue culture.....	47
2.1.1 Cell lines	47
2.1.1.1 Culture conditions	47
2.1.1.2 Cell passaging	48
2.1.1.3 Cryopreservation	48
2.1.2 Transactivation assays	49
2.1.2.1 Vectors/plasmids	49
2.1.2.1.1 pTAL-luc	49
2.1.2.1.2 pAP1 ₃ -luc	49
2.1.2.1.3 pNF κ B ₄ -luc	49
2.1.2.2 Transfection.....	51
2.1.2.3 Luciferase assay.....	52
2.2 Gene expression analysis	53
2.2.1 RNA extraction	53
2.2.2 DNA/RNA quantification	54
2.2.3 Reverse-transcription PCR	54
2.2.4 Gene amplification and sequencing	55
2.3 Protein expression analysis	56
2.3.1 Tissue processing	56
2.3.2 Immunohistochemistry	56
2.3.3 Preparation of whole cell lysates	58
2.3.4 Protein quantification	59
2.3.5 Western blot	59
2.3.5.1 Sodium dodecyl sulfate polyacrylamide gel electrophoresis (SDS-PAGE)	59
2.3.5.2 Protein transfer	60
2.3.5.3 Antibody stripping	61
 Chapter 3 PPARγ activation augments anticancer effects of XIAP inhibition in ovarian granulosa cell tumor (publication).....	 62

Chapter 4 Targeting XIAP and PPAR γ in granulosa cell tumors alters metabolic signaling (publication)..... 115

Chapter 5 Regulation of the constitutive NF- κ B and AP-1 signalling in GCT 164

5.1 Introduction	165
5.2 Methods	169
5.2.1 Cell lines	169
5.2.1.1 GCT-derived cell lines	169
5.2.1.2 hGrC1	169
5.2.1.3 Lenti-X HEK293T	169
5.2.1.4 Chinese Hamster Ovary (CHO)	170
5.2.2 Transactivation assays	170
5.2.2.1 Vectors/plasmids	170
5.2.2.2 Drug treatment.....	171
5.2.3 Cell proliferation assay	172
5.2.4 xCELLigence assay	173
5.2.5 Primer design and PCR	175
5.2.5.1 DNA extraction from agarose gels	177
5.2.5.2 Sequencing.....	177
5.2.6 Transcriptome data processing and statistical analyses	178
5.2.7 Generation of shRNA-resistant XIAP wildtype and mutant plasmids	178
5.2.7.1 Plasmids	178
5.2.7.1.1 XIAP plasmid constructs	178
5.2.7.1.2 GEV16 plasmid	179
5.2.7.1.3 pTRIPz plasmid	179
5.2.7.2 Site-directed mutagenesis	183
5.2.7.3 Plasmid miniprep	185
5.2.7.4 Plasmid maxiprep	186
5.2.8 Re-introduction of XIAP into XIAP-deficient cell line	187
5.2.8.1 Generation of lentivirus	187
5.2.8.2 Lentiviral titration	189
5.2.8.3 Lentiviral transduction of CHO cells	189
5.2.9 Statistical analyses	190
5.3 Results	191
5.3.1 IC50 of 5Z-7-oxozeaenol	191
5.3.1.1 Cell proliferation assay	191

5.3.1.2 xCELLigence assay	194
5.3.2 AP-1 transactivation is abolished by XIAP and TAK1 inhibition in GCT-derived cell lines	194
5.3.3 XIAP and TAK1 regulates NF- κ B signalling in GCT-derived cell lines	197
5.3.4 Absence of mutations in the <i>TAK1</i> gene in KGN and COV434	199
5.3.5 mRNA levels of the TAK-TAB complex in GCT, KGN, COV434 and hGrC1	199
5.3.6 Establishment of stable inducible XIAP knockdown cell lines	203
5.3.6.1 Protein level of XIAP in XIAP knockdown KGN and COV434	203
5.3.6.2 shRNA binding site on XIAP	208
5.3.6.3 Screening successful shRNA-resistant expression vectors using BsrB1 restriction digestion	208
5.3.6.4 Generation of lentivirus in CHO cells	211
5.4 Discussion	214
Chapter 6 Discussion and Conclusions	220
6.1 Discussion and conclusions	221
6.2 Future directions	235
Bibliography	237
Appendix A Electropherogram of <i>TAK1</i> coding sequence	xix
Appendix B Publications.....	xxxvi

Copyright notice

© Tan Hung (Dilys) Leung (2017)

I certify that I have made all reasonable efforts to secure copyright permissions for third-party content included in this thesis and have not knowingly added copyright content to my work without the owner's permission.

Thesis including published works declaration

I hereby declare that this thesis contains no material which has been accepted for the award of any other degree or diploma at any university or equivalent institution and that, to the best of my knowledge and belief, this thesis contains no material previously published or written by another person, except where due reference is made in the text of the thesis.

This thesis includes 2 submitted publications (Chapter 3 and 4) and 3 invited reviews (Appendix) published in peer reviewed journals. The core theme of the thesis is the pathophysiology of ovarian granulosa cell tumours. The ideas, development and writing up of all the papers in the thesis were the principal responsibility of myself, the student, working within the *Hudson Institute of Medical Research and Department of Molecular Sciences, Monash University* under the supervision of Prof. Peter Fuller and Dr Simon Chu.

The inclusion of co-authors reflects the fact that the work came from active collaboration between researchers and acknowledges input into team-based research.

In the case of Chapter 3, 4 and 5, my contribution to the work involved the following:

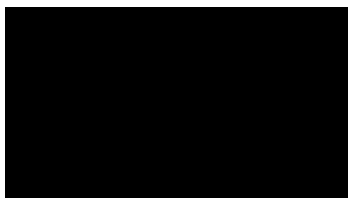
Thesis Chapter	Publication Title	Status (published, in press, accepted or returned for revision, submitted)	Nature and % of student contribution	Co-author name(s) Nature and % of Co-author's contribution*	Co-author(s), Monash student Y/N*
3	PPAR γ activation augments anticancer effects of XIAP inhibition in ovarian granulosa cell tumors	Submitted	50% - input into experiments and intellectual input	1. Trang Nguyen, <i>input into experiments 10%</i> 2. Edwina Oliver, <i>input into experiments*</i> 3. Juliana Matti, <i>input into experiments*</i> 4. Maria Alexiadis, <i>input into experiments*</i> 5. John Silke, <i>intellectual and materials input 2%</i> 6. Peter J Fuller, <i>intellectual input 8%</i> 7. Simon Chu, <i>intellectual input 25%</i> *combined contribution of 5%	No No No No No No No
4	Differentially expressed proteins and genes after combined XIAP inhibition and PAPR γ activation in ovarian	Submitted	80% - input into experiments and intellectual input	1. Adam Rainczuk, <i>input into data analyses and manuscript 5%</i> 2. Trang Nguyen, <i>input into experiments 5%</i> 3. Peter J Fuller, <i>input into manuscript 5%</i> 4. Simon Chu, <i>input into manuscript 5%</i>	No No No No

	granulosa cell tumors				
--	--------------------------	--	--	--	--

I have not renumbered sections of submitted or published papers in order to generate a consistent presentation within the thesis.

The submitted papers are written in American English in accordance to the submission requirement of *Molecular Cancer Therapeutics*.

Student signature:



Date: 1st September 2017

The undersigned hereby certify that the above declaration correctly reflects the nature and extent of the student's and co-authors' contributions to this work. In instances where I am not the responsible author I have consulted with the responsible author to agree on the respective contributions of the authors.

Main Supervisor signature:



Date: 1st September 2017

Acknowledgements

I have read the acknowledgements in several PhD theses throughout the course of my PhD years. Each time, I can't help but think how rewarding/tough their journeys have been and how lucky I am to have my own.

I would like to thank my two supervisors, Prof. Peter Fuller and Dr Simon Chu, for their unequivocal support and guidance throughout my PhD. I really cannot thank them enough for all the time and effort, challenges and opportunities that they have given me which help shape the researcher I am today. I will always be proud to have been their student.

Thank you Peter, for your ever intelligent and constructive advices (with an occasional touch of humour). I am wholeheartedly impressed by and truly grateful for your prompt feedback of my work despite your fully packed schedule! There is always something new to learn from you! Thank you for all the support throughout the years – I highly treasure your compliments/words of encouragement with every award/scholarship outcome. Thank you for always fighting for me when I needed it.

Thank you Simon for believing in me from day 1. You really are a great teacher and you are one of the most patient person I have ever met. Transitioning from psychology to biomedical science could not be made possible without your patience in teaching and confidence in me. Thank you for honestly sharing all the ups and downs of research with me. Being an international student has been an enjoyable experience but can also be financially tough at times! It was with the job that I have in the lab (thank you Peter, Morag and Ann!), and the numerous scholarship and grant applications you and Peter had assisted me with such that I could afford my tuition fees and put food on the table.

I would like to acknowledge my collaborator, Dr Adam Rainczuk. Thank you for sharing your knowledge in mass spectrometry and all your generous help and advice that assisted my learning of this previously completely unfamiliar field. I would like to thank Prof. John Silke for the Smac mimetic and plasmids which are undoubtedly crucial elements in my project.

I am so fortunate to have supportive and encouraging panel members, Dr Peter Stanton, A/Prof Tim Cole and Prof Vincent Harley, who generously took their time and effort to supervise my progress. Your resourceful advices and reminders always ensure I keep achieving in this journey.

Members of the Steroid Receptor Biology Laboratory, both past and present, are amazing researchers – thank you all. Thank you Maria for showing me all the correct techniques and lab etiquettes to kick start my career in research. Trang and Edwina, thank you for all your help and support, and for sharing the ups and downs inside and outside the lab with me. I would like to acknowledge Dr Ann Drummond, Medina and Vicky for their help in the lab. I would like to thank the Cardiovascular Endocrinology division headed by Dr Morag Young, and team members, Dr Amanda Rickard, Dr Elizabeth Fletcher, James, Dr Jimmy Shen, Dr Jun Yang and Dr Greg Ong, who are always keen to share their valuable experiences in lab techniques and presentations. It has been a great pleasure knowing you all.

I would like to say a big thank you to my families and friends, who have supported my journey in all shapes and forms. Thank you for the amazing someone who reminds me to always fight for my dream and accomplish for myself. This has been an incredibly rewarding journey and I have learnt a great deal from the skills and knowledge that I have gained, friendships and collaborations that I have established and most importantly, the attributes and mentality to survive and succeed.

Publications during enrolment

Publications arising from this thesis

Leung DTH, Oliver E, Chee YN, Stewart C, Alexiadis M, Silke J, Fuller PJ and Chu S. “PPAR γ activation augments anticancer effects of XIAP inhibition in ovarian granulosa cell tumors”. Submitted to *Molecular Cancer Therapeutics*.

Leung DTH, Adam Rainczuk, Trang Nguyen, Peter J Fuller and Simon Chu. “Targeting XIAP and PPAR γ alters protein and gene expression in ovarian granulosa cell tumors.” Submitted to *Molecular Cancer Therapeutics*.

Invited Reviews

Leung, DTH, Fuller, PJ and Chu, S. 2016. Impact of FOXL2 mutations on signaling in ovarian granulosa cell tumors. *International Journal of Biochemistry and Cell Biology*. 72: 51-54.

Fuller, PJ, **Leung, DTH**. and Chu, S. 2016. Genetics and genomics of ovarian sex-cord stromal tumors. *Clinical Genetics*. 91(2): 285-291.

Publications arising indirectly during my studies

Fuller PJ, **Leung, DTH** and Chu S. 2017. Genetics and genomics of ovarian sex cord-stromal tumors. *Clinical genetics*. 91(2): 285-291.

Leung, DTH and Chu, S. 2017. Measurement of oxidative stress – mitochondrial function using the Seahorse system. *Methods in Pre-eclampsia*. Murthi, P. and Vaillancourt, C. Springer Publishing. (Accepted)

Alexiadis, M, Chu, S, **Leung, DTH**, Gould, J and Fuller, PJ. 2016. Transcriptomic analysis of stage I versus advanced adult granulosa cell tumors. *Oncotarget*. 7(12): 14207-14219.

Abstracts for Scientific Meetings

Abstracts accepted for oral presentations

Leung DTH, Fuller PJ, Chu S. Combined PPAR γ and XIAP therapy as a new treatment paradigm in ovarian granulosa cell tumors. 99th Annual meeting and expo of the Endocrine Society, Orlando, Florida, U.S.A. *ORA40-1*

Leung DTH, Fuller PJ, Chu S. Combined PPAR γ and XIAP treatment alters invasive properties of ovarian granulosa cell tumours. 59th Annual Scientific Meeting of the Endocrine Society of Australia, Adelaide, Australia 2016. *id #193*

Leung DTH, Fuller PJ, Chu S. Combined PPAR γ and XIAP treatment sensitises granulosa cell tumours to PPAR γ -mediated apoptosis. 58th Annual Scientific Meeting of the Endocrine Society of Australia, Adelaide, Australia 2015. *id #27606*

Leung DTH, Fuller PJ, Chu S. PPAR γ and XIAP as potential targets for combination treatment of ovarian granulosa cell tumours. 57th Annual Scientific Meeting of the Endocrine Society of Australia, Melbourne, Australia 2014. *Abs #22*

Leung DTH, Oliver E, Fuller PJ, Chu S. PPAR γ agonists augment anticancer effects of XIAP inhibition on human granulosa cell tumour-derived cells. Australia Society for Medical Research (ASMR) Student Research Symposium, Melbourne, Australia 2014. *ORA 10*

Chu S, **Leung DTH**, Alexiadis M, Fuller PJ. Effects of nuclear receptor activation in ovarian granulosa cell tumours. 13th Asian Conference on Transcription. Melbourne, Australia 2014.

Leung DTH. Characterisation of a potential therapeutic target – X-linked inhibitor of apoptosis protein (XIAP) in granulosa cell tumours (GCT). 20th Anniversary Student Symposium, Prince Henry's Institute of Medical Research 2013.

Abstracts accepted for poster presentations

Leung DTH, Fuller PJ, Chu S. Combined PPAR γ and XIAP treatment alters invasive properties of ovarian granulosa cell tumours. Research Week, Monash Health and Monash Health Translational Precinct, Melbourne, Australia 2016. *EN4*

Leung DTH, Fuller PJ, Chu S. Combined PPAR γ and XIAP treatment sensitises granulosa cell tumours to PPAR γ -mediated apoptosis. Australia Society for Medical Research (ASMR) Student Research Symposium, Melbourne, Australia 2016. *P2A03*

Leung DTH, Chu S, Fuller PJ. PPAR γ agonists augment anticancer effects of XIAP inhibition on human granulosa cell tumour-derived cells. Research Week 2015, Monash Health and Monash Health Translational Precinct, Melbourne, Australia. *PO15*

Leung DTH, Fuller PJ, Chu S. PPAR γ and XIAP as potential targets for combination treatment of ovarian granulosa cell tumours. Australia Society for Medical Research (ASMR) Student Research Symposium, Melbourne, Australia 2015. *POS50*

Leung DTH, Fuller PJ, Chu S. PPAR γ agonists augment anticancer effects of XIAP inhibition on human granulosa-cell-tumour-derived cells. Australia Society for Medical Research (ASMR) Student Research Symposium, Melbourne, Australia 2013. *PO48*

Abstracts arising indirectly from during my studies

Fuller PJ, Alexiadis M, Chu S, **Leung DTH**, Rowley SM, Li J, Amarasinghe KC, Campbell IG. Mutational landscape of adult granulosa cell tumours of the ovary from whole exome sequencing. 99th Annual meeting and expo of the Endocrine Society, Orlando, Florida, U.S.A. 2017. *SAT157. Poster*

Chu S, **Leung DTH**, Alexiadis M, Fuller FJ. PPAR γ agonists augment anticancer effects of XIAP inhibition on human granulosa cell tumor-derived cells. The Rivkin

Center for Ovarian Cancer Ovarian Cancer Research Symposium 2016, Seattle, USA.
Abstract NTOC-085. *Poster*

Chu S, **Leung DTH**, Alexiadis M, Fuller PJ. Effects of Nuclear Receptor Activation in Ovarian Granulosa Cell Tumours. 13th Asian Conference on Transcription 2014, Melbourne. *Oral*

Leung DTH, Oliver E, Alexiadis M, Fuller PJ, Chu S. Ovarian sex cord tumours. Proc ESA Ann Meeting Melbourne, 2014 *Abstract 72. Oral*

Chu S, **Leung DTH**, Oliver E, Alexiadis M, Silke J, Fuller PJ. PPAR-gamma agonists augment anticancer effects of XIAP inhibition on human ovarian granulosa cell tumor-derived cells. Proceedings 15th Biennial Meeting of the International Gynecologic Cancer Society 2014, *Abstract 47. Poster.*

Chu S, Oliver E, **Leung DTH**, Chee YN, Alexiadis M, Silke J, Fuller PJ. Thiazolidinediones augment anticancer effects of XIAP inhibition on human ovarian granulosa cell tumor-derived cells through PPAR γ activation. US Endocrine Society Annual Meeting, San Francisco, U.S.A. 2013. *SAT327. Poster*

Chu S, **Leung DTH**, Heathcock D, Alexiadis M, Fuller PJ. Expression and cellular activation of peroxisome proliferator-activated receptor γ in granulosa cell tumours. Southern Health Research Week, Monash Medical Centre, Clayton, Australia 2012. *Oral*

Chu S, **Leung DTH**, Alexiadis M, Fuller PJ. Effects of ligand activation of peroxisome proliferator-activated receptor γ in granulosa cell tumours. 55th Annual Scientific Meeting of the Endocrine Society of Australia 2012. *Abs #192. Poster*

Abbreviations

3'	Three prime, the downstream region of a nucleotide sequence
5'	Five prime, the upstream region of a nucleotide sequence
AF	Activation function
AMH	Anti-Müllerian hormone
AP1	Activator protein 1
BIR	Baculovirus IAP repeat
bp	Base pairs
CL	Corpus luteum
CRE	cAMP regulatory element
DBD	DNA-binding domain
DISC	Death-inducing signalling complex
E ₂	Estradiol
ER	Estrogen receptor
ERK	Extracellular-signal-regulated kinase
FOXL2	Forkhead box L2
FSH	Follicle stimulating hormone
GC	Granulosa cells
GCT	Granulosa cell tumours
GnRH	Gonadotrophin-releasing hormone
IAP	Inhibitor of apoptosis protein
IBM	IAP-binding motif
IGF	Insulin-like grown factor
IHC	Immunohistochemistry
IL	Interleukin
IRAK	IL-1 receptor-associated kinase

JNK	Jun-n-terminal kinase
LBD	Ligand-binding domain
LBP	Ligand-binding pocket
LH	Luteinising hormone
MAP	Mitogen-activated protein
NF- κ B	Nuclear factor-kappa B
NR	Nuclear receptors
O	Oocyte
PBS	Phosphate buffered saline
PGZ	pioglitazone
PKA	Protein kinase A
PPAR γ	Peroxisome proliferator-activated receptor gamma
PPRE	PPAR-response element
RA	Retinoic acid
RGZ	Rosiglitazone
RING	Really interesting new gene
rpm	Revolutions per minute
RT-PCR	Real time-polymerase chain reaction
RXR	Retinoid X receptor
SMAC	Second mitochondrial activator of caspases
ST	Stromal cell
TAB	TAK-binding protein
TAK	Transforming growth factor- β -activated kinase 1
TGF β	Transforming growth factor beta
TGZ	Troglitazone
TH	Theca cell

TLR	Toll-like receptor
TMA	Tissue microarray
TNF	Tumour necrosis factor
TNFR	Tumour necrosis factor receptor
TRAF	TNF receptor-associated factor
TRE	TPA responsive element
TZD	Thiazolidinediones
XIAP	X-linked inhibitor of apoptosis protein

Abstract

Ovarian granulosa cell tumours (GCT) are hormonally-active neoplasms characterised by indolent growth and late, invasive relapse. Our research has established that several nuclear receptors, including the anti-proliferative peroxisome proliferator-activated receptor (PPAR) γ , are upregulated in GCT. NF- κ B and AP-1 are constitutively activated in the GCT-derived cell lines, KGN and COV434. NF- κ B induces a key effector protein, X-linked inhibitor of apoptosis protein (XIAP). Small molecule inhibitors of XIAP, smac-mimetics (SM or compound A; CmpdA) and PPAR γ agonists, thiazolidinediones (TZD), are potential anti-tumour agents. The aim of this study is to characterise XIAP and PPAR γ as potential therapeutic targets for the treatment of GCT.

Methods: Tissue microarrays with immunohistochemistry were used to establish XIAP and PPAR γ expression and distribution in GCT and other ovarian pathologies. Transactivation assays were used to assess the transcriptional activity of PPAR γ , as well as the effect of transforming growth factor (TGF) β -activated kinase (TAK) 1 and XIAP inhibition on NF- κ B and AP-1 signalling. The anti-tumour effects of the combined XIAP inhibition (SM) and PPAR γ activation (rosiglitazone, RGZ, and retinoic acid, RA) were investigated using both monolayer and 3D culture of the KGN cells. Digital PCR and stable isotope labelling of amino acids in cell culture coupled with mass spectrometry were used to assess the SM/RGZ/RA-induced changes at the proteomic and message levels in the KGN cells.

Results: XIAP and PPAR γ overexpression was observed in GCT and serous papillary epithelial ovarian cancers when compared to normal ovaries and other benign ovarian pathologies. I demonstrated that PPAR γ -mediated transcription is repressed by NF- κ B

but can be relieved by BAY11-7082 (NF- κ B inhibition) or SM, and activated when combined with RGZ/RA. XIAP regulates NF- κ B activity as part of a feed-forward loop, and inhibition of TAK1 or XIAP significantly abolished both NF- κ B- and AP-1-mediated transactivation in the KGN and COV434 cells. As a result of the SM/RGZ/RA-treatment, a significant induction in apoptosis and reduction in cell viability was observed in the KGN cells. Cell invasion was significantly delayed and no proliferation was detected after invasion. The cells were metabolically compromised with an impairment in their ability to respond to an increased energy demand. The proteomic analysis identified an overrepresentation of proteins associated with the canonical glycolytic pathways following the combined treatment. Stearoyl-CoA desaturase (SCD) was upregulated and an increased expression of a PPAR γ binding site in the SCD promoter region was observed. mRNA expression of several metabolic proteins was confirmed using digital PCR.

Discussion and conclusion: This is the first time a systemic review of XIAP expression has been established across a variety of ovarian pathologies and normal ovary. The overexpression of XIAP and PPAR γ , as well as the effects we observed in the 3D culture warrant further investigation of the two proteins as potential therapeutic targets. Given its role in lipid and glucose metabolism, restoration of PPAR γ activity is consistent with the upregulation of proteins associated with metabolism. Our findings suggested PPAR γ activation and XIAP inhibition works synergistically to exert anti-neoplastic effects in tumours that co-express PPAR γ and XIAP.

List of Figures

The following is a list of figures included in this thesis. Figures that are part of the publications (Chapter 3 and 4) are not included in this list.

Chapter 1

Figure 1.1. Schematic diagram showing various stages of follicle development within a female ovary.

Figure 1.2. Hormonal fluctuations and morphological changes of the follicle during menstrual cycle.

Figure 1.3. Histology of GCT.

Figure 1.4. Schematic diagram showing the hormonal regulation at various developmental stages of normal follicle.

Figure 1.5. Structure of PPAR γ .

Figure 1.6. Expression of nuclear receptors in a panel of 14 GCT and two GCT-derived cell lines, KGN and COV434.

Figure 1.7. PPRE₄-mediated transactivation in KGN.

Figure 1.8. X-linked inhibitor of apoptosis protein (XIAP).

Figure 1.9. *XIAP* mRNA expression in postmenopausal ovaries, GCT and GCT-derived cell lines.

Figure 1.10. Effects of combined XIAP inhibition and PPAR γ activation on GCT *in vitro*.

Figure 1.11. XIAP in TGF β signalling pathway.

Figure 1.12. The intrinsic and extrinsic apoptotic pathways.

Figure 1.13. Microscopic images of the two human GCT-derived cell lines.

Chapter 2

Figure 2.1. Generalised map of vector.

Chapter 5

Figure 5.1. Regulation of the TAK-TAB protein complex.

Figure 5.2. Map of the pF-5UAS SV40-puro expression vector.

Figure 5.3. Map of the pF-5UAS SV40-puro expression-empty vector.

Figure 5.4. Map of the GEV16 plasmid.

Figure 5.5. IC₅₀ of 5Z-7 from MTT assay.

Figure 5.6. IC₅₀ of 5Z-7 from xCELLigence.

Figure 5.7. AP-1 transactivation assay in GCT-derived cell lines.

Figure 5.8. NF- κ B transactivation assay in GCT-derived cell lines.

Figure 5.9. Microarray analysis of *TAK1*, *TAB1*, *TAB2*, *TAB3* and *TRAF6* mRNA levels.

Figure 5.10. Expression of XIAP and β -actin in two KGN Δ XIAP clones.

Figure 5.11. Expression of XIAP and β -actin in COV434 Δ XIAP.

Figure 5.12. COV434 Δ XIAP under fluorescence microscope.

Figure 5.13. The shRNA binding region on the full length *XIAP* gene.

Figure 5.14. Incorporation of a silent mutation of the shRNA binding site of XIAP expression vectors detected by BsrB1 restriction digestion.

Figure 5.15. Electropherogram of the XIAP sequence following site-directed mutagenesis.

Figure 5.16. Lentiviral transduction of CHO cells.

List of Tables

The following is a list of tables included in this thesis. Tables that are part of the publications (Chapter 3 and 4) are not included in this list.

Chapter 2

Table 2.1. Culture conditions for KGN and COV434.

Chapter 5

Table 5.1. Compounds used in AP-1 and NF- κ B transactivation assay.

Table 5.2. Serial concentration of 5Z-7 for KGN and COV434 in the MTT assay.

Table 5.3. Experimental schedule for the xCELLigence assay.

Table 5.4. Serial concentration of 5Z-7 for KGN and COV434 in xCELLigence assay.

Table 5.5. Primer sequences for the *TAK1* gene.

Table 5.6. Primer sequences for site-directed mutagenesis.

Table 5.7. Preparation of plasmid DNA and polymer solutions.

Table 5.8. IC₅₀ and Hill slope of 5Z-7 in KGN and COV434 at 24 and 48 hours from the MTT assay.

Table 5.9. IC₅₀ and Hill slope of 5Z-7 in KGN and COV434 at 24 and 48 hours from the xCELLigence assay.

Table 5.10. Fold changes and *p* values of significant differences in *TAK1* and *TAB2* levels.

CHAPTER 1
LITERATURE REVIEW

1.1 The ovary

The ovaries are the primary female sex organs, responsible for producing ova or oocytes (egg cells), as well as the steroid and peptide hormones necessary for reproductive function. The following outlines the structure and the biological events that take place in this organ.

1.1.1 Anatomy and physiology

The ovaries are paired organs, held in place by connective tissue ligaments bilateral to the uterus. Each ovary is indistinctly divided into an outer cortex where germ cells develop, and a central medulla where connective tissues, nerves, blood vessels and lymphatics are found (Figure 1.1). The primary function of the ovary is to work in concert with the intraovarian and endocrine axes to nurture the oocyte to maturity. This is achieved by the functional unit of the ovary, the follicle, which consists of an immature egg (oocyte) surround by granulosa cells (GC) and theca cells.

1.1.1.1 Follicle and folliculogenesis

Folliculogenesis is the progressive development of the ovarian follicle (Figure 1.1). Current knowledge of this process has been primarily determined using animal models, which corresponds closely to what occurs in humans, albeit with differences in temporal and cellular localisation of some genes and proteins (Sarraj and Drummond, 2012). The various fundamental biological processes involved in folliculogenesis are the result of the bidirectional interaction between intraovarian (e.g. insulin-like growth factor-1 (IGF-1)) and endocrine (follicle-stimulating hormone

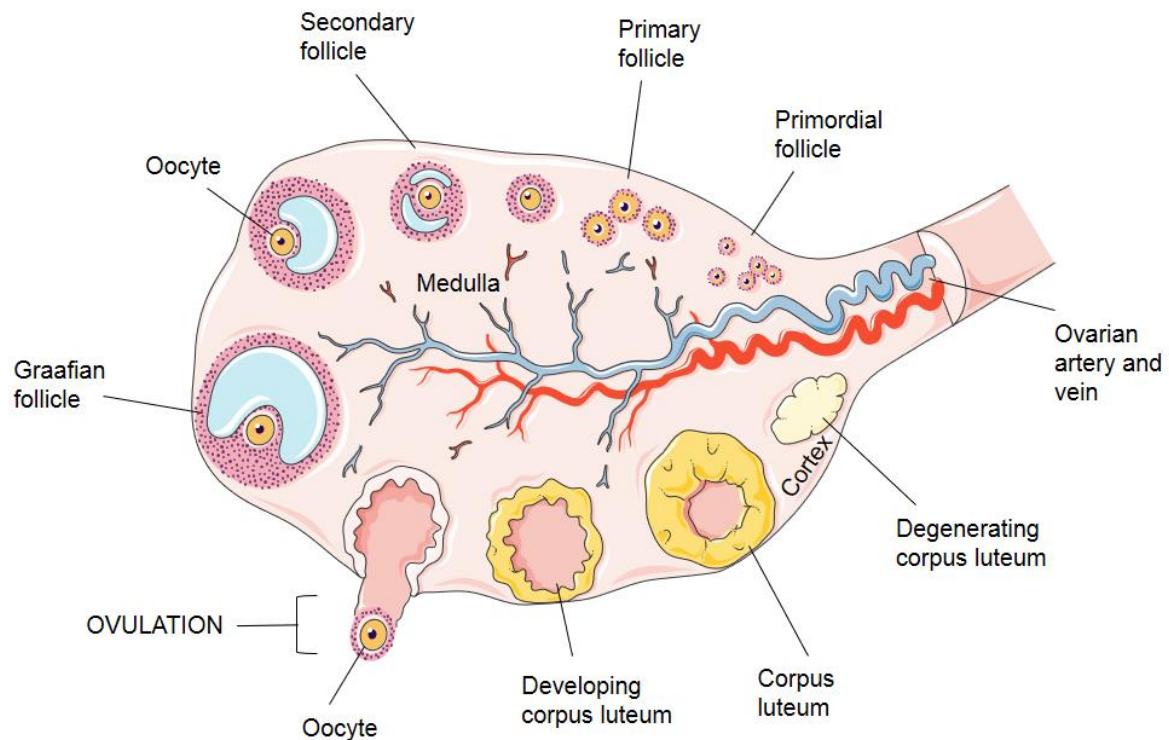


Figure 1.1. Schematic diagram showing various stages of follicle development within a female ovary. The outer cortex of the ovary is the site of folliculogenesis where primordial follicles develop into primary, secondary and Graafian follicles, and then differentiate into the corpus luteum. The medulla contains blood vessels and nerves (adapted from Servier, 2012).

(FSH), luteinising hormone (LH) and estradiol (E_2) factors (Figure 1.2) (Zuccotti et al., 2011). IGF-1 in the ovary not only stimulates E_2 production and follicular growth, but is also thought to be involved in the regulation of FSH-induced follicular development (Zuccotti et al., 2011, Zhou et al., 2013). In addition, GC of the growing follicle also produce activating/inhibitory factors to regulate follicular development. Many of these autocrine and paracrine signals including activin and inhibin which belong to the transforming growth factor (TGF) β superfamily (Zuccotti et al., 2011).

The two phases of folliculogenesis are defined by the period before (preantral) and after (antral) the follicle develops a fluid-filled cavity, the antrum. At birth, about two million primary oocytes are present in the human ovary. Only a very small proportion of these are recruited to developing follicles (primordial to primary). Under the stimulation of the pituitary gonadotrophins at puberty, the primordial follicles resume the first division of meiosis. The single layer of squamous follicular cells surrounding the oocyte in a primordial follicle becomes cuboidal and proliferates to become the zona granulosa in the primary and secondary follicles. FSH and other paracrine factors regulate the pre-antral to antral transition.

The antral stage of folliculogenesis is characterised by the presence of secondary follicles which feature the antrum within the now multi-layered granulosa cells surrounding the oocyte. The follicular fluid within the antrum contains high concentrations of E_2 , along with other nutritional factors that are essential to nourish the growing follicle. Of this pool, a dominant follicle is destined to ovulate once a month while the fate of most follicles is to undergo cell death (atresia) (Sarraj and Drummond, 2012). Prior to ovulation, pituitary gonadotrophins signal the completion of meiosis I in the dominant follicle, which is now the Graafian follicle. The LH surge

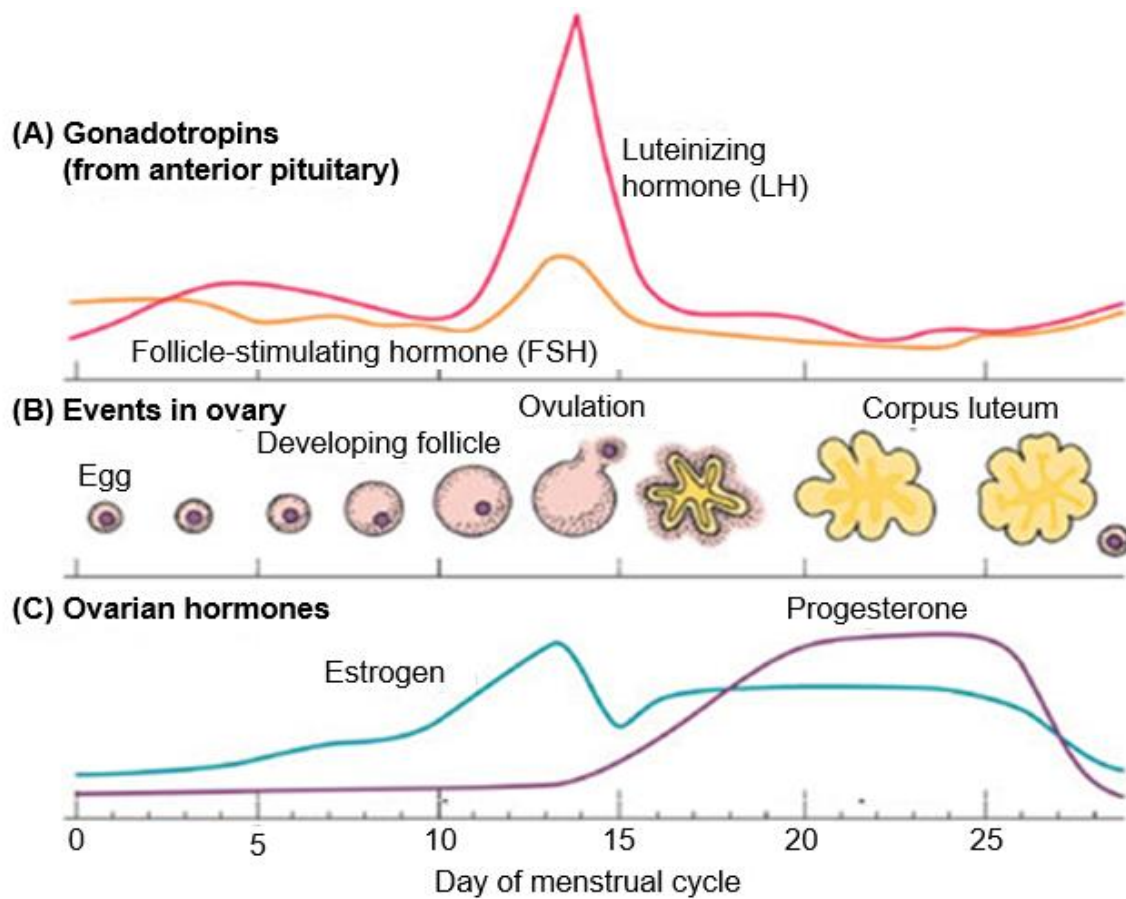


Figure 1.2. Hormonal fluctuations and morphological changes of the follicle during menstrual cycle. Endocrine hormones including FSH and estrogen control follicular development, while LH stimulates ovulation and differentiation of GC into corpus luteum (Fernandes, 2008).

stimulates the release of oocyte from the mature follicle, or ovulation. The exposure to LH also ceases GC proliferation and along with FSH by acting through cAMP-dependent protein kinase A (PKA), induces GC differentiation (Zuccotti et al., 2011). Following ovulation, terminal differentiation of GC and theca cells takes place and forms the corpus luteum (CL) (Robker and Richards, 1998, Richards et al., 2002).

1.1.1.2 Granulosa cells (GC)

GC play a critical role in nurturing a healthy oocyte during folliculogenesis. Each month throughout the course of a female's reproductive life, GC undergo squamous-to-cuboidal transition as a result of the expression of the Forkhead box L2 (FOXL2) transcription factor (Schmidt et al., 2004). It has been suggested that FOXL2-regulated activating/inhibitory factors trigger the primordial to primary follicle transition, which coincides with the squamous-to-cuboidal transition in GC. These processes occur as a gateway to GC proliferation (Schmidt et al., 2004). Without the support of cuboidal GC, atresia is observed in most of the oocytes, and subsequently, no maturation into secondary follicles (Schmidt et al., 2004).

GC increase in numbers and layers as they progress through the stages of folliculogenesis. Under the influence of FSH, they differentiate into cumulus cells and mural GC. Both cell types possess the capacity to communicate with the oocyte in a bidirectional manner. Peripheral GC are called mural GC. They differ slightly from the cumulus cells in their responsiveness to gonadotropins (Armstrong et al., 1996). As the dominant follicle is selected, GC acquire aromatase activity, leading to a rise in E₂ and thus a decrease in FSH levels. Low levels of FSH result in an atretic fate for the less mature follicles (Vegetti, 2006). After ovulation occurs, mural GC undergo

further differentiation and luteinisation; together with theca cells they form the CL which secretes progesterone and maintains pregnancy (Eppig, 2001).

GC are the major site of E₂ production during a female's reproductive years (Jamieson and Fuller, 2012). Elevated E₂ is crucial to GC proliferation and differentiation, and represents a hallmark of the GC of the dominant and preovulatory follicles (Chu et al., 2002, Fuller and Chu, 2004, Zuccotti et al., 2011, Jamieson and Fuller, 2012). Receptors for oocyte-secreted paracrine factors such as growth differentiation factor (GDF)-9 and bone morphogenetic protein (BMP)-15 are present on GC. This intercommunication between GC and the oocyte plays facilitative/regulatory role in differentiation and function of GC, as well as in oocyte maturation (Peng et al., 2013). Other crucial factors for GC proliferation and maturation include a series of FSH-regulated genes, some of which regulate estrogen receptor beta (ER β), inhibin subunits and the LH receptor (LHR) (Chu et al., 2002), which will be discussed in detail in later sections.

1.2 Ovarian cancer

Annually, ovarian cancer accounts for an estimated 238,719 new cases as well as 151,917 reported deaths worldwide (Ferlay et al., 2013). It is the leading cause of death from gynaecological diseases, and in Australia/New Zealand, the fourth most common cause of cancer mortality in women. The incidence and mortality rates of ovarian cancer increase with age (Ferlay et al., 2013).

Neoplasms of the ovary develop from the three ovarian regions – epithelial (85-95%), sex cord-stromal (5-8%) and germ cells (3-5%) (Roett and Evans, 2009). The majority of ovarian tumours are of epithelial in origin and have the potential to differentiate into various subtypes that take on different histopathological appearances. Varying morphologies are also observed among the much rarer germ cell tumours, which are believed to be derived from the primitive germ cells of the embryonic gonad. Sex cord-stromal tumours arise either from theca and stromalutein cells (of stromal origin), and/or granulosa cells (of sex-cord origin) (Jamieson and Fuller, 2012, Fuller et al., 2017).

Surgical debulking is the recommended initial management for ovarian malignancies. It is also necessary to enable definitive diagnosis and staging of the disease, which is defined by the International Federation of Obstetrics and Gynaecology (FIGO). Biopsies of common metastatic sites such as the peritoneum and diaphragm etc. are required if metastasis is suspected (Benedet et al., 2000, Schumer, 2003).

1.2.1 Granulosa cell tumours (GCT)

GCT of the ovary contribute approximately 5-8% of all ovarian cancers (Jamieson and Fuller, 2012, Fuller et al., 2017). They are the most common ovarian sex-cord stromal tumours. There are two subtypes of GCT; the adult form (95%) characterised by a FOXL2 C134W mutation and the much rarer juvenile form. The following discussion will refer to the more common adult subtype of GCT, unless otherwise stated.

GCT can occur at any age but the incidence peaks in women between 50 and 54 years of age (Schumer, 2003, Jamieson and Fuller, 2012). In its early stage, GCT present with non-specific symptoms such as abdominal distension and bloating, which unfortunately, may not alert women to the need to see a clinician. As the disease advances, persistent, localised abdominal or pelvic pain is common due to the presence of a large ovarian mass (GCT can be > 10-15 cm in diameter at diagnosis). Due to tumour-derived estrogen secretion, prepubertal females may present with endocrine symptoms such as precocious breast development, while in the reproductive-age group women present with menstrual irregularities and in postmenopausal women, inappropriate vaginal bleeding (Benedet et al., 2000, Schumer, 2003, Jamieson and Fuller, 2012).

Diagnosis of GCT was previously based on tumour morphology. The distinct nuclear appearance is the classical feature of GCT. Well-differentiated tumours have pale, grooved nuclei (nuclear grooves) with a “coffee-bean” appearance (Figure 1.3A) (Ali et al., 2008). Some tumours have nuclei denuded of cytoplasm, or “naked nuclei” (Figure 1.3B and C). Call-Exner bodies, the small eosinophilic fluid-filled space

between GC, were seen in 30-70% of cases (Stenwig et al., 1979, Ali et al., 2008). Tumour cells are arranged in various growth pattern; “microfollicular” or “diffuse” pattern presents with or without Call-Exner bodies, respectively (Figure 1.3B). Tumour cells are organised in bands, islands, zigzag cords or wavy rows in “trabecular”, “insular”, “gyriform” or “watered-silk” pattern (Figure 1.3C – F). Cysts of varying sizes are seen in GCT with a “macrofollicular” pattern (Figure 1.3G). “Luteinised” tumour cells contain eosinophilic cytoplasm (Figure 1.3H) (Esheba, 2015). These growth patterns have not been found to be of prognostic significance (Esheba, 2015). In addition to the distinct morphological features of GCT, a robust diagnostic criterion is the presence of the unique FOXL2 mutation.

1.2.1.1 FOXL2 C134W mutation

Recent studies have consistently identified a single somatic missense mutation in the *FOXL2* gene (402C→G) in GCT (Kobel et al., 2009, Shah et al., 2009, Jamieson et al., 2010, Jamieson and Fuller, 2012). The mutation results in a single amino acid substitution of tryptophan for cysteine at position 134 (C134W). Although it is still unclear how the mutation contributes to the development of GCT, it is regarded as a specific marker for differential diagnosis within the category of sex cord-stromal tumours (Kobel et al., 2009, Shah et al., 2009, Jamieson and Fuller, 2012). In the current literature, FOXL2 C134W mutations are reported in 90-97% of adult GCT samples. It is noteworthy that some of the GCT samples that were negative for the FOXL2 C134W mutation were found to be misclassified during retrospective re-evaluation (Shah et al., 2009, Jamieson et al., 2010). This mutation is not present in the juvenile GCT, where protein expression of FOXL2 is either low or absent and often coincides with aggressive progression of the disease

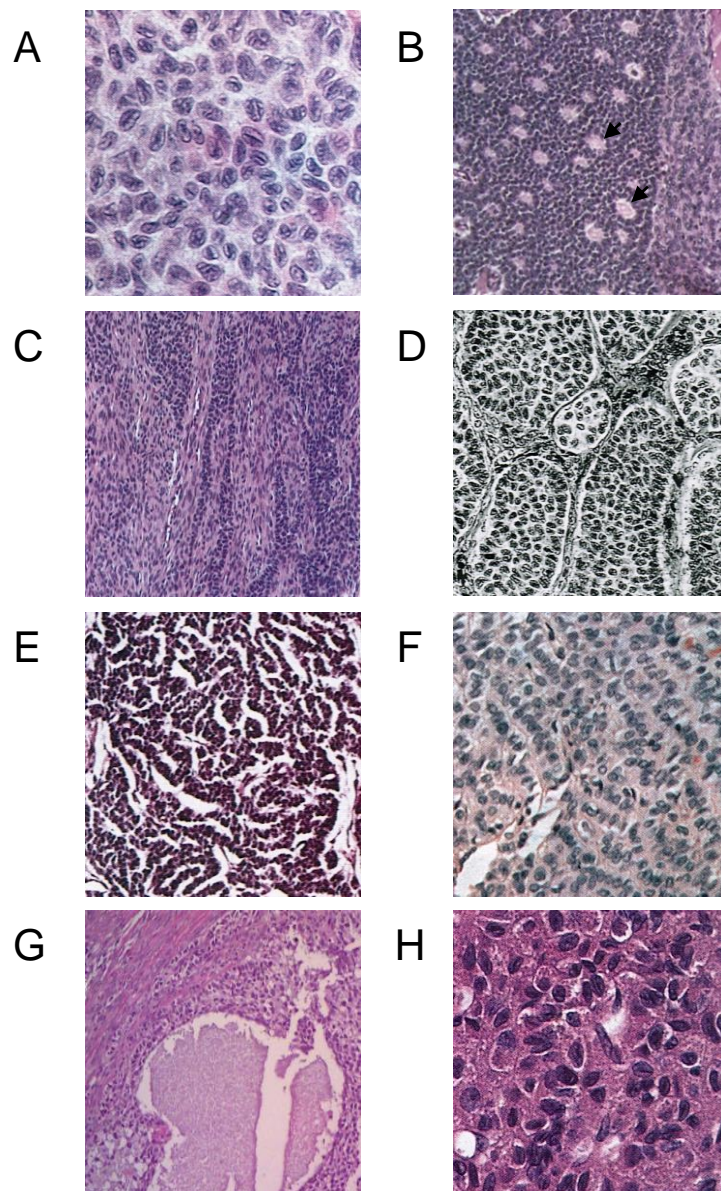


Figure 1.3. Histology of GCT. A. Tumour cells with pale nuclei with nuclear grooves. B. Call-Exner bodies (arrow; “microfollicular”) surrounded by a diffuse pattern of tumour cells. C – F. Tumour cells organised in bands, islands, zigzag cords or wavy rows in “trabecular” (C), “insular” (D), “gyriform” (E) or “watered-silk” (F) pattern (modified from Ehdaivand, 2016). G. GCT with a cyst – “macrofollicular” (modified from Parodo et al, 2013). H. Luteinised tumour cells with eosinophilic cytoplasm (modified from Ehdaivand, 2016).

(Jamieson and Fuller, 2012). Further, the FOXL2 C134W mutation is not detected in other ovarian or sex-cord stromal carcinomas, suggesting the mutation is characteristic of adult GCT of the ovary (Jamieson et al., 2010).

1.2.1.2 Prognostic factors

Many patients present with FIGO stage I disease and have a relatively good prognosis (Schumer, 2003). Those who present with stage III/IV have a five-year survival rate of no greater than 50% (Schumer, 2003). In addition, the characteristic indolent development of GCT often results in the disease relapses many years after primary treatment. An 18-year follow-up study has reported the median time to relapse was 75 months (range = 55-137 months) (Lee et al., 2008). Studies have also demonstrated that stage of disease correlates with disease recurrence in univariate but not multivariate analysis, suggesting other significant prognostic factors affect overall survival (Benedet et al., 2000, Lee et al., 2008). When GCT recur, up to 80% of patients die of the disease (Jamieson and Fuller, 2012).

1.2.1.3 Aetiology and risk factors

The aetiology of GCT is poorly understood. Molecular characterisation of GCT shows that they exhibit a phenotype similar to that of a proliferating GC of the preovulatory follicle (Chu et al., 2002, Jamieson and Fuller, 2012) (Figure 1.4). These similarities include expression of functional FSH receptors with FSH binding (Chu et al., 2002), synthesis of E₂ and anti-Müllerian hormone (AMH) (Schumer, 2003). Another prominent feature of proliferating GC is the synthesis and secretion of another gonadal peptide, inhibin (Ferlay et al., 2010).

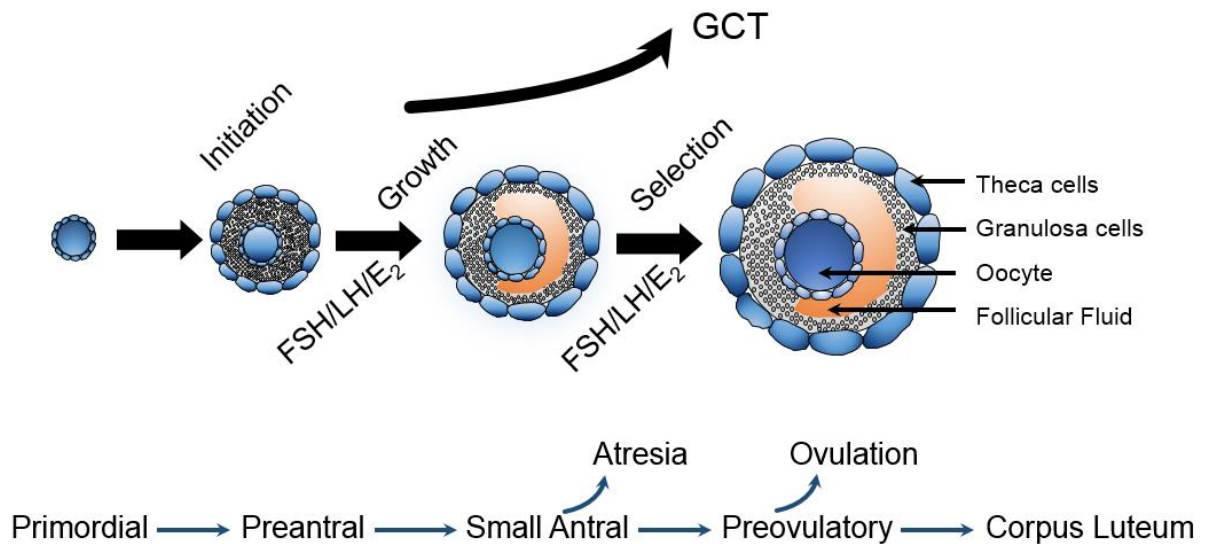


Figure 1.4. Schematic diagram showing the hormonal regulation at various developmental stages of normal follicle. The proliferation of GC and selection of antral follicles which develop into dominant follicles are under tight regulation of hormones including FSH, LH and E₂. There is a the speculation that GCT may arise from GC of a proliferating, late preovulatory follicle (modified from Richards, 1994).

Like the molecular pathogenesis and aetiology of GCT, associated risk factors of the disease are still unclear. For instance, menopausal status and low parity do not seem to have biological significance in GCT development and inheritance of the *BRCA1* or *BRCA2* mutation is associated consistently only with epithelial ovarian cancer, not with GCT (Schumer, 2003, Palermo, 2007)

1.2.1.4 Current therapeutic strategies for GCT

The standard management for GCT is surgical excision of the tumour. In reproductive-age women with early-stage GCT, conservative fertility-sparing surgery without hysterectomy has been a standard approach and remains the best evidenced treatment for this disease (Park et al., 2012, Seagle et al., 2017). In post-menopausal women and patients who present with advanced disease, total hysterectomy and bilateral salpingo-oophorectomy (removal of the Fallopian tube and ovary) is recommended (Jamieson and Fuller, 2012, Seagle et al., 2017). However, optimal treatment has yet to be established for advanced or recurrent GCT. Postoperative chemotherapy is mainly platinum-based, of which the BEP regimen (bleomycin, etoposide and cisplatin) is the most commonly used (Park et al., 2012, Gurumurthy et al., 2014). Hormonal therapies include tamoxifen, GnRH (gonadotrophin-releasing hormone) agonists and more recently aromatase inhibitors. In general, hormonal therapy is better tolerated but the lack of randomised controlled trials makes it difficult to evaluate the efficacy of these modalities (van Meurs et al., 2014). Although adjuvant therapy is an option, the efficacy of chemotherapy or hormonal therapy for GCT remains controversial (Jamieson and Fuller, 2012, Park et al., 2012, van Meurs et al., 2014). Findings from a recent retrospective analysis of 2,680 women

concluded that adjuvant chemotherapy does not increase survival (Seagle et al., 2017). Hence, there is a need for a more targeted approach to treating this disease.

1.2.2 Signal transduction in GC and GCT

GCT synthesise several steroid hormones and are in turn, regulated by their effects (Fuller and Chu, 2004). The existing literature contains reports which have considered subversion of growth and differentiation mechanisms in normal GC, as well as examining molecular changes that may contribute to the malignant phenotype in GCT. Genetic events that control key signalling pathways are also thought to be involved in tumourigenesis of GCT (Chu et al., 2002, Fuller and Chu, 2004). The following discussion identifies some of the major signalling pathways in normal GC that are of relevance to the pathogenesis of GCT.

1.2.2.1 Follicle-stimulating hormone (FSH) and luteinising hormone (LH)

Both FSH and LH are glycoprotein hormones of the hypothalamo-pituitary-gonadal axis. They are synthesised and secreted by the anterior pituitary gland under the pulsatile stimulus of gonadotropin-releasing hormone (GnRH). Serum levels of FSH and LH vary with age and stage of menstrual cycle, and are subjected to complex control via feedback from E₂, inhibin and GnRH (Palermo, 2007). Both hormones act by binding to their specific receptors in the ovary. Unlike LH receptors (LHR) that are expressed in theca cells early in folliculogenesis, it is generally accepted that in human GC, FSH receptors (FSHR) become functional from the primary follicle onward, but not during earlier follicular development (Vegetti, 2006, Palermo, 2007). Around mid-cycle where a dominant follicle is selected, LHR are also expressed in GC, which after LH binding to LHR, continue to support follicular growth during the

decline in levels of FSH. Only the dominant follicle with increased FSH sensitivity continues to be nurtured and is destined to ovulate (Palermo, 2007).

Upon binding to its receptor, FSH stimulates the production of intracellular cAMP and activates genes required for proliferation and differentiation. In GC, FSH promotes the secretion of inhibin and AMH, which in turn have regulatory/inhibitory roles on FSH secretion (Fuller and Chu, 2004). It also induces LHR expression, preparing the ovary for the LH surge that subsequently triggers ovulation. As early as the beginning of a female's reproductive years, the LH surge resumes meiosis of the resting oocytes (Palermo, 2007). After ovulation occurs, the LH surge causes the remaining granulosa and theca cells to undergo terminal differentiation to become a CL. FSH and LH are responsible for adequate steroidogenesis; FSH promotes progesterone and E₂ secretion from GC while LH stimulates progesterone and androgen production by luteal and theca cells, respectively (Palermo, 2007).

As mentioned in the previous section, GCT exhibit functional FSHR and FSH binding (Jamieson and Fuller, 2012). FSH levels in GCT, however, appear to be suppressed by GCT-derived inhibin, indicating tumour growth is FSH-independent. There has been speculation that activating mutations of FSHR may play a role in tumorigenesis but efforts to identify any *FSHR* gene mutations were not successful (Fuller et al., 1998, Fuller and Chu, 2004). In contrast to FSHR, expression of LHR is low to absent in GCT (Chu et al., 2002, Fuller and Chu, 2004). This finding coincides with the failure of GCT to undergo terminal differentiation into a luteinised phenotype.

1.2.2.2 Estrogen receptor (ER)

ER belong to the nuclear receptor (NR) superfamily of ligand-activated transcription factors. Both ER members, ER α and ER β are present in the normal ovary (GC and theca cells), although ER β is the predominant subtype in GC of the growing follicle, CL and oocyte (Chu et al., 2002, Drummond and Fuller, 2010, Fan et al., 2010a). In the ovary, ER mediate important physiological responses by modulating activity of estrogen, principally E₂ secreted by GC (Drummond and Fuller, 2010). Studies of ER α and ER β knockout mice have revealed distinct functionality between the two ERs (Couse et al., 2003, Fan et al., 2010a). For instance, ER α , but not ER β , knockout mice failed to exert negative feedback on LH levels from the pituitary via the regulatory action of estrogen. Hyperstimulation by elevated LH in ER α knockout mice reflects the fact that LH synthesis and secretion are dependent upon ER α action (Couse et al., 2003). It is thought that ER α mediates the proliferative action of estrogen, whereas ER β represses proliferation and promotes differentiation (Fan et al., 2010a). Actions of ER β appear to be more directly relevant from the perspective of GC. ER β -mediated estrogenic activity plays a pivotal role in follicular development, namely, antrum formation and FSH-induced GC proliferation (Drummond and Fuller, 2010). ER β -null mice are subfertile; their ovaries contain fewer antral follicles and their GC fail to differentiate in response to FSH, they also have heightened apoptotic events and yield fewer oocytes (Couse et al., 2003, Couse et al., 2005, Drummond and Fuller, 2010, Fan et al., 2010a). *ER* gene expression is regulated by FSH activity; together they promote cell survival and proliferation of GC (Chu et al., 2002, Richards et al., 2002).

There is growing evidence that abnormalities in ER β expression contribute to tumour development. In estrogen-secreting GCT, ER β (mRNA and protein) is predominantly and abundantly expressed (Chu et al., 2004, Alexiadis et al., 2011). When one considers the anti-proliferative and pro-differentiating effects of ER β , it is not clear as to why there is high expression of ER β in GCT cells. Findings from two GCT-derived cell lines (refer to Chapter 1 Section 1.6) revealed that ER β , although able to bind E₂, fails to transactivate an estrogen-responsive reporter in the presence of E₂ (Chu et al., 2004). Further analysis by our laboratory discovered that ER β signalling is inhibited by the constitutive activation of NF- κ B signalling, and that knockdown of NF- κ B restores ER β activity (Chu et al., 2004).

1.2.2.3 Peroxisome proliferator-activated receptor-gamma (PPAR γ)

Other members of the NR superfamily include the peroxisome proliferator-activated receptors (PPAR). Three isoforms, α , β and γ , encoded by three separate genes, have been identified (Dupont et al., 2012). The *PPAR γ* gene has 4 isoforms produced by alternative splicing, which give rise to 2 translational products. Of the 4 splice variants, *PPAR γ ₁*, *γ ₃* and *γ ₄* encode the same protein, PPAR γ ₁, which is expressed in most human tissues. Isoform 2, or *PPAR γ ₂*, yields the adipocyte-specific PPAR γ ₂ and has 28 additional amino acids in the N-terminus (Froment et al., 2006). The following will focus on PPAR γ ₁, referred to as PPAR γ , unless otherwise stated.

Common to all NR, PPAR γ comprises three domains: i) the N-terminal ligand-independent activation function 1 (AF1); ii) a highly-conserved DNA-binding domain

(DBD) that recognises and targets the specific PPAR-response elements (PPRE); and iii) a carboxy-terminal ligand-binding domain (LBD) with a ligand-binding pocket (LBP) and an activation function 2 (AF2) that controls transactivation via the recruitment of co-regulators (Figure 1.5). Linking the DBD and LBD is a non-conserved hinge region (Khorasanizadeh and Rastinejad, 2016). Hinge regions in some NR serve to provide additional DNA-binding specificity. In PPAR γ however, the hinge region changes shape following DNA distortion but does not involve in allosteric pathway (Ricci et al., 2016).

Upon activation by fatty acids and their derivatives, PPAR γ forms heterodimers with retinoid X receptor (RXR) α whose ligand is 9-cis retinoic acid. This elicits a classical activation mechanism of NR, also observed in PPAR γ , via the activation of AF2 and subsequent conformational changes which stabilise the orientation of LBP. Co-activators or co-repressors compete for binding near AF2 to regulate transactivation. The PPAR γ -RXR α heterodimer binds to PPRE within the promoter region of target genes to exert transcriptional regulation (Khorasanizadeh and Rastinejad, 2016, Ricci et al., 2016). Besides ligand binding, other regulatory mechanisms of PPAR γ expression include phosphorylation, ubiquitylation and nitration (addition of a nitro group). The site of phosphorylation and the subsequently activated kinase cascade will dictate the effects of phosphorylation (reviewed in Gelman et al., 2005). Both nitration and ligand binding negatively regulates PPAR γ expression; nitration of the tyrosine kinase prevents nuclear translocation of PPAR γ (Shibuya et al., 2002) while ligand binding induces ubiquitylation of the receptor (Hauser et al., 2000).

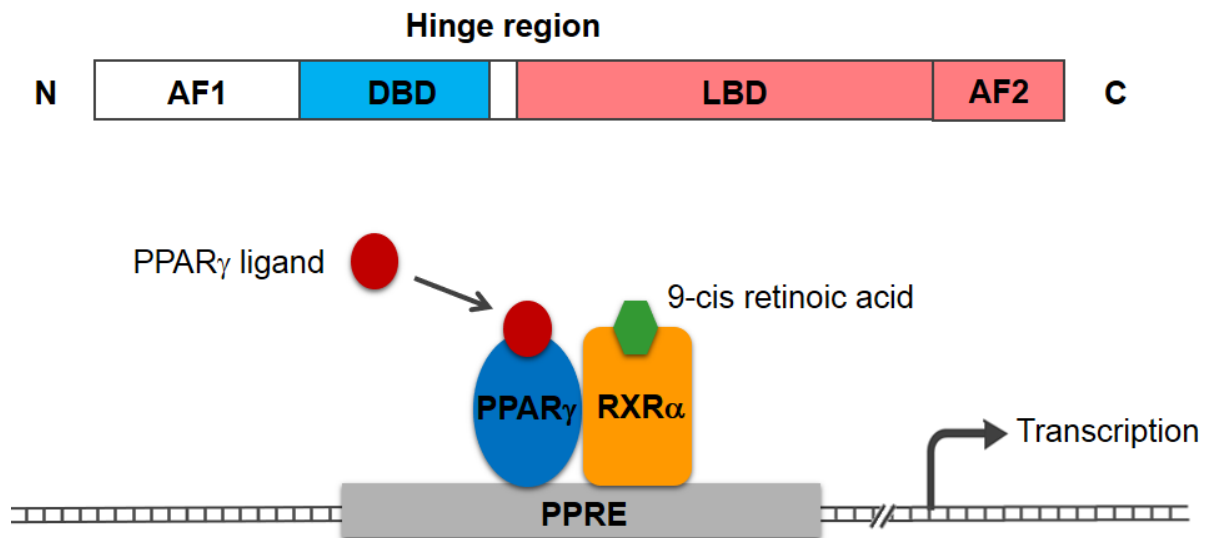


Figure 1.5. Structure of PPAR γ . PPAR γ has a classical three-domain structure of NR – the activation function 1 (AF1), DNA-binding domain (DBD) and ligand-binding domain (LBD). DBD and LBD, which comprises AF2, are linked through the hinge region. Ligands for PPAR γ and RXR α are fatty acids and 9-cis retinoic acid, respectively. Upon activation by their ligands, PPAR γ heterodimerises with RXR α , recruits co-activators or co-repressors and then binds to PPRE within the promoter of target genes and modulates their expression.

PPAR γ has been shown to have a role in the immune response, lipid and glucose metabolism, apoptosis and differentiation (Vignati et al., 2006). In the rat ovary, PPAR γ is first detected at day 7 (Long et al., 2009). PPAR γ is expressed strongly in GC in primary and secondary follicles, as well as oocytes of various species (Dupont et al., 2012). Its expression increases as follicular development progresses, consistent with its role in regulating the synthesis of steroid hormones and oocyte maturation (Long et al., 2009, Dupont et al., 2012). PPAR γ also modulates steroidogenesis in the ovary. The rate-limiting enzyme, aromatase (CYP19A1), is responsible for the conversion of androgens to E₂. Studies have shown that activation of PPAR γ reduces CYP19A1 expression in GC *in vivo* (Lovekamp-Swan et al., 2003). PPAR γ also regulates progesterone production although effects depend on cell types, levels of other steroid hormones and stage of folliculogenesis (Puttabyatappa et al., 2010, Mehta et al., 2013). Conversely, PPAR γ also appears to be regulated by progesterone (Kim et al., 2008). Another target of PPAR γ is the steroidogenic acute regulatory protein-encoding *StAR* gene, which is downregulated by PPAR γ activation (Puttabyatappa et al., 2010). The importance of PPAR γ is demonstrated in GC-specific PPAR γ knockout mice which developed an impairment of ovulation and subsequent sterility (Kim et al., 2008), echoing the critical role of PPAR γ in normal ovarian function, and particularly, in terminal differentiation and the ovulatory response.

PPAR γ also exhibits pro-apoptotic and anti-proliferative effects which are achieved by the activation of caspases and other cell cycle-regulatory proteins. The balance between proliferation and differentiation/apoptosis is regulated by the mitogen-

activated protein (MAP) kinase pathways, where phosphorylation of MAP kinase has been shown to inhibit PPAR γ expression (Burgermeister and Seger, 2007).

PPAR γ has been of interest in the context of cancer biology. Surprisingly, overexpression of PPAR γ has been reported in a number of human malignancies including colon (Tsukahara and Haniu, 2012), thyroid (Ferrari et al., 2016) and epithelial ovarian cancers (Dupont et al., 2012). In a screen of all 48 nuclear receptors in GCT, PPAR γ showed elevated expression across 14 GCT samples and two GCT-derived cell lines (see Chapter 1 Section 6) (Figure 1.6) (Alexiadis et al., 2011). The authors speculated that the presence of high levels of anti-neoplastic gene may reflect resistance to PPAR γ that has developed in these tumours (Alexiadis et al., 2011). The therapeutic potential of PPAR γ activation has been explored with the aid of synthetic PPAR γ ligands, the thiazolidinediones (TZD). TZD include troglitazone (TGZ), rosiglitazone (RGZ) and pioglitazone (PGZ). RGZ and PGZ are in clinical use as anti-diabetic drugs (Chou et al., 2007).

An increasing amount of research has reported TZD-induced growth arrest and apoptosis in cancer cell lines of various origins (Chou et al., 2007). The anti-tumour effect of PPAR γ agonists has also been observed in xenograft models of solid tumours (Shimazaki et al., 2008). These pre-clinical data have led to the use of TZD in humans to examine the effect of TZD-induced growth arrest and apoptosis in the treatment of various cancers (Burstein et al., 2003, Smith et al., 2004, Hau et al., 2007). Notably, a third generation TZD, efatutazone, was tested alone (Murakami et al., 2014) or in combination (Smallridge et al., 2013, Komatsu et al., 2014) with other

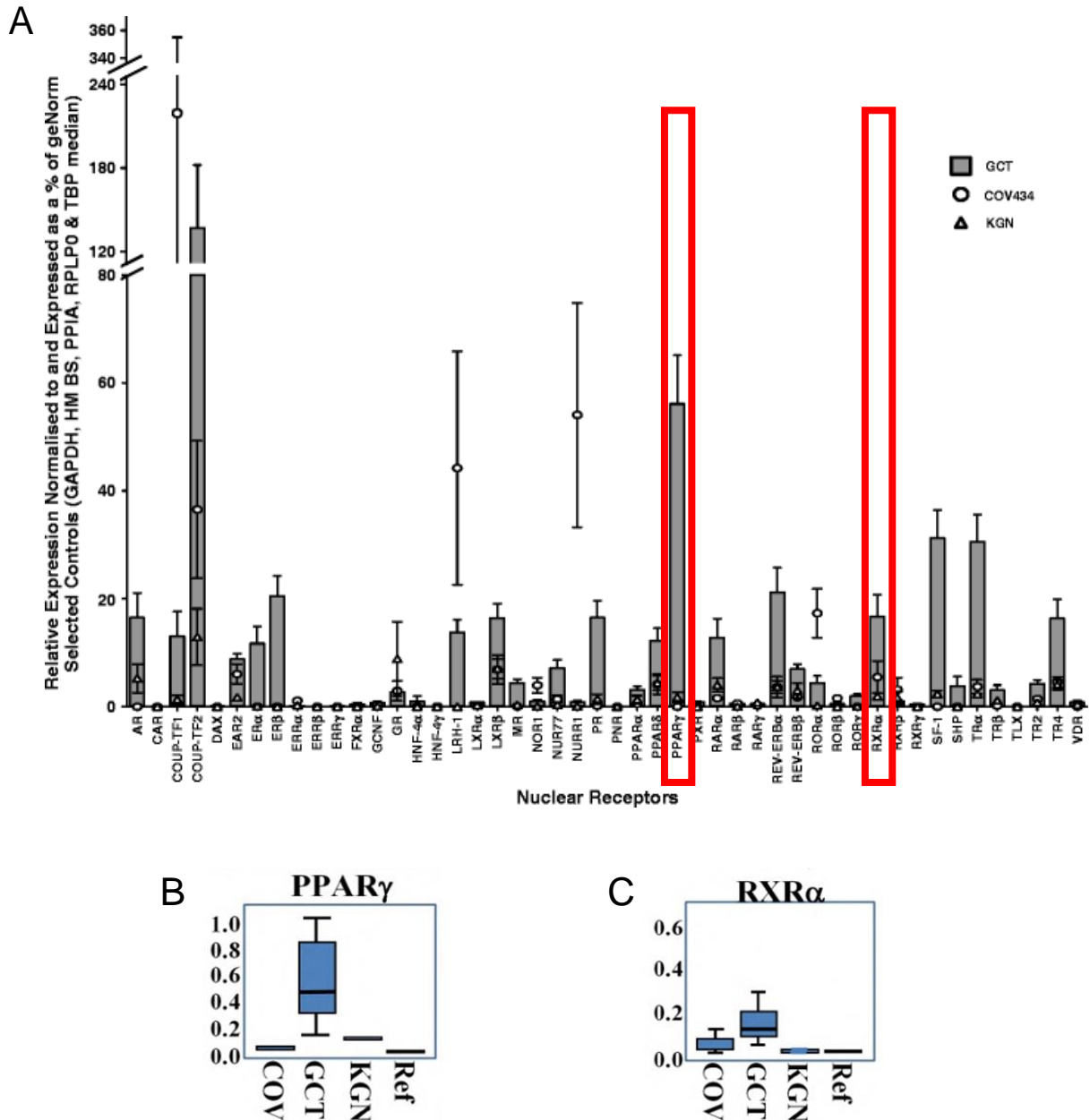


Figure 1.6. Expression of nuclear receptors in a panel of 14 GCT and two GCT-derived cell lines, KGN and COV434. A. Gene expression of nuclear receptors were analysed using the relative quantification method of ΔC_t and normalised to the median of *HMBS*, *PPIA* and *RPLP0*. Overexpression of *PPAR γ* and *RXR α* was seen in GCT, KGN and COV434. B and C. Whisker plot analysis. The line in the box represents the median and the whiskers indicate the highest and lowest values. Ref = Universal tumour RNA reference. (reproduced from Alexiadis et al. 2011) .

chemotherapy in several phase I studies. These trials reported an acceptable safety profile and disease stabilisation with the use of efatutazone.

Despite this, the current literature has contradicting views about the anti-proliferative effects of TZD in cancer treatment. It is argued that there is insufficient clinical data regarding the therapeutic effects of PPAR γ agonists when used alone (Ondrey, 2009). This makes it difficult to conclude whether PPAR γ -dependent or -independent effects contribute to any anti-cancer activities. For epithelial ovarian cancer, the use of the most potent PPAR γ agonists, RGZ and PGZ, did not inhibit PPAR γ -mediated cell proliferation in three ovarian cancer cell lines when used alone (Al-Alem et al., 2011). Ferrari et al. (2016) argued that the anti-tumour effects of PPAR γ agonists are more potent in PPAR γ -expressing tumour cells. Despite the overexpression of PPAR γ , studies in our laboratory have demonstrated that PPAR γ and RXR α agonist treatment alone does not induce apoptosis in GCT (refer to Section 1.2.2.5). This is consistent with the concept that there is potential resistance to PPAR γ . Further studies have shown that this is indeed the case, and the resistance is due to constitutive NF- κ B activity in GCT cells (see Chapter 1 Section 1.2.2.4).

1.2.2.4 Nuclear factor kappa B (NF- κ B)

The NF- κ B signalling pathway plays an important role in apoptosis, inflammation and immunity. The inactive NF- κ B protein is bound with the inhibitor of NF- κ B (I κ B) protein (thus, NF- κ B:I κ B complex) and resides in the cytoplasm. Not until the degradation of I κ B by phosphorylation is NF- κ B able to translocate to the nucleus and become activated. Activated NF- κ B upregulates a subset of target genes, whose subsequent activity leads to stimulation of growth with inhibition of differentiation and

apoptosis (Prasad et al., 2010). Characterisation of the role of NF- κ B signalling in the normal ovary has been limited, although effects on one of its target genes, X-linked Inhibitor of Apoptosis Protein (XIAP), have been described (see Chapter 1 Section 1.2.2.5) (Wang, 2002).

The pro-survival properties of NF- κ B are believed to contribute to a variety of human cancers. The GCT-derived KGN and COV434 cell lines (refer to Section 1.2.4), as well as many tumour cell lines of various origins, demonstrated constitutive activation of NF- κ B (Chu et al., 2004, Imbert and Peyron, 2017). Cancers characterised by constitutive NF- κ B signalling are more aggressive and correlate with a poor prognosis (Drummond and Fuller, 2010). The mechanism by which NF- κ B is constitutively activated appears to vary with tumour types, but the specific details in GCT remain to be elucidated (Chu et al., 2004, Imbert and Peyron, 2017). Recently it has been demonstrated in the KGN and COV434 cell lines, that abrogating NF- κ B activity using an I κ B inhibitor (BAY11-7082; BAY) leads to restoration of ER β (Chu et al., 2004) and also PPAR γ functional activity (Figure 1.7) (see Chapter 3). Considering the role of ER β and PPAR γ in initiating differentiation and apoptosis, respectively, the transrepression of ER β and PPAR γ by NF- κ B inhibition could be an exciting therapeutic target for treating GCT. Due to the critical role of NF- κ B in normal physiology, however, the consequences of long-term inhibition need to be first determined before NF- κ B inhibition is adopted as a therapeutic option. Another feasible option is to examine target genes that are part of the NF- κ B pathway, such as XIAP.

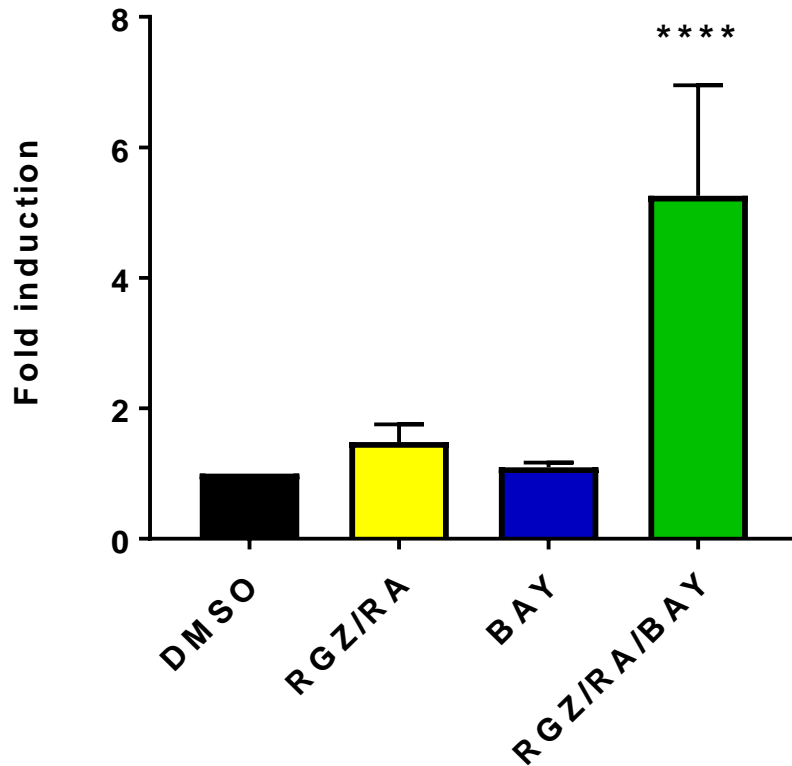


Figure 1.7. PPRE₄-mediated transactivation in KGN. PPAR_γ activation using RGZ (20 μM) and RA (5 μM) did not induce PPAR_γ-mediated transactivation (PPRE₄-Luc) in the KGN cells. Upon NF-κB inhibition using BAY11-7082 (BAY; 5 μM), RGZ and RA treatment significantly induced PPAR_γ-mediated transactivation in KGN cells. This suggested that PPAR_γ is transrepressed by the constitutive NF-κB signalling in the KGN cells (Chapter 3). n = 5 in duplicate wells; One-way ANOVA; Tukey's post-hoc analysis; *p* < 0.0001 when compared to DMSO.

1.2.2.5 X-linked inhibitor of apoptosis protein (XIAP)

The cellular Inhibitors of Apoptosis Protein (IAP) family are a subset of NF- κ B target genes whose function is to block programmed apoptotic cell death by inhibiting caspase activities (Fulda and Vucic, 2012, Bai et al., 2014). Members of the family share at least one copy of a well-conserved Baculovirus IAP Repeat (BIR) domain. Some BIR domains were found to interact with proteins, such as the caspases, which contain an IAP-binding motif (IBM) at their N-termini (Lin et al., 2007). Amongst the eight members of the IAP family, XIAP, also known as BIRC4, is the most potent caspase inhibitor, being the only member of this family able to directly suppress apoptosis triggered by both intrinsic and extrinsic apoptotic signals (Fulda and Vucic, 2012).

XIAP consists of three BIR domains (BIR1, BIR2 and BIR3), followed by a C-terminal RING (Really Interesting New Gene) domain (Figure 1.8A). Each domain possesses distinct functional properties. Unlike the BIR2 and BIR3 domains, BIR1 does not possess caspase-binding activity nor does it contain an IBM-binding groove (Lin et al., 2007). Instead, structural analysis revealed that the IBM-interacting residues on BIR2 and BIR3 domains significantly overlap with the self-dimerisation residues on the BIR1 domain (Lin et al., 2007, Lu et al., 2007). Self-dimerisation of the BIR1 domain is critical for inducing NF- κ B activation, which is dependent on the successful interaction between the BIR1 domain and the transforming growth factor (TGF)- β -activated kinase (TAK) 1 at the surface opposite to the site of BIR1 self-dimerisation (Lu et al., 2007).

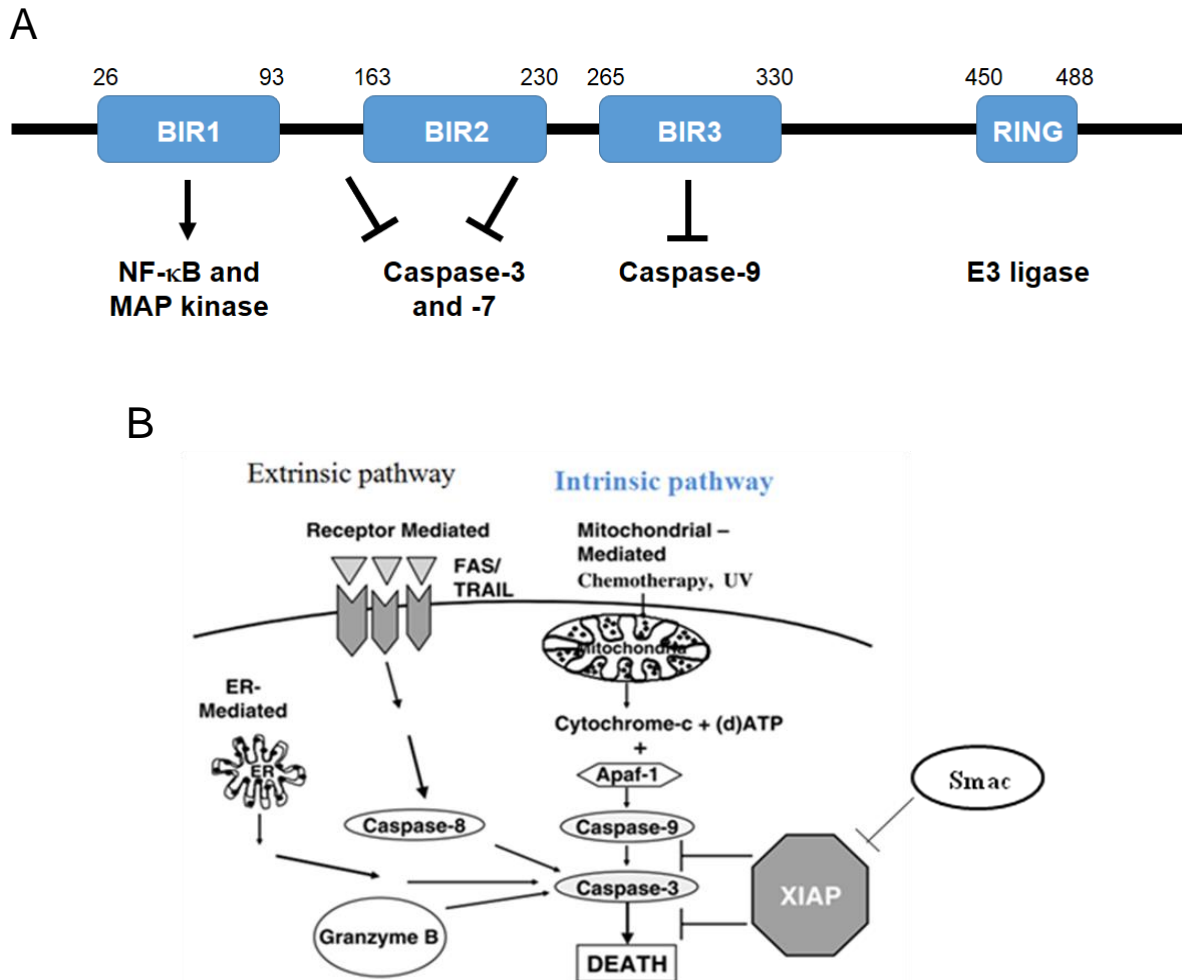


Figure 1.8. X-linked inhibitor of apoptosis protein (XIAP). A. Structure and function of XIAP. XIAP contains three BIR domains and a RING finger motif. BIR1 domain is crucial for XIAP-mediated NF- κ B and MAP kinase activation. The anti-apoptotic BIR2 domain blocks caspase-3 and -7 while the BIR3 domain inhibits caspase-9. The RING domain acts as an E3 ubiquitin ligase. XIAP inhibits apoptosis in response to multiple stimuli. B. XIAP inhibits caspase activity (caspase-3, -7 and -9) within the intrinsic pathway. By inhibiting effector caspases, XIAP blocks the downstream pathway and thus inhibits apoptosis via the extrinsic and intrinsic pathways. The expression of XIAP is regulated by an endogenous inhibitor, Smac (second mitochondrial activator of caspases) (adapted from Schimmer et al., 2006).

The BIR2 domain and the linker region between the BIR1 and BIR2 domains are responsible for the anti-apoptotic mechanism by binding to the effector caspases, caspase-3 and -7 (Figure 1.8B) (Sun et al., 1999, Chai et al., 2001). Sun et al. (1999) has reported that aspartate 148 in the BIR1-BIR2 linker region is essential for the caspase-3 inhibition where a substitution of an alanine at position 148 completely abolished the inhibitory activity. Other residues important for caspase interaction such as L141, V147 and I149 retained some degree of caspase-3 inhibition when mutated (Sun et al., 1999). While an intact BIR2 domain is necessary to inhibit caspase-3 (Silke et al., 2001), it serves as a facilitator to the BIR1-BIR2 linker region in caspase-7 binding (Huang et al., 2001). In addition, the BIR2 domain plays a regulatory role in caspase binding by interacting with the endogenous XIAP inhibitor, a mitochondrial protein called second mitochondrial activator of caspases (Smac) (Huang et al., 2001).

The isolated fragment of BIR3 domain selectively targets the initiator caspase, caspase-9 (Figure 1.8B). Crystallographic analysis revealed that the BIR3 domain dimerises with caspase-9 at the site which is required for caspase-9 homodimerisation (Shiozaki et al., 2003). Homodimerisation of caspases enables the formation of an active site which requires the critical supporting loop (L2') of the adjacent monomer (Shi, 2002). As such, the BIR3 domain inhibits caspase-9 activity by "trapping" the caspase in a monomeric state (Shiozaki et al., 2003).

The RING domain exhibits E3 ubiquitin ligase activity; it mediates ubiquitylation and the subsequent protein degradation that are necessary for normal cellular function (Fulda, 2007). RING dimerisation is a prerequisite for the transfer of ubiquitin and recruitment of the ubiquitin-conjugating enzyme, or the E2 ligase (Nakatani et al.,

2013). Potent targets for ubiquitylation in the context of XIAP-induced apoptosis are caspases-3 and -9 (Suzuki et al., 2001, Morizane et al., 2005). The RING domain also regulates XIAP expression by promoting the ubiquitylation of cytosolic mature Smac (Morizane et al., 2005). Although the RING domain has a role in the regulation of apoptosis, the literature suggests that mutation of the RING finger does not abolish the anti-apoptotic effects; the E3-ligase activity however is found to be less effective (Nakatani et al., 2013). In addition to its role as a caspase inhibitor, XIAP also inhibits apoptosis via other mechanisms. The E3 ubiquitin ligase activity of the RING domain promotes I κ B degradation and NF- κ B translocation to the nucleus, and consequently NF- κ B activation (Hofer-Warbinek et al., 2000, Levkau et al., 2001).

In silico molecular docking studies and *in vitro* studies have sought to identify molecules/pathways that regulate XIAP expression. As mentioned previously, one such important regulator is the endogenous XIAP inhibitor, Smac (Figure 1.8B). In the mitochondria, Smac co-localises with cytochrome c, another protein which promotes caspase activation (Du et al., 2000). Upon cleavage, the mature Smac possesses caspase activation activity and is released into the cytosol during apoptosis (Du et al., 2000). The mature form has an exposed IAP-binding tetrapeptide motif (Ala-Val-Pro-Ile) which allows the dimeric Smac to interact with the BIR 3 domain of XIAP at the site of caspase-9 binding (Du et al., 2000, Wu et al., 2000). This results in effective relief of caspase-9 inhibition by XIAP. In addition, the Smac dimer also binds to the linker region between the BIR2 and 3 domains to compete with the XIAP-caspase-7 interaction (Huang et al., 2003).

Similar to Smac, the mitochondrial serine protease Omi/HtrA2 is released into the cytosol in the mature form following proteolytic cleavage. The mature Omi/HtrA2

contains an IAP-binding tetrapeptide motif (Ala-Val-Pro-Ser) and the trimerisation of Omi/HtrA2 is indispensable for its pro-apoptotic function (Li et al., 2002). Conversely, the nuclear XIAP-associated factor (XAF) 1 does not require proteolytic activity for its activation. XAF1 antagonises XIAP by sequestering the anti-apoptotic protein in the nucleus (Liston et al., 2001).

Since the inhibition of apoptosis is a critical mechanism in tumourigenesis, there has been a lot of conjecture about whether XIAP overexpression leads to a heightened anti-apoptotic activity which could play an important role in the oncogenic process (Fulda, 2007). Our laboratory has shown XIAP to be overexpressed in numerous GCT (Figure 1.9). XIAP has been found to be an FSH-regulated gene in concert with NF- κ B – this led our laboratory to study XIAP expression in GCT. Indeed, the XIAP gene is significantly overexpressed in GCT and in two GCT-derived cell lines when compared to normal ovary (Figure 1.9) (Chu et al., 2009). It is worth noting that overexpression of XIAP is oftentimes seen in patients resistant to chemotherapy (Ma et al., 2009). There are XIAP inhibitors currently in clinical trials for various malignancies such as pancreatic cancer (Jiang et al., 2012) and acute myeloid leukaemia (Carter et al., 2011). The development of XIAP inhibitors has taken two approaches – antisense oligonucleotides and small molecule inhibitors. Antisense oligonucleotides against XIAP work by degrading *XIAP* mRNA and therefore knocking down translation into protein. This downregulation of XIAP has also been shown to restore sensitivity to chemotherapy and directly induce apoptosis (Vogler et al., 2008).

The pro-apoptotic action of Smac is thought to be therapeutically useful. Smac-mimetics (SM) have been developed to mimic the action of the endogenous XIAP

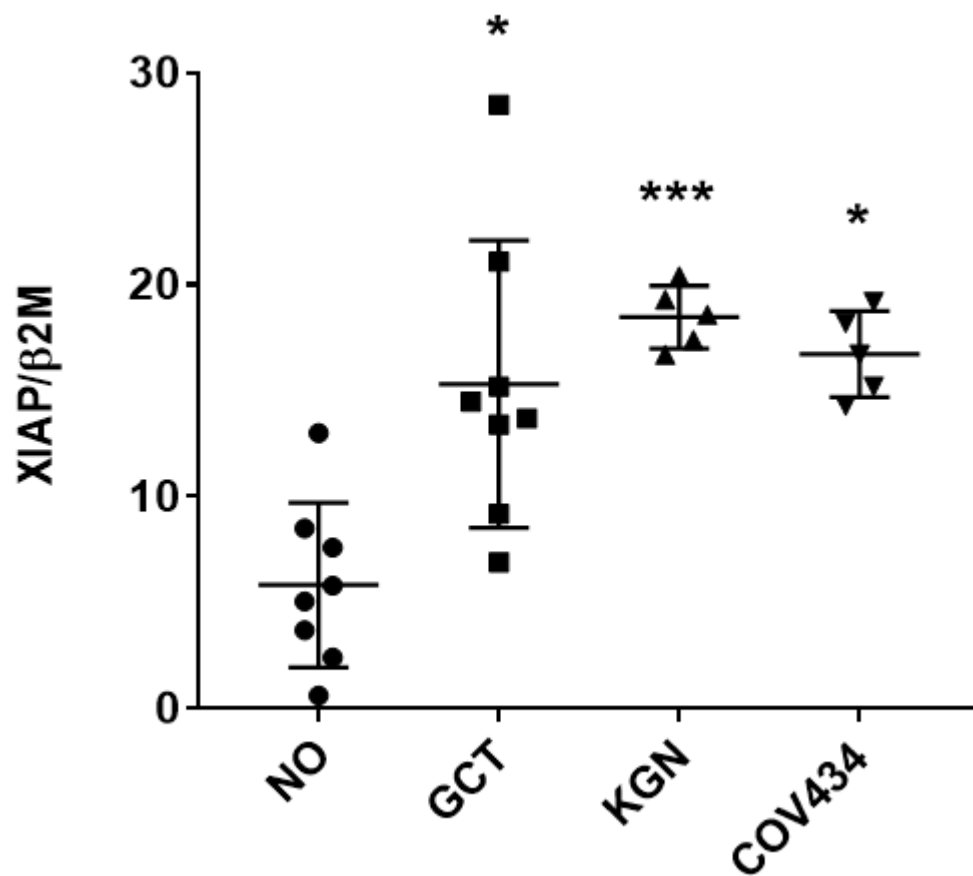


Figure 1.9. mRNA Expression of *XIAP* in pre-menopausal ovaries, GCT and GCT-derived cell lines. *XIAP* mRNA expression is normalised to the housekeeping gene beta-2 microglobulin (β_2M). Significant overexpression of *XIAP* is reported in 8 human GCT, the KGN and COV434 cells compare to 8 pre-menopausal ovaries (NO) collected from unrelated gynaecological conditions (NO). Horizontal lines indicate the mean value for each cohort. Kruskal-Wallis; Dunn's post-hoc analysis; * $p < 0.05$, *** $p < 0.001$ when compared to NO.

inhibitor. Keeping in mind that the BIR domains are well-conserved across the IAP family, it is not surprising that SM are reported to also antagonise other member of the IAP family (e.g. cIAP1). Much work needs to be done to characterise the functions of SM and/or other XIAP inhibitors. Additionally, it is also important to investigate other essential IAP functions that could be potentially targeted (Fulda and Vucic, 2012). Small molecules direct against the BIR2 or BIR3 domains of XIAP have been developed to inhibit XIAP-induced apoptosis. Similar to SM, small molecule inhibitors block IAP binding to caspases, and thus prevent IAP from impeding caspase activities. These have led to reports that show this approach leads to induction of apoptosis and sensitisation of malignant cell lines to chemotherapy (Matzinger et al., 2015). One promising example of a BIR3 inhibitor is embelin. This compound demonstrates anti-tumour effects and has also been shown to be well tolerated in animal studies (Lunardi et al., 2013).

Studies in our laboratory have shown that combined treatment of GCT cells with PPAR γ /RXR α agonists, as well as XIAP inhibitors causes a significant increase in apoptotic cells in GCT-derived cell lines (Chapter 3). This finding is consistent with studies that used the same approach but in the context of colorectal cancer (Dai et al., 2008). Increased apoptosis did not occur when cells were treated with PPAR γ /RXR α agonists or XIAP inhibitor alone (Figure 1.10). These findings raise the question of how XIAP inhibition sensitises GCT to PPAR γ -mediated apoptosis, and whether or not a combination of XIAP antagonist and PPAR γ agonist would be a more efficacious therapeutic strategy for treating GCT, and indeed other ovarian cancer subtypes expressing both PPAR γ and XIAP.

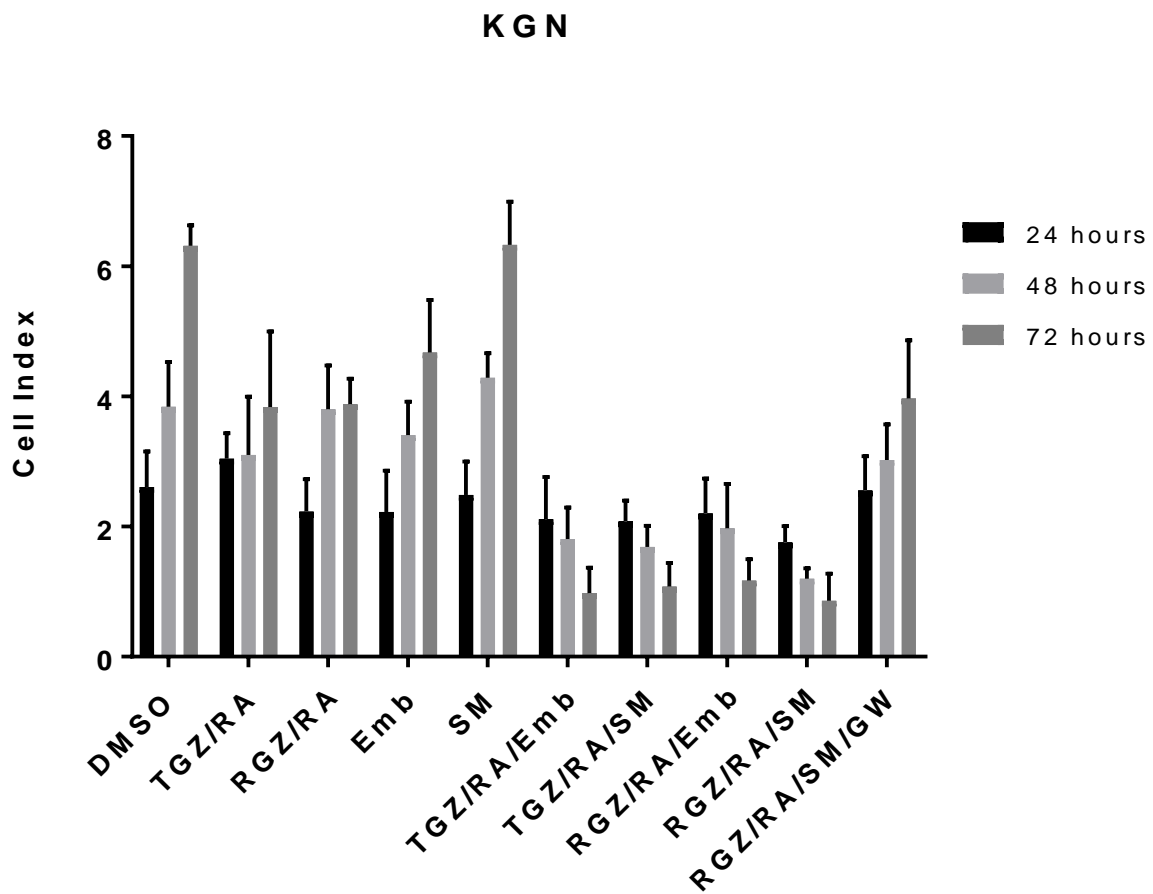


Figure 1.10A. Effects of combined XIAP inhibition and PPAR γ activation in GCT *in vitro*. The KGN cells were subjected to PPAR γ activation (TGZ or RGZ/RA) and XIAP inhibition (Emb or SM) singularly or in combination for 24 to 72 hours to assess proliferation. PPAR γ activation or XIAP inhibition alone had no effects on proliferation. However, when combined TGZ or RGZ/RA with Emb or SM, reduction of cell proliferation was observed in the KGN cells. GW9662 (GW) is a PPAR γ antagonist which was demonstrated to reverse the anti-proliferative effects of PPAR γ in the RGZ/RA/SM treatment. n = 3 in duplicate wells.

COV434

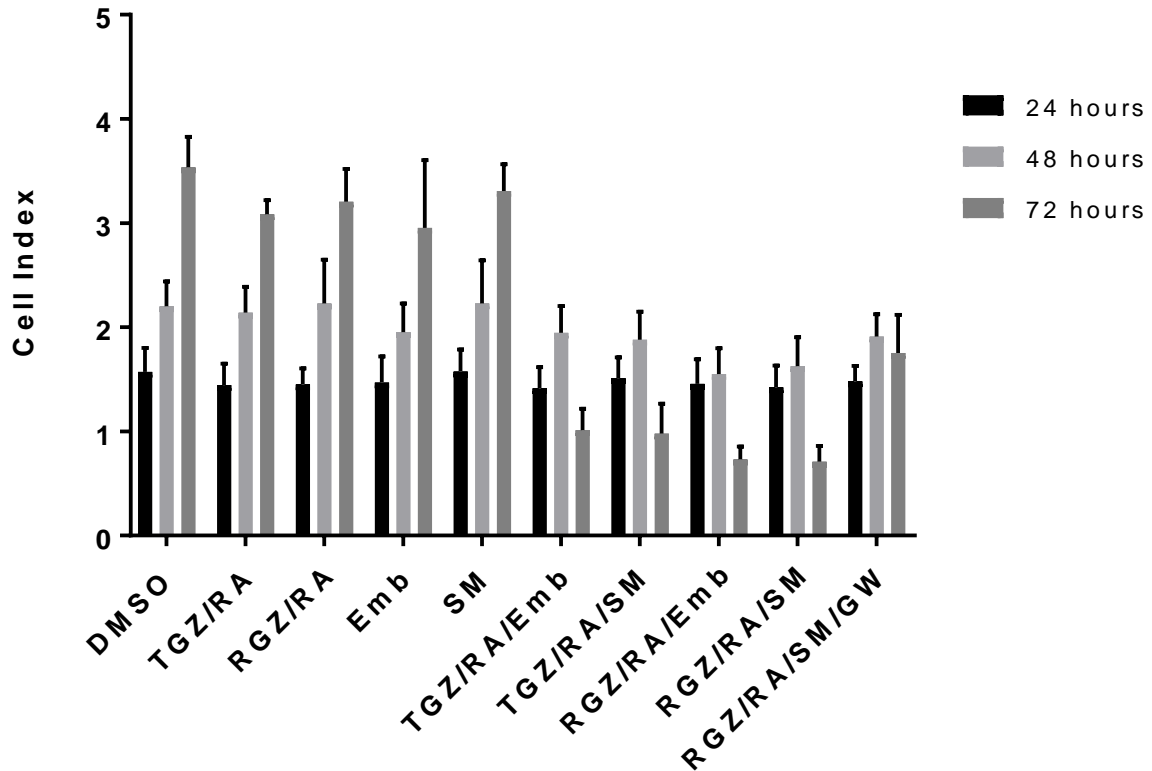


Figure 1.10B. Effects of combined XIAP inhibition and PPAR γ activation in GCT *in vitro*. The COV434 cells were subjected to PPAR γ activation (TGZ or RGZ/RA) and XIAP inhibition (Emb or SM) singularly or in combination for 24 to 72 hours in cell proliferation assay. Singular treatment did not affect proliferation of the COV434 cells. However, cessation of proliferation was observed when TGZ or RGZ/RA was combined with Emb or SM in the COV434 cells. The PPAR γ antagonist, GW, was added in combination with the RGZ/RA/SM treatment to reverse the anti-proliferative effects of PPAR γ . n = 3 in duplicate wells.

1.2.2.6 Mitogen-activated protein (MAP) kinase pathway

MAP kinases are proline-directed serine/threonine kinases that influence a number of cell signalling pathways. In response to G protein-coupled receptors, receptor tyrosine kinases, inflammatory cytokines and environmental stresses, MAP kinases are activated by dual phosphorylation of threonine and tyrosine residues. Thus far, six MAP kinases signalling pathways have been identified; extracellular-signal-regulated kinase (ERK) 1/2, ERK3/4, ERK5, ERK7/8, c-Jun-n-terminal kinase (JNK) 1/2/3 and p38/ERK6 (Shaulian and Karin, 2002). In GC, FSH and LH have been demonstrated as potent activators of MAPK via ERK1/2 (Seger et al., 2001). In particular, the activator protein-1 (AP-1) as a downstream transcription factor has regulatory roles in GC differentiation and proliferation (Sharma and Richards, 2000).

1.2.2.7 Activator protein-1 (AP-1)

AP-1 describes a class of basic leucine zipper (bZIP) transcription factors. It is a collective term that refers to a dimeric protein composed of Jun (c-Jun, JunB and JunD), Fos (c-Fos, FosB, Fra-1 and Fra-2) or activating transcription factor (ATF) subunits, which can form homo- or hetero-dimers (Sharma and Richards, 2000). They partly depend on the relative abundance, or the combination of specific Jun/Fos factors (Karin, 2002). The involvement of AP-1 in cell cycle regulation is therefore multi-factorial. In the ovary, each AP-1 factor exhibits specific expression patterns in response to endocrine factors, which correlates with different stages of ovarian development (Sharma and Richards, 2000, Rusovici and LaVoie, 2003). For instance, JunD and Fra2 expression is associated with the terminal differentiation of GC (Sharma and Richards, 2000). In a context-dependent manner, AP-1 inhibits or promotes cell proliferation, differentiation and apoptosis (Matthews et al., 2007).

Accumulating evidence has confirmed the ability of AP-1 to regulate angiogenesis and inflammation. Thus it is not surprising that it contributes to tumour promotion (Shaulian, 2010). Overexpression of various AP-1 factors has been detected in human malignancies and cancer cell lines (Matthews et al., 2007). Similarly, deletion of an upstream kinase, JNK2, was found to be protective against ultraviolet-induced tumour development in a knockout mouse model, suggesting that AP-1 may be fundamental to tumorigenesis (Matthews et al., 2007).

The increase in AP-1 activity in cancer has been attributed to enhanced signalling through the MAPK pathways (Leaner et al., 2007, Matthews et al., 2007). In ovarian cancer, activation of AP-1 has been linked to cancer invasion and metastasis (Matthews et al., 2007). Studies in our laboratory have demonstrated that AP-1 signalling is constitutively activated in two GCT-derived cell lines (see Chapter 1 Section 1.2.4) (Chu et al., 2004). As discussed previously, GCT cells also have NF- κ B constitutive activity. A common regulatory molecule key for activating both NF- κ B and AP-1 is the transforming growth factor- β -activated kinase 1 (TAK1) (Hofer-Warbinek et al., 2000).

1.2.2.8 Transforming growth factor- β -activated kinase (TAK) 1

TAK1 is a member of the MAP kinase kinase kinase (MAP3K) family. It is activated by exogenous stressors (e.g. UV irradiation) and endogenous ligands, namely TGF β , tumour necrosis factor (TNF) and interleukin-1 (IL-1) (Mihaly et al., 2014). Following stimulation, TAK1 forms complexes with its regulatory subunits, TAK-binding protein (TAB) 1, 2 or 3 (Figure 1.11) (Besse et al., 2007). These complexes play an essential

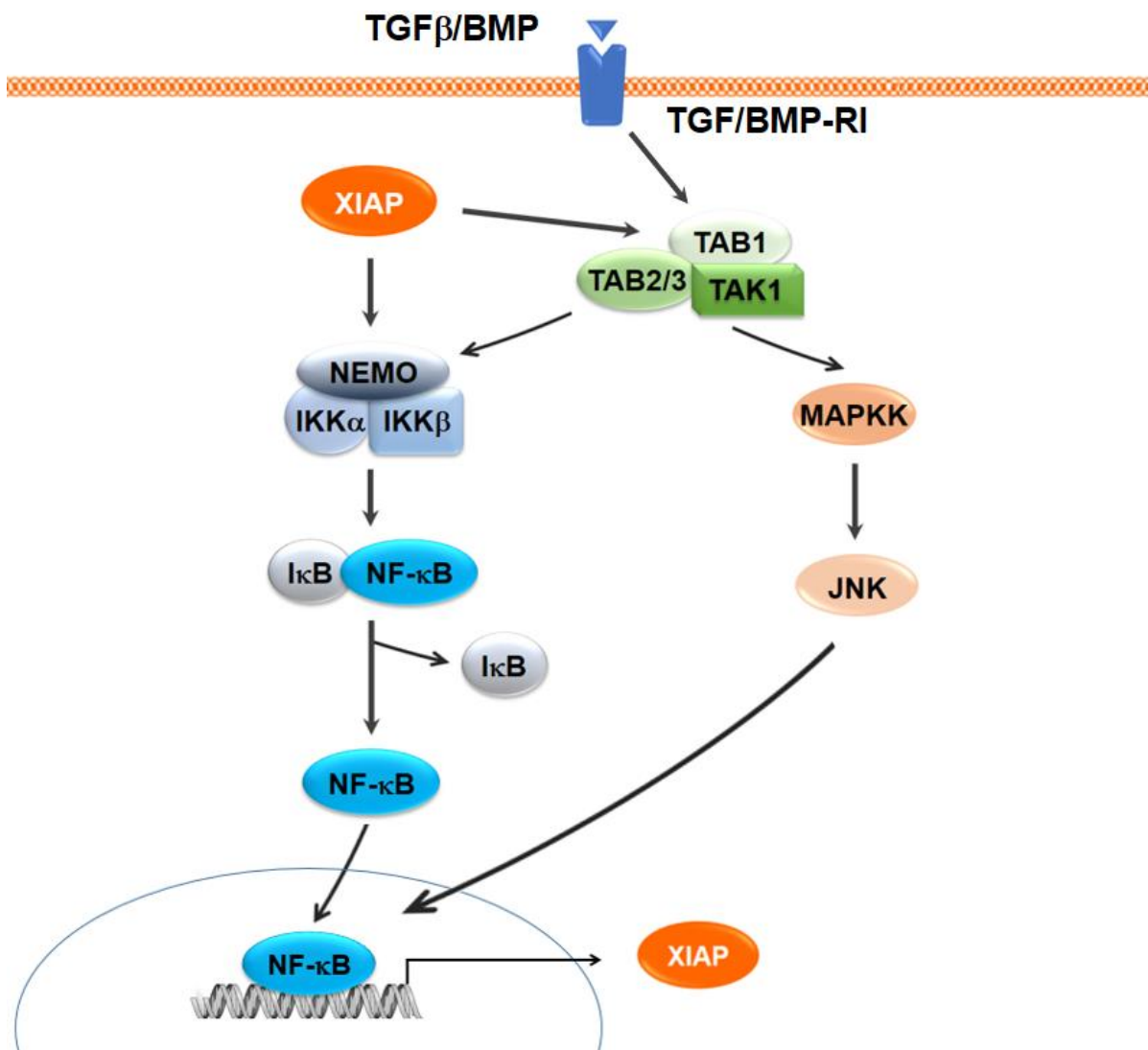


Figure 1.11. XIAP in TGFβ signalling pathway. XIAP directly interacts with TAB1 to activate TAK1. The TAK-TAB complex of the TGFβ pathway stimulates MAPKK and NF-κB transcription, which subsequently increases the expression of XIAP.

role in the activation of I κ B kinase and JNK, which subsequently upregulate NF- κ B and AP-1 signalling (Besse et al., 2007, Fan et al., 2010b, Kim et al., 2012). TAK1 also modulates NF- κ B signalling via TNF α and IL-1 β (Fan et al., 2010b). TAK1 appears to be regulated by XIAP in a signal-dependent manner (Kaur et al., 2005). Following TGF- β 1 stimulation, the RING domain of XIAP targets TAK1 for proteosomal degradation. As a result, JNK1 activity is downregulated, and TGF β -mediated apoptosis is abolished (Kaur et al., 2005). On the other hand, mapping studies using unstimulated purified XIAP and TAB1 constructs found that only the BIR1 domain interact with TAB1 via dimerisation, and such process is critical for TAK1 activation (Figure 1.11) (Lu et al., 2007). Disruption of this dimerisation abolishes the activation of NF- κ B, the downstream effectors of TAK1 activation (Lu et al., 2007). Given that both NF- κ B and AP-1 activities are upregulated in GCT cells (refer to Section 1.2.2.4), our laboratory has speculated on the potential involvement of TAK1 in GCT pathophysiology. As mentioned previously, XIAP activates TAK1 via TAB1, which in turn regulates NF- κ B and AP-1 signalling. As XIAP may be a key regulator of the constitutive NF- κ B and AP-1 signalling pathways in GCT, we have investigated the effect of XIAP inhibition on NF- κ B and AP-1 signalling. In GCT-derived cell lines (Chapter 1 Section 1.2.4), XIAP inhibition was found to inhibit both AP-1 (Chapter 3) and NF- κ B (Chapter 3) constitutive activities. The next question of interest is, whether or not XIAP overexpression contributes to NF- κ B and AP-1 constitutive activities via a dysregulation in TAK1 signalling, leading to a downregulation of apoptosis.

1.2.3 Apoptosis

Apoptosis is a process of programmed cell death that has a pivotal role in maintaining the integrity and homeostasis of tissues and organs (Malladi et al., 2010, Wong, 2011). It serves to eliminate harmful cells by a process of active signalling in an orderly fashion in contrast to necrosis, where cells die from damage and from the induced inflammatory response (Wong, 2011). Morphological changes occurring during apoptosis are well-documented and biochemical markers of apoptosis have been identified (Malladi et al., 2010, Wong, 2011). Major contributors to apoptosis include caspases and other apoptotic regulators (Fiandalo and Kyprianou, 2012). Caspases are classified based on their functions: in apoptosis, adaptor proteins interact with and activate the initiator caspases (caspases-2, -8, -9 and -10), which in turn activate the effector caspases (caspases-3, -6 and -7) (Malladi et al., 2010).

There are two main pathways to apoptosis – the intrinsic and extrinsic pathways (Figure 1.12). The intrinsic pathway is activated by internal stimuli within the cells while the extrinsic pathway involves death receptor binding. The intrinsic pathway takes place in the mitochondria in response to irreparable DNA damage, growth factor withdrawal, endoplasmic reticulum stress and the like (Malladi et al., 2010, Wong, 2011). The stimulus triggers the release of apoptotic factors (e.g. cytochrome-c, Smac) from mitochondria into the cytoplasm; this is closely regulated by the pro-apoptotic and anti-apoptotic members of the Bcl-2 protein family (Figure 1.12). Smac, for instance, then binds to and suppresses cIAP action which subsequently results in activation of caspases-3 and -9 (Wong, 2011). Alternatively, XIAP can inhibit both the intrinsic and extrinsic pathways (described previously in Section 1.2.2.5).

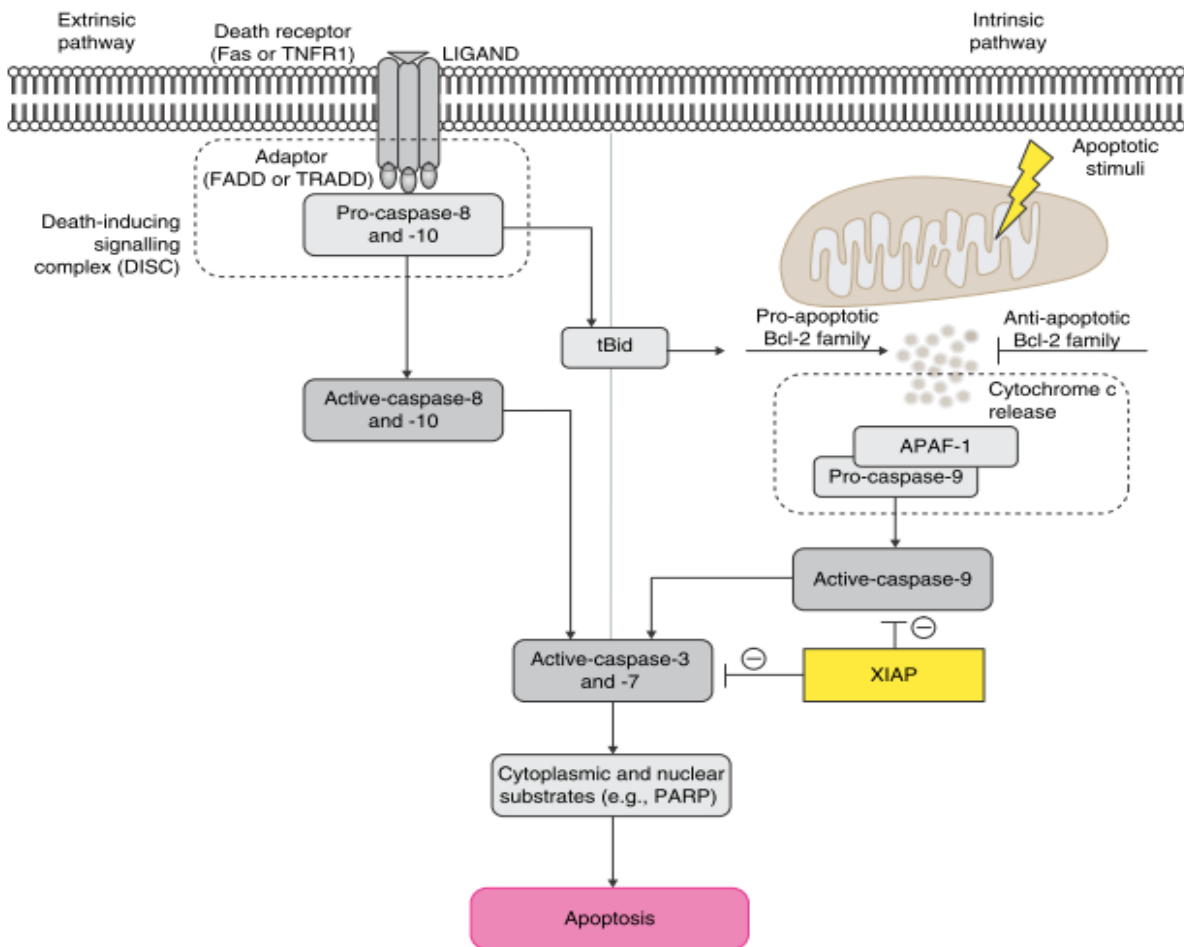


Figure 1.12. The intrinsic and extrinsic apoptotic pathways. The intrinsic apoptotic pathway is initiated in the mitochondria by stress stimuli. This triggers the release of cytochrome c into the cytoplasm, a process which is closely regulated by both pro- and anti-apoptotic Bcl-2 family. The extrinsic apoptotic pathway involves the death receptors (Fas or TNFR). Upon binding by death ligands such as FADD or TRADD, caspase-8 and -10, and subsequently caspase-3 and -7 are activated to initiate apoptosis. Caspase-3 and -7 can also be activated by cytochrome c-activated caspase-9. XIAP binds to caspase-3, -7 and -9 to inhibit their apoptotic activity (Dean et al., 2007). FADD = Fas-associated death domain; TRADD = TNF receptor-associated death domain; tBID = truncated BID.

The extrinsic apoptotic pathway involves the death receptors, which refers to members of the tumour necrosis factor (TNF) receptor (TNFR) superfamily. These receptors have a death domain for death ligand, for example, TNF or Fas, binding. This gives rise to a death-inducing signalling complex (DISC) which then activates caspase-8 to initiate apoptosis (Wong, 2011) (Figure 1.12). Regulatory mechanisms of this pathway include NF- κ B signalling, which has inhibitory effects on TNF-induced apoptosis (Westwick et al., 2009). Inappropriate apoptosis can lead to pathological conditions; some examples include cancers where there is insufficient apoptosis, and autoimmune disorders in which there is increased apoptosis (Wong, 2011). For GCT, it is speculated that failure of the apoptotic regulators discussed previously could contribute to tumour development.

1.2.4 GCT-derived cell lines

The study will use two human GCT-derived cell lines, KGN and COV434, as models to study GCT pathogenesis *in vitro*. The KGN cell line was established from a recurrent GCT isolated from a 64-year-old postmenopausal woman. The cultured KGN cells have a fibroblast-like morphology; they initially grow in a monolayer but as the cells proliferate, they are found in multilayers and a lack of contact inhibition is noted (Figure 1.13A) (Nishi et al., 2001). The COV434 granulosa cells were isolated from a GCT of a 27-year-old female. Unlike KGN cells, they grow as small aggregates with intercellular connections formed between cells (Figure 1.13B) (van den Berg-Bakker et al., 1993). Both cell lines demonstrate physiological activities similar to that in normal human GC, including the expression of functional FSH receptors and some level of steroidogenesis (van den Berg-Bakker et al., 1993, Zhang et al., 2000, Nishi et al., 2001). For instance, E₂ is detected and its production

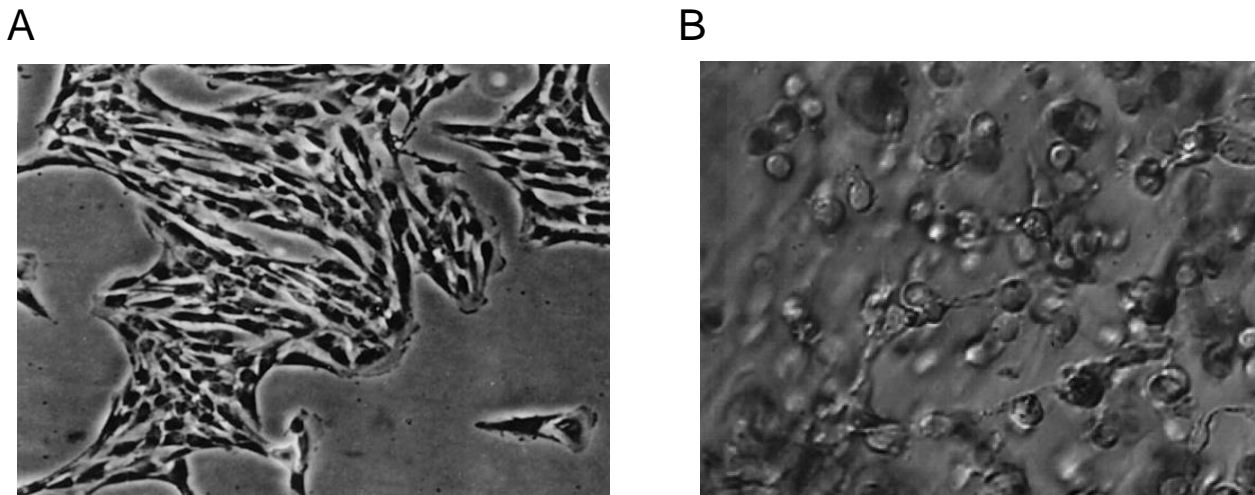


Figure 1.13. Microscopic images of the two human GCT-derived cell lines. A. The KGN cells exhibit a spindle shape morphology. They grow as adherent cells in a monolayer (Nishi et al., 2001). B. The COV434 cells grow as small aggregates with a granular appearance. Intercellular junctions are seen between some cells (van den Berg-Bakker et al., 1993).

responds to cAMP stimulation in both KGN and COV434 cells, indicating aromatase activity in these cells (van den Berg-Bakker et al., 1993, Nishi et al., 2001). Both cell lines exhibit basal level of progesterone secretion but only progesterone synthesis in the KGN cells responds to stimulation by cAMP (van den Berg-Bakker et al., 1993, Nishi et al., 2001). The FOXL2 C134W mutation is present in the KGN cells, but not the COV434 cell line, suggesting these cell lines represent an adult and juvenile GCT, respectively (Jamieson et al., 2010). Reflective of what is observed in adult GCT, the FOXL2 protein is expressed in the KGN cells. The COV434 cells however, do not express FOXL2 which is similar to the juvenile GCT whose FOXL2 expression is reported low or undetectable (Jamieson et al., 2010).

1.3 Hypotheses and aims

Our laboratory has demonstrated high expression of XIAP in GCT cells (Figure 1.9) and constitutive activation of NF- κ B signalling in the GCT-derived cell lines, KGN and COV434. Additionally, we observed the overexpression of PPAR γ (Figure 1.6) with suspected resistance to it in the GCT-derived cell lines. By treating GCT cells with a combination of PPAR γ /RXR α agonists and XIAP or NF- κ B inhibitors, there is a significant increase in apoptosis in GCT cells. Such changes do not occur when cells are treated with PPAR γ /RXR α agonists or XIAP inhibitors alone (Figure 1.10). This finding raises the question as to how XIAP sensitises PPAR γ -mediated apoptosis. We hypothesise that the overexpression of XIAP contributes to GCT pathogenesis and that XIAP antagonism sensitises GCT cells to PPAR γ -mediated differentiation and apoptosis.

To address these hypotheses, the aims of this study are to

- 1) analyse XIAP and PPAR γ expression in GCT, other ovarian cancers and postmenopausal ovaries;
- 2) investigate XIAP regulation in KGN and COV434; and
- 3) determine the effects of XIAP inhibition and PPAR γ activation in KGN and COV434.

An understanding of the underlying mechanisms of XIAP action in GCT should lead to improvements in classification, prognostication and therapy in these tumours.

CHAPTER 2

GENERAL METHODS

2 GENERAL METHODS

This chapter outlines the methodologies/techniques that are commonly used across this thesis.

2.1 Tissue culture

Tissue culture techniques that are included in Chapter 3, 4 and 5 are described in the following sections.

2.1.1 Cell lines

The two GCT-derived cell lines, KGN and COV434 are described in Chapter 1 Section 1.2.4.; they were established by Nishi et al (2001) and van den Berg-Bakker et al (1993), respectively. The KGN cell line was derived from a recurrent GCT in a 64-year-old woman. It is heterozygous for the FOXL2 C134W mutation (Jamieson et al., 2010), which has been exclusively reported in adult GCT. The COV434 cell line was isolated from a GCT of a 27-year-old female. The COV434 cells harvest wild-type *FOXL2* gene and do not express FOXL2 (Jamieson et al., 2010) , they are used as a model of juvenile GCT. Given this project focuses primarily on adult GCT, most experiments were performed on KGN only.

2.1.1.1 Culture conditions

Cells were cultured in T75 media flasks in a humidified incubator, 5% CO₂ at 37°C. Table 2.1 listed the specific growth medium for each cell line. These culture conditions were used consistently unless otherwise stated in a specific experiment.

All tissue culture products are from Invitrogen Life Technologies, Thermo Fisher Scientific (Waltham, WA, U.S.A.). Cells were passaged at 80-90% confluency.

Table 2.1 Culture conditions for KGN and COV434.

Cell lines	Medium	Supplements
KGN	Dulbecco's Modified Eagle Medium (DMEM): Nutrient Mixture F-12 (DMEM:F-12)	10% fetal bovine serum (FBS); 2.4% HEPES buffer;
COV434	DMEM	1% penicillin/streptomycin/amphotericin B

2.1.1.2 Cell passaging

Existing media was decanted into a 1% bleach solution. Cells were rinsed twice with 5 ml of PBS (Invitrogen) to remove all traces of media that contains trypsin inhibitor. 1 ml of 0.25% (w/v) trypsin-EDTA (Invitrogen) was added into the flask, which was left in 37°C incubator for 5-10 minutes. The cells were dissociated with gentle tapping. The cell suspension was mixed by gentle pipetting; approximately 0.2 ml of cell suspension was added into a new flask with 20 ml of respective media and returned to the incubator.

2.1.1.3 Cryopreservation

Cells were washed with PBS and trypsinised by the standard protocol described above. Trypsinised cells were pelleted by centrifugation at 1,000 rpm for 5 minutes. Supernatant was decanted and pellet was re-suspended in 3 ml of respective media with 10% DMSO (Invitrogen). 1 ml of the re-suspended cells was transferred to each cryovial and stored in liquid nitrogen for long term storage.

2.1.2 Transactivation assays

2.1.2.1 Vectors/plasmids

2.1.2.1.1 pTAL-luc

pTAL-luc (Clontech Laboratories, Takara Bio Inc., Japan) lacks the enhancer element, but contains a TATA-like promoter (P_{TAL}) and a firefly luciferase (*luc*) gene. It was used to study putative enhancers that were inserted upstream of the luciferase reporter gene. Figure 2.1 shows the generalised map of the vectors used in this study.

2.1.2.1.2 pAP1₃-luc

The pAP1₃-Luc vector (Clontech Laboratories) contains 3 specific AP-1 enhancer elements which are located upstream from a TATA promoter (Figure 2.1). The vector has a luciferase reporter gene that encodes an enzyme, luciferase, which upon binding to its substrate luciferin, emits light. When the AP-1 enhancer element is stimulated, the transcriptional activity can be assessed by measuring the signals from the light-emitting luciferin.

2.1.2.1.3 pNF κ B₄-luc

The pNF κ B₄-Luc vector (Clontech Laboratories) contains 4 NF- κ B enhancer elements which are located upstream from a TATA promoter and a luciferase coding sequence (Figure 2.1). Upon stimulation of the NF- κ B enhancer element, the transcriptional activity can be assessed by measuring the signals from the light-emitting luciferin.

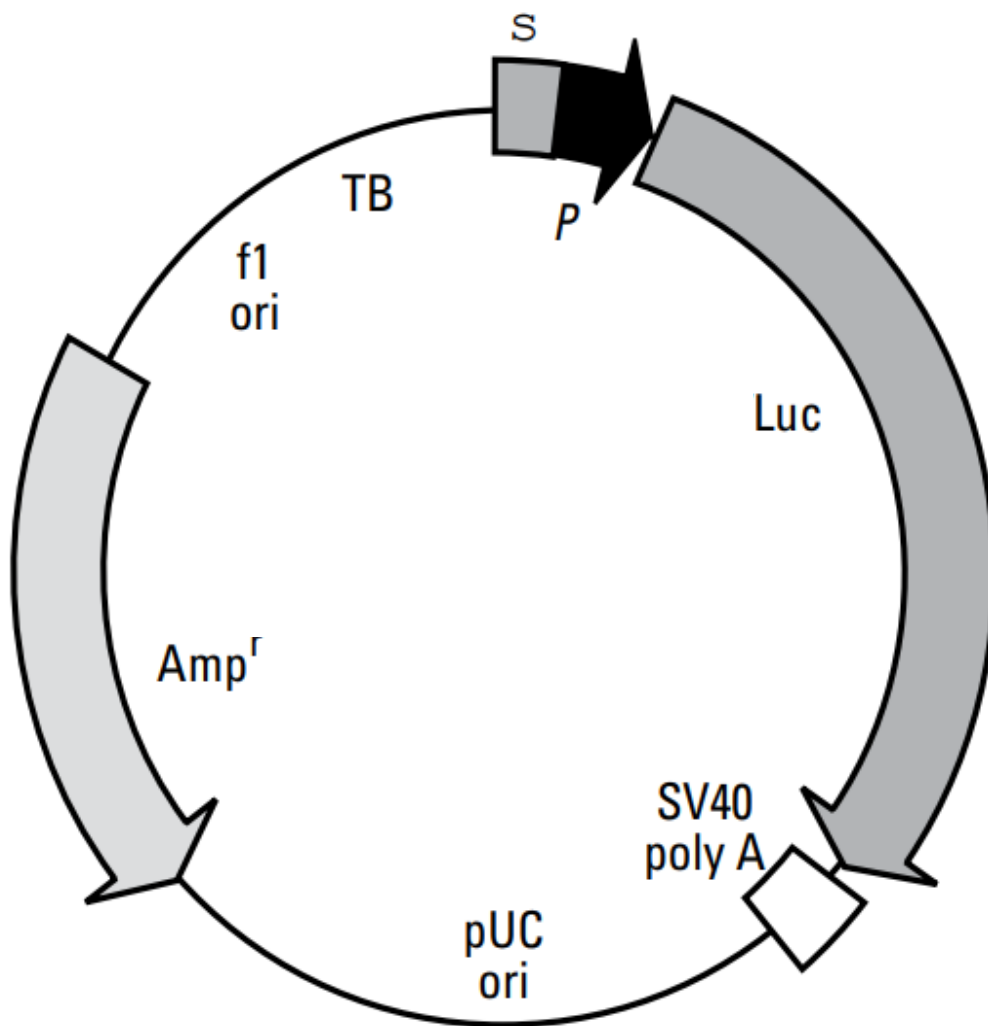


Figure 2.1. Generalised map of vector. The vector contains a TATA-like promoter (pTAL) region from the herpes simplex virus (HSV-TK). The luciferase coding sequence (Luc) is followed by the SV40 late polyadenylation signal to ensure efficient processing of luciferase transcript. The *cis*-acting response elements are located upstream from the pTAL region. The transcription blocker (TB) serves to reduce background transcription.

2.1.2.2 Transfection

Cells were seeded in 24-well plates at 2×10^4 KGN cells or 1×10^5 COV434 cells per well, maintained in 500 μ l of respective media. Approximately 4 hours after seeding, cells were checked to ensure adhesion to the wells. Cells were then washed once with PBS, and maintained overnight in 500 μ l of serum-free DMEM:F12 or DMEM to synchronise the cells.

From day two onwards, cells were maintained in respective media with 2% charcoal-stripped FBS, unless otherwise stated. The two cell lines were transfected with different transfection reagents, with conditions optimised previously by our laboratory (Chu et al., 2004), for optimal transfection efficiency and minimal toxicity. Cells were transfected with pTAL-luc or other plasmid reporters. All reagents were warmed to room temperature and vortexed gently before use.

For KGN, the transfection reagent used was SuperFect (Qiagen). The master mix of transfection reagent-DNA complexes (or transfection mixture, in brief) contained 42 μ l of opti-MEM (Invitrogen), 0.5 μ g of plasmid reporter and 1.26 μ l of SuperFect, for each well. The transfection mixture was spun and vortexed briefly, incubated at room temperature for 5-10 minutes. 128 μ l of DMEM:F12 per well was calculated and added to the transfection mixture. Of this master mix, 170 μ l was added into each well.

For COV434, the transfection reagent used was Trans IT-LT1 (Mirus Bio LLC, Madison, WI, U.S.A.). The transfection mixture contained 52 μ l of opti-MEM, 1.58 μ l of Trans IT-LT1 and 1 μ g of plasmid reporter for each well. The transfection mixture was spun and vortexed briefly, incubated at room temperature for 15-30 minutes. In

each well, 500 μ l of DMEM was first added, then 54 μ l of the incubated transfection master mix was added drop-wise, with gentle swirling of the plate.

Both cell lines were incubated for 4 hours in 37°C humidified incubator. 400 μ l of DMEM:F12 was added to KGN cells and incubated overnight. COV434 were washed once with PBS and maintained in DMEM overnight.

On day three, the cells were washed twice with PBS prior to the drug treatment. All drugs were diluted at desired concentration in DMEM:F12 or DMEM; 500 μ l was added to each well. The cell lines were treated for 24 hours with specific drug treatment regime outlined in the respective study.

2.1.2.3 Luciferase assay

The luciferase reporter assay was conducted using the Luciferase Reporter Assay System (Promega, Madison, WI, USA), according to the manufacturer's instructions. Briefly, 5X passive lysis buffer was diluted with Milli-Q H₂O (dH₂O) to make up 1X lysis buffer. The cells were washed with 500 μ l of PBS and 50 μ l of 1X lysis buffer was added to each well. The bottom of the wells was gently scraped to collect the cell lysate; 20 μ l was transferred to an opaque 96-well plate. 50 μ l of luciferase assay substrate was added. Light emission was measured using the EnVision® Multilabel Reader (PerkinElmer Inc).

2.2 Gene expression analysis

2.2.1 RNA extraction

The cell lines were cultured to 90% confluency and approximately 1×10^6 cells were seeded in triplicates in a 6-well plate. RNA was isolated using the RNeasy® mini kit (Qiagen, Hilden, Germany), according to the manufacturer's instructions. Briefly, cell lysis was performed by adding 350 μ l of lysis buffer (buffer RLT, with 10 μ l of β -mercaptoethanol per ml) to pool triplicate wells. Each sample was homogenised for 30 seconds at 50 oscillation/second using a bead in a TissueLyser (Qiagen). Next, 350 μ l of 70% ethanol was added directly to the homogenised lysate to enhance RNA binding to the silica membrane. For RNA binding, a collection tube with a spin column was prepared; the lysate was pipetted up and down 2 to 3 times then loaded onto the spin column. The lysate was centrifuged for 15 seconds at 13,000 rpm. The flow-through was discarded. 350 μ l of wash buffer (buffer RW1) was added to the spin column, followed by centrifugation for 15 seconds at 13,000 rpm. On column DNase treatment was performed after this step using the RNase-free DNase set (Qiagen). 10 μ l of DNase I stock solution was added to 70 μ l of a RNase-free buffer (buffer RDD); 80 μ l of this DNase I mix was added to each sample and incubated at room temperature for 15 minutes. At the end of the incubation, 350 μ l of wash buffer (buffer RW1) was added to the spin column to remove the DNase I, followed by centrifugation for 15 seconds at 13,000 rpm. 500 μ l of a second wash buffer (buffer RPE) was added to the spin column twice, followed by centrifugation at 13,000 rpm for 15 seconds and then 2 minutes to remove residual ethanol. After each RPE wash the flow-through was discarded, and the spin column was returned to the collection

tube. After the last wash, the spin column was placed in a new collection tube. RNA was eluted by 30 μ l of RNase-free water and centrifuged at 13,000 rpm for 1 minute. RNA was quantified and purity assessed with the NanoDrop Spectrophotometer (Thermo Fisher Scientific, Waltham, MA, U.S.A.) as stated in section 2.1.2. RNA was kept at -80°C until further use.

2.2.2 DNA/RNA Quantification

A NanoDrop Spectrophotometer (Thermo Fisher Scientific) was used to measure DNA or RNA concentration. In brief, 1.5 μ l of each sample was assessed by spectrophotometry and the absorbance was measured using 260 nm and 280 nm wavelengths. RNA purity is assessed by the ratio of sample absorbance at 260 and 280 nm; a ratio of >1.9 is taken as high purity. The NanoDrop was also used when making up primer stocks. Primers (in powder) were reconstituted with nuclease-free water as indicated in the manufacturer's datasheet, the concentration was calculated using the following formula:

$$\text{Concentration in } \mu\text{M} = A_{260} \times \text{Weight per OD} / 1 \text{ mM (molecular weight in g/L)}$$

Once the stock concentration was determined, primers are diluted to a 10 μ M working solution.

2.2.3 Reverse-transcription PCR

A reverse-transcription PCR (RT-PCR) was performed to enable determination of mRNA expression levels of genes of interest. RNA was extracted from the GCT-derived cell lines and stored at -80°C. cDNA was synthesised from total RNA using SuperScript® III First-Strand Synthesis System (Invitrogen) for RT-PCR. According

to manufacturer's protocol, a reaction mixture containing 1 µg of RNA, 1 µl of random hexamer, 1 µl of 10 mM dNTP was made up to a total volume of 10 µl with nuclease-free H₂O. The reaction mixture was incubated at 65°C for 5 minutes. For each sample, the following were added prior to a PCR for cDNA amplification: 2 µl of 10X RT buffer, 4 µl of 25 mM MgCl₂, 2 µl of 0.1M DTT, 1 µl of RNase Out (40 U/µl) and 1 µl of Superscript® III RT (200 U/µl). The PCR conditions were as follow: 25°C for 10 minutes, 50°C for 50 minutes, 85°C for 5 minutes. Following the PCR reaction, 1 µl of RNase H was into each sample and incubated for 20 minutes at 37°C.

2.2.4 Gene amplification and sequencing

The PCR reaction contained 12.5 µl of GoTaq® Green Master Mix (Taq DNA polymerase, MgCl₂, dNTPs and reaction buffers) (Promega, Madison, WI, USA), 1 µl of cDNA, 0.5 µl of 10 mM gene-specific primers and nuclease-free H₂O to make up a total volume of 25 µl. The PCR conditions were as follow: 95°C for 5 minutes, 1 cycle; 95°C for 30 seconds, primer-specific annealing temperature for 30 seconds and 72°C for 40 seconds, 30 cycles; followed by a final extension at 72°C for 7 minutes. PCR products were examined on a SYBR® Safe-stained (Invitrogen) 1.5% agarose gel using gel electrophoresis.

The isolated DNA samples were submitted to the Gandel Sequencing Trust Sequencing Facility (Monash Health Translational Precinct, Clayton, Victoria) for Sanger sequencing. The sequence data were then aligned against the sequence of the specific gene using the 'human genomic plus transcript' database on the NCBI (National Center for Biotechnology Information) BLAST website.

2.3 Protein expression analysis

The expression of the proteins of interest was visualised using immunohistochemistry or determined by obtaining protein from the GCT-derived cell lines. Both approaches are outlined below.

2.3.1 Tissue processing

Mouse tissues were obtained for the immunohistochemical analyses presented in Chapter 3. Female mice were culled at 9-weeks (XIAP^{-/-}) and 19-weeks of age (control) when the ovaries were collected. Kidneys were collected from 8-week old male mice.

Mouse tissues were fixed with 4% paraformaldehyde overnight before washing in PBS (3 times, 30 minutes each). Tissues were dehydrated with 30% and 70% ethanol for 2 hours each, and kept in 70% ethanol. Tissues were then processed using Medite Tissue Processor, the processing parameters were as follow: 70% and 90% ethanol (2 hours each), 100% ethanol (3 times, 2 hours each), histosol (3 times, 2 hours each) and paraffin at 60°C (twice, 2 hours each).

4 µm sections were cut from the paraffin blocks using a microtome, floated on warm water and picked up on Menzel-Glä ser Superfrost® Plus slides (Lomb Scientific, Thermo Fisher Scientific, Waltham, MA, U.S.A.). The slides were air-dried on a rack.

2.3.2 Immunohistochemistry

Prior to staining, the sections were oven-baked at 60°C for an hour. Sections were dewaxed in histolene (twice, 10 minutes each), rehydrated in 100% and 70% ethanol

(twice, 2 minutes each) and dH₂O (2 minutes). Antigens were retrieved by boiling the slides in a microwave at high power in sodium citrate (10 mM trisodium citrate (dehydrate) in dH₂O) for 2 minutes, then at medium-low for 6 minutes. The slides were cooled down under running tap water for 10 minutes, followed by two 5 minute-washes in TN buffer (10 mM Tris-Cl and 15 mM NaCl in dH₂O). Endogenous peroxidase was quenched by 3% hydrogen peroxide (H₂O₂) made up with TN buffer. The washed slides were slightly dried with paper towel and the cut sections were circled; slides were placed on a "humidified" chamber, with water added underneath the chamber rack. 50-100 µl of 3% H₂O₂ was added onto the marked tissue sections and allowed to incubate at room temperature for 30 minutes. After two washes with TN buffer (5 minutes each), 50-100 µl of avidin and biotin (3 drops of avidin or biotin per 1 ml of TN buffer; Vector Laboratories, Burlingame, CA, U.S.A.), were added onto the marked sections; 15-minute incubation was allowed for each of avidin and biotin, with quick rinse in TN buffer in between. 10% goat serum (Sigma Aldrich, St. Louis, MO, USA) was made up in 3% bovine serum albumin (BSA; Roche Applied Science, Penzberg, Germany). Washed slides were tap-dried and placed in the humidified chamber. 50-100 µl of 10% goat serum was added onto the marked sections, incubated for 60 minutes at room temperature. Primary antibodies were diluted at desired concentration in 3% BSA. After a quick wash of slides in TN buffer, the marked sections were covered with antibody dilution and incubated in the humidified chamber at 4°C overnight.

On day two, all washes were performed on a shaker at 72 rpm. The incubated slides were washed with TNT buffer (1 ml of Tween 20 per 1 L of TN buffer; three times, 10 minutes each). 1:200 of the appropriate secondary antibody was made up in TN

buffer, added to sections and incubated in humidified chamber for 60 minutes at room temperature. Vectastain® Avidin-biotinylated enzyme complex (ABC; Vector Laboratories) was made up 30 minutes prior to application (15 µl of solution A and B per 1 ml of TN buffer). The ABC reagent was left on the slides for 45 minutes at room temperature. Following each application of secondary antibody and ABC vector, slides were washed with TNT buffer (twice, 10 minutes each). Using the DAB kit, 50-100 µl of DAB chromagen solution (1 drop of DAB per 1 ml of buffer; Dako, Agilent Technologies, Santa Clara, CA, USA) was added onto marked sections. Colour development (brown) was observed under microscope within 3 minutes; the reaction was stopped by dipping the slide into dH₂O. Slides were immersed into Harris haemotoxylin (diluted 1:2 with tap water; Sigma Aldrich) for 1 minute 10 seconds, then left under tap water for 5 minutes. To dehydrate, the slides were immersed in 70% ethanol (twice, 2 minutes each), 100% ethanol (twice, 2 minutes each) and histolene (twice, 10 minutes each). A cover slip was mounted on the slides with DPX mounting medium.

2.3.3 Preparation of whole cell lysates

Lysis buffer was prepared by dissolving one protease inhibitor cocktail tablet (Roche Applied Science) in 10 ml of Universal Immunoprecipitation (UIP) buffer (50 mM Tris-Cl, 150 mM NaCl, 2 mM EDTA, 2 mM EGTA, 25 mM NaF, 0.2% (v/v) Triton X-100, 0.3% (v/v) Nonidet P-40 and 25 mM β-glycerolphosphate in dH₂O). 75 µl of the lysis buffer was added into each well of a 6-well plate. After 10 minute-incubation at room temperature, the plate was gently tapped to ensure complete dissociation of the cells. The cell lysates for each duplicate well were pooled, and stored at -80°C until further analyses using BCA and western blot.

2.3.4 Protein quantification

Total protein quantification was performed by utilising the Pierce® BCA Protein Assay Kit (Thermo Fisher Scientific). The preparation of albumin (BSA) standards was performed prior as per manufacturer's protocol. 25 µl of each BSA standard was loaded onto a 96-well reading plate in duplicate. Protein samples were diluted 1:10 in PBS then 25 µl of each sample was added to the plate in duplicate. The BCA working reagent was prepared by mixing 50 parts of BCA Reagent A with 1 part of Reagent B. 200 µl of this working reagent was added to each of the samples/standards. The solutions were mixed thoroughly on a shaker at 72 rpm for 30 seconds. The plate was covered and incubated at 37°C for 30 minutes. Absorbance at 560 nm was measured using the EnVision® Multilabel Reader (PerkinElmer Inc., Waltham, MA, U.S.A.).

2.3.5 Western blot

2.3.5.1 Sodium dodecyl sulfate polyacrylamide gel electrophoresis (SDS-PAGE)

SDS-PAGE gel was used to separate proteins: 10% resolving gel (1.4 ml of dH₂O, 3.3 ml of 30% Bis/acrylamide mix, 2.5 ml of 1.5 M Tris-HCl (pH 8.8), 100 µl of 10% SDS, 100 µl of 10% ammonium sulfate, 4 µl of TEMED) and 5% stacking gel (2.1 ml of dH₂O, 495 µl of 30% Bis/acrylamide mix, 375 µl of 1 M Tris-HCl (pH 6.6), 30 µl of 10% SDS, 30 µl of 10% ammonium sulfate, 4 µl of TEMED). Using a pipette, the resolving gel solution was poured carefully between the glass plates. dH₂O was added to cover the top of the resolving gel, which was then allowed to polymerise for

30 minutes. When the resolving gel had set, the water was tipped off. The stacking gel solution was poured then the comb was inserted; allowed to set for 30 minutes.

The SDS-PAGE gel was placed into an electrophoresis tank containing 1X western running buffer (25 mM Tris-Cl, 192 mM glycine and 0.1% (w/v) SDS in dH₂O). For each sample, 50 µg of total protein was mixed with loading dye (0.5 M Tris-HCl (pH 8.8), 10% (v/v) glycerol, 10% (w/v) SDS, 0.5% w/v bromophenol blue in dH₂O) containing 5% beta-mercaptoethanol, prior to heating at 95°C for 5 minutes. A pre-stained Precision Plus Protein Standards (~10-180 kDa; Bio-Rad, Hercules, CI, USA) was used to identify the correct size of the desired protein. Proteins were separated by electrophoresis using the Protean Gel System (Bio-Rad) at 120V and 50 mA for 1.5 hours.

2.3.5.2 Protein transfer

Amersham Hybond™-P PDVF membranes (GE Healthcare Life Sciences, Chicago, IL, U.S.A.) were pre-soaked in methanol. PDVF membranes, blotting paper and gels were immersed in transfer buffer (25 mM Tris-Cl, 192 mM glycine and 20% (v/v) methanol in dH₂O) for five minutes to prepare for protein transfer. The proteins were transferred out of the gel to a PDVF membrane using the Bio-Rad Mini Trans-Blot electrophoretic transfer system at 30V at 4°C overnight or 120V at room temperature for 1.5 hours.

In the following procedures, all washes were performed at room temperature with gentle rocking. The membrane was blocked with 5% BSA in TBS (137 mM NaCl, 2.7 mM KCl, 25 mM Tris in dH₂O; pH 7.4) for 1 hour at room temperature with gentle

rocking. Primary antibody was diluted in 1% BSA in TBS and incubated overnight with gentle rocking.

Following primary antibody incubation, the membranes were washed with TBS 4 times for 15 minutes each. The secondary antibody was diluted in TBS; membranes were incubated for 2 hours at room temperature with gentle rocking. Following the incubation period, the membrane was washed with TBST (1 ml of Tween-20 in 1 L of TBS; 4 times, 10 minutes each). The membrane was blotted dry after the last wash to ensure all traces of TBST were removed. 4 ml of ECL Plus Western Blotting Detection System (GE Healthcare) was freshly prepared as per manufacturer's instructions, and added ensuring the entire membrane was covered. The membrane was imaged using the Bio-Rad ChemiDoc™ XRS+ System.

2.3.5.3 Antibody Stripping

1X Reblot Plus-Strong antibody stripping solution (Merck Millipore, Kenilworth, NJ, U.S.A.) was made up using dH₂O (1:10 dilution). The membrane was first incubated in 1X stripping solution for 20 minutes, followed by washing with TBST (three times, 15 minutes each). The membrane was then re-probed with an antibody to β -actin as an internal loading control.

CHAPTER 3

***PPAR γ ACTIVATION AUGMENTS ANTICANCER EFFECTS
OF XIAP INHIBITION IN GRANULOSA CELL TUMORS OF
THE OVARY (publication)***

PPAR γ activation augments anticancer effects of XIAP inhibition in granulosa cell tumors of the ovary

Dilys TH Leung¹, Trang Nguyen¹, Edwina Oliver¹, Juliana Matti¹, Maria Alexiadis¹, John Silke², Peter Fuller¹ and Simon Chu¹

¹Hudson Institute of Medical Research and Monash University Department of Molecular and Translational Science, Clayton, Victoria 3168, Australia

²Walter and Eliza Hall Institute, Parkville, Victoria 3052, Australia

Running title: Anticancer effects of PPAR γ activation and XIAP inhibition

Keywords: granulosa cell tumors, PPAR γ , X-linked inhibitor of apoptosis

Financial support

This work was supported by grants-in-aid from the Cancer Council Victoria; the Ovarian Cancer Research Foundation (SC); the Granulosa Cell Tumour of the Ovary Foundation; and the National Health & Medical Research Council of Australia through a Project Grant (grant number #1058334, 2014-2016) and a Senior Principal Research Fellowship to PJF (grant number #1002559, since 2001; Endocrine Society of Australia Research Higher Degree Scholarship to DL. The Hudson Institute is supported by the Victorian Government's Operational Infrastructure Scheme.

Corresponding author: Dr Simon Chu

Hudson Institute of Medical Research

██
██
██
██

Declaration of interest

The authors declare no conflict of interest.

Abstract

Ovarian granulosa cell tumors (GCT) are characterized by a FOXL2 mutation and exhibit an indolent growth and late relapse. No therapeutic modalities aside from surgical debulking at initial diagnosis have been proven effective. We previously reported the paradoxical overexpression of the anti-proliferative nuclear receptor, peroxisome proliferator-activated receptor-gamma (PPAR γ) and constitutive activity of the NF- κ B and AP-1 signaling pathways. PPAR γ is a transcription factor that impedes proliferation and promotes terminal differentiation and may present a potential therapeutic target. Overexpression of PPAR γ in GCT suggests resistance to the actions of PPAR γ , these studies show that in GCT-derived cells (KGN and COV434), this is caused by NF- κ B transrepression. Abrogation of NF- κ B signaling in GCT cells enables PPAR γ agonists to initiate apoptosis. Additionally, we identified overexpression of an effector protein of NF- κ B, X-linked inhibitor of apoptosis protein (XIAP), in GCT and GCT-derived cell lines. XIAP has emerged as an attractive therapeutic target by virtue of its role in inhibiting key portions of the apoptotic pathway and also its regulatory role of the NF- κ B signaling pathway. We thus aim to investigate the anti-tumor effects of combined XIAP inhibition using Smac-mimetics and PPAR γ activation using thiazolidinediones in the GCT-derived cells. Transactivation assays revealed that NF- κ B transrepresses PPAR γ in GCT-derived cells and can be relieved by NF- κ B or XIAP inhibition. The combined XIAP inhibition and PPAR γ activation sensitizes the KGN cells and COV434 cells to PPAR γ -mediated apoptosis. KGN in 3D culture and GCT explant models both demonstrated significant reduction in cell viability and proliferation, and significant induction of apoptosis following the combination treatment. Real-time monitoring of cell invasion showed that the Smac-

mimetic and thiazolidinediones co-treatment delayed onset of invasion by 8 hours and ceased proliferation of the invaded KGN cells. The combined treatment also upregulated pro-apoptotic genes and compromised cellular energetics in the KGN cells. This study provides supportive data that the combined PPAR γ and XIAP treatment has anti-neoplastic effects in GCT. The overexpression of PPAR γ and XIAP in GCT and other malignancies warrant further investigation of this approach as cancer therapeutics.

Introduction

Granulosa cell tumors (GCT) which comprise the majority of ovarian stromal tumors, arise from proliferating granulosa cells of the ovarian follicle, and represent a specific subset of malignant ovarian tumors (1). They frequently present with endocrine manifestations such as estrogenization in prepubertal girls and postmenopausal women. GCT exhibit many features of normal ovarian GC (1), including expression of the follicle stimulating hormone (FSH) receptor gene, estrogen synthesis, ER β expression, inhibin subunit expression with synthesis of biologically active inhibin, and anti-Müllerian hormone (AMH) expression. Adult GCT are defined by the presence of the FOXL2 C134W mutation. GCT are unusual in that they exhibit an indolent course, and have an unexplained propensity for late recurrence. ~80% of patients with aggressive or recurrent tumors die from their disease (1). At present there are no reliable methods for predicting relapse and, aside from surgery, no therapeutic modalities have proven effective (1).

Nuclear receptors play a central pathogenic role in several endocrine malignancies and as such represent established therapeutic targets. We have previously shown that a member of the nuclear receptor superfamily, peroxisome proliferator-activated receptor-gamma (PPAR γ) is highly expressed in GCT (2), and thus presents a potential therapeutic target. PPAR γ has been implicated in the pathology of numerous diseases including obesity and diabetes. PPAR γ binds to DNA at specific sites as obligate functional heterodimers with RXR α which we also have shown to be expressed in GCT (2). The potential of PPAR γ agonists as anticancer agents has attracted considerable interest, including the treatment of endocrine malignancies such as thyroid cancer (3).

The role of the NF- κ B family of proteins in immune, inflammatory and anti-apoptotic responses is well documented (4,5). NF- κ B and the signaling pathways that are involved in its activation are also important for tumor development; activated NF- κ B increases the expression of genes involved in cell proliferation, metastasis, and anti-apoptosis (6,7). In GCT, we have previously demonstrated that many nuclear receptors are transrepressed by constitutive activity of the critical pro-survival NF- κ B signaling pathway (8).

Apoptosis is directed by activated caspases. The Inhibitors of Apoptosis Proteins (IAP) suppress apoptosis through the inhibition of the caspases. IAP are defined by the presence of the baculovirus IAP repeat (BIR) domains. Of the eight human IAP identified, the X-linked Inhibitor of Apoptosis Protein (XIAP) is the best characterized and also the most potent caspase inhibitor, blocking both intrinsic and extrinsic apoptotic signals by directly inhibiting caspases-3, -7 and -9 (9). XIAP has three BIR domains, and a RING finger domain conferring E3-ubiquitin ligase activity (9). The BIR2 and BIR3 domains are responsible for caspase inhibition (9). XIAP is predominantly regulated by the mitochondrial protein, Second mitochondria-derived activator of caspases (Smac) (9). Released Smac interacts with XIAP through conserved amino acid residues in the BIR3 domain of XIAP and eliminates the inhibitory effect of XIAP on caspase activation (9).

Constitutive NF- κ B signaling can be a consequence of a positive feed-forward loop involving XIAP (10). Due to its prominent ability to control cell death and elevated expression in several human cancers (11-13), XIAP has been an attractive therapeutic target for novel anti-cancer treatment (11-13).

Small-molecule inhibitors of XIAP are in various stages of development, from preclinical to phase II clinical trials (11-13). Smac-mimetics are drugs designed to

mimic the inhibitory Smac and bind directly to XIAP with high affinity to neutralize the pro-oncogenic functions of this protein, by preventing caspase binding. Various Smac-mimetics have been designed which monovalently inhibit either the BIR2 or BIR3 functional domains, or both domains as bivalent mimetics (11-13). A number of these compounds have demonstrated good anti-cancer activity in preclinical studies, and several have already passed primary phase clinical trials, suggesting that these compounds are well tolerated (11-13).

In this study, we investigated the effects of PPAR γ agonists on GCT-derived cells *in vitro*, and determined that when used in combination with inhibiting XIAP using Smac-mimetics causes a release of NF- κ B transrepression, resulting in induction of apoptosis in GCT-derived cells.

Material and Methods

Patients and Tissue Acquisition and Tissue Microarray (TMA)

For the expression studies, we have utilized the previously characterized ovarian GCT samples (n=14) collected sequentially at our institution (14). Normal ovarian tissue was obtained from eight premenopausal women who had undergone elective hysterectomy with oophorectomy for a range of conditions not associated with ovarian malignancy. TMAs were provided as a gift from Professor Colin Stewart (University of WA). The GCT samples used in this study have been verified to possess the C134W mutation in the *FOXL2* gene, that is characteristic of the adult GCT phenotype (14). The study protocol was approved by the Research and Ethics Committee of Monash Medical Centre, and all women gave written informed consent for the studies.

Cell Lines

Cell lines used in these studies: granulosa cell carcinoma, COV434 and KGN (15,16), and normal non-luteinized granulosa cells, hGrC1 (17). The cells were maintained in DMEM (COV434 and hGrC1) or DMEM/F12 (KGN) supplemented with 10% FCS at 37°C in a 95% air/5% CO₂ humidified incubator.

Chemicals and Antibodies

Troglitazone (TGZ) and rosiglitazone (RGZ) were purchased from Sigma-Aldrich. Chemical inhibitors used were: BAY11-7082 (BAY; Sigma-Aldrich); GW9952 (GW; Sigma-Aldrich); PD-98059 (PD; Sigma-Aldrich); XIAP inhibitors used in these studies were embelin (2,5-dihydroxy-3-undecyl-1,4-benzoquinone; Emb) (Sigma-Aldrich), a cell-permeable inhibitor of XIAP which binds to the BIR3 domain of XIAP; Compound A (18) (bivalent Smac-mimetic; CmpdA) (gift from Professor John Silke, WEHI); AZD5582 (monovalent Smac-mimetic; AZD) (Tocris). PPAR γ agonists: TGZ and RGZ. PPAR γ antagonist: GW. RXR α agonist: 9-cis-retinoic acid (RA). NF- κ B inhibitor: BAY. High Content Screening dyes: Hoechst 33342; YoPro-1; ToPro-3 (Life Technologies). The following antibodies were used for these studies: PPAR γ (ab27649; Abcam, Cambridge, UK); XIAP (PRS3331; Sigma-Aldrich), cIAP-1 (ab2399; Abcam) and cIAP2 (sc-7944; Santa-Cruz, Dallas, TX, USA).

xCELLigence Assay

Cell proliferation was assessed in a real-time, non-invasive, and label-free manner using the xCELLigence Real-Time Cell Analyzer (RTCA) (Acea Biosciences), measuring the electrical resistance of cells that adhere to electrodes on the surface of the wells in an E-plate 96. Proliferation was assessed as per the manufacturer's instructions. Briefly, after a background reading of cell-free 2% charcoal-stripped serum DMEM/F12 was measured, 10,000 KGN cells were seeded in each well of an

E-plate 96 in a total volume of 100 μ l of 2% charcoal-stripped serum media. Proliferation was then measured using the xCELLigence RTCA DP apparatus in a 37°C incubator, cell index was measured every 2-15 minutes for 120 hours. Each condition was performed in triplicate.

Relative cell proliferation is measured as the final cell index values show the difference between the resistance generated by the cells in each time point and the resistance of the medium without cells.

The xCELLigence RTCA system was also utilized to assess invasion of the KGN cells. Electrical current passes through the electrodes on the bottom of the upper chamber of the cell culture plate (CEM-16). As cells seeded in the upper chamber invaded across a layer of Matrigel® into the lower chamber, which contains 10% FCS as chemoattractant, they attach onto the electrodes and electrode resistances increase. The electrode resistance is indicative of cell invasion and is represented by cell index. The maximum cell indices across a 72-hour period which is indicative of number of cells invaded, were compared between the control and treatment groups.

High Content Screening Apoptosis Assays

Cells were grown in 24-well plates and incubated either DMSO (0.1%), embelin (25 μ M), CmpdA (500nM), BAY (2 μ M), TGZ/RA (20 μ M/5 μ M), TGZ/RA in the presence of BAY, TGZ/RA in the presence of Emb or CmpdA, RGZ/RA (20 μ M/5 μ M), RGZ/RA in the presence of BAY, or TGZ/RA in the presence of Emb or CmpdA for 24 hours. Media containing Hoechst 33342 dye, YoPro-1 dye (to detect early apoptosis) and ToPro-3 dye (to detect late apoptosis or necrosis) was added to the cells before imaging and analysis on a Cellomics Arrayscan VTI High Content Screening Reader.

Reverse Transcription and Real Time RT-PCR

The comparative Ct ($\Delta\Delta C_t$) method was used to validate XIAP expression. FAM labeled TaqMan Gene Expression assays for XIAP, TNFRSF1B, BIRC3 and TGM2 were purchased along with a FAM labeled RPLP0 probe which was used as an endogenous control. A 10 μ l reaction was prepared with 1X TaqMan universal PCR master mix (Applied Biosystems, Foster City, CA) and diluted cDNA. All PCR reactions were carried out in triplicate in MicroAmp optical 384-well reaction plates (Applied Biosystems). The cycling parameters were initiated by 2 minutes at 50°C and 10 minutes at 95°C, followed by 40 cycles of 15 seconds at 95°C and 60°C for 1 minute using the 7900HT fast real-time PCR system (Applied Biosystems).

TaqMan Low-Density Array

Commercial micro-fluidic cards, the TLDA (Applied Biosystems, catalogue no. 4378701), that contain an exclusive set of TaqMan gene expression assays for 93 apoptosis genes and 3 internal controls (eukaryotic 18S rRNA (18S), glyceraldehyde-3-phosphate dehydrogenase (GAPDH), beta-actin (ACTB)) were used to profile gene expression. These controls span the relative abundance/Cl range of the genes on the card. The geNorm software imbedded within the ABI/Intergromics StatMiner V4.1 software package was used to compute least expression variation and select the most appropriate, stable, and robust combination of internal control genes with which to normalize the expression data (against the mean of the most stable controls).

For each sample, 1.5 μ g of total RNA was reverse-transcribed using random hexamers with SuperScript III reverse transcriptase (Invitrogen) in a total volume of 45 μ l. A total of 100 μ l reaction mixture containing 50 μ l cDNA template (333ng) in RNase-free water and an equal volume of TaqMan[®] universal master mix (Applied Biosystems) was added to each TLDA fill reservoir. Each GCT sample was run once while the cell lines

were run as three biological replicates. Four reservoirs per sample were filled. The TLDA includes all apoptosis genes and endogenous controls in triplicate. After sealing the plate, it was run on an ABI 7900HT Real-Time instrument (Applied Biosystems).

Immunohistochemistry

Frozen GCT were blocked with OCT (optimal cutting temperature) compound and 4 μ m sections were prepared using the cryostat. All incubation and washes were performed at room temperature unless stated otherwise. Frozen GCT sections were fixed in 4% paraformaldehyde for 30 minutes followed by quenching of endogenous peroxidase using 0.3% hydrogen peroxide/PBS for 30 minutes. For membrane permeation, slides were incubated in 0.1% triton X-100/PBS for 10 minutes. Nonspecific binding was blocked by 10% goat serum in 3% BSA for an hour. Incubation with primary antibody, rabbit polyclonal PPAR γ (Abcam; ab27649; 1:350), XIAP (Sigma-Aldrich; PRS3331; 1:200) was performed at 4°C overnight. Goat serum was used as a negative control. After PBS washes, slides were incubated with biotinylated goat anti-rabbit secondary antibody (Dako; 1:200) for an hour. VECTORSTAIN® avidin/biotinylated enzyme complex was made up as per manufacturer's instructions, added to sections and incubated for an hour. Staining was visualized by incubation of DAB solution (Dako) for 3 minutes. Sections were counterstained with hematoxylin, dehydrated with ethanol (70% and 100%) and mounted with DPX.

Transactivation Assays

The KGN cells were transfected using Superfect reagent (Qiagen, Valencia, CA), according to the manufacturer's instructions. The reporter constructs, NF κ B₄-luc or AP1₃-luc, were transfected at 1 μ g/well in the KGN cells. Following transfection, cells were treated for 24 hours with 0.1% DMSO as vehicle control, CmpdA (500nM), BAY (5 μ M) or PD (20 μ M) to inhibit either NF- κ B or AP-1.

Seahorse

Cellular energetics of the KGN cells was assessed using the mito-stress kit paired with the Seahorse Extracellular Flux XFp Analyzer according to manufacturer's protocol. Briefly, the sensor cartridge was hydrated with calibrant overnight prior to cell seeding. 10,000 KGN cells in 80 μ l of DMEM/F12 were plated in wells B to G; wells A and H are background correction wells with media only. Moats around the wells were hydrated with PBS and incubated overnight. Treatment was performed in duplicate with 0.1% DMSO, RGZ/RA (20 μ M/5 μ M) or RGZ/RA/CmpdA (20 μ M/5 μ M/500nM). Following 24-hour treatment, cells were washed twice with the XFp base medium (1mM pyruvate, 2mM glutamine and 10mM glucose; adjusted to pH 7.4; filter-sterilized). The plate was de-gassed for an hour in a non-CO₂, humidified, 37°C incubator for 60 minutes. Stressors were prepared with the supplemented XFp base medium as previously optimized – oligomycin at 1 μ M, FCCP at 2 μ M, antimycin A/rotenone at 0.5 μ M in the well. Stressors were loaded into the sensor cartridge and calibration of the plate was initiated in the analyzer. At the end of the calibration and de-gassing of the miniplate, the miniplate was loaded onto the analyzer to commence the mito-stress assay. Pierce BCA protein assay (ThermoFisher Scientific) was performed at the end of the assay for normalization. Data analysis was performed with the analyzer's Wave software.

Spheroids

To generate spheroids, 3,000 KGN cells were seeded in DMEM/F12 with 20% methylcellulose, no additives or serum. Spheroids formed within 24-72 hours post seeding. Treatments were performed in quadruplicate, once spheroids were formed, and replenished every 3 days in 2% charcoal-stripped serum-containing DMEM/F12. Spheroids were treated in with 0.1% DMSO, RGZ/RA (20 μ M/5 μ M) or RGZ/RA/CmpdA (20 μ M/5 μ M/500nM). Cell viability was assessed at the end of the treatment using

resazurin (Sigma-Aldrich). 1% resazurin in Milli-Q water was further diluted to 0.005% in 2% charcoal-stripped FCS-containing DMEM/F12 prior to use. 150 μ l of the resazurin solution was added to each and incubated for an hour. Fluorescence signal was measured using excitation at 560nm and emission at 595nm.

Primary GCT culture

Two GCT were sequentially collected following surgery and maintained in DMEM/F12 until processing. The tumor was sliced into 6 equal-sized pieces, which were then halved and minced into approximately 1mm³. The primary GCT was plated in a 6-well plate and then treated with 0.1% DMSO, RGZ/RA (20 μ M/5 μ M) or RGZ/RA/CmpdA (20 μ M/5 μ M/500nM) in 10% serum-containing DMEM/F12 for 24 hours. At the end of the treatment, the explant culture was pooled to extract RNA or blocked with OCT compound for further analysis.

Statistics

Drug treatments for all experiments were performed in duplicates and repeated at least three times. Data are presented as mean \pm SD. Student t-test, One-way ANOVA or the non-parametric equivalent, Kruskal-Wallis test was used for statistical analyses where $p < 0.05$ is considered statistically significant.

Results

Expression of XIAP and PPAR γ in GCT and GCT-derived Cell Lines

We have previously described *PPAR γ* mRNA overexpression in GCT and the GCT-derived cell lines (2). In this study, *XIAP* expression was assessed using quantitative RT-PCR (Figure 1A); XIAP and PPAR γ protein expression was determined using immunohistochemistry (IHC) (Figure 1B). The GCT samples for RT-PCR analysis were obtained as previously described (2,14,19,20), their clinical details have also

been previously described (19). All cases were heterozygous for the FOXL2 C134W mutation (14). We performed expression profiles for 12 tumors, and also for the KGN and COV434 cell lines. The KGN cell line is heterozygous for the FOXL2 C134W mutation, and thus was derived from an adult GCT (14). The COV434 cell line is wild-type for FOXL2, and thus likely to have been derived from a juvenile GCT (14).

Using quantitative RT-PCR, we observed that XIAP was significantly more highly expressed in the GCT than in whole normal ovary (Figure 1A). The results are presented as a scatterplot; the levels observed in KGN and COV434 cells are also indicated, showing high expression of XIAP in these cell lines (Figure 1A). There was no discrimination of the expression levels for XIAP between stage 1 tumors compared to advanced stage tumors (Supplementary figure 1). The expression of XIAP and PPAR γ was examined at the protein level using IHC (Figure 1B). Tissue microarray analysis revealed that XIAP expression was high in 52/76 (68%) primary tumor samples (Figure 2 and Table 1). For those tumor samples where both primary and recurrent cores were available, we observed that the level of expression for XIAP did not alter for any of the tumor samples (Table 1). XIAP expression was observed in the granulosa cells of both small follicles and a preovulatory follicle, as well as in the surrounding theca in a normal preovulatory ovarian sample (Figure 2).

We also determined the expression levels of the related members of the IAP family, cIAP1 and cIAP2. We observed very low expression of cIAP-1 in all tissues examined (Figure 2), while no expression of cIAP2 was observed.

Consistent with our previous observation of high expression of PPAR γ at the message level, we observed high expression of PPAR γ in the majority of the GCT cores in the TMA. Moderate to high expression of PPAR γ was observed for 49/76 (64%) of primary GCT (Figure 2 and Table 1), with only 1 tumor showing less expression in a recurrent

tumor compared to the primary tumor (data not shown). Nuclear staining was observed in the granulosa cells of the small follicles and preovulatory follicle in the normal preovulatory ovarian sample (Figure 2), while both nuclear and cytoplasmic staining was observed in the cells of the surrounding stroma. Clinical information of the patient cohort is summarized in Supplementary Table 1. No clinical data was available to correlate expression with progression-free survival or overall survival.

NF- κ B causes transrepression of PPAR γ in GC- and GCT-derived cell lines

In KGN cells, activation of PPAR γ and its obligate heterodimeric partner RXR α using the PPAR γ agonist, rosiglitazone (RGZ; 20 μ M), and the RXR α agonist, 9-cis-retinoic acid (RA; 5 μ M), results in a 30% reduction in cell proliferation compared to vehicle that did not reach significance (Supplementary Figure 2A). When cells were transfected with a PPAR γ reporter construct (PPRE $_4$ -luciferase) and treated with RGZ/RA, there was a small but significant activation of the reporter compared to vehicle (Supplementary Figure 2B). However, after 24 hours of RGZ/RA treatment, no significant increase in apoptosis (as assessed by high content screening cytofluorometry) was observed for either KGN or COV434 cells (Supplementary Figure 4C). A sub-lethal dose of the NF- κ B inhibitor, BAY (2 μ M) alone, does not affect cell proliferation (Supplementary Figure 2A), nor does it activate the PPAR γ reporter (Supplementary Figure 2B). When RGZ/RA is combined with BAY we observed that proliferation ceases (Supplementary Figure 2A), with a significant increase in apoptosis (Supplementary Figure 2C and D). This occurs at the receptor level, as this effect is reversed by the PPAR γ antagonist (GW9662 (GW); 20 μ M) (Supplementary Figure 2A). The robust activation of the reporter by RGZ/RA in combination with BAY (Supplementary Figure 2B), demonstrates that NF- κ B transrepresses PPAR γ

signaling. Similar results were observed when another PPAR γ agonist, TGZ, was used in these assays (data not shown).

Inhibiting XIAP decreases NF- κ B and AP-1 transactivation

We have previously reported that the NF- κ B and AP-1 signaling pathways are constitutively activated in KGN and COV434 cells (8). NF- κ B transcriptionally activates the expression of XIAP. There is also a modulatory role for XIAP in NF- κ B activation as a consequence of a positive feed-forward loop. XIAP regulates NF- κ B, through the ubiquitin ligase activity of its RING domain (10). XIAP also activates the NF- κ B and AP-1 signaling pathways via the activation of TGF β -activated kinase 1 (TAK1) (21). We thus sought to determine if inhibiting XIAP could decrease NF- κ B and AP-1 transactivation in the GCT-derived cell lines. When cells were transfected with either an NF- κ B or AP-1 reporter, there was an approximate 6-fold induction of luciferase activity under basal conditions compared with cells transfected with an enhancer-less reporter (pTAL-Luc) (Figure 3). Treating KGN cells with 5 μ M BAY (NF- κ B inhibitor) or 20 μ M PD (ERK/AP-1 inhibitor) suppressed the respective constitutive activity. When we treated KGN cells with the Smac-mimetic, CmpdA (500nM) (18), we observed that the constitutive activity was abrogated for both pathways, indicating that XIAP is regulating both pathways, potentially through the TAK1/TAB1/2/3 complex (Figure 3). A similar result was observed for the COV434 cells line (data not shown).

XIAP inhibition removes NF- κ B transrepression and potently sensitizes KGN cells and COV434 cells to PPAR γ -mediated apoptosis

As inhibition of XIAP using the Smac-mimetic abrogates the constitutive activity of both the NF- κ B and AP-1 signaling pathways, we hypothesized that inhibition of XIAP would remove NF- κ B transrepression of PPAR γ . Using the xCELLigence RTCA to

assess cell proliferation in real-time, we assessed the effect of CmpdA either as a single treatment, or in combination with the PPAR γ agonists. We tested these in the GCT-derived cell lines (KGN and COV434) and a non-luteinized granulosa cell line (hGrC1). When cells were treated with 500nM CmpdA alone, there was no effect on cell proliferation for either the GCT-derived cell lines (Figure 4A and B) or the hGrC1 cells (Figure 4C) over 72 hours. Additionally, inhibiting XIAP on its own also had no effect on PPAR γ transactivation (Figure 4D) or apoptosis (Figure 4E and F). When CmpdA was combined with both 20 μ M RGZ and 5 μ M RA, we observed cessation of cell proliferation in both KGN (Figure 4A) and COV434 (Figure 4B) cells over 72 hours. This was accompanied by robust PPAR γ -mediated transactivation of the reporter construct (Figure 4D) and significant increase in apoptosis (Figure 4E and F) in both cell lines, similar to that seen with combined NF- κ B inhibition and PPAR γ activation (Supplementary Figure 2). Consistent results were observed when a monomeric Smac-mimetic AZD5582 or a small molecule XIAP inhibitor embelin were used in combination with RGZ/RA or indeed with another PPAR γ agonist, TGZ (data not shown).

Combined XIAP inhibition and PPAR γ activation causes disruption to KGN cells grown as 3D spheroids

To determine whether the drug combination would be successful in a 3D setting, we tested the combined XIAP inhibition and PPAR γ activation in a 3D cell culture model for KGN cells. We observed that the combination treatment (RGZ/RA/CmpdA) at the same concentrations used for the 2D monolayer experiments, caused disruption of spheroid architecture from 24-hour treatment (Figure 5A), with gradual but complete spheroid dissociation occurring over 12-day treatment (Figure 5A). We confirmed that

this was due to a significant decrease in cell viability (Figure 5B) as assessed using the resazurin viability assay.

Combined XIAP inhibition and PPAR γ activation causes disruption to primary patient-derived GCT explants

Further, to reinforce that the combination treatment is effective not just for continuous cell lines, we have determined whether the drug combination would be successful for primary GCT samples obtained from surgery and grown in an explant model. As shown in Figure 6A, the combination treatment also causes disruption of the GCT explant after 7-day treatment, with complete disruption and no cell viability (Figure 6 – a representative of 2 GCT explant studies). We also measured the gene expression levels of stearoyl-CoA desaturase-1, which we have previously identified as a PPAR γ -induced gene, and is highly induced after the combination treatment in KGN cells (*Leung DTH et al – concurrent submitted manuscript*). We observed that there was also robust induction of SCD gene expression after the combination treatment in two GCT explant samples (Figure 6B), indicating that PPAR γ is being activated by the combined treatment.

Combined XIAP inhibition and PPAR γ activation causes delayed onset of invasion

A major problem for ovarian cancer patients is that cancer cells inherently aggregate into multicellular structures, contributing to the metastatic process by attaching to and invading the peritoneal lining to form secondary tumors. In order to determine whether combined inhibition of XIAP and PPAR γ activation can prevent the metastatic process, we employed the xCELLigence RTCA system to investigate invasiveness of the KGN cells after treatment with either vehicle or with RGZ/RA/CmpdA. We observed that

RGZ/RA/CmpdA-treated KGN cells were 30% less invasive than vehicle treated cells (Figure 7A), and that there was a delayed onset of invasion by 8 hours (Figure 7B).

Combined XIAP inhibition and PPAR γ activation decreases mitochondrial respiration and reduces spare respiratory capacity

The increased cell death of GCT-derived cells implies cytotoxicity of the combined treatment at the mitochondria, raising questions regarding the underlying mechanism. As PPAR γ plays a pivotal role in lipid and glucose metabolism, we have reported that there is upregulation of proteins associated with metabolic processes that is consistent with the restoration of PPAR γ activity (*Leung DTH et al – concurrent submitted manuscript*). Additionally, as mitochondria also play a critical role in determining whether cells live or die, and the critical role of XIAP and Smac signaling pathways in oxidative stress, we thus investigated whether the combined treatment would affect mitochondrial oxygen consumption rate in the KGN cells. We performed mitochondrial respiratory analysis using Extracellular Flux Analyzer (XFp) to determine whether the oxygen consumption rate (OCR) was altered by the combined treatment in the mitochondria of living cultured KGN cells under our experimental settings. A schematic representation of the design and interpretation of this assay is shown in Figure 8A. During the course of the assay, multiple mitochondrial inhibitors, including oligomycin, FCCP, and antimycin A/rotenone, were added to the KGN cells in the presence or absence of the treatment, and the OCR in compound-exposed or non-exposed cells was measured every 9 minutes. The fluctuation of OCR is summarized in Figure 8B. While RGZ/RA causes a non-significant reduction in OCR over the time-course of the experiment, the combined inhibition of XIAP and PPAR γ activation significantly decreased OCR (Figure 8B). By measuring the spare respiratory capacity, which is an estimate of the potential bioenergetic reserve the cell can call upon in times of stress,

we observed a significant reduction in the combined treated cells compare to vehicle- or RGZ/RA-treated cells. This indicates that the combined treatment has affected the mitochondrial function, inhibiting the ability of the mitochondria to function at its full potential, causing the reserve capacity to be significantly reduced.

TLDA analysis of XIAP inhibition and PPAR γ activation in KGN cells

Analysis of gene expression for 98 apoptosis-related genes were analyzed using Taqman Low Density Arrays. The relative expression of each gene was normalized against the median of geNorm software selected controls (which is in effect the inverse of the Ct value). The genes that showed the highest fold change after the combined treatment compared to vehicle control were *TNFRSF1B* (2.33-fold) and *BIRC3* (139.77-fold). Additionally, the combined treatment in KGN cells also increased the protein expression of TGM2 (8.01-fold), using a proteomic approach of SILAC (*Leung DTH et al – concurrent submitted manuscript*). TGM2 is a protein with a known role in apoptosis (22).

Given the statistically significant differential expression, *TNFRSF1B*, *BIRC3* and *TGM2* were selected for selected for further analysis using qRT-PCR. Individual cell lines were treated with DMSO 0.1% (vehicle control), PPAR γ /RXR α agonists (RGZ/RA 20 μ M/5 μ M), Smac-mimetics (Cmpd A and AZD at 500nM, for *BIRC3*) alone and a combination of Smac-mimetics and PPAR γ /RXR α agonists (CmpdA/RGZ/RA and AZD/RGZ/RA (for *BIRC3*) both at 500nM/20 μ M/5 μ M). Gene expression is presented as a change in fold induction, relative to *RPLP0* control and normalized to vehicle control. *TNFRSF1B* expression following RGZ/RA treatment alone is not significantly increased. However, *TNFRSF1B* is shown to be significantly upregulated following RGZ/RA/CmpdA treatment (Figure 9A). A similar trend was observed for *TGM2* mRNA expression (Figure 9B). For *BIRC3* mRNA expression, CmpdA and AZD treatments

resulted in significantly increased induction as well as significantly increased induction in both combination groups. RGZ/RA treatment did not affect *BIRC3* mRNA expression (Figure 9C).

Discussion

Granulosa cell tumors (GCT) arise from granulosa cells (GC) of the ovarian follicle, and represent a specific subset of malignant ovarian tumors (1). GCT are unusual in that they have an unexplained propensity for late recurrence. ~80% of patients with aggressive or recurrent tumors die from their disease (1). At present there are no reliable methods for predicting relapse and, once surgery is no longer an option, no therapeutic modalities have proven effective (1). Hence the need for more novel, targeted therapy cannot be overstated.

Nuclear receptors (NR) represent established therapeutic targets, as they play a central pathogenic role in several endocrine malignancies. We have previously reported the gene expression profile for all 48 NR in our cohort of GCT samples (2). One of the most highly expressed NR in GCT is PPAR γ (2), which also has detectable expression in the two GCT-derived cell lines (KGN and COV434), and in a transformed human “non-luteinized” GC (hGrC1) cell line (17). PPAR γ binds to DNA at specific sites as obligate functional heterodimers with RXR α which is also expressed in GCT and these cell lines.

The molecular mechanisms of PPAR γ action in ovarian function are poorly understood. PPAR γ is anti-proliferative, promoting terminal differentiation in GC and alterations in steroidogenesis (23). It is also involved in atresia as activation of PPAR γ induces apoptosis in primary rat GC (23). PPAR γ has been implicated in the pathology

of several diseases including obesity, diabetes and polycystic ovarian syndrome (23). The synthetic thiazolidinediones (TZD) (e.g. troglitazone and rosiglitazone) are PPAR γ agonist ligands, developed to treat patients with type II diabetes (24). The potential of PPAR γ agonists as anticancer agents has attracted considerable interest for the treatment of endocrine malignancies (3). Modulation of PPAR γ action using TZD has also been found to exert anti-neoplastic effects in various solid tumors (25-27). The pro-differentiating role of PPAR γ has been associated with tumor development and progression (28). Previous studies have demonstrated the overexpression of PPAR γ in many tumor types and in various cancers such as the colon (29) and thyroid (30), activation of PPAR γ reduced cell viability and inhibited cell proliferation. This anti-tumor effect of PPAR γ agonists has also been observed in xenograft model of solid tumors (31).

The high levels of PPAR γ in the GCT at the mRNA level (2) and subsequently in this study at the protein level were unexpected given the anti-proliferative properties of PPAR γ suggesting that, though potentially targetable, there is resistance to the actions of PPAR γ in GCT. The evidence we have presented showing that the TZDs have only a small effect on GCT cell proliferation and transactivation activity indicate that this is the case.

We have previously reported that for both GCT-derived cell lines, the estrogen receptor-beta (ER β) gene that has anti-proliferative activity, is also upregulated. We reported that ER β signaling was inhibited by constitutive activation of NF- κ B signaling, providing at least circumstantial evidence that ER β may be a tumor suppressor gene (8). Like human GCT (32), the cell lines were shown to predominantly express both ER β mRNA and protein, with no ER α protein observed (8). Interestingly, however,

despite ER β expression and the ability to functionally bind estradiol, when cells were transfected with estrogen-responsive reporter constructs and treated with estradiol, no response was observed (8). To investigate whether this transcriptional repression was restricted to ER β , a range of other reporter constructs were employed, containing the glucocorticoid receptor (GR) response element, as well as reporter constructs containing enhancer elements for second messenger pathways, including CREB, heat shock, and the MAPK reporters AP-1 and NF- κ B. The results revealed two interesting findings; first, GR-mediated transactivation was also repressed, demonstrating that transrepression was not limited to the ER, and second, although the CREB, heat shock, and MAPK reporters could all be induced by the appropriate stimulus, both the AP-1 and NF- κ B reporters exhibited constitutive activation under serum-free conditions (8). Furthermore, although inhibition of AP-1 using MAPK inhibitors had no effect on ER transcriptional repression, inhibition of the NF- κ B pathway using the inhibitor of κ B α ($\text{I}\kappa\text{B}\alpha$)-specific inhibitor, BAY11-7082, restored both ER- and GR-mediated transactivation (8). These data demonstrate that the functional consequence of both constitutive and ligand-dependent NF- κ B activity is the transrepression of ER β -mediated transcription in the COV434 and KGN cell lines (8). Consistent with this published data, in this study we have demonstrated that this PPAR γ resistance in the GCT-derived cells is also mediated by constitutive NF- κ B activity causing transrepression of PPAR γ .

We observed that when PPAR γ agonists (troglitazone or rosiglitazone) were used with the RXR α agonist (9-cis-retinoic acid), that there was just a small, but significant decrease in proliferation. When the cells were transfected with a PPAR γ reporter construct and treated with the agonists, again there was a small but significant

activation of the reporter compared to vehicle. It was only after inactivation of NF- κ B signaling by inhibition of I κ B phosphorylation that we saw the most profound effect on decreased proliferation, increased apoptosis, and PPAR γ -mediated transactivation at the PPRE, leading to a 5-fold induction in response to ligand.

Members of the nuclear receptor superfamily and NF- κ B subunits have been shown to physically interact. The best characterized interactions are those of NF- κ B and GR, resulting in a mutual transcriptional antagonism (33). It has been demonstrated, in an *in vivo* system, that p65, p50, and I κ B α interact with the GR not only in nucleus but also in the cytosol in absence of ligand (34). This mutual transrepression is thought to play a part in the modulation of inflammation and immunosuppression. Other nuclear receptors that have been demonstrated to physically interact with NF- κ B in similar experimental systems include the mineralocorticoid, androgen, and progesterone receptors (35,36).

The significance of constitutive activation of NF- κ B with consequent transrepression of PPAR γ in the pathogenesis of GCT remains speculative. There are several lines of evidence to suggest that the role of PPAR γ in granulosa cells may be antiproliferative (23,37). Thus activation of NF- κ B signaling in GCT may provide a survival advantage not only through its antiapoptotic and pro-proliferative effects but also by its repression of PPAR γ signaling. GCT exhibit a poor response to endocrine therapy. The lack of a response to the PPAR γ agonists may be due to activation of the NF- κ B pathway in GCT. It is well established that the NF- κ B pathway and upstream components involved in its activation are important for cancer development; activated NF- κ B increases the expression of genes involved in cell proliferation, metastasis, angiogenesis and anti-apoptosis (4).

The Inhibitor of Apoptosis Proteins (IAP) are critical modulators of apoptosis as they inhibit activation of caspases, a process which initiates apoptosis. Members of the IAP family are characterized by the well conserved baculovirus IAP repeat (BIR) domain. XIAP is the best characterized and most potent caspase inhibitor amongst the 8-member IAP family. XIAP has three BIR domains, and a RING finger domain conferring E3 ubiquitin ligase activity (9). The BIR2 and BIR3 domains are responsible for blocking both intrinsic and extrinsic apoptotic signals by directly inhibiting caspase-3, -7 and -9 (9). The expression of XIAP is regulated by the mitochondrial protein, Second Mitochondria-derived Activator of Caspases (Smac) (9). Released Smac interacts with the conserved amino acid residues in the XIAP BIR3 domain to antagonize the caspase-binding activity of XIAP.

NF- κ B transcriptionally activates the expression of XIAP. In addition, XIAP has a reciprocal modulatory role in NF- κ B activation as a consequence of a positive feed-forward loop. The ubiquitin ligase activity of XIAP RING domain targets I κ B for proteosomal degradation to regulate NF- κ B activity. XIAP also activates the NF- κ B and AP-1 signaling pathways involving the TAK-TAB protein complex. Activation of this complex is induced by the physical interaction between XIAP BIR1 domain and the TGF β -activated kinase-binding (TAB) protein 1 (10). In this context, we have demonstrated that NF- κ B and TGF β coordinately regulate cell survival in GCT (38). The constitutive activity of both NF- κ B and AP-1 in the GCT-derived cell lines is also interesting in this context (8,39). It remains to be determined if the constitutive activity for both pathways is regulated through TAK1.

XIAP is a critical regulator of follicular atresia (40). XIAP expression is upregulated in response to FSH, suppressing GC apoptosis and facilitating FSH-induced follicular

growth (40). XIAP is highly expressed in proliferating GC of gonadotropin-primed follicles and downregulated in apoptotic cells from atretic follicles after gonadotropin withdrawal (40). FSH induces XIAP expression in GC *in vitro* via the NF- κ B pathway (41). In this correspondence, we have shown that XIAP gene and protein is overexpressed in our cohort of primary GCT and in KGN and COV434 cells, likely due to constitutive activation of the NF- κ B pathway, and that GCT cells are show similarity to an FSH-stimulated preovulatory granulosa cell (42).

Due to its elevated expression and prominent ability to control cell death in many human cancers, XIAP has become an attractive therapeutic target for novel anti-cancer treatment (11,12). Small-molecule inhibitors are in various stages of development, from preclinical to phase II clinical trials (11,12). Smac-mimetics are drugs designed to mimic the inhibitory Smac and bind directly to XIAP with high affinity to neutralize the pro-oncogenic functions of this protein, by preventing caspase binding. Mono- or bi-valent Smac-mimetics have been designed to target the BIR2 and/or BIR3 functional domains. Preclinical studies have reported high anti-neoplastic activity by both monovalent and bivalent compounds. Several of these compounds have also demonstrated favorable safety profile and evidence of anti-tumor activity in early clinical trials (11,12). Inhibiting XIAP using single agents has shown some signs of anti-tumor activity, however, by far the majority of studies indicate that the promise of XIAP inhibitors as cancer therapeutics primarily resides in rational drug combinations in order to exploit synergistic lethality (11,12). Although originally designed to inactivate XIAP, Smac-mimetics are also effective in producing rapid ubiquitylation and proteosomal degradation of other members of the IAP family, in particular cIAP-1 and cIAP2 (43,44), which also binds to caspases-3, -7 and -9 but with a lower affinity than XIAP (11). We have shown that XIAP is the predominant IAP expressed in GCT, the

levels of other members are low. In our studies, we utilized a bivalent Smac-mimetic, Compound A (CmpdA) (18), a commercial monovalent compound, AZD5582, and a cell-permeable inhibitor of XIAP, embelin (45). We demonstrated that when either of these compounds were used on their own as a single treatment, there was no effect on cell proliferation, PPAR γ transactivation or apoptosis. However we did observe that if cells were transfected with either an NF- κ B or AP-1 reporter, that inhibition of XIAP abrogated constitutive activity for both pathways, indicating that XIAP is regulating both pathways, potentially through the TAK1/TAB1/2/3 complex.

Antagonism of XIAP *in vitro* and *in vivo* has been shown to lower the apoptotic threshold and thereby sensitize tumor cells to the effects of chemotherapy (11,12), enabling the use of lower doses with the potential for fewer toxicities (11,12). In this study, we thus sought out to determine whether combining the anti-proliferative/pro-apoptotic effects of PPAR γ activation with XIAP inhibition presents a potential therapeutic strategy to treat GCT.

We have presented strong proof that targeting the peroxisome proliferator-activated receptor-gamma protein (PPAR γ) and the X-linked inhibitor of apoptosis protein (XIAP) provides a novel and specific therapeutic strategy for GCT. These studies show that PPAR γ agonism in combination with inhibition of NF- κ B signaling is a potential efficacious, molecular-targeted therapy for GCT treatment. The key NF- κ B effector protein, XIAP, is an attractive therapeutic target due to (i) inhibition of intrinsic anti-apoptotic properties, (ii) blocking NF- κ B activation, and (iii) relative tissue specificity. Our data shows that not only is this the case for GCT-derived cell lines, whether monolayer, or as 3D spheroids which mimic the tumor microenvironment, but is also likely relevant for primary GCT as well given that we saw similar effects on two *in vivo*

GCT explants from patient tumor samples. The use of orthotopic models of patient-derived GCT xenotransplantation would more closely mimic the *in vivo* feature of GCT, hence further studies using an orthotopic PDX model would confirm our current results with more convincing data.

Given that PPAR γ controls the networks of genes involved in adipogenesis, lipid metabolism, inflammation and maintenance of metabolic homeostasis, we were interested to determine what the effect of the combined treatment would be on metabolic function. Using the Seahorse extracellular flux system, we were able to measure mitochondrial respiration to determine whether this would provide some insight into the mechanisms involved in the effect from the combined treatment. Generation of ATP by mitochondrial respiration is an indispensable source of energy. Many cells and tissues operate at a basal level that only requires a part of their total bioenergetic capability, allowing a reserve respiratory capacity for sudden surges in energy requirement. Our observation that the combined treatment caused a reduction in the available reserve respiratory capacity can provide, indicates that the combined treatment sensitizes the GCT-derived cells to a sudden surge in ATP demand, however as the reserve is depleted, it causes the cells to undergo cell death.

The evidence that the XIAP and PPAR γ targeted treatment induces apoptosis and alters cellular bioenergetics, also echoes the gene expression analysis where pro-apoptotic genes such as TNFRSF1B and TGM2 were upregulated at the message level. A major challenge for GCT treatment is that cancer cells inherently aggregate into multicellular structures, contributing to the metastatic process by attaching to and invading the peritoneal lining to form secondary tumors. Additionally, we have also identified from our proteomic study (*Leung DTH et al – concurrent submitted manuscript*), the downregulation of fascin, which is a protein associated with cell

motility. Utilizing the xCELLigence RTCA system to assess the effects of the compounds on cell invasion, we observed that compared to vehicle control, the RGZ/RA/CmpdA-treated KGN cells significantly delayed the onset of invasion by 8 hours. The treated cells were also 30% less invasive. No increase in cell numbers was observed 4 hours post onset of invasion, suggesting proliferation of the RGZ/RA/CmpdA-treated cells had ceased. This may indicate the cells were undergoing differentiation as PPAR γ activity is restored. It also suggests that the combined treatment strategy will also be advantageous in preventing the metastatic process.

This study provides a proof-of-concept for combination therapeutic targeting involving XIAP inhibition and PPAR γ activation for GCT. We anticipate this targeted therapy will contribute to reducing the use of broad non-specific standard chemotherapy. As these drugs are already in clinical or pre-clinical use, expedient translation to the clinic is possible. The findings presented in this study may also have broader significance beyond GCT, specifically for malignancies that co-express these proteins, e.g. epithelial ovarian cancer (46,47), colorectal cancer (48) and thyroid cancer (49,50).

Acknowledgements

This work is supported by grants-in-aid from the Ovarian Cancer Research Foundation (SC); the Cancer Council Victoria; the Granulosa Cell Tumor of the Ovary Foundation; and the National Health & Medical Research Council of Australia through a Project Grant (#1058334) and a Senior Principal Research Fellowship to PJF (#1002559).

The Hudson Institute is supported by the Victorian Government's Operational Infrastructure Scheme. DTHL is supported by the Endocrine Society of Australia through a Research Higher Degree Scholarship.

The authors thank Calvin Chee (Hudson Institute of Medical Research), Nicholas Chee (Hudson Institute of Medical Research), Daniel Heathcote (Hudson Institute of Medical Research) and the MHTP Research Platforms for technical support.

References

1. Jamieson S, Fuller PJ. Molecular pathogenesis of granulosa cell tumors of the ovary. *Endocrine reviews* **2012**;33:109-44
2. Alexiadis M, Eriksson N, Jamieson S, Davis M, Drummond AE, Chu S, *et al.* Nuclear receptor profiling of ovarian granulosa cell tumors. *Hormones & cancer* **2011**;2:157-69
3. Catalano MG, Poli R, Pugliese M, Fortunati N, Boccuzzi G. Emerging molecular therapies of advanced thyroid cancer. *Molecular aspects of medicine* **2010**;31:215-26
4. Baldwin AS. Regulation of cell death and autophagy by IKK and NF-kappaB: critical mechanisms in immune function and cancer. *Immunological reviews* **2012**;246:327-45
5. Baldwin AS, Jr. The NF-kappa B and I kappa B proteins: new discoveries and insights. *Annual review of immunology* **1996**;14:649-83
6. Karin M, Cao Y, Greten FR, Li ZW. NF-kappaB in cancer: from innocent bystander to major culprit. *Nat Rev Cancer* **2002**;2:301-10
7. Ghosh S, Karin M. Missing pieces in the NF-kappaB puzzle. *Cell* **2002**;109 Suppl:S81-96
8. Chu S, Nishi Y, Yanase T, Nawata H, Fuller PJ. Transrepression of estrogen receptor beta signaling by nuclear factor-kappaB in ovarian granulosa cells. *Mol Endocrinol* **2004**;18:1919-28
9. Vaux DL, Silke J. IAPs, RINGs and ubiquitylation. *Nature reviews Molecular cell biology* **2005**;6:287-97
10. Lu M, Lin SC, Huang Y, Kang YJ, Rich R, Lo YC, *et al.* XIAP induces NF-kappaB activation via the BIR1/TAB1 interaction and BIR1 dimerization. *Mol Cell* **2007**;26:689-702
11. Fulda S. Smac Mimetics to Therapeutically Target IAP Proteins in Cancer. *International review of cell and molecular biology* **2017**;330:157-69
12. Fulda S. Promises and Challenges of Smac Mimetics as Cancer Therapeutics. *Clin Cancer Res* **2015**;21:5030-6
13. Fulda S. Smac mimetics as IAP antagonists. *Semin Cell Dev Biol* **2015**;39:132-8
14. Jamieson S, Butzow R, Andersson N, Alexiadis M, Unkila-Kallio L, Heikinheimo M, *et al.* The FOXL2 C134W mutation is characteristic of adult granulosa cell tumors of the ovary. *Modern pathology : an official journal of the United States and Canadian Academy of Pathology, Inc* **2010**;23:1477-85
15. Nishi Y, Yanase T, Mu Y, Oba K, Ichino I, Saito M, *et al.* Establishment and characterization of a steroidogenic human granulosa-like tumor cell line, KGN, that expresses functional follicle-stimulating hormone receptor. *Endocrinology* **2001**;142:437-45
16. van den Berg-Bakker CA, Hagemeyer A, Franken-Postma EM, Smit VT, Kuppen PJ, van Ravenswaay Claasen HH, *et al.* Establishment and characterization of 7 ovarian carcinoma cell lines and one granulosa tumor cell line: growth features and cytogenetics. *Int J Cancer* **1993**;53:613-20
17. Bayasula, Iwase A, Kiyono T, Takikawa S, Goto M, Nakamura T, *et al.* Establishment of a human nonluteinized granulosa cell line that transitions from the gonadotropin-independent to the gonadotropin-dependent status. *Endocrinology* **2012**;153:2851-60
18. Vince JE, Wong WW, Khan N, Feltham R, Chau D, Ahmed AU, *et al.* IAP antagonists target cIAP1 to induce TNFalpha-dependent apoptosis. *Cell* **2007**;131:682-93
19. Alexiadis M, Chu S, Leung D, Gould JA, Jobling T, Fuller PJ. Transcriptomic analysis of stage 1 versus advanced adult granulosa cell tumors. *Oncotarget* **2016**;7:14207-19
20. Jamieson S, Fuller PJ. Characterization of the inhibitor of kappaB kinase (IKK) complex in granulosa cell tumors of the ovary and granulosa cell tumor-derived cell lines. *Horm Cancer* **2013**;4:277-92
21. Resch U, Schichl YM, Winsauer G, Gudi R, Prasad K, de Martin R. Siva1 is a XIAP-interacting protein that balances NFkappaB and JNK signalling to promote apoptosis. *Journal of cell science* **2009**;122:2651-61

22. Roszer T. Transcriptional control of apoptotic cell clearance by macrophage nuclear receptors. *Apoptosis : an international journal on programmed cell death* **2017**;22:284-94
23. Froment P, Gizard F, Defever D, Staels B, Dupont J, Monget P. Peroxisome proliferator-activated receptors in reproductive tissues: from gametogenesis to parturition. *J Endocrinol* **2006**;189:199-209
24. Aleman-Gonzalez-Duhart D, Tamay-Cach F, Alvarez-Almazan S, Mendieta-Wejbe JE. Current Advances in the Biochemical and Physiological Aspects of the Treatment of Type 2 Diabetes Mellitus with Thiazolidinediones. *PPAR Res* **2016**;2016:7614270
25. Smallridge RC, Copland JA, Brose MS, Wadsworth JT, Houvras Y, Menefee ME, *et al.* Efatutazone, an oral PPAR-gamma agonist, in combination with paclitaxel in anaplastic thyroid cancer: results of a multicenter phase 1 trial. *J Clin Endocrinol Metab* **2013**;98:2392-400
26. Komatsu Y, Yoshino T, Yamazaki K, Yuki S, Machida N, Sasaki T, *et al.* Phase 1 study of efatutazone, a novel oral peroxisome proliferator-activated receptor gamma agonist, in combination with FOLFIRI as second-line therapy in patients with metastatic colorectal cancer. *Investigational new drugs* **2014**;32:473-80
27. Murakami H, Ono A, Takahashi T, Onozawa Y, Tsushima T, Yamazaki K, *et al.* Phase I study of Efatutazone, an oral PPARgamma agonist, in patients with metastatic solid tumors. *Anticancer research* **2014**;34:5133-41
28. Ferrari SM, Materazzi G, Baldini E, Ulisse S, Miccoli P, Antonelli A, *et al.* Antineoplastic Effects of PPARgamma Agonists, with a Special Focus on Thyroid Cancer. *Current medicinal chemistry* **2016**;23:636-49
29. Tsukahara T. The Role of PPARgamma in the Transcriptional Control by Agonists and Antagonists. *PPAR research* **2012**;2012:362361
30. Antonelli A, Fallahi P, Ulisse S, Ferrari SM, Minuto M, Saraceno G, *et al.* New targeted therapies for anaplastic thyroid cancer. *Anti-cancer agents in medicinal chemistry* **2012**;12:87-93
31. Shimazaki N, Togashi N, Hanai M, Isoyama T, Wada K, Fujita T, *et al.* Anti-tumour activity of CS-7017, a selective peroxisome proliferator-activated receptor gamma agonist of thiazolidinedione class, in human tumour xenografts and a syngeneic tumour implant model. *Eur J Cancer* **2008**;44:1734-43
32. Chu S, Mamers P, Burger HG, Fuller PJ. Estrogen receptor isoform gene expression in ovarian stromal and epithelial tumors. *J Clin Endocrinol Metab* **2000**;85:1200-5
33. De Bosscher K, Vanden Berghe W, Haegeman G. The interplay between the glucocorticoid receptor and nuclear factor-kappaB or activator protein-1: molecular mechanisms for gene repression. *Endocrine reviews* **2003**;24:488-522
34. Widen C, Gustafsson JA, Wikstrom AC. Cytosolic glucocorticoid receptor interaction with nuclear factor-kappa B proteins in rat liver cells. *The Biochemical journal* **2003**;373:211-20
35. McKay LI, Cidlowski JA. Molecular control of immune/inflammatory responses: interactions between nuclear factor-kappa B and steroid receptor-signaling pathways. *Endocr Rev* **1999**;20:435-59
36. McKay LI, Cidlowski JA. Cross-talk between nuclear factor-kappa B and the steroid hormone receptors: mechanisms of mutual antagonism. *Mol Endocrinol* **1998**;12:45-56
37. Komar CM. Peroxisome proliferator-activated receptors (PPARs) and ovarian function-implications for regulating steroidogenesis, differentiation, and tissue remodeling. *Reprod Biol Endocrinol* **2005**;3:41
38. Bilandzic M, Chu S, Wang Y, Tan HL, Fuller PJ, Findlay JK, *et al.* Betaglycan alters NFkappaB-TGFbeta2 cross talk to reduce survival of human granulosa tumor cells. *Molecular endocrinology* **2013**;27:466-79

39. Chu S, Alexiadis M, Fuller PJ. Proteasome inhibition by bortezomib decreases proliferation and increases apoptosis in ovarian granulosa cell tumors. *Reprod Sci* **2009**;16:397-407
40. Wang Y, Rippstein PU, Tsang BK. Role and gonadotrophic regulation of X-linked inhibitor of apoptosis protein expression during rat ovarian follicular development in vitro. *Biology of reproduction* **2003**;68:610-9
41. Wang Y, Chan S, Tsang BK. Involvement of inhibitory nuclear factor-kappaB (NFkappaB)-independent NFkappaB activation in the gonadotropic regulation of X-linked inhibitor of apoptosis expression during ovarian follicular development in vitro. *Endocrinology* **2002**;143:2732-40
42. Chu S, Rushdi S, Zumpe ET, Mamers P, Healy DL, Jobling T, *et al.* FSH-regulated gene expression profiles in ovarian tumours and normal ovaries. *Mol Hum Reprod* **2002**;8:426-33
43. Darding M, Feltham R, Tenev T, Bianchi K, Benetatos C, Silke J, *et al.* Molecular determinants of Smac mimetic induced degradation of cIAP1 and cIAP2. *Cell death and differentiation* **2011**;18:1376-86
44. Feltham R, Bettjeman B, Budhidarmo R, Mace PD, Shirley S, Condon SM, *et al.* Smac mimetics activate the E3 ligase activity of cIAP1 protein by promoting RING domain dimerization. *The Journal of biological chemistry* **2011**;286:17015-28
45. Nikolovska-Coleska Z, Xu L, Hu Z, Tomita Y, Li P, Roller PP, *et al.* Discovery of embelin as a cell-permeable, small-molecular weight inhibitor of XIAP through structure-based computational screening of a traditional herbal medicine three-dimensional structure database. *J Med Chem* **2004**;47:2430-40
46. Zhang GY, Ahmed N, Riley C, Oliva K, Barker G, Quinn MA, *et al.* Enhanced expression of peroxisome proliferator-activated receptor gamma in epithelial ovarian carcinoma. *British journal of cancer* **2005**;92:113-9
47. Wu M, Yuan S, Szporn AH, Gan L, Shtilbans V, Burstein DE. Immunocytochemical detection of XIAP in body cavity effusions and washes. *Modern pathology : an official journal of the United States and Canadian Academy of Pathology, Inc* **2005**;18:1618-22
48. Qiao L, Dai Y, Gu Q, Chan KW, Ma J, Lan HY, *et al.* Loss of XIAP sensitizes colon cancer cells to PPARgamma independent antitumor effects of troglitazone and 15-PGJ2. *Cancer Lett* **2008**;268:260-71
49. Zhang Y, Yu J, Lee C, Xu B, Sartor MA, Koenig RJ. Genomic binding and regulation of gene expression by the thyroid carcinoma-associated PAX8-PPARG fusion protein. *Oncotarget* **2015**;6:40418-32
50. Hussain AR, Bu R, Ahmed M, Jehan Z, Beg S, Al-Sobhi S, *et al.* Role of X-Linked Inhibitor of Apoptosis as a Prognostic Marker and Therapeutic Target in Papillary Thyroid Carcinoma. *The Journal of clinical endocrinology and metabolism* **2015**;100:E974-85

Table 1. XIAP and PPAR γ protein expression on GCT tissue microarray¹.

Marker	Total GCT Tissue Microarray (<i>n</i> = 76: 52 primary tumors only; 4 recurrent tumors only) ²			
	Low		Medium/High	
	<i>n</i>	(%)	<i>n</i>	(%)
XIAP	24	(32)	52	(68)
PPAR γ	27	(36)	49	(64)

¹ Staining was analyzed using “positive pixel count v9” algorithm in the Aperio ImageScope version 12.3.0.5056 (Leica Biosystems, Wetzlar, Germany). Percentage of positive (brown) staining indicating protein levels was determined as low (0-30%), medium (31-79%) or high (>80%).

² Each sample represents a GCT collected from an individual patient. Of the 52 primary tumours, 20 have matched samples and 4 patients have developed recurrent diseases which were included in the cohort. Clinical information of patient cohort is summarized in Supplementary Table 1.

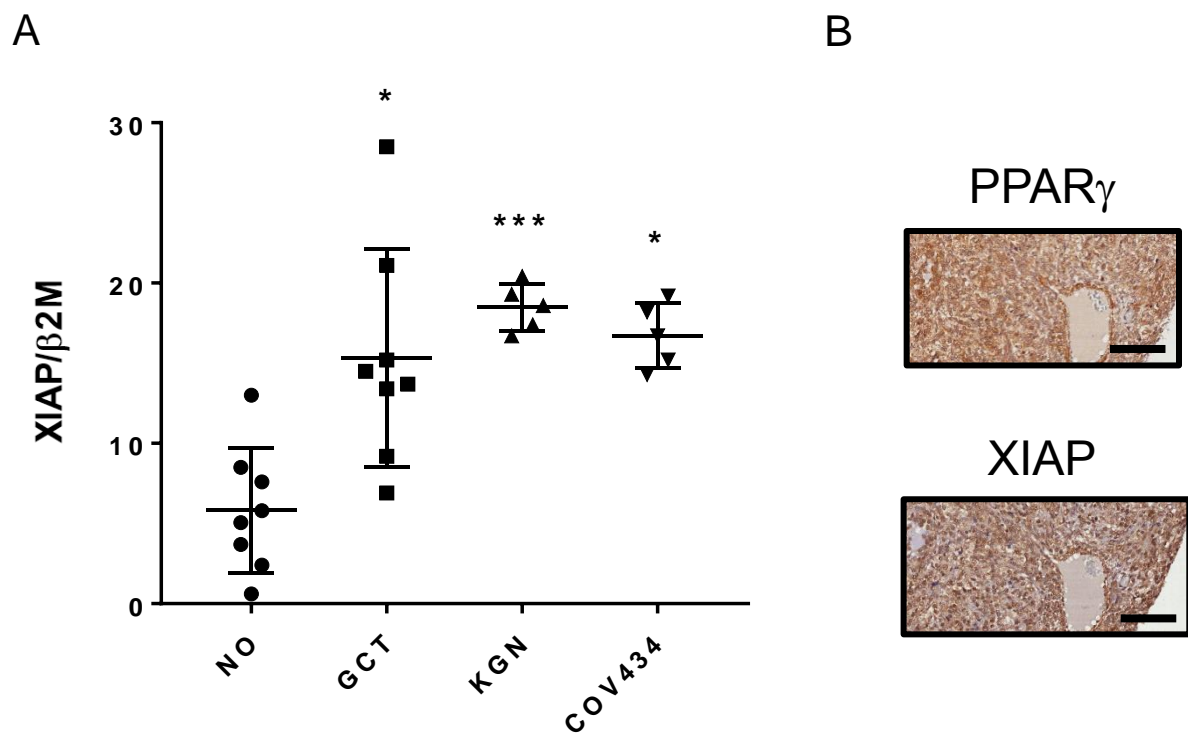


Figure 1. XIAP and PPAR γ expression in GCT and GCT-derived cell lines. A. XIAP mRNA expression was assessed using RT-PCR and normalized to that of the housekeeping gene, β -2-microglobulin (β 2M). The panel includes 8 premenopausal ovary (NO), 8 GCT and the two human GCT-derived cell lines, KGN and COV434. Kruskal-Wallis; Dunn's post-hoc analysis; * $p < 0.05$, *** $p < 0.001$ when compared to NO. B. PPAR γ and XIAP protein expression in GCT was determined using immunohistochemistry. All images are shown in x40 magnification. Scale bar is at 50 μ m.

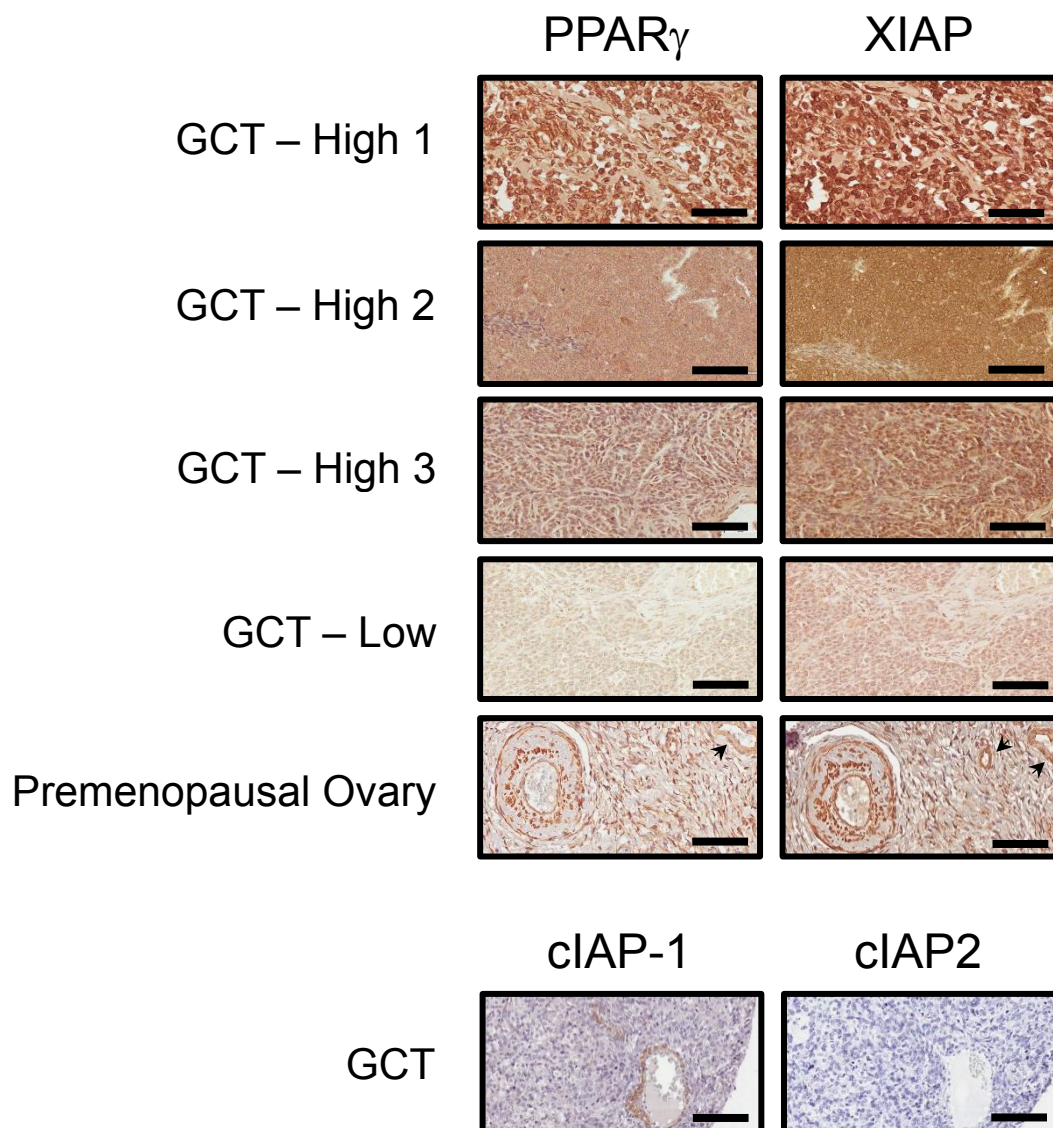


Figure 2. Protein expression of XIAP, PPAR γ , cIAP1 and cIAP2 in primary GCT samples and premenopausal ovaries. Low to high expression of XIAP and PPAR γ was observed in the GCT cores in the TMA. XIAP and PPAR γ was also detected in the granulosa cells and theca cells in a normal preovulatory ovarian sample. Very low levels of cIAP-1 and no expression of cIAP2 was observed in GCT samples. All images are shown in x40 magnification. Scale bar is at 50 μ m. Arrow heads point to blood vessels in the premenopausal ovaries.

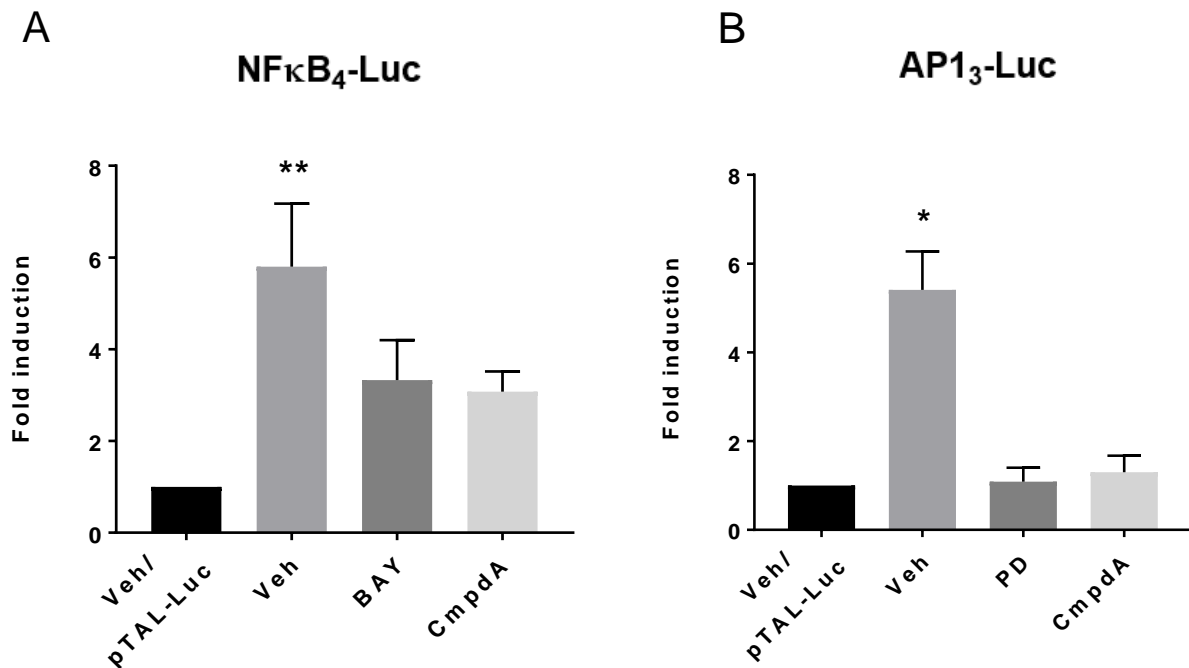


Figure 3. NF- κ B and AP-1-mediated transactivation assays in the KGN cells.

Cells transfected with either an NF- κ B (A) or AP-1 (B) reporter showed an approximate 6-fold induction of luciferase activity under basal conditions (Veh; with 0.1% DMSO) compared with cells transfected with an enhancer-less reporter (pTAL-Luc; with 0.1% DMSO). This suggests constitutive activity of NF- κ B and AP-1 in the KGN cells. NF- κ B inhibitor, BAY11-7082 (BAY), or ERK/AP-1 inhibitor, PD98095 (PD), suppressed the respective constitutive activity. XIAP inhibition using CmpdA also abrogated NF- κ B and AP-1 constitutive activity. $n = 4$ in duplicate wells. Kruskal-Wallis; Dunn's post-hoc analysis; * $p < 0.05$, ** $p < 0.01$ when compared to Veh/pTAL-Luc.

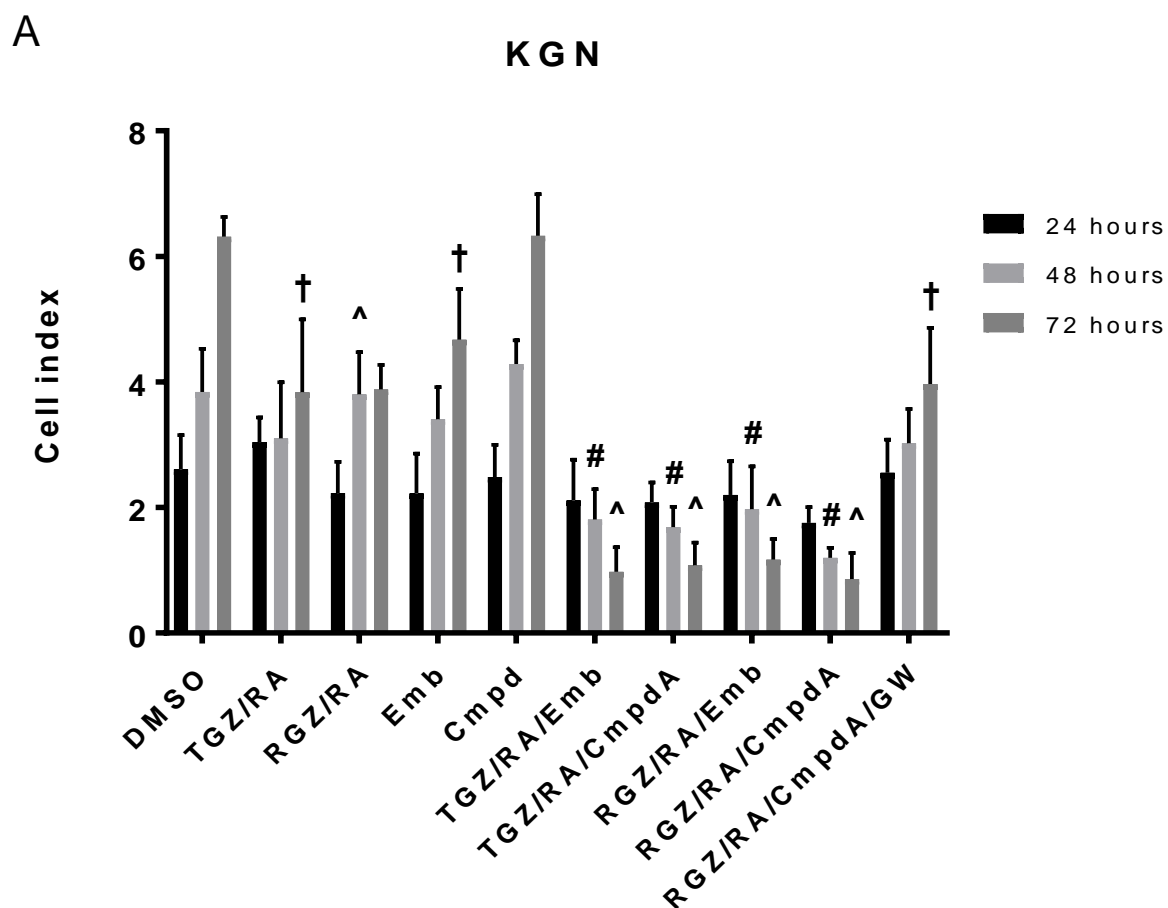


Figure 4A. Proliferation assay in the KGN cells. The KGN cells were subjected to PPAR γ activation (20 μ M TGZ or RGZ and 5 μ M RA) alone or in combination with XIAP inhibition (10 μ M Emb or 500nM CmpdA) for 24 to 72 hours. No effect on proliferation was observed with singular treatment. Significant reduction in proliferation was seen with combined PPAR γ activation and XIAP inhibition. GW9662 (GW; 20 μ M) is a PPAR γ antagonist used to reverse the effects of PPAR γ activation. # $p < 0.01$ compared to Veh (0.1% DMSO) at 48 hours; † $p < 0.05$ compared to Veh at 72 hours; ^ $p < 0.01$ compared to Veh at 72 hours. $n = 3$ in duplicate wells.

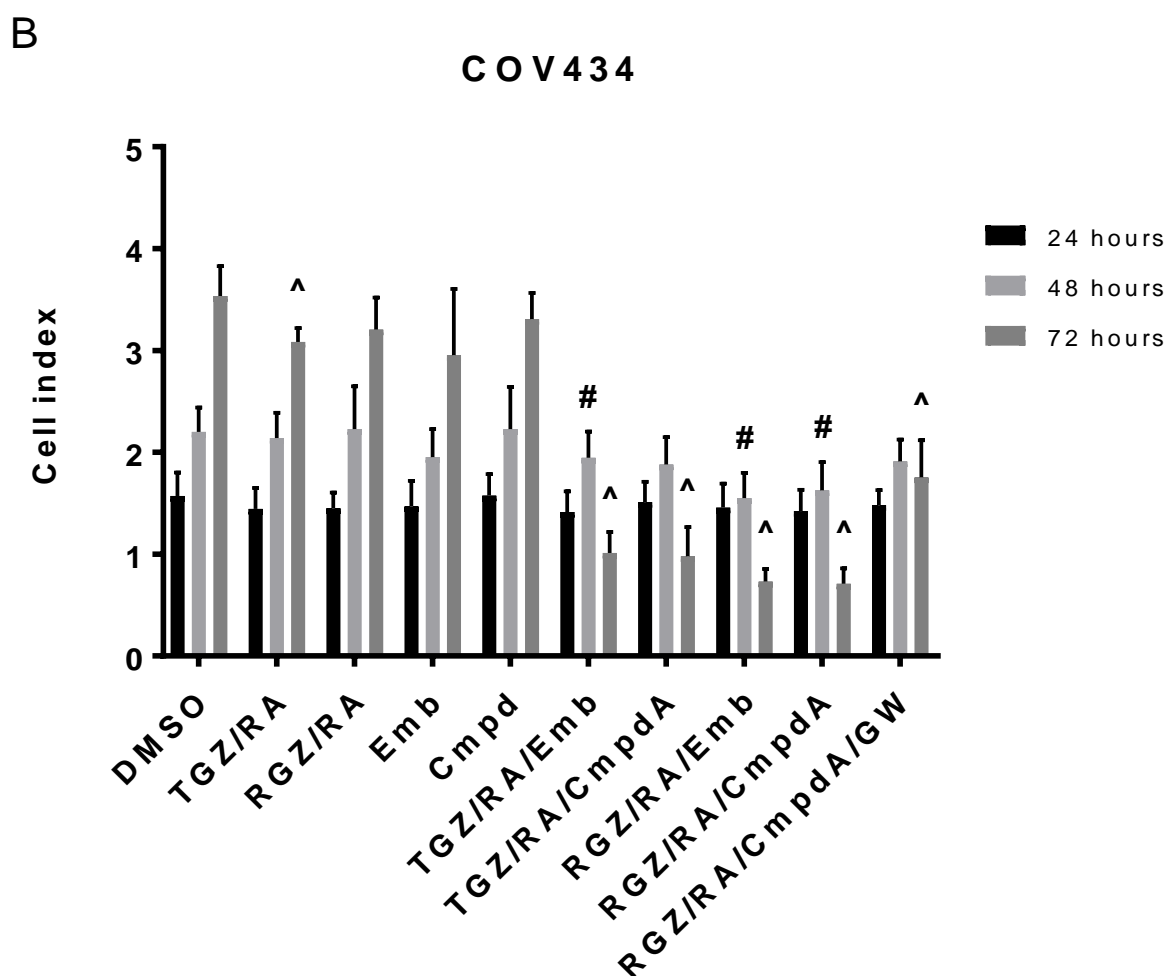


Figure 4B. Proliferation assay in the COV434 cells. The COV434 cells were subjected to the same treatment regimen as the KGN cells: 20 μ M TGZ or RGZ and 5 μ M RA (PPAR γ activation), 10 μ M Emb or 500nM SM (XIAP inhibition) alone or in combination for 24 to 72 hours. Similar to what was observed in the KGN cells, there was no effect on proliferation when the COV434 cells were treated with PPAR γ activation or XIAP inhibition alone. The combined PPAR γ and XIAP treatment reduced cell proliferation in the COV434 cells. # $p < 0.01$ compared to Veh (0.1% DMSO) at 48 hours; ^ $p < 0.01$ compared to Veh at 72 hours. $n = 3$ in duplicate wells.

C

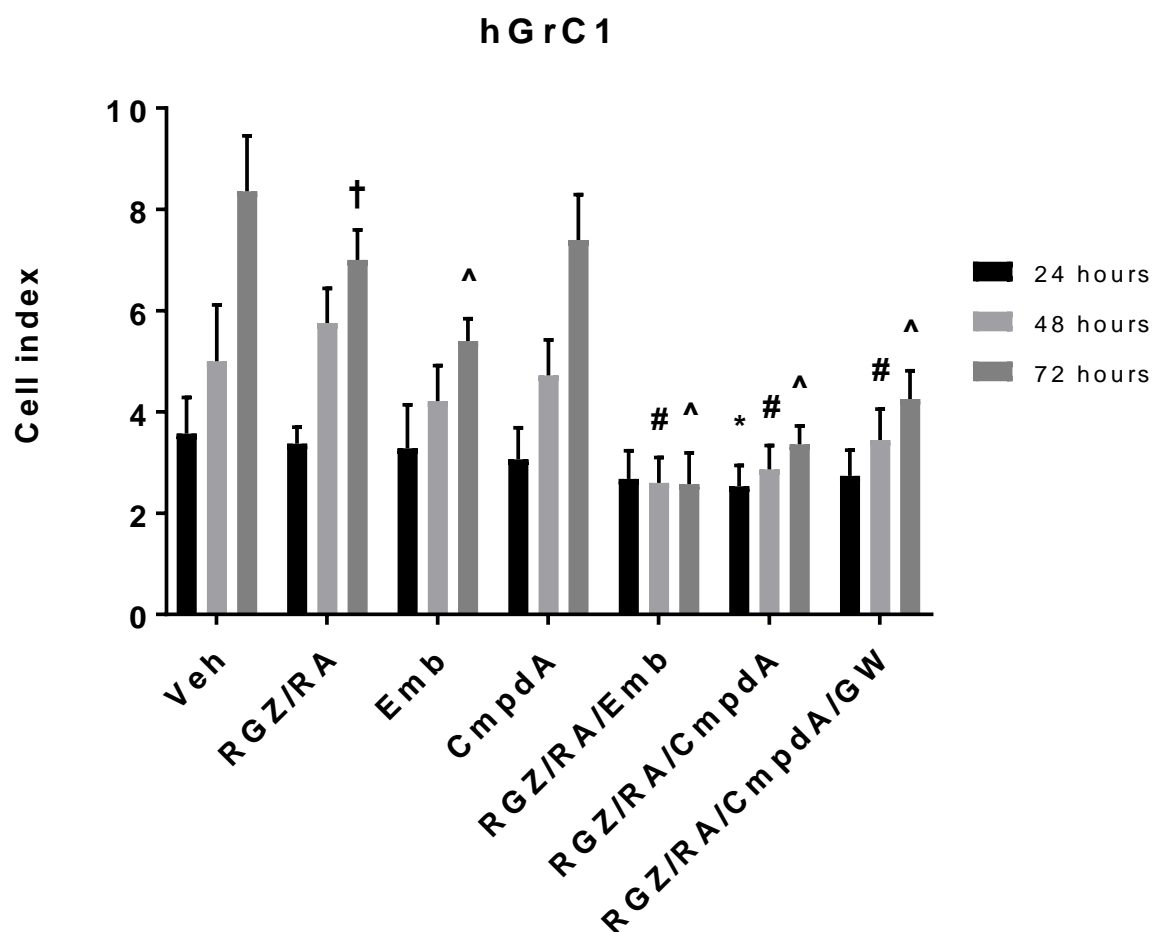


Figure 4C. Proliferation assay in the hGrC1 cells. Effects of PPAR γ activation (20 μ M RGZ/5 μ M RA) and XIAP inhibition (10 μ M Emb or 500nM CmpdA) on the hGrC1 cells was assessed over 24, 48 and 72 hours. No significant effect on cell proliferation was observed with the singular treatment. * $p < 0.05$ compared to Veh (0.1% DMSO) at 24 hours; # $p < 0.01$ compared to Veh at 48 hours; † $p < 0.05$ compared to Veh at 72 hours; ^ $p < 0.01$ compared to Veh at 72 hours. $n = 3$ in duplicate wells.

D

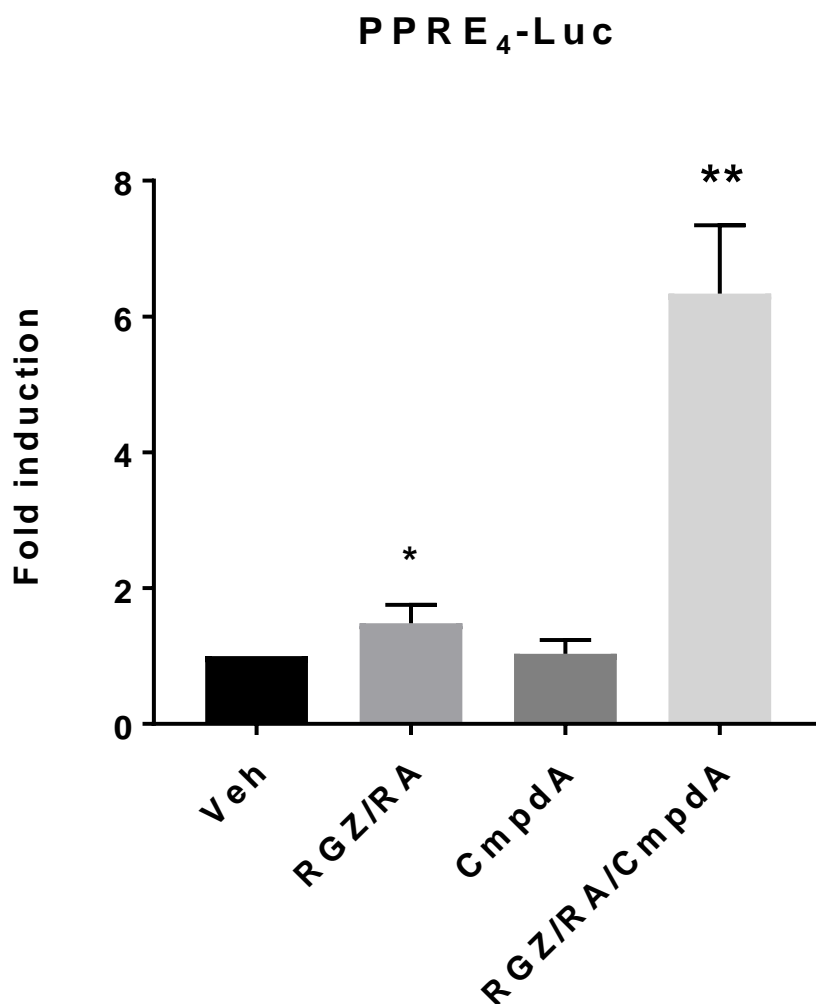


Figure 4D. Effects of RGZ/RA/CmpdA on PPAR γ -mediated transactivation.

PPRE₄-luc reporter transfected in the GCT-derived cell lines showed little activity when the cells were treated with PPAR γ .RXR α ligand, 20 μ M RGZ/5 μ M RA. Robust PPAR γ -mediated transactivation was observed when the cells were treated with RGZ/RA in combination with 500nM CmpdA. $n = 5$ in duplicate wells; Kruskal-Wallis; Dunn's post-hoc analysis; * $p < 0.05$, ** $p < 0.01$ when compared to Veh (0.1% DMSO).

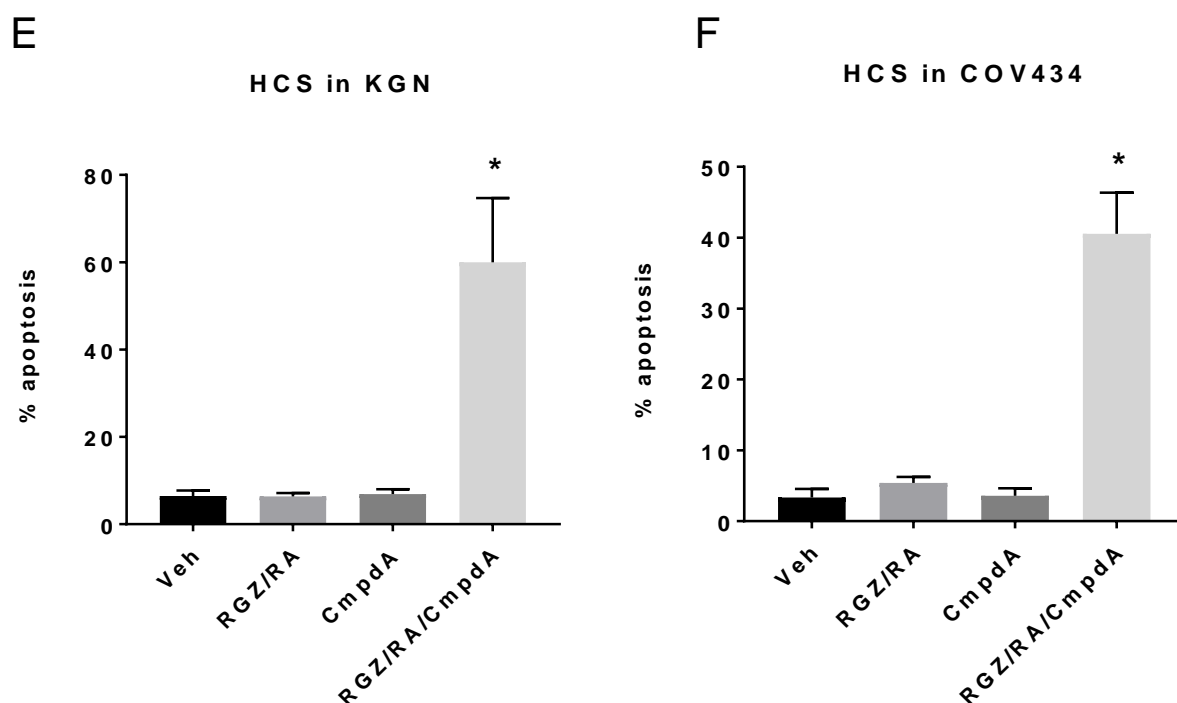


Figure 4E and F. Effects of RGZ/RA/CmpdA on apoptosis. High content screening (HCS) was used to assess apoptosis after 24-hour treatment of 20 μ M RGZ/5 μ M RA, 500nM CmpdA and RGZ/RA/CmpdA in the KGN (E) and COV434 (F) cells. No apoptosis was observed with singular treatment. Significant induction in apoptosis was seen in both cell lines following RGZ/RA/CmpdA treatment. $n = 5$ in triplicate wells; Kruskal-Wallis; Dunn's post-hoc analysis; * $p < 0.05$ when compared to Veh (0.1% DMSO).

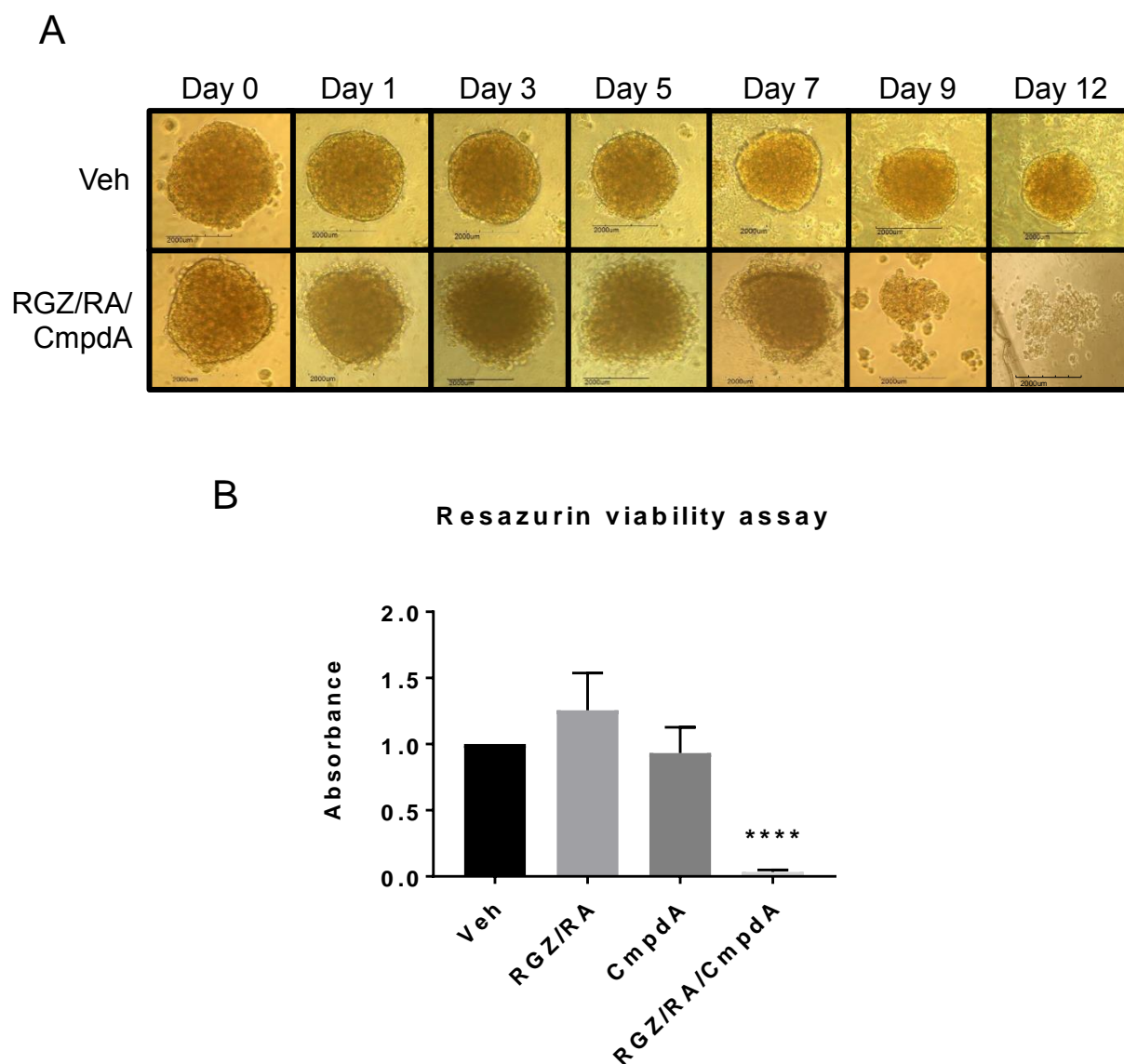
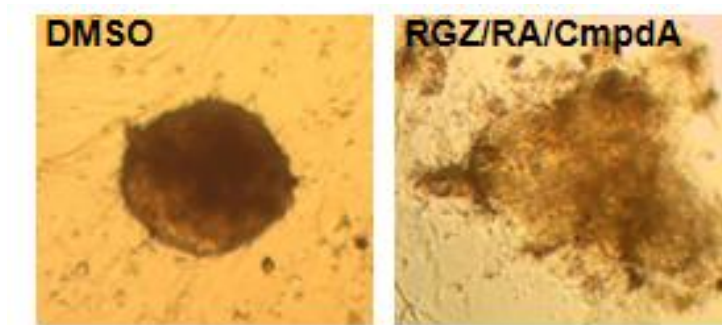


Figure 5. Effects of combined PPAR γ activation and XIAP inhibition in KGN spheroids. Combination treatment (RGZ/RA/CmpdA) at the same concentrations used for the 2D monolayer experiments caused disruption of KGN spheroid architecture from 24-hour treatment with gradual but complete spheroid dissociation occurring over 12-day treatment (A). This was due to a significant decrease in cell viability (B) as assessed using the resazurin viability assay. $n = 3$ with 4 spheroids in each experiment; One-way ANOVA; Tukey's post-hoc analysis; $*p < 0.05$ when compared to Veh (0.1% DMSO).

A



B

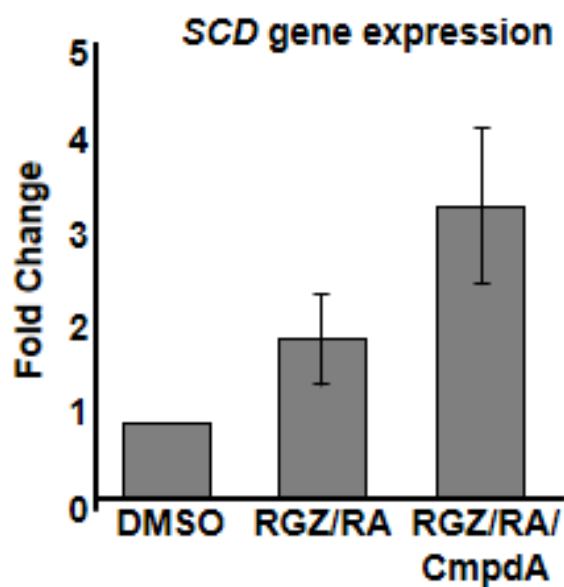


Figure 6. Effects of combined PPAR γ activation and XIAP inhibition in GCT explants. The combination treatment (20 μ M RGZ/5 μ M RA/500nM CmpdA) caused disruption of the GCT explants (n = 2) after 7-day treatment, with complete disruption and no cell viability (A). A robust induction of a PPAR γ -induced gene, steraoyl-CoA desaturase 1 (SCD), was also observed after the combination treatment in these GCT explants.

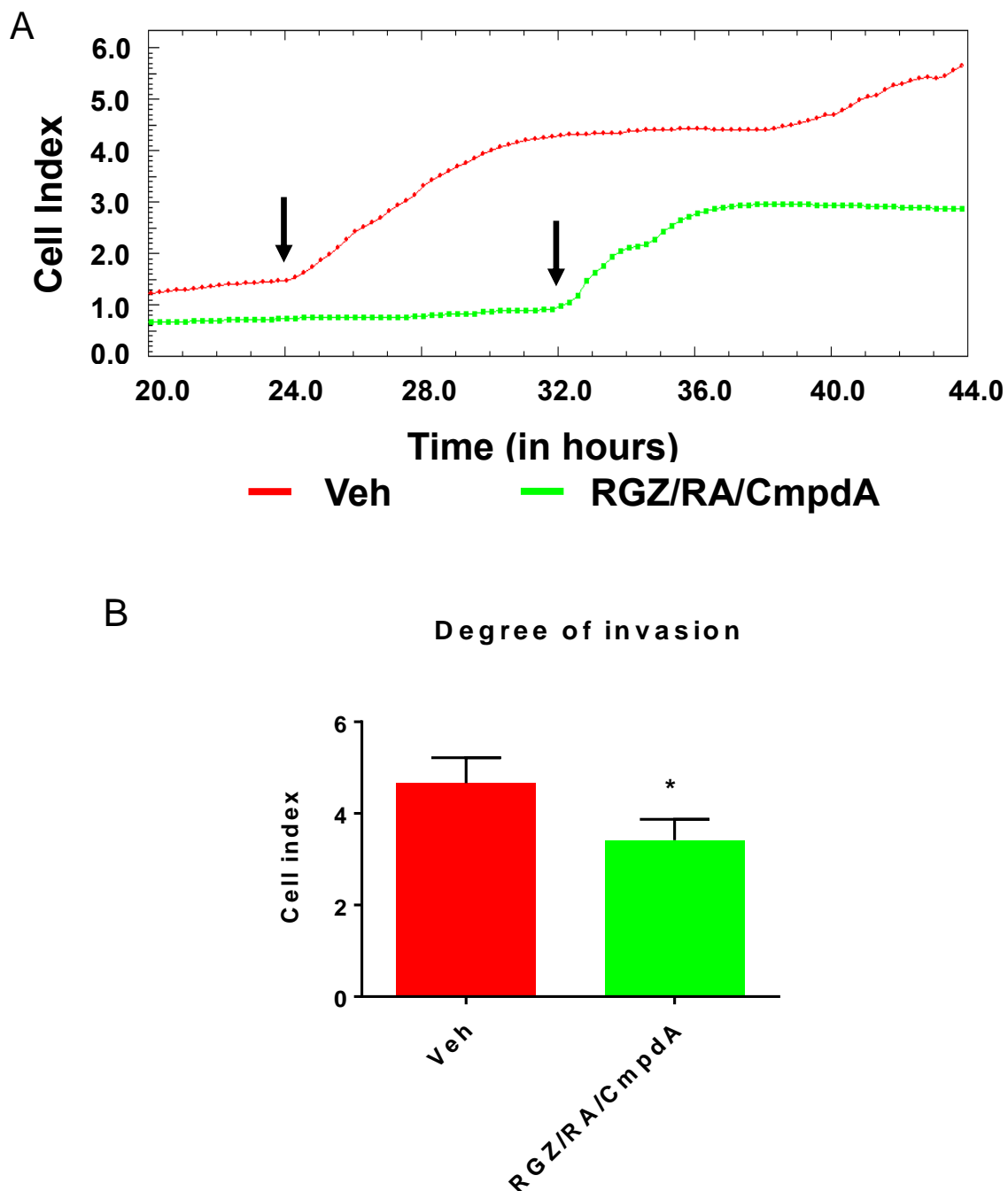


Figure 7. Effects of combined PPAR γ activation and XIAP inhibition on invasion using the xCELLigence RTCA system. The combination treatment (20 μ M RGZ/5 μ M RA/500nM CmpdA) caused a delayed onset of invasion by 8 hours (A; onset of invasion indicated by arrows) and 30% reduction in invasion in the treated cells than the vehicle (veh; 0.1% DMSO) treatment. $n = 3$ in duplicate wells; Student's t -test; $*p < 0.05$.

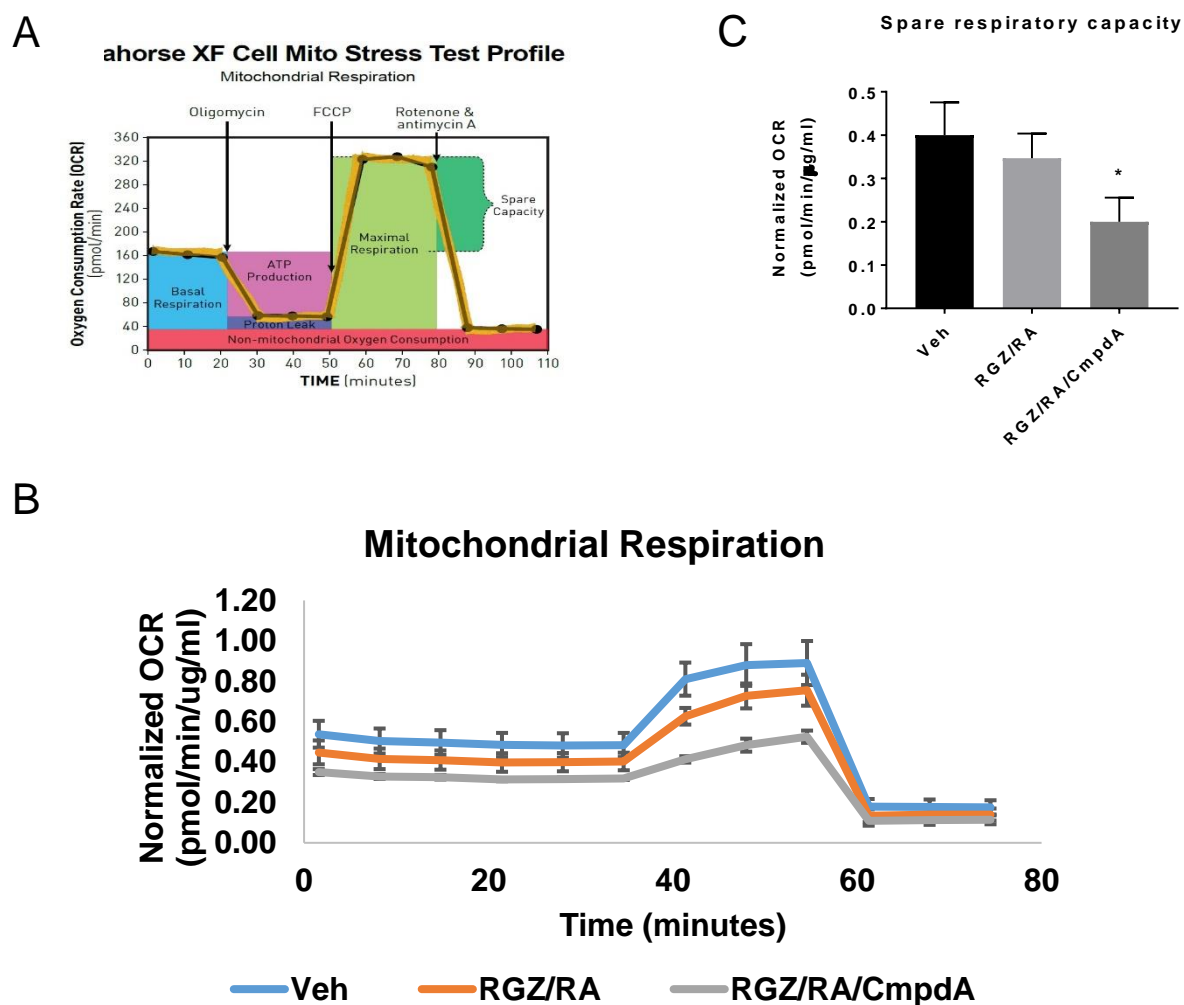


Figure 8. Effects of combined PPAR γ activation and XIAP inhibition on cellular energetics using the Seahorse Extracellular Flux Analyzer (XFp). A schematic representation of the design and interpretation of the assay. Mitochondrial respiration, represented by the oxygen consumption rate (OCR), was measured as the KGN cells were subjected to metabolic stressors, oligomycin, FCCP and antimycin A/rotenone (B). While the 20 μ M RGZ/5 μ M RA alone did not alter the spare respiratory capacity, when CmpdA was combined, significant reduction in the cells' ability to respond to an increased energy demand was observed. $n = 3$ in duplicate wells; One-way ANOVA; Tukey's post-hoc analysis; * $p < 0.05$ when compared to Veh (0.1% DMSO).

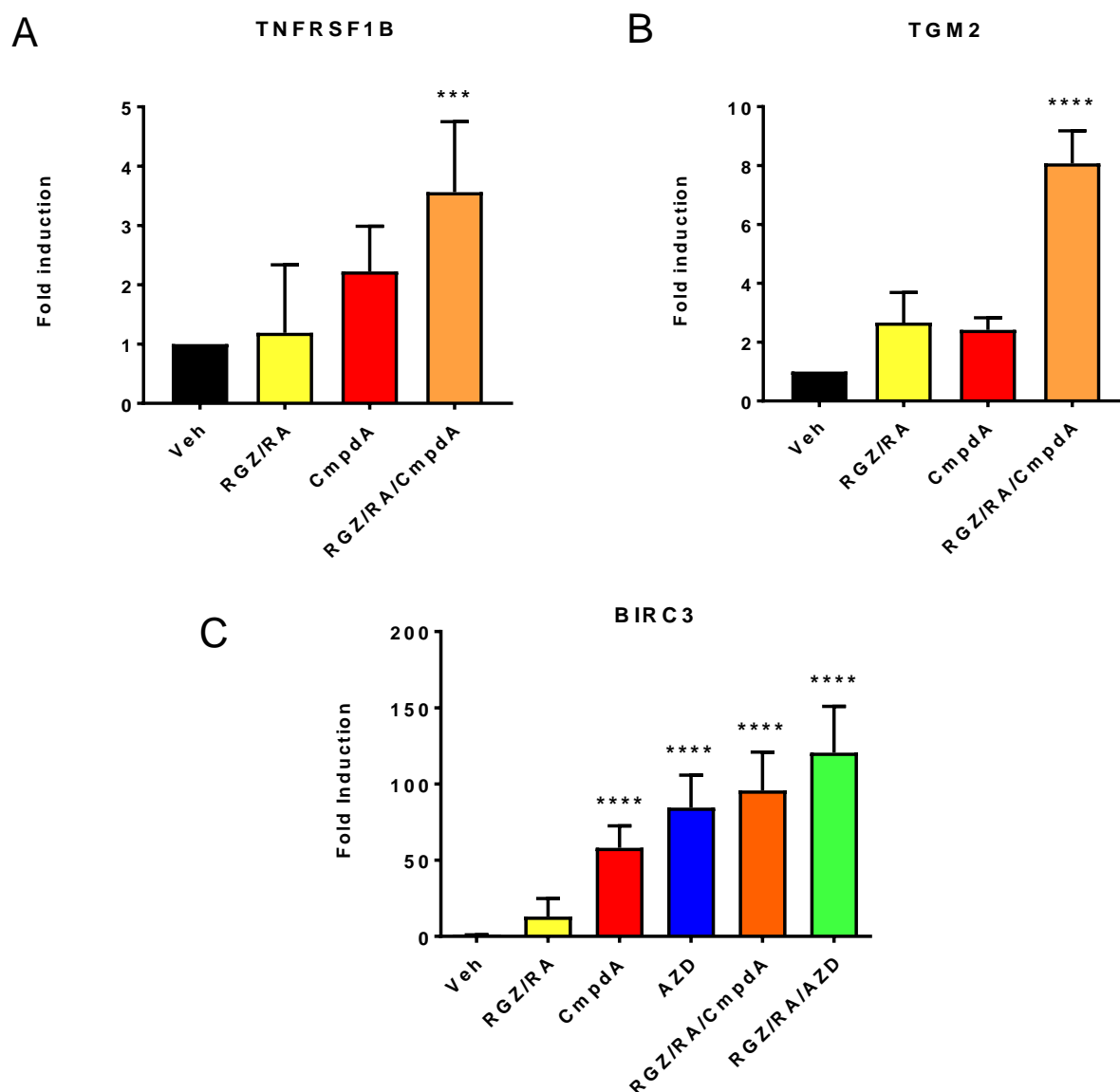
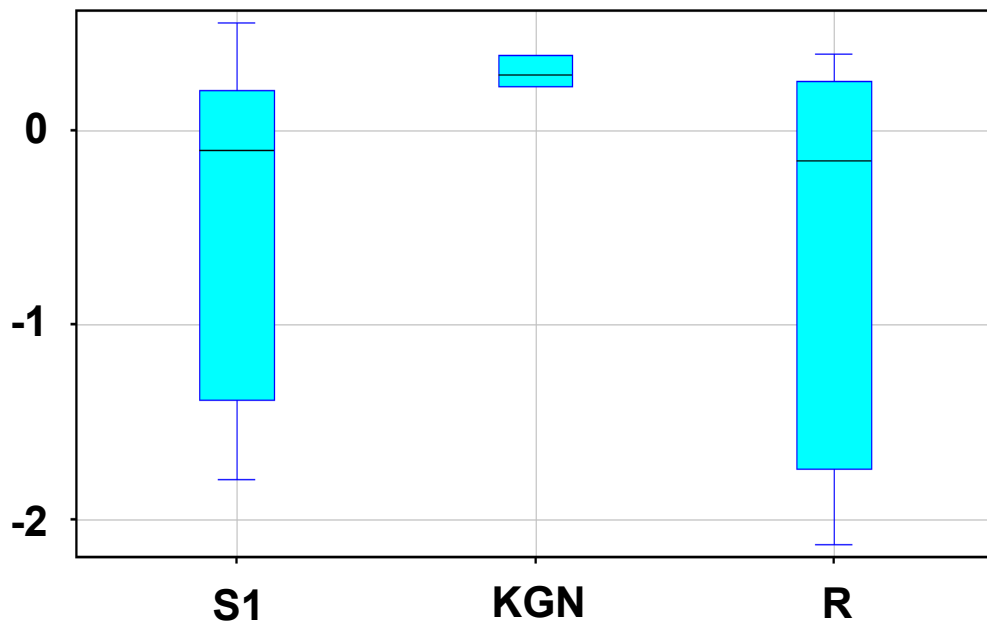
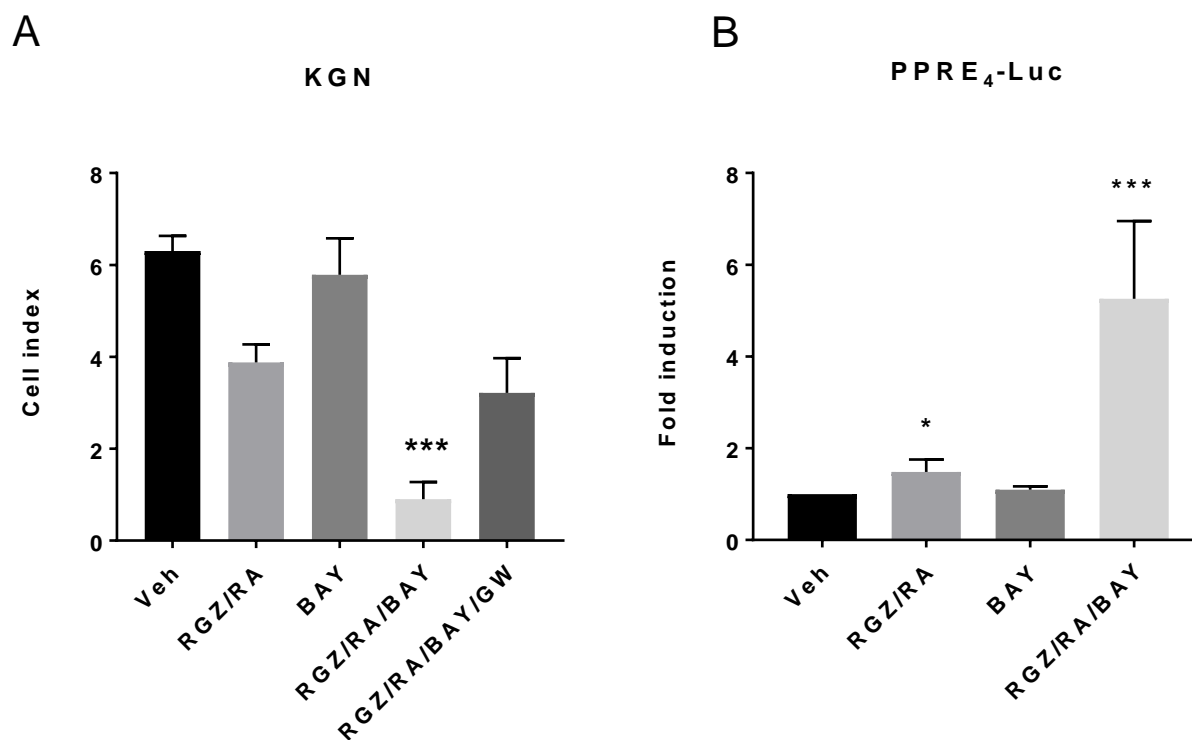


Figure 9. Effects of combined PPAR γ activation and XIAP inhibition on gene expression. Digital PCR showed significantly upregulated mRNA expression of the pro-apoptotic gene, *TNFRSF1B* (A) and *TGM2* (B), following the combined PPAR γ activation (20 μ M RGZ/5 μ M RA) and XIAP inhibition (10 μ M Emb or 500nM CmpdA). An IAP member, cIAP2, was also induced by the two Smac-mimetics, CmpdA and AZD (both at 500nM), alone or in combination with RGZ/RA. n = 3 – 7 in duplicate wells; Kruskal-Wallis; Dunn's post-hoc analysis; * $p < 0.05$, *** $p < 0.001$, **** $p < 0.0001$ when compared to Veh (0.1% DMSO).

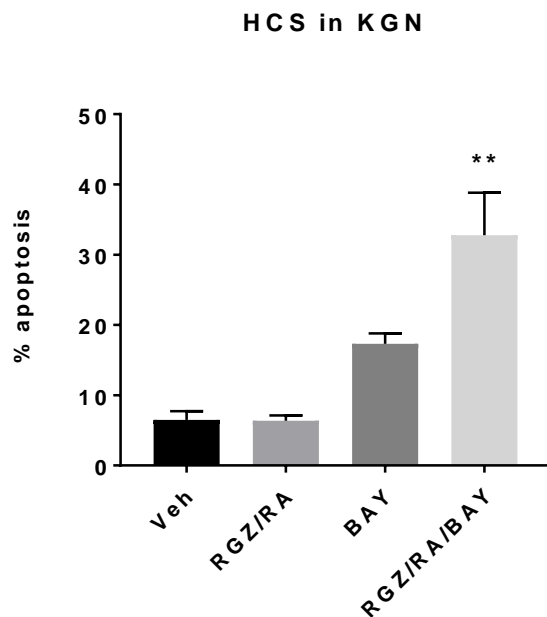


Supplementary figure 1. XIAP mRNA expression in GCT and GCT-derived cell line. Results from quantitative RT-PCR demonstrated no difference between the XIAP mRNA expression among 8 stage 1 GCT (S1), 8 recurrent GCT (R) and the GCT-derived cell line, KGN.

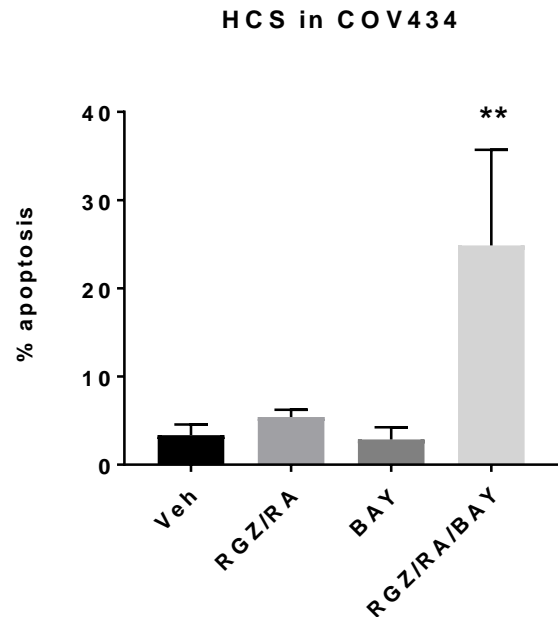


Supplementary figure 2A and B. Effects of combined PPAR γ activation and NF- κ B inhibition. A. Cell proliferation assay ($n = 6$ in duplicate wells) showed that a small but non-significant effect was observed when RGZ/RA and BAY was used singularly. Cell proliferation was ceased in KGN cells treated with RGZ/RA/BAY; this effect was reversed by the addition of GW. B. The KGN cells were transfected with the PPRE₄-luc reporter and subjected to 24-hour treatment ($n = 5$ in duplicate wells). A small but significant induction of the reporter activity was observed with RGZ/RA treatment while BAY alone showed no effect. Combined RGZ/RA/BAY treatment significantly induced PPAR γ -mediated transactivation in the KGN cells. Kruskal-Wallis; Dunn's post-hoc analysis; * $p < 0.05$; *** $p < 0.001$ when compared to Veh (0.1% DMSO).

C



D

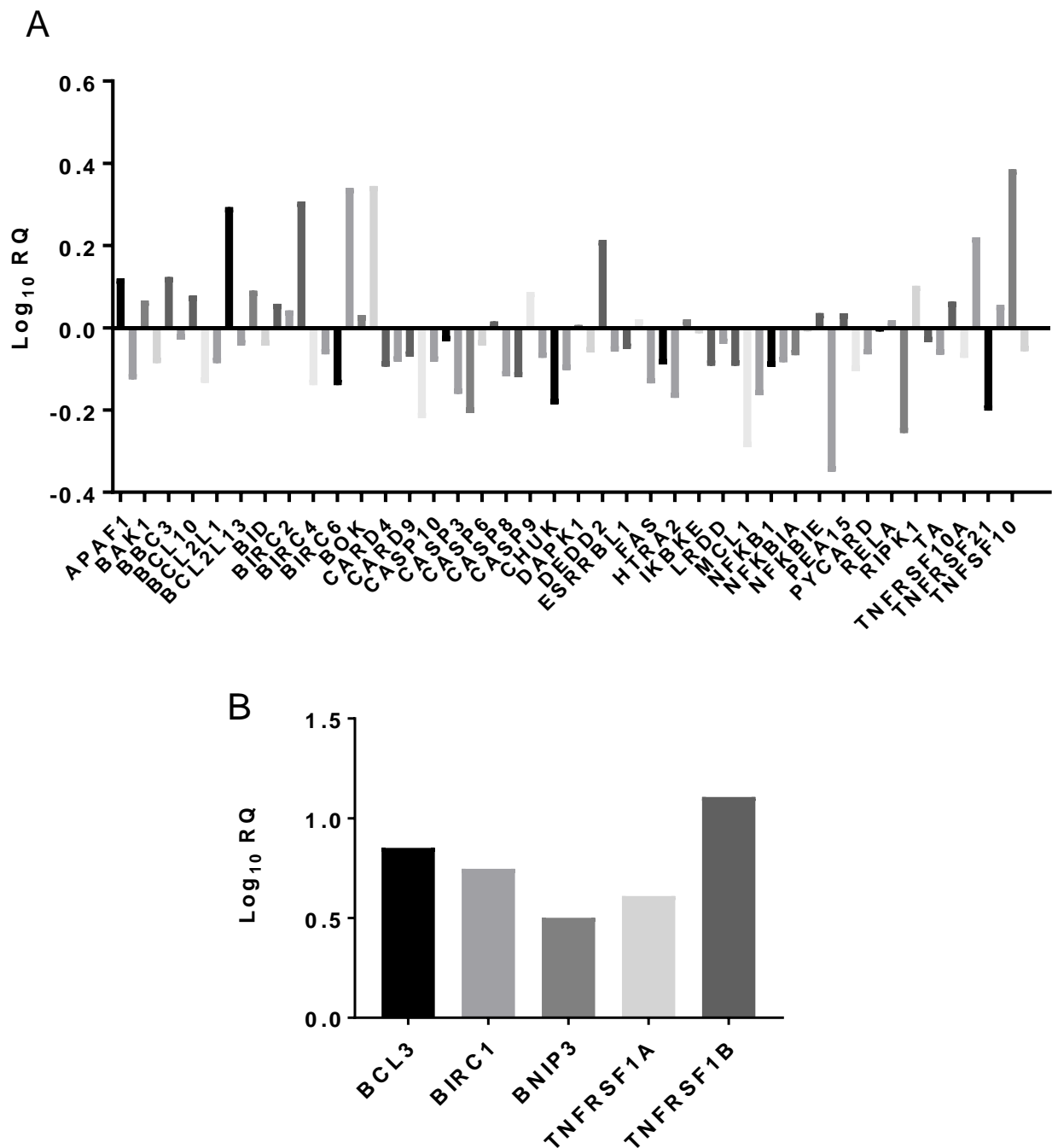


Supplementary figure 2C and D. Effects of combined PPAR γ activation and NF- κ B inhibition on apoptosis. High content screening (HCS) was used to assess apoptosis after 24-hour treatment of 20 μ M RGZ/5 μ M RA, 2 μ M BAY and RGZ/RA/BAY in the KGN (C) and COV434 (D) cells. No apoptosis was observed with singular treatment. Significant induction in apoptosis was seen in both cell lines following RGZ/RA/BAY treatment. $n = 5$ in triplicate wells; Kruskal-Wallis; Dunn's post-hoc analysis; * $p < 0.05$ when compared to Veh (0.1% DMSO).

Supplementary Table 1. Clinical information of patients of the GCT cohort.

GCT no.	Age	Stage	Type
GCT001	65	IC	Primary; Recurrence
GCT002	43	Unknown	Recurrence
GCT003	58	IC	Primary; Recurrence
GCT004	67	IA	Primary; Recurrence
GCT006	43	IC	Primary
GCT007	55	IC	Primary; Recurrence
GCT008	71	IA	Primary
GCT009	48	IIIC	Primary; Metastasis; Recurrence
GCT010	76	IA	Primary
GCT011	68	IA	Primary
GCT012	66	IA	Primary
GCT014	54	IA	Primary; Recurrence
GCT015	67	IIIC	Primary
GCT016	37	IA	Primary
GCT017	50	IA	Primary
GCT018	45	IA	Primary
GCT019	63	IA	Primary
GCT020	50	IC	Primary
GCT021	26	IC	Primary; Recurrence
GCT022	51	IA	Primary
GCT023	56	IIIC	Primary; Metastasis; Recurrence
GCT024	38	IIIC	Primary; Metastasis
GCT025	75	IIIC	Primary; Metastasis; Recurrence
GCT026	62	IA	Primary; Recurrence
GCT027	65	IIA	Primary
GCT028	48	IIC	Primary; Recurrence
GCT029	63	IV	Primary; Recurrence
GCT030	38	IA	Primary; Recurrence
GCT031	76	IA	Primary; Recurrence
GCT032	55	IC	Primary; Recurrence
GCT033	31	IA	Primary
GCT034	57	IA	Primary; Recurrence
GCT035	67	IA	Primary
GCT036	46	IA	Primary
GCT037	40	IA	Primary
GCT038	58	IA	Primary
GCT039	41	IA	Primary
GCT040	55	IA	Primary
GCT041	64	IA	Primary
GCT042	40	IA	Primary

GCT043	64	IA	Primary
GCT044	54	IIA	Primary
GCT045	46	IIIA	Primary
GCT046	60	IC	Primary
GCT047	35	IC	Primary
GCT048	54	IA	Primary
GCT049	43	IC	Primary
GCT050	44	IA	Primary
GCT051	77	IA	Primary
GCT052	35	IA	Primary; Recurrence
GCT053	42	IA	Primary
GCT054	38	IA	Primary
GCT055	55	IA	Primary
GCT056	40	IA	Primary
GCT057	Unknown	IA	Primary
GCT058	Unknown	IA	Primary
GCT059	Unknown	IA	Primary
GCT060	89	IA	Primary
GCT061	39	IA	Primary
GCT062	Unknown	IA	Primary
GCT063	Unknown	IA	Primary
GCT064	Unknown	IC	Primary
GCT065	84	IA	Primary
GCT066	49	IA	Primary; Recurrence
GCT067	Unknown	IIIA	Primary
GCT068	Unknown	IA	Primary
GCT069	Unknown	IA	Primary
GCT070	48	IA	Primary
GCT071	Unknown	IC	Primary
GCT072	52	IC	Primary
GCT073	48	IC	Primary
GCT074	40	IC	Primary
GCT075	34	IA	Primary
GCT076	Unknown	IA	Primary
GCT077	Unknown	IA	Primary
GCT078	Unknown	IC	Primary



Supplementary Figure 1. Gene expression analysis by TaqMan Low-Density Array. mRNA levels of apoptotic genes in the TGZ/Emb-treated cells were normalized to that of the housekeeping genes, and subsequently to that of the vehicle treatment. Log₁₀ of the relative quantification (RQ) value was calculated for genes that did not reach (A) or reached (B) statistical significance between the vehicle and treatment groups.

CHAPTER 4

**TARGETING XIAP AND PPAR γ IN GRANULOSA CELL
TUMORS ALTERS METABOLIC SIGNALING (publication)**

Targeting XIAP and PPAR γ in granulosa cell tumors alters metabolic signaling

Dilys TH Leung, Adam Rainczuk, Trang Nguyen, Peter J Fuller and Simon Chu

Hudson Institute of Medical Research and Monash University Department of Molecular Translational Science, Clayton, Victoria 3168, Australia

Running title: Targeting XIAP and PPAR γ in GCT

Keywords: Apoptosis; Granulosa cell tumors; Ovary; Proteomics; Receptor binding

Financial support

This work was supported by grants-in-aid from the Cancer Council Victoria; the Ovarian Cancer Research Foundation (SC); the Granulosa Cell Tumor of the Ovary Foundation; and the National Health & Medical Research Council of Australia through a Project Grant (grant number #1058334, 2014-2016) and a Senior Principal Research Fellowship to PJF (grant number #1002559, since 2001; Endocrine Society of Australia Research Higher Degree Scholarship to DL. The Hudson Institute is supported by the Victorian Government's Operational Infrastructure Scheme.

Corresponding author: Dr Simon Chu

Hudson Institute of Medical Research

██
██
██
██

Declaration of interest

The authors declare no conflict of interest.

Abstract

Ovarian granulosa cell tumors (GCT) are hormonally-active cancers characterized by indolent growth and late, invasive relapse. No therapies have been proven efficacious to date. We previously reported that inhibition of the X-linked inhibitor of apoptosis protein (XIAP) removes transrepression of the nuclear receptor, peroxisome proliferator-activated receptor (PPAR)- γ , in a GCT-derived cell line (KGN). Both PPAR γ and XIAP are abundantly expressed in human GCT. Inhibition of the anti-apoptotic XIAP with restoration of pro-differentiative PPAR γ signaling using a SMAC mimetic (SM) and rosiglitazone (RGZ)/retinoic acid (RA), respectively, results in a reduction of cell proliferation and induction of apoptosis in the KGN cells. To investigate the proteomic changes of this combined treatment, we utilised stable isotope labelling with amino acids in cell culture (SILAC) to identify differentially expressed proteins in the KGN cells following SM/RGZ/RA treatment. We identified a total of 32 differentially expressed proteins, 22 of which were upregulated by ≥ 1.5 fold with the combined treatment. The protein with the greatest magnitude of change, stearoyl-CoA desaturase (SCD), was further examined for putative binding sites for PPAR γ using in silico screening. Chromatin immunoprecipitation using KGN cell lysates confirmed the two identified putative binding sites and demonstrated increased binding in the SM/RGZ/RA-treated KGN cells. This is the first report to demonstrate the direct binding of PPAR γ on the promoter region of *SCD*. As PPAR γ plays a pivotal role in lipid and glucose metabolism, upregulation of proteins associated with metabolic processes such as SCD is consistent with the restoration of PPAR γ activity.

Introduction

Granulosa cell tumors (GCT) of the ovary are the most common type of ovarian sex-cord stromal tumors which contribute to approximately 5% of all ovarian cancers (1,2). The predominant adult GCT subtype (up to 97% compared to juvenile GCT) is defined by a single somatic FOXL2 C134W mutation (1). The incidence of these tumors peaks between 50 and 54 years. Patients who present with FIGO stage I disease have a relatively good prognosis. However, those who present with stage III/IV disease have a five-year survival rate of no greater than 50% (1). The characteristic indolent development of GCT implies that the disease often relapses in aggressive form many years after primary treatment. Hormonal or radiotherapies have limited efficacy; they are generally based on the regimen for the treatment of the more common epithelial ovarian cancer which despite a shared 'organ of origin' is a separate disease (2).

We have used the human GCT-derived cell lines, KGN, to identify potential therapeutic targets for the treatment of these cancers. The KGN cell line was established from a recurrent GCT (3). It harvests a FOXL2 C134W mutation and is used as a model of adult GCT (4). Using these human GCT-derived cell lines, we have identified using these human GCT-derived cell lines that the X-linked inhibitor of apoptosis protein (XIAP) and the peroxisome proliferator-activated receptor (PPAR)- γ are potential therapeutic targets. Both proteins are abundantly expressed in GCT (5,6). PPAR γ is involved in lipid and glucose metabolism. PPAR γ agonists, thiazolidinediones (TZD) such as rosiglitazone (RGZ) or pioglitazone are anti-diabetic drugs in current clinical use (7). In the ovary, PPAR γ is expressed in granulosa cells (GC) of developing follicles (8). It promotes terminal differentiation (9), inhibits proliferation and induces apoptosis in rat GC and primary GC (9,10). Overexpression of PPAR γ is seen in many

tumor types, namely thyroid (11) and colon (12) cancers. Given the involvement of PPAR γ in apoptosis and differentiation, the anti-tumor effects of TZDs have been investigated in various solid tumors (13-15). Abundant expression of PPAR γ in GCT despite its obvious anti-neoplastic effects appears paradoxical. In the KGN, the constitutively activated nuclear factor- κ B (NF- κ B) signaling (16) upregulates its effector protein, the anti-apoptotic XIAP, as well as transrepresses the pro-differentiating transcription factor, PPAR γ . Our study found that combining a specific inhibitor of NF- κ B, BAY11-7082, with RGZ (and retinoic acid (RA) to activate RXR α , the obligate heterodimeric partner), PPAR γ activity was induced in GCT cells.

The constitutive NF- κ B signaling in the KGN cells also upregulates its effector protein XIAP. XIAP is the most potent member of the Inhibitor of Apoptosis Protein (IAP) family. It physically interacts with caspase-3 and -7 via the linker region between the Baculoviral IAP Repeat (BIR) 1 and 2 domains, as well as caspase-9 via the BIR3 domain to inhibit both intrinsic and extrinsic apoptotic pathways (17). It is ubiquitously expressed across the body. In the ovary, XIAP is highly expressed in healthy follicles (18) and protects rat GC from apoptosis *in vitro* (19) and *in vivo* (20). XIAP has been implicated in malignancies including ovarian (21), pancreatic (22), nasopharyngeal (23) and acute myeloid leukaemia (24). Endogenous XIAP is inhibited by the mitochondrial protein, second mitochondrial-derived activator of caspases (SMAC). It binds and blocks the BIR2 and 3 domains of XIAP to inhibit their caspase-binding activity (25,26). SMAC mimetics (SM), the synthetic analogues of the endogenous SMAC, are in clinical trials for various cancers (27,28). Similar to SM, there are small molecule inhibitors that have been designed to block IAP binding to caspases, and thus unable to block caspase activities. These have led to reports that show this approach leads to

induction of apoptosis and sensitizing of malignant cell lines to chemotherapy (26,29). One promising example of a BIR3 inhibitor is embelin. Embelin is a cell-permeable, small molecular weight inhibitor of XIAP. It inhibits growth and induces apoptosis by binding to BIR3 domain of XIAP, activates caspase 9 activity (30) as well as caspase-3 and BAX (31).

In the ovary, XIAP is regulated by follicle stimulating hormone (FSH) and NF- κ B (32). We also identified the involvement of XIAP in a feed-forward loop which contributes to the constitutive NF- κ B activity in GCT cells (Leung *et al.*, concurrent publication). Given the regulatory role of XIAP in NF- κ B signaling, we used SM to inhibit XIAP and remove the NF- κ B transrepression of PPAR γ . By combining XIAP inhibition (SM) with PPAR γ activation (RGZ and RA), we observed significant induction of apoptosis, a significant reduction in cell viability and proliferation in the KGN cell line. In this study, we have identified differentially expressed proteins after combined XIAP inhibition and PPAR γ activation of the KGN cells.

Materials and methods

Cell culture and Stable Isotope Labelling with Amino Acids in Cell Culture (SILAC)

Human GCT-derived cell line, KGN, was established as previously described (3). The cells were cultured in SILAC DMEM:F12 containing no arginine and lysine at a 37 °C humidified incubator with 5% CO₂.

For labelling, DMEM:F12 was first supplemented with 10% dialysed foetal bovine serum (FBS), 1% penicillin/streptomycin and 2.4% HEPES buffer. The medium was supplemented with either ¹³C6-¹⁵N4-arginine (*Arg-10*) and ¹³C6-¹⁵N2-lysine (*Lys-8*) or

the naturally occurring $^{12}\text{C}_6$ -arginine and -lysine to produce heavy or light SILAC medium, respectively. Incorporation of heavy or light amino acids (>95%) was confirmed after five passages using mass spectrometry.

Drug treatments

All treatments were performed in media containing 2% dialysed FBS. Compounds used include RGZ (20 μm) and RA (5 μm) in combination with SM (500 nm) or embelin (Emb; 20 μm). RGZ, RA and Emb were purchased from Sigma Aldrich, St. Louis, MO, USA; SM is a gift from A/Prof John Silke, Walter Eliza Hall Institute, Melbourne, Australia. 'Light' cells were used as vehicle control with 0.1% DMSO (Sigma Aldrich) while 'heavy' cells were treated with the compounds listed above. A reciprocal experiment was performed where 'heavy' cells were the control and 'light' cells were treated with the compounds. After 24-hour treatment, the cells were lysed with Universal Immunoprecipitation (UIP) lysis buffer (50 mM Trizma base, 150 mM NaCl, 2 mM EDTA, 2 mM EGTA, 25 mM NaF, 0.2% Triton X-100, 0.3% Nonidet P-40 and 25 mM β -glycerolphosphate) and protease inhibitor cocktail tablet (Roche Applied Science, Penzberg, Germany; 1 tablet per 10 ml of UIP lysis buffer). The lysates were precipitated using acetone to remove undesirable substances that may interfere with downstream analyses. Following incubation with acetone for 60 minutes at $-20\text{ }^\circ\text{C}$, the proteins were pelleted by centrifugation and the supernatant was removed.

Sample preparation

Acetone-precipitated protein pellets were kept at $-80\text{ }^\circ\text{C}$ until processed. All centrifugation was performed at 14,000 x g. Each pellet was resuspended in 7 M urea and incubated in a sonicating water bath. 15 μg of each sample was mixed with 7 M urea, added to spin column and centrifuged for 15 minutes; the flow-through was discarded. 100 μl of 20 mM dithiothreitol was added to each spin column, centrifuged

for 10 minutes and the flow-through discarded. This was followed by the addition of 100 μ l of 55 mM iodoacetamide in 7 M urea with 20 minutes of incubation and 10 minutes of centrifugation. After discarding the flow-through, 100 μ l of 7 M urea was added to a Vivacon® 500 spin column (10 kDa molecular weight cut-off; Sartorius Stedium Biotech, Goettingen, Germany) and centrifuged for 15 minutes – this step was repeated three times. Next, 100 μ l of 50 mM ammonium bicarbonate was added and centrifuged for 15 minutes three times. For digestion, trypsin solution (Promega, Madison, WI, USA; enzyme to protein ratio = 1:50) was added to each column filter and incubated overnight at 37 °C. The digested peptides were centrifuged for 10 minutes and the flow-through was collected. 50 μ l of 1% formic acid (FA) then 100 μ l of 1% FA was added to the column filter, each followed by centrifugation for 10 minutes. The peptide extracts were lyophilised by vacuum centrifugation to approximately 2 μ l and then re-suspended with 0.1% trifluoroacetic acid in 2% acetonitrile (ACN) to a total volume of 100 μ l.

Liquid Chromatography – electrospray ionization tandem mass spectrometry

5 μ l (15 μ g) of each peptide sample was separated on a HPLC system (Thermo Fisher Scientific, Berman, Germany) using a separation column (Acclaim PepMap RSLC, C18, pore size 100 Å, particle size 2 μ m, 75 μ m inner diameter \times 15 cm length; Thermo Fisher Scientific) and a trapping column (Acclaim PepMap100, C18, pore size 100 Å, particle size 3 μ m, 75 μ m ID \times 2 cm length; Thermo Fisher Scientific). The HPLC system was coupled to a LTQ Orbitrap XL mass spectrometer (Thermo Fisher Scientific), using the following buffer system: (A) 2% ACN, 0.1% FA in water; (B) 80% ACN, 0.1% FA in water. For direct injection into the mass spectrometer, 1 μ l of the digests was loaded onto the trap column and washed for 5 minutes with 100% A at a flow rate 5 μ l/min. Peptides were eluted at a 300 nl/min flow rate with the following 100

min gradient: 4% B for 10 minutes, gradient to 40% B over 50 minutes, gradient to 90% B in 20 minutes, 90% B for 10 minutes, gradient from 90% to 4% B in 30 s, 4% B for 19.5 minutes. The LTQ Orbitrap XL instrument was operated in data-dependent mode to automatically switch between full scan MS and MS/MS acquisition. Instrument control was through Thermo Tune Plus and Xcalibur software (Thermo Scientific).

Full scan MS spectra ($m/z = 300\text{--}1700$) was acquired in the orbitrap analyzer and resolution in the orbitrap system was set to $r = 60,000$. The standard mass spectrometric conditions for all experiments were: spray voltage, 1.25 kV; no sheath and auxiliary gas flow; heated capillary temperature, 200 °C; predictive automatic gain control enabled, and an S-lens radio frequency level of 50–60%. All unassigned charge states and charge state of one were rejected. The 6 most intense peptide ions with charge states ≥ 2 and minimum signal intensity of 1000 were sequentially isolated and fragmented in the high-pressure linear ion trap by low-energy collision-induced dissociation. An activation $q = 0.25$, activation time of 30 ms and normalized collision energy of 35% were used. The resulting fragment ions were scanned out in the low-pressure ion trap at the “normal scan rate” (33,333 amu/s) and recorded with the secondary electron multipliers.

Data analysis

Raw data were processed with MaxQuant software (version 2.3.02) and its built-in Andromeda search engine using the following parameter settings: trypsin as enzyme with two missed cleavages allowed, *Homo sapiens* as organism, oxidation (M) as variable modification, carbamidomethylation (C) as a fixed modification, 10 ppm MS tolerance, 0.8 Da fragment mass tolerance, peptide and protein false discovery rate both at 1% ($P < 0.05$ significance threshold). The peak lists were searched against the Swiss-Prot database (version 2014_02).

Protein ratio quantification was adjusted for lysine/arginine labelling bias and a normalized ratio was calculated for each protein within each sample. Proteins that were identified in both reciprocal experiments and differentially expressed by ≥ 1.5 -fold were retained. At least one unique peptide must be identified for any protein to be included in further analyses. Protein ratios from the reciprocal experiments were averaged to calculate the final fold change.

Construction of protein-protein interaction network and functional annotation analysis

Regulated proteins were subjected to association analysis using STRING database (Search Tool for the Retrieval of Interacting Genes/Proteins version 10: (33)) to build a protein-protein interaction network. Identification of the over- or under-represented Gene Ontology (GO) biological processes was performed using GO Enrichment Analysis (<http://geneontology.org/>) (34).

SDS PAGE and western blot analysis

For western blot analysis, 50 μ g of total protein was separated by SDS-PAGE gel (10% resolving and 5% stacking). Proteins were transferred to a PDVF membrane using the Bio-Rad Mini Trans-Blot electrophoretic transfer system at 4 °C overnight. The membrane was blocked for 1 hour at room temperature with TBS (50 mM Tris-HCl, 150 mM NaCl; pH 7.6) containing 5% BSA (Roche Applied Science). Incubation with mouse monoclonal anti-SCD1 antibody (1:1000; Abcam, Cambridge, UK) in 1% TBST (TBS with 1% Tween 20) was performed at 4 °C overnight with gentle rocking. Subsequently, the membrane was incubated with goat anti-mouse horseradish peroxidase-conjugated secondary antibody (1:4000; Dako, Agilent Technologies, Santa Clara, CA, USA) for 2 hours at room temperature. Proteins were detected by applying Amersham ECL Prime Western Blotting Detection Reagent (GE Healthcare,

Little Chalfont, UK). The membrane was imaged and quantified using the Bio-Rad ChemiDoc™ XRS+ System and Image Lab version 4.1 (Bio-Rad, Hercules, CI, USA).

Digital PCR Fluidigm® Biomark HD™ System

RNA was extracted from the KGN cells following drug treatments with DMSO, RGZ/RA, SM or Emb alone, SM/RGZ/RA or Emb/RGZ/RA. The integrity of the RNA was assessed using Agilent 2100 Bioanalyzer at the Single Cell Genomic Centre, Monash Health Translation Precinct, Melbourne, Australia. All RNA samples have a 260:280 ratio of between 1.5 to 1.8 and a RNA Integrity Number (RIN) of greater than 9.500 of RNA was used for cDNA synthesis with SuperScript III Reverse Transcriptase (Invitrogen, Thermo Fisher Scientific, Waltham, MA, USA). The RIN algorithm ranks the quality of RNA based on the presence or absence of degradation products at a scale of 1 to 10, where level 10 RNA is completely intact. For gene expression analysis using the Fluidigm® Biomark HD™ System, all cDNA was pre-amplified to increase the number of copies of each gene to detectable levels as per Fluidigm® Gene Expression Specific Target Amplification Quick Reference PN 68000133 RevC. 45 genes were selected based on several proteins identified from the SILAC study, as well as genes that are involved in apoptosis, cell cycle and steroidogenesis. 48 Taqman gene expression assays and 48 samples including 3 housekeeping genes and 2 negative controls were combined in a 48.48 Dynamic array IFC according to Fluidigm® 48.48 Real-Time PCR Workflow Quick Reference PN 6800088. Data was analyzed using the Fluidigm® Real-Time PCR Analysis software version 4.1.2.

Screening for putative binding sites

We screened a region of 10 kb upstream of the *SCD* transcriptional start site (www.ensembl.org/index.html) for PPAR γ binding using the JASPAR dataset (<http://jaspar.genereg.net/>; relative profile score threshold 80%) (35). Primers were

designed to amplify regions capturing the putative binding sites to confirm binding following chromatin immunoprecipitation (ChIP).

Chromatin preparation

2×10^7 KGN cells were plated on 150 mm dish. Cell viability of >90% was confirmed using the Countess Automated Cell Counter (Thermo Fisher Scientific). The KGN cells were subjected to 0.1% DMSO, RGZ/RA (20 μ M/5 μ M) or SM/RGZ/RA (500 nM/20 μ M/5 μ M) for 6 hours. Chromatin was cross-linked by formaldehyde at a final concentration of 1% added directly to the cells, mixed gently and incubated at room temperature for 10 minutes. The cross-linking reaction was quenched by glycine at a final concentration of 0.125 M. Cells were washed with an equal volume of cold (4 °C) PBS and lysed with 5 ml of cold Farnham lysis buffer (5 mM PIPES pH 8.0, 85 mM KCL, 0.5% Nonidet P-40, Roche cOmplete™ EDTA-free protease inhibitor cocktail tablet). Cells were pelleted at 2,000 rpm for 5 minutes at 4 °C and then passed through a 21-gauge needle 20 times. Following centrifugation at 2,000 rpm for 5 minutes at 4 °C, the supernatant was removed and the pellet was resuspended in 300 μ l of cold RIPA buffer (1X PBS, 1% NP-40, 0.5% sodium deoxycholate, 0.1% SDS, Roche cOmplete™ EDTA-free protease inhibitor cocktail tablet). The DNA was sheared with Covaris® S220 Focused-ultrasonicator in a circulating water bath using the following parameters: peak power of 105 watts, duty factor of 2 and 200 cycles per burst for 4 minutes at 4 °C. 50 μ l of the sonicated DNA was set aside as the input DNA.

Immunoprecipitation

250 μ l chromatin was incubated with 50 μ l of goat anti-rabbit IgG magnetic beads (New England Biolabs, Ipswich, MA, USA) pre-coupled with 5 μ g of anti-PPAR γ antibody (Abcam #ab45036) on a rotator platform for 1 hour at 4 °C. Beads containing immune-

bound chromatin were washed 5 times with cold IP wash buffer (100 mM Tris pH 7.5, 500 mM lithium chloride, 1% NP-40, 1% sodium deoxycholate) with mixing for 3 minutes for each wash on a rotator. Following washing and mixing with 1 ml of TE buffer (10 mM Tris-HCl pH 7.5, 0.1 mM Na₂EDTA) for 1 minute on the rotator, the bead pellet was resuspended in 200 µl of IP elution buffer (1% SDS, 0.1 M NaHCO₃). To elute the immune-bound chromatin from the beads, the bead pellet was incubated in a 65 °C water bath for 1 hour and vortexed every 15 minutes. The supernatant containing the DNA was collected following centrifugation at 14,000 rpm at room temperature for 3 minutes. The cross-linking was reversed by incubation in a 95 °C water bath for 15 minutes.

400 µg of proteinase K (Roche Applied Science) was added to the DNA and incubated at room temperature for 2 minutes. The DNA was then cleaned up using the PCR purification kit (Qiagen, Hilden, Germany) according to the manufacturer's instructions. The DNA was eluted in two 15 µl aliquots of warmed buffer EB.

Confirmation of PPAR_γ putative binding sites

PCR amplifying the putative binding site was performed to confirm PPAR_γ binding on *SCD*. Primers were as follows: for -3293 to -3274, sense, 5'-CCACCAATCTACTTTCTGTCTC-3' and antisense, 5'-GGTAACAAAGTGAGACCCTATC-3'; for -7908 to -7889, sense, 5'-GGCAGCTGTGGCATAGTCA-3' and antisense, 5'-GGGCTGAGGCTGTCATTTCT-3'. The samples were denatured at 95 °C for 5 minutes, amplified for 32 (-3293 to -3274) or 27 (-7908 to -7889) cycles at 95 °C for 30 seconds, 60 °C for 30 seconds and 72 °C for 40 seconds, with a final extension step at 72 °C for 7 minutes. The PCR

products were loaded on a 1.5% agarose gel stained with SYBR® Safe (Thermo Fisher Scientific).

Statistical analyses

Drug treatments for ChIP, RNA or protein extraction were performed in duplicates and repeated at least three times. Data are presented as mean \pm SD. One-way ANOVA or the non-parametric equivalent, Kruskal-Wallis test was used for statistical analyses where $P < 0.05$ is considered statistically significant.

Results

Combined XIAP inhibition (SM or Emb) and PPAR γ (RGZ and RA) activation leads to induction of apoptosis in human GCT-derived cell lines (Leung *et al.*, concurrent publication). In order to understand the underlying mechanisms of this response, we utilised SILAC to identify the proteomic changes. Incorporation of the heavy and light amino acids was confirmed using mass spectrometry prior to drug treatment in the KGN cells (Supplementary figure 1). Altogether, a total of 569 proteins were identified in the KGN cells after SM/RGZ/RA or Emb/RGZ/RA treatment. Of these, 22 were upregulated and 10 downregulated by ≥ 1.5 fold after the combined treatment (Supplementary table 1 and 2). We then used the *Search Tool for the Retrieval of Interacting Genes/Proteins* (STRING v10) to identify any interactions between the regulated proteins and classify these proteins according to their biological processes. GO Enrichment Analysis identified several subsets of proteins which were enriched for various steps involved in the canonical glycolysis pathways ($P < 0.05$) (Supplementary table 3). The significant upregulation of metabolic pathways is consistent with the restoration of PPAR γ activity upon removal of the NF- κ B transrepression by the XIAP

inhibitors, SM and Emb. No pathway was found to be over- or under-represented amongst the downregulated proteins.

Stearoyl-CoA desaturase was upregulated by combined XIAP and PPAR γ treatment

Among the 22 upregulated and 10 downregulated proteins, stearoyl-CoA desaturase (SCD) showed the greatest fold of change after SM/RGZ/RA treatment compared to vehicle. Orbitrap mass spectrometry analysis identified 4.50- and 4.59-fold (average change of reciprocal experiments) of induction in SCD in the KGN cells after combined SM/RGZ/RA and Emb/RGZ/RA treatment, respectively (Supplementary table 4).

In KGN cells, western blot analysis demonstrated that SCD protein levels were significantly increased after SM/RGZ/RA (3.47 fold) and Emb/RGZ/RA (4.28 fold) treatment (Figure 1A and B) confirming the mass spectrometry findings. We also investigated the response of SCD at the messenger RNA level. SCD is encoded by the stearoyl-CoA desaturase (*SCD*) gene. Digital PCR using the Fluidigm® Biomark HD™ system demonstrated that *SCD* mRNA was upregulated by 3.31- and 3.97-fold after 24-hour treatment with SM/RGZ/RA and Emb/RGZ/RA in the KGN cells, respectively (Figure 1C).

Upregulation of proteins and genes associated with metabolism

Besides SCD, functional annotation of differentially regulated proteins performed by GO Enrichment Analysis revealed an over-representation of the canonical glycolysis pathway ($P < 0.05$) (Supplementary table 5). Following selection based on the magnitude of change, we quantified the levels of the mRNA that encode for the proteins involved in this biological process using the Fluidigm® Biomark HD™ system. Besides SCD, we also identified other targets that are regulated by the combined PPAR γ and XIAP treatment. This includes acyl-CoA synthetase long-chain family

member 3 (ACSL3) and α -enolase (ENO1). ACSL3 protein levels were significantly increased by Emb/RGZ/RA as identified by mass spectrometry (data not shown). ACSL3 mRNA expression was increased by both SM/RGZ/RA and Emb/RGZ/RA treatment (Figure 2). ENO1 demonstrated an induction consistent at both the mRNA (Figure 3) and protein level (data not shown) following Emb/RGZ/RA treatment.

PPAR γ binding sites on *SCD* promoter region

SCD plays a role in fatty acid and cholesterol synthesis (36). To date, no known function of SCD in the ovary has been documented. It has been previously shown that PPAR γ agonists increase SCD protein and mRNA in adipose tissue (36,37). However, there are no reports whether there are PPAR γ binding sites in the promoter. To test this, we screened a region 10 kb upstream of the *SCD* transcriptional start site (www.ensembl.org/index.html) for putative PPAR γ binding using the JASPAR dataset (<http://jaspar.genereg.net/>; relative profile score threshold 80%) (35). Two putative binding sites for PPAR γ were identified between nucleotide point -7908 to -7889 and -3293 to -3274 relative to the start site of transcription.

Following 6-hour of drug treatment with DMSO, RGZ/RA or SM/RGZ/RA, ChIP-PCR analysis demonstrated a significant increase in PPAR γ binding at nucleotide point -3293 to -3274 (Figure 4A). There appears to be an increase at -7908 to -7889, however, this does not reach significance (Figure 4B).

SCD, ACSL3 and ENO1 were detected in untreated KGN cells and human GCT samples

We have previously performed a whole transcriptome analysis of 12 human GCT and the KGN cells (38) which enabled us to analyze the levels of SCD, ACSL3 and ENO1 mRNA in untreated KGN cells and human GCT using this data set. *SCD* mRNA was

detected in all samples. The stage (stage 1 versus recurrent) of the disease does not alter the level of expression; the KGN cells showed similar level of *SCD* mRNA as the human GCT samples (Figure 5). Similarly, *ACSL3* and *ENO1* were both detected in all samples with similar levels of expression in the stage 1 and recurrent GCT (Supplementary figure 2 and 3). Statistical analysis was not performed with only one cell line included in the data set.

Discussion

XIAP is considered as an attractive therapeutic target due to its impact on both the intrinsic and extrinsic apoptotic pathways (17). XIAP inhibitors, SM, which mimic the function of endogenous SMAC, has been tested as anti-tumor agents in clinical trials (27,28,39). Downregulation of XIAP has also been shown to induce apoptosis in chemoresistant human ovarian cancer cell lines (40,41). Although originally designed to inactivate XIAP, SM is also effective in producing rapid ubiquitylation and proteosomal degradation of cIAP1 (42,43), another member of the IAP family which also binds to caspases-3, -7 and -9 but with a lower affinity than XIAP (44). We have shown that XIAP is the predominant IAP expressed in GCT, the levels of other members are low. Thus the effect that we see is likely XIAP-specific.

PPAR γ is a transcription factor which promotes differentiation and induces apoptosis in the ovary (9). PPAR γ is also involved in the regulation of lipid and glucose metabolism. PPAR γ agonists, the TZD, have been developed to treat patients with type II diabetes (7). Modulation of PPAR γ action using TZD has also been found to exert anti-neoplastic effects in various solid tumors (13-15). The pro-differentiating role of PPAR γ has been associated with tumor development and progression (11).

Previous studies have demonstrated the overexpression of PPAR γ in many tumor types and in various cancers such as the colon (12) and thyroid (45), activation of PPAR γ reduced cell viability and inhibited cell proliferation. This anti-tumor effect of PPAR γ agonists has also been observed in xenograft model of solid tumors (46).

The use of XIAP inhibitors or PPAR γ agonists as anti-cancer treatment has been shown more efficient in malignancies that express the XIAP or PPAR γ proteins as might be expected (11,21). As with GCT, several cancers have been reported to co-express XIAP and PPAR γ proteins including glioblastoma (47), colon cancer (48,49) and leukaemia (50). In these studies, XIAP inhibition using small molecule inhibitor (50) or XIAP knockout (48) sensitized the cancers to PPAR γ -dependent cell death induced by TZD.

We have found that combining an XIAP inhibitor with PPAR γ agonists induces both differentiation and apoptosis in GCT cells (Leung *et al.*, concurrent publication). In the current study, we have sought to understand the mechanism of the response by utilising SILAC labelling coupled with mass spectrometry analysis to investigate the proteomic changes in the cells following the combined treatment.

Of the 32 proteins that were differentially regulated by the combined treatment, SCD stands out as the most interesting target with the greatest magnitude of change. SCD messenger and protein level is upregulated by both SM/RGZ/RA and Emb/RGZ/RA treatment in the KGN cells. Further we provide evidence that this is a transcriptional response mediated via a direct interaction of PPAR γ with the *SCD* gene.

Stearoyl-CoA desaturase (SCD), also called acyl-CoA desaturase or Δ -9-desaturase, is an enzyme which converts saturated fatty acids to monounsaturated fatty acids (MUFA), namely, palmitoyl- and stearoyl-CoA to palmitoleic and oleic acid, which are

preferred substrates for cholesterol biosynthesis. *SCD* is predominantly expressed by adipocytes but is also detected in other organs including the ovary. We have used microarray analysis to examine the levels of *SCD* in six stage 1, six recurrent GCT and in the KGN cells using microarray analysis (38). *SCD* mRNA was detected in all samples; no significant difference was observed amongst the GCT samples regardless of the stage of disease, and the untreated KGN cells.

There is no existing literature on the function of *SCD* in the ovary. Arguably it may have a role in steroidogenesis given its function in synthesizing the precursors for the steroidogenic pathways. Zhao and colleagues (51) identified in a group of women with polycystic ovarian syndrome (PCOS) an increase in MUFA to saturated fatty acids ratio, which is indicative of increased *SCD* activity. No direct link has been reported between PCOS and *SCD* as yet. However, it is plausible that the hormone imbalance and increased cholesterol level is associated with the heightened *SCD* activity in PCOS patients (51).

Altered *SCD* expression has been associated with the metabolic syndrome (52). Previous studies have consistently reported that *SCD* expression is increased upon PPAR γ activation by TZD in individuals with diabetes. Treatment with the anti-diabetic TZD including one that was used in this study, RGZ (37), as well as pioglitazone (36), increased *SCD* mRNA and protein expression in adipose tissues and adipocytes of humans with varying insulin sensitivity. These subjects demonstrated improved insulin sensitivity after TZD treatment. However, it is difficult to determine from these studies if it is a primary or secondary effect of PPAR γ activation, given the treatments varied between hours and days *in vitro*, and months *in vivo*. Despite the activation, no existing literature has reported direct evidence that PPAR γ regulates/activates *SCD* expression or activity. Using promoter analysis, we identified two putative binding sites of PPAR γ

to the promoter region of *SCD*; cells treated with XIAP inhibitor and PPAR γ agonist showed an increase in *SCD* gene expression.

ACSL3 catalyses long chain fatty acids to form acyl-CoA in fatty acid metabolism. It is expressed in various tissues including the ovary. No specific role of ACSL3 in the ovary has been described. Bu and colleagues (53) reported that ACSL3 siRNA suppressed PPAR γ transcriptional activity in hepatocytes, suggesting a positive relationship between ACSL3 and PPAR γ . In our study, we found that ACSL3 mRNA and protein expression was upregulated following the restoration of PPAR γ activity. This points to a possible reciprocity in the regulation. A downregulation of ACSL3 was noted in 1,648 ovarian cancers and higher expression was correlated with a better prognosis in these patients (54). From the microarray analysis of six stage 1, six recurrent GCT and in the KGN cells (38), the levels of ACSL3 were similar regardless of the stage of the disease; no difference was observed compared to the untreated KGN cells (Supplementary figure 3).

The glycolytic enzyme, α -enolase (ENO1), catalyses the production of phosphoenolpyruvate from 2-phospho-D-glycerate in the cytoplasm (55). A short variant of ENO1, Myc promoter-binding protein-1 (MBP-1), represses Myc transcription in the nucleus and may serve as a tumor suppressor (55). ENO1 is widely expressed across the body. *ENO1* mRNA expression was observed in GC and theca cells of the rat ovary (56) and ENO1 protein was detected in human ovary (57). *ENO1* mRNA expression remains unchanged throughout the oestrous cycle and is not altered by human chorionic gonadotropin (hCG) (58). Consistent with potential tumor suppressive effects, knockdown of ENO1 using siRNA has been shown to increase cell growth in Chinese hamster ovary (CHO) cells (59).

The increased expression of targets associated with metabolism is consistent with restoration of PPAR γ activity. This is achieved by the release of PPAR γ from transrepression by NF- κ B through inhibition of XIAP. Despite the link of heightened metabolism with unfavourable outcomes in cancer, we found using extracellular flux analysis that the GCT-derived cells subjected to the combinational treatment are less metabolically active (data not shown). Additionally, these cells failed to respond to the increased energy demand under stressed condition (data not shown). The combined XIAP and PPAR γ approach also induced apoptosis in the GCT-derived cells, as shown by high content screening (data not shown).

This proteomic analysis is a proof of concept that the transrepression of PPAR γ signaling can be removed by small molecular inhibitor of XIAP in the GCT cells. Without the repressive effect, the anti-neoplastic function of PPAR γ is reinstated by PPAR γ agonists. Co-expression of XIAP and PPAR γ at high levels are not only seen in the GCT but also in other solid tumors. This phenomenon thus makes these two proteins unique candidates of a targeted therapy which has a broader implication beyond GCT.

Acknowledgements

The authors wish to acknowledge Dr Peter Hoffmann and Dr Georgia Arentz at Adelaide Proteomics Centre for mass spectrometry analysis of the samples, Maria Alexiadis for the microarray data.

References

1. Jamieson S, Fuller PJ. Molecular pathogenesis of granulosa cell tumors of the ovary. *Endocr Rev* **2012**;33:109-44
2. Fuller PJ, Leung D, Chu S. Genetics and genomics of ovarian sex cord-stromal tumors. *Clin Genet* **2017**;91:285-91
3. Nishi Y, Yanase T, Mu Y, Oba K, Ichino I, Saito M, *et al.* Establishment and characterization of a steroidogenic human granulosa-like tumor cell line, KGN, that expresses functional follicle-stimulating hormone receptor. *Endocrinology* **2001**;142:437-45
4. Jamieson S, Butzow R, Andersson N, Alexiadis M, Unkila-Kallio L, Heikinheimo M, *et al.* The FOXL2 C134W mutation is characteristic of adult granulosa cell tumors of the ovary. *Mod Pathol* **2010**;23:1477-85
5. Alexiadis M, Eriksson N, Jamieson S, Davis M, Drummond AE, Chu S, *et al.* Nuclear receptor profiling of ovarian granulosa cell tumors. *Horm Cancer* **2011**;2:157-69
6. Chu S, Alexiadis M, Fuller PJ. Proteasome inhibition by bortezomib decreases proliferation and increases apoptosis in ovarian granulosa cell tumors. *Reprod Sci* **2009**;16:397-407
7. Aleman-Gonzalez-Duhart D, Tamay-Cach F, Alvarez-Almazan S, Mendieta-Wejebe JE. Current Advances in the Biochemical and Physiological Aspects of the Treatment of Type 2 Diabetes Mellitus with Thiazolidinediones. *PPAR Res* **2016**;2016:7614270
8. Long MJ, Sairam MR, Komar CM. Initiation of the expression of peroxisome proliferator-activated receptor gamma (PPAR gamma) in the rat ovary and the role of FSH. *Reprod Biol Endocrinol* **2009**;7:145
9. Froment P, Gizard F, Defever D, Staels B, Dupont J, Monget P. Peroxisome proliferator-activated receptors in reproductive tissues: from gametogenesis to parturition. *J Endocrinol* **2006**;189:199-209
10. Zhang H, Li Q, Lin H, Yang Q, Wang H, Zhu C. Role of PPARgamma and its gonadotrophic regulation in rat ovarian granulosa cells in vitro. *Neuro Endocrinol Lett* **2007**;28:289-94
11. Ferrari SM, Materazzi G, Baldini E, Ulisse S, Miccoli P, Antonelli A, *et al.* Antineoplastic Effects of PPARgamma Agonists, with a Special Focus on Thyroid Cancer. *Curr Med Chem* **2016**;23:636-49
12. Tsukahara T, Haniu H. Peroxisome proliferator-activated receptor gamma overexpression suppresses proliferation of human colon cancer cells. *Biochem Biophys Res Commun* **2012**;424:524-9
13. Komatsu Y, Yoshino T, Yamazaki K, Yuki S, Machida N, Sasaki T, *et al.* Phase 1 study of efatutazone, a novel oral peroxisome proliferator-activated receptor gamma agonist, in combination with FOLFIRI as second-line therapy in patients with metastatic colorectal cancer. *Invest New Drugs* **2014**;32:473-80
14. Smallridge RC, Copland JA, Brose MS, Wadsworth JT, Houvras Y, Menefee ME, *et al.* Efaturazone, an oral PPAR-gamma agonist, in combination with paclitaxel in anaplastic thyroid cancer: results of a multicenter phase 1 trial. *J Clin Endocrinol Metab* **2013**;98:2392-400
15. Murakami H, Ono A, Takahashi T, Onozawa Y, Tsushima T, Yamazaki K, *et al.* Phase I study of Efaturazone, an oral PPARgamma agonist, in patients with metastatic solid tumors. *Anticancer Res* **2014**;34:5133-41
16. Chu S, Nishi Y, Yanase T, Nawata H, Fuller PJ. Transrepression of estrogen receptor beta signaling by nuclear factor-kappaB in ovarian granulosa cells. *Mol Endocrinol* **2004**;18:1919-28

17. Obexer P, Ausserlechner MJ. X-linked inhibitor of apoptosis protein - a critical death resistance regulator and therapeutic target for personalized cancer therapy. *Front Oncol* **2014**;4:197
18. Phillipps HR, Kokay IC, Grattan DR, Hurst PR. X-linked inhibitor of apoptosis protein and active caspase-3 expression patterns in antral follicles in the sheep ovary. *Reproduction* **2011**;142:855-67
19. Wang Y, Rippstein PU, Tsang BK. Role and gonadotrophic regulation of X-linked inhibitor of apoptosis protein expression during rat ovarian follicular development in vitro. *Biol Reprod* **2003**;68:610-9
20. Li J, Kim JM, Liston P, Li M, Miyazaki T, Mackenzie AE, *et al.* Expression of inhibitor of apoptosis proteins (IAPs) in rat granulosa cells during ovarian follicular development and atresia. *Endocrinology* **1998**;139:1321-8
21. Li X, Chen W, Zeng W, Wan C, Duan S, Jiang S. microRNA-137 promotes apoptosis in ovarian cancer cells via the regulation of XIAP. *Br J Cancer* **2017**;116:66-76
22. Moon JH, Shin JS, Hong SW, Jung SA, Hwang IY, Kim JH, *et al.* A novel small-molecule IAP antagonist, AZD5582, draws Mcl-1 down-regulation for induction of apoptosis through targeting of cIAP1 and XIAP in human pancreatic cancer. *Oncotarget* **2015**;6:26895-908
23. Yang S, Li SS, Yang XM, Yin DH, Wang L. Embelin prevents LMP1-induced TRAIL resistance via inhibition of XIAP in nasopharyngeal carcinoma cells. *Oncol Lett* **2016**;11:4167-76
24. Yang T, Lan J, Huang Q, Chen X, Sun X, Liu X, *et al.* Embelin sensitizes acute myeloid leukemia cells to TRAIL through XIAP inhibition and NF-kappaB inactivation. *Cell Biochem Biophys* **2015**;71:291-7
25. Holcik M, Gibson H, Korneluk RG. XIAP: apoptotic brake and promising therapeutic target. *Apoptosis* **2001**;6:253-61
26. Schimmer AD, Dalili S, Batey RA, Riedl SJ. Targeting XIAP for the treatment of malignancy. *Cell Death Differ* **2006**;13:179-88
27. Mahadevan D, Chalasani P, Rensvold D, Kurtin S, Pretzinger C, Jolivet J, *et al.* Phase I trial of AEG35156 an antisense oligonucleotide to XIAP plus gemcitabine in patients with metastatic pancreatic ductal adenocarcinoma. *Am J Clin Oncol* **2013**;36:239-43
28. Carter BZ, Mak DH, Morris SJ, Borthakur G, Estey E, Byrd AL, *et al.* XIAP antisense oligonucleotide (AEG35156) achieves target knockdown and induces apoptosis preferentially in CD34+38- cells in a phase 1/2 study of patients with relapsed/refractory AML. *Apoptosis* **2011**;16:67-74
29. Dean EJ, Ranson M, Blackhall F, Dive C. X-linked inhibitor of apoptosis protein as a therapeutic target. *Expert Opin Ther Targets* **2007**;11:1459-71
30. Nikolovska-Coleska Z, Xu L, Hu Z, Tomita Y, Li P, Roller PP, *et al.* Discovery of embelin as a cell-permeable, small-molecular weight inhibitor of XIAP through structure-based computational screening of a traditional herbal medicine three-dimensional structure database. *J Med Chem* **2004**;47:2430-40
31. Xu XM, Zhang ML, Zhang Y, Zhao L. Osthole induces lung cancer cell apoptosis through inhibition of inhibitor of apoptosis family proteins. *Oncol Lett* **2016**;12:3779-84
32. Phillipps HR, Hurst PR. XIAP: a potential determinant of ovarian follicular fate. *Reproduction* **2012**;144:165-76
33. Szklarczyk D, Franceschini A, Wyder S, Forslund K, Heller D, Huerta-Cepas J, *et al.* STRING v10: protein-protein interaction networks, integrated over the tree of life. *Nucleic Acids Res* **2015**;43:D447-52
34. Gene Ontology C. Gene Ontology Consortium: going forward. *Nucleic Acids Res* **2015**;43:D1049-56

35. Mathelier A, Fornes O, Arenillas DJ, Chen CY, Denay G, Lee J, *et al.* JASPAR 2016: a major expansion and update of the open-access database of transcription factor binding profiles. *Nucleic Acids Res* **2016**;44:D110-5
36. Yao-Borengasser A, Rassouli N, Varma V, Bodles AM, Rasouli N, Unal R, *et al.* Stearoyl-coenzyme A desaturase 1 gene expression increases after pioglitazone treatment and is associated with peroxisomal proliferator-activated receptor-gamma responsiveness. *J Clin Endocrinol Metab* **2008**;93:4431-9
37. Kolak M, Yki-Jarvinen H, Kannisto K, Tiikkainen M, Hamsten A, Eriksson P, *et al.* Effects of chronic rosiglitazone therapy on gene expression in human adipose tissue in vivo in patients with type 2 diabetes. *J Clin Endocrinol Metab* **2007**;92:720-4
38. Alexiadis M, Chu S, Leung D, Gould JA, Jobling T, Fuller PJ. Transcriptomic analysis of stage 1 versus advanced adult granulosa cell tumors. *Oncotarget* **2016**;7:14207-19
39. Fulda S. Smac Mimetics to Therapeutically Target IAP Proteins in Cancer. *Int Rev Cell Mol Biol* **2017**;330:157-69
40. Ma JJ, Chen BL, Xin XY. XIAP gene downregulation by small interfering RNA inhibits proliferation, induces apoptosis, and reverses the cisplatin resistance of ovarian carcinoma. *Eur J Obstet Gynecol Reprod Biol* **2009**;146:222-6
41. Sasaki HS, Y.; Kotsuji, F.; Tsang, B. K. Down-regulation of X-linked inhibitor of apoptosis protein induces apoptosis in chemoresistant human ovarian cancer cells. *Cancer research* **2000**;60:9
42. Darding M, Feltham R, Tenev T, Bianchi K, Benetatos C, Silke J, *et al.* Molecular determinants of Smac mimetic induced degradation of cIAP1 and cIAP2. *Cell death and differentiation* **2011**;18:1376-86
43. Feltham R, Bettjeman B, Budhidarmo R, Mace PD, Shirley S, Condon SM, *et al.* Smac mimetics activate the E3 ligase activity of cIAP1 protein by promoting RING domain dimerization. *The Journal of biological chemistry* **2011**;286:17015-28
44. Wei Y, Fan T, Yu M. Inhibitor of apoptosis proteins and apoptosis. *Acta Biochim Biophys Sin (Shanghai)* **2008**;40:278-88
45. Antonelli A, Ferrari SM, Fallahi P, Piaggi S, Di Domenicantonio A, Galleri D, *et al.* Variable modulation by cytokines and thiazolidinediones of the prototype Th1 chemokine CXCL10 in anaplastic thyroid cancer. *Cytokine* **2012**;59:218-22
46. Shimazaki N, Togashi N, Hanai M, Isoyama T, Wada K, Fujita T, *et al.* Anti-tumour activity of CS-7017, a selective peroxisome proliferator-activated receptor gamma agonist of thiazolidinedione class, in human tumour xenografts and a syngeneic tumour implant model. *Eur J Cancer* **2008**;44:1734-43
47. Kang DW, Choi CH, Park JY, Kang SK, Kim YK. Ciglitazone induces caspase-independent apoptosis through down-regulation of XIAP and survivin in human glioma cells. *Neurochem Res* **2008**;33:551-61
48. Qiao L, Dai Y, Gu Q, Chan KW, Ma J, Lan HY, *et al.* Loss of XIAP sensitizes colon cancer cells to PPARgamma independent antitumor effects of troglitazone and 15-PGJ2. *Cancer Lett* **2008**;268:260-71
49. Dai Y, Qiao L, Chan KW, Zou B, Ma J, Lan HY, *et al.* Loss of XIAP sensitizes rosiglitazone-induced growth inhibition of colon cancer in vivo. *Int J Cancer* **2008**;122:2858-63
50. Liu JJ, Guo YW, Fang ZG, Si XN, Wu XY, Liu PQ, *et al.* Activation of peroxisome proliferator-activated receptor-gamma induces apoptosis on acute promyelocytic leukemia cells via downregulation of XIAP. *Int J Mol Med* **2009**;24:623-32
51. Zhao X, Xu F, Qi B, Hao S, Li Y, Li Y, *et al.* Serum metabolomics study of polycystic ovary syndrome based on liquid chromatography-mass spectrometry. *J Proteome Res* **2014**;13:1101-11
52. Singh V, Chassaing B, Zhang L, San Yeoh B, Xiao X, Kumar M, *et al.* Microbiota-Dependent Hepatic Lipogenesis Mediated by Stearoyl CoA Desaturase 1 (SCD1) Promotes Metabolic Syndrome in TLR5-Deficient Mice. *Cell Metab* **2015**;22:983-96

53. Bu SY, Mashek MT, Mashek DG. Suppression of long chain acyl-CoA synthetase 3 decreases hepatic de novo fatty acid synthesis through decreased transcriptional activity. *J Biol Chem* **2009**;284:30474-83
54. Chen WC, Wang CY, Hung YH, Weng TY, Yen MC, Lai MD. Systematic Analysis of Gene Expression Alterations and Clinical Outcomes for Long-Chain Acyl-Coenzyme A Synthetase Family in Cancer. *PLoS One* **2016**;11:e0155660
55. Subramanian A, Miller DM. Structural analysis of alpha-enolase. Mapping the functional domains involved in down-regulation of the c-myc protooncogene. *J Biol Chem* **2000**;275:5958-65
56. Sugiura K, Pendola FL, Eppig JJ. Oocyte control of metabolic cooperativity between oocytes and companion granulosa cells: energy metabolism. *Dev Biol* **2005**;279:20-30
57. Gillott DJ, Eldib A, Iammarrone E, Leung KY, Thornhill AR, Grudzinskas JG. Glycolytic enzyme expression in human granulosa cells. *Fertil Steril* **2008**;90:1405-10
58. Yoshioka N, Takahashi N, Tarumi W, Itoh MT, Ishizuka B. Gonadotropins up-regulate the expression of enolase 2, but not enolase 1, in the rat ovary. *Endocr J* **2011**;58:941-8
59. Doolan P, Meleady P, Barron N, Henry M, Gallagher R, Gammell P, *et al.* Microarray and proteomics expression profiling identifies several candidates, including the valosin-containing protein (VCP), involved in regulating high cellular growth rate in production CHO cell lines. *Biotechnol Bioeng* **2010**;106:42-56

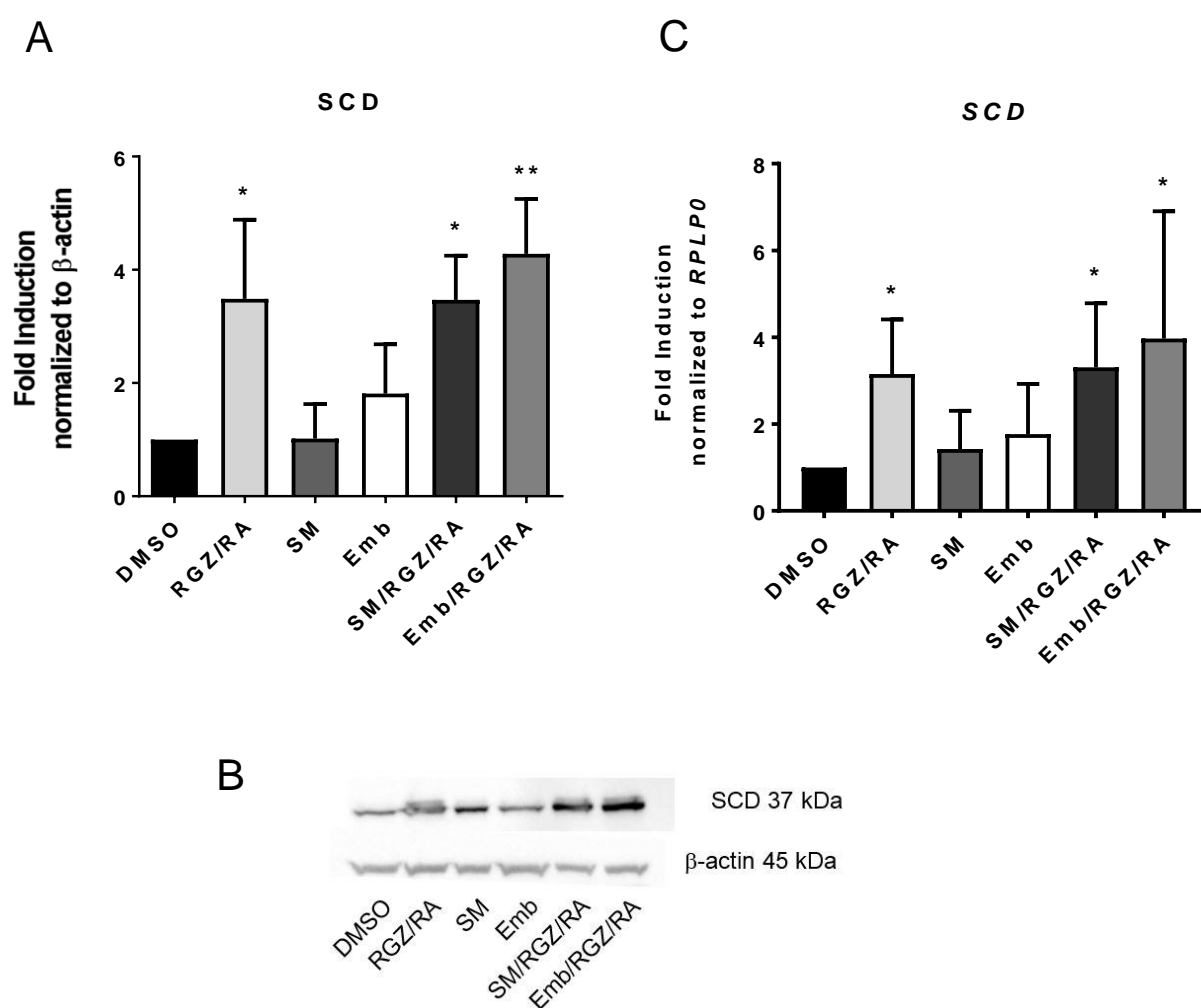


Figure 1. SCD protein and mRNA levels in KGN cells. A. Densitometry analysis of western blot showing an induction of SCD expression following 24-hour treatment of RGZ/RA, SM/REGZ/RA or Emb/REGZ/RA in KGN. $n = 3$; mean \pm SD; One-way ANOVA; Bonferroni post-hoc analysis. * $p < 0.01$; ** $p < 0.005$ when compared to DMSO. B. Western blot of SCD and β -actin as loading control. C. SCD mRNA expression is induced following 24-hour treatment of RGZ/RA, SM/REGZ/RA or Emb/REGZ/RA in KGN demonstrated using digital PCR (Fluidigm® Biomark HD™ system). mRNA expression was normalised to that of the housekeeping gene *RPLP0*. $n = 4-7$; mean \pm SD; Kruskal-Wallis test; Dunn's post-hoc analysis. * $p < 0.05$ when compared to DMSO.

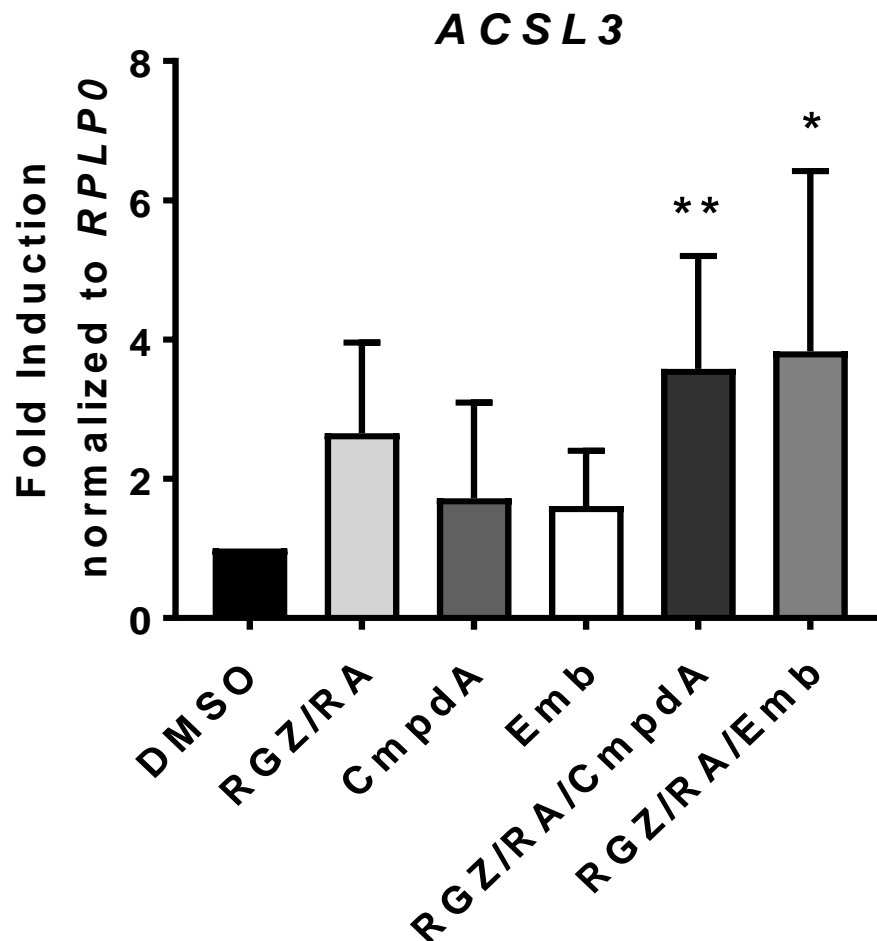


Figure 2. ACSL3 mRNA level in KGN cells. ACSL3 mRNA expression following drug treatments in KGN using digital PCR (Fluidigm® Biomark HD™ system). mRNA expression was normalised to that of RPLP0. n = 4-7; mean ± SD; Kruskal-Wallis test; Dunn's post-hoc analysis. * $p < 0.05$; ** $p < 0.01$ when compared to DMSO.

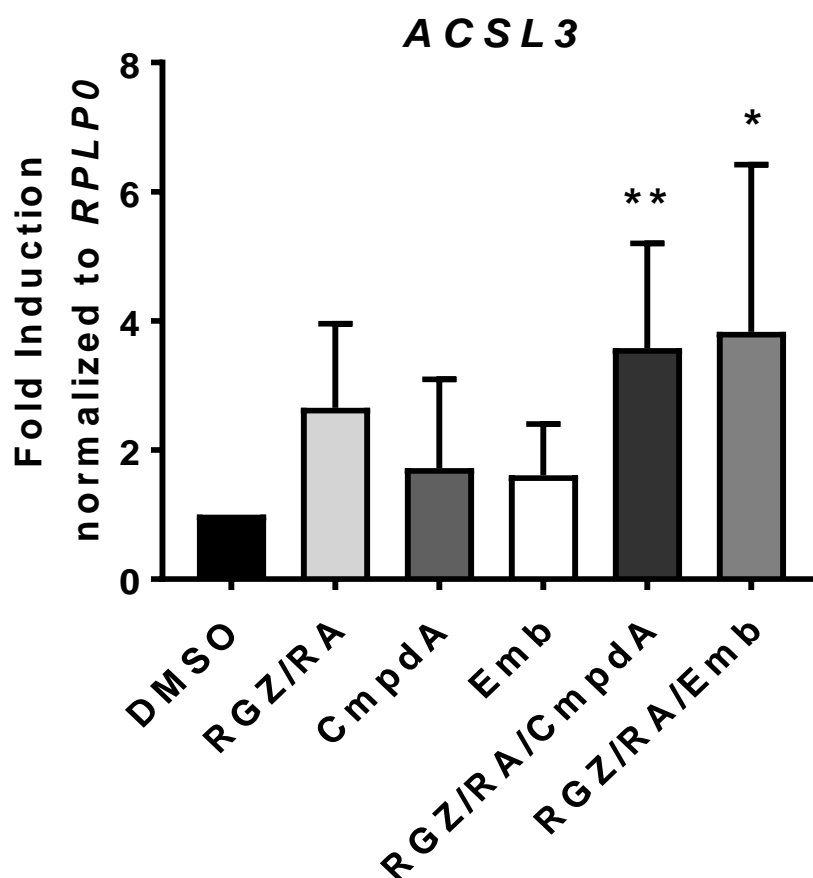


Figure 3. *ENO1* mRNA level in KGN. *ENO1* mRNA expression following drug treatments in KGN using digital PCR (Fluidigm® Biomark HD™ system). mRNA expression was normalised to that of RPLP0. n = 4-7; mean ± SD; Kruskal-Wallis test; Dunn's post-hoc analysis. * $p < 0.05$ when compared to DMSO.

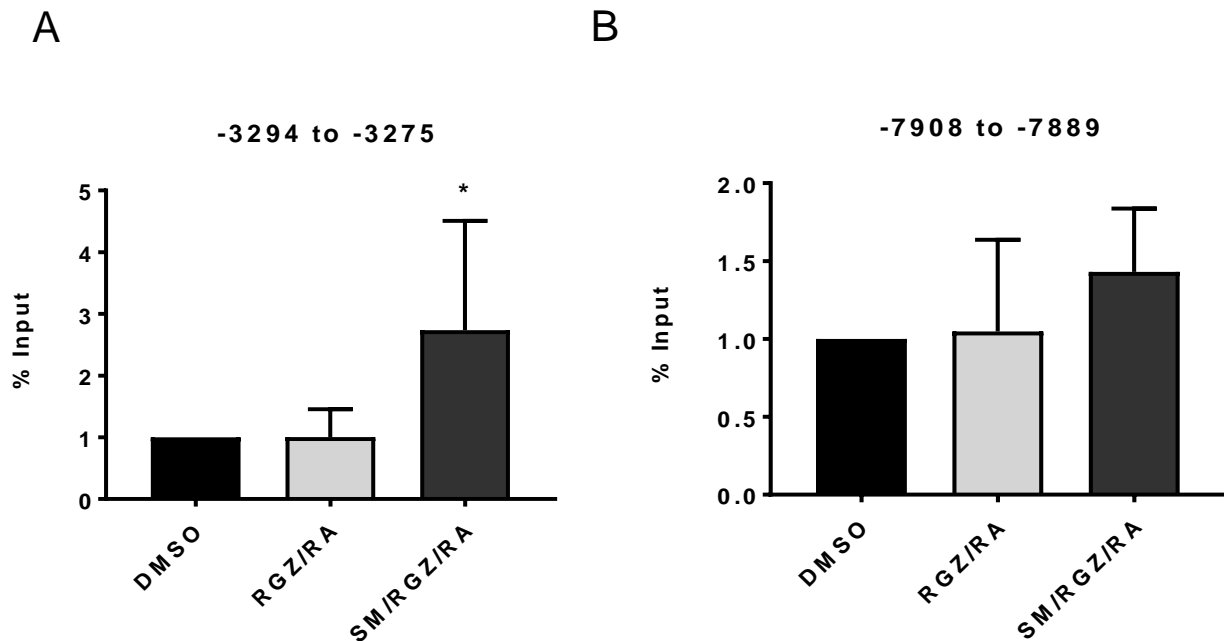


Figure 4. ChIP-PCR analysis of PPAR γ binding on SCD promoter region in KGN.

A. PPAR γ binding on SCD (-3294 to -3275). The KGN cells were treated with DMSO (control), RGZ/RA or SM/RGZ/RA for 6 hours. Binding intensity following singular treatment, RGZ/RA, was not significant. Increased binding of PPAR γ on the predicted binding site was observed following SM/RGZ/RA treatment in the KGN cells ($*P < 0.05$ when compared to DMSO). $n = 4$; mean \pm SD; Kruskal-Wallis test; Dunn's post-hoc analysis. B. PPAR γ binding on SCD (-7908 to -7889). RGZ/RA did not alter the intensity of PPAR γ binding on SCD promoter region. Binding intensity was increased following SM/RGZ/RA treatment but did not reach significant difference. $n = 4$; mean \pm SD; Kruskal-Wallis test; Dunn's post-hoc analysis.

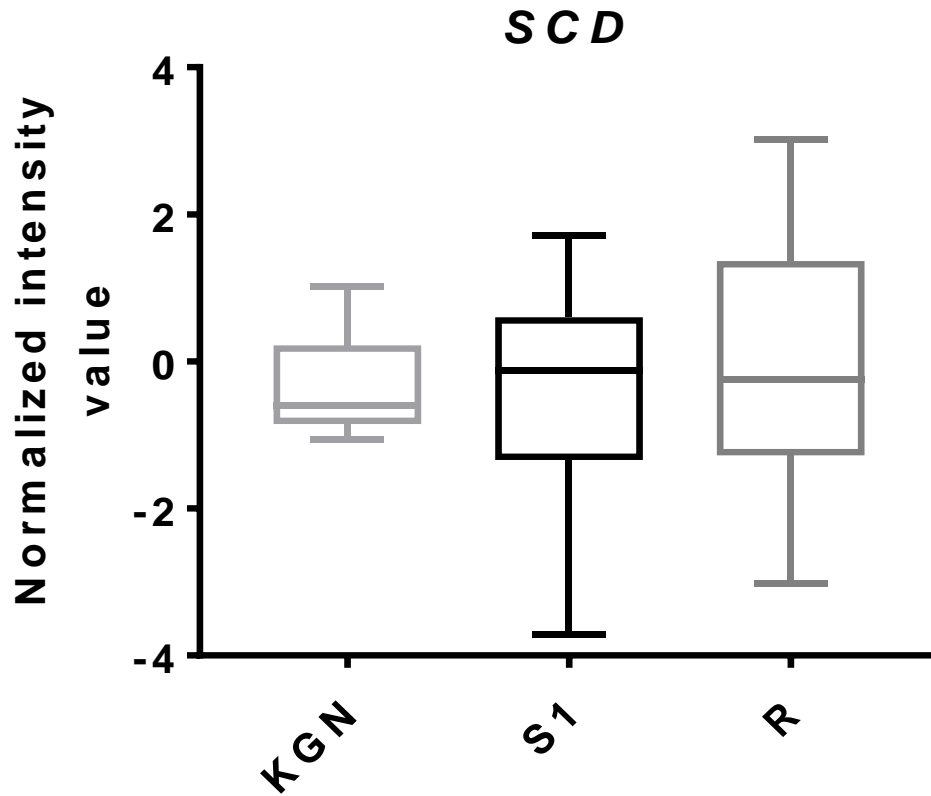


Figure 5. Microarray analysis of *SCD* mRNA in the KGN cells, stage 1 and recurrent GCT. Values were averaged and normalised over six stage 1 (S1), six recurrent (R) GCT samples and three replicate samples of the KGN cell line. The box and whiskers plot show the minimum and maximum values of all samples

Supplementary Table 1. Upregulated proteins in KGN cells. ¹

Protein ID	Gene	Protein	SM/RGZ/RA	Emb/RGZ/RA	Sequence	Protein score	% Sequence coverage
O00767	SCD	Acyl-CoA desaturase	4.50	4.59	FSETHADPHNSRR GSTLDLSDLEAEKLVMFQR FSETHADPHNSR VEYVWR GSTLDLSDLEAEK	87 344	3.6 10.6
P08648*	ITA5	Integrin alpha-5	nd	3.23	TPDGRPQEVGR AHGSSILACAPLYSWR LGFFKRSLPYGTAMEK	- 53	2.6 4.1
P00558	PGK1	Phosphoglycerate kinase I	nd	2.87	AAVPSIK ELNYFAK ALMDEVVK DCVGPEVEK VLPGVDALSNI NNQITNNQR FHVEEEGK GK NNQITNNQRIK AHSSMVGVNLPQK VVMRVDFNVPMK	875 1118	55.6 53.5

¹ Mass spectrometry analysis identified 22 proteins that were upregulated by ≥ 1.5 fold by the 24-hour combination treatment in the KGN cells. Protein ratios from the reciprocal experiments were averaged to calculate the final fold change. Protein scores and sequence coverage for each individual protein from the reciprocal experiments were listed. nd = not detected. *6 proteins were identified previously but due to a change of personnel for analysis, these were not found in the final list of differentially expressed proteins. These proteins were excluded from GO enrichment analysis.

					LGDVYVNDAFGTAHR GCITIIGGGDTATCCA ACANPAAGSVILLENLR ALESERPFLAILGGAK ITLPVDFVTADKFDENAK AHSSMVGVNLPQKAGGFLMK QIVWNGPVGVEAFAR TGQATVASGIPAGWMGLDCGPESKK		
O95573	ACSL3	Acyl-CoA synthetase long chain family member 3	nd	2.56	THYQADIER AKPVNSKPDSAYR LSPEPWTPETGLVTDAFK VSEMSSFQR GRNTPLCDSFVFR SVNSLDGLASVLYPGCDTLDKVFTYAKNK	51 84	4.4 5.6
P07602	PSAP	Prosaposin	1.79	2.32	KHEVPAK SLPCDICK QEILAALEK KLVGYLDRNLEK EMPMQTLVPAKVASK SDVYCEVCEFLVK EIVDSYLPVILDIK MYALFLLASLLGAALAGPVLGLKECTRGSA VWCQNVK EMPMQTLVPAK	SM/RGZ/RA: 361 190 Emb/RGZ/RA: 177 240	SM/RGZ/RA: 22.1 9.4 Emb/RGZ/RA: 7.3 19.3
P21980*	TGM2	Protein-glutamine gamma-glutamyltransferase 2	2.30	nd	-	- 221	2.6 9.3
P08670	VIM	Vimentin	2.21	nd	LDLER SSVPGVR FANYIDK FLEQQNK SYVTTSTR LLEGEESR QQYESVAAK	4165 2682	84.5 69.5

					LQEMLQR QVDQLTNDK KLEGEESR DNLAEDIMR QVDNASLAR FADLSEAANR VELQELNDR LQDEIQNMK EYQDLLNVK ILLAELEQLK RQVDQLTNDK LGDLYEEEMR EKLQEMLQR MALDIEIATYR NLQEAEWYK EEAENTLQSFR SLYASSPGGVYATR QVQSLTCEVDALK TYSLGSALRPSTSR KVESLQEEIAFLK ILLAELEQLKGQK ISLPLPNFSSLNLR TNEKVELQELNDR KVESLQEEIAFLK ETNLDLPLVDTHSK VEVERDNLAEDIMR LQDEIQNMKEEMAR DGQVINETSQHDDLE LLQDSVDFSLADAINTEFK EMEENFAVEAANYQDTIGR LQEMLQREEAENTLQSFR QVQSLTCEVDALKGTNESLER RMFGGPGTASRPSSRSYVTTSTR LHEEEIQELQAQIQEQHVQIDVDVSKPDLTA ALR		
--	--	--	--	--	---	--	--

P07858	CTSB	Cathepsin B	1.56	1.97	DIMAEIYK VMFTEDLK GQDHCGIESEVVAGIPR NGPVEGAFSVYSDFLLYK LCGTFLGGPKPPQRVMFTEDLK EQWPQCPTIK DQGSCGSCWAFGAVEAISDR	SM/RGZ/RA: 225 254 Emb/RGZ/RA: 170 362	SM/RGZ/RA: 19.2 18 Emb/RGZ/RA: 10 23.9
P61769	B2M	Beta 2 microglobulin	1.74	1.90	VNHVTLISQPK SNFLNCYVSGFHPSDIEVDLLK	SM/RGZ/RA: 83 28 Emb/RGZ/RA: 79 141	SM/RGZ/RA: 26.9 26.9 Emb/RGZ/RA: 26.9 26.9
P04083	ANXA1	Annexin A1	nd	1.83	CLTAIVK NALLSLAK ALYEAGER VYREELKR LHQAMKGVGTR DITSDTSGDFR TPAQFDADELK VLDLELKGDIK HDMNKVLDLELK GTDVNVFNTILTTR GVDEATIIDILTKR ALTGHLEEVVLALLK GLGTDEDTLIEILASR AAYLQETGKPLDETLKK GDRSEDFGVNEDLADSDAR SYPQLR VYREELK CATSKPAFFAEK QAWFIENEEQEYVQTVK GGPGSAVSPYPTFNPSSDVAALHK	759 43	50.9 2.7
P11279*	LAMP1	Lysosome- associated	nd	1.75	SHAGYQTI ALQATVGNSYK	- 134	6.8 14.4

		membrane glycoprotein 1			FFLQGIQLNTILPDAR YNSVSGTNGTCLLASMGLQLNLTYER		
Q16777	H2A2C	Histone H2A type 2-C	1.70	nd	HLQLAIR AGLQFPVGR TESHKAKSK HLQLAIRNDEELNK VTIAQGGVLPNIQAVLLPK	273 95	35.9 14
P00338	LDHA	L-lactate dehydrogenase A chain	nd	1.69	LNLVQR LVIITAGAR FIIPNVVK VHPVSTMIK SADTLWGIQK DQLIYNLLK VTLTSEEEAR VIGSGCNLDSAR QVVESAYEVIK GEMMDLQHGSFLR DLADELALVDVIEDK LKGEMMDLQHGSFLR TLHPDLGTDKDKEQWK DLADELALVDVIEDK LLIVSNPVDILTYVAWK GYTSWAIGLSVADLAESIMK GLYGIKDDVFLSVPCILGQNGISDLVK LGVHPLSCHGWVLGEHGDSSVPVWSGMN VAGVSLK ISGFVK YLMGER DDVFLSVPCILGQNGISDLVK	158	15.7
P13473*	LAMP2	Lysosome-associated membrane glycoprotein 2	nd	1.67	SHTALLR EQTVSVSGAFQINTFDLR EKPEAGTYSVNNGNDTCLLATMGLQLNITQ DK	- 1422	9.7 72.9
Q13162	PRDX4	Peroxioredoxin-4	nd	1.67	GLFIIDDK QITLNDLPVGR	84 290	16.6 21

					IPLLSDLTHQISK SINTEVVACSVDSQFTHLAWINTPR QGGLGPIR GLFIIDDKGILR		
P60174	TPI1	Triosephosphate isomerase	nd	1.64	VVFEQTK LGSSAMAPSRK IAVAAQNCYK SNVSDAVAQSTR IIYGGSVTGATCK TATPQQAQEVHEK HVFGEDELIGQK DCGATWVVLGHSER VVLAYEPVWAIGTGK VAHALAEGLVACIGEK ELASQPDVDGFLVGGASLKPEFVDIINAK VPADTEVVCAPPTAYIDFAR	693 705	54.2 52.8
P07237	P4HB	Protein disulfide isomerase	nd	1.59	LKAEGSEIR MDSTANEVEAVK NGDTASPKEYTAGR TGPAATTLPDGAAAESLVESSEVAVIGFFK SNFAEALAAHK KSNFAEALAAHK YQLDKDGVVLFK VDATEESDLAQQYGVR LITLEEEMTKYKPESEELTAER	149 274	12.8 15.9
P45880*	VDAC2	Voltage-dependent anion-selective channel protein 2	1.57	nd	-	- -	5.7 9.9
P17516*	AKRIC4	Aldo-keto reductase family 1 member C4	1.56	nd	-	133 58	15.8 8
P06733	ENO1	Alpha enolase	nd	1.55	GVPLYR EIFDSR EGLELLK YNQLLR	1456 1790	68.4 78.6

					TIAPALVSK SGKYDLDFK IGAEVYHNLK GNPTVEVDLFTSK YISPDQLADLYK KLVNTEQEKIDK LAQANGWGVMSHR VVIGMDVAASEFFR VNQIGSVTESLQACK AAVPSGASTGIYEALER SGKYDLDFKSPDDPSR LAMQEFMILPVGAANFR DATNVGDEGGFAPNILENK FTASAGIQVVGDDLTVTNPK AGYTDKVVIGMDVAASEFFR SGETEDTFIADLVVGLCTGQIK LAMQEFMILPVGAANFREAMR DYPVVSIEDPFDQDDWGAWQK HIADLAGNSEVILPVPFNVINGGSHAGNK IEEELGSK LNVTEQEK KLVNTEQEK TRYMGKGVSK IDKLMIEMDGTENKSK FGANAILGVSLAVCKAGAVEK DATNVGDEGGFAPNILENKEGLELLK SFIKDYPVVSIEDPFDQDDWGAWQK		
P11021	HSPA5	78 kDa glucose-regulated protein	nd	1.52	FLPFK VLEDSDLK LTPEEIER ITITNDQNR VYGERPLTK DAGTIAGLNVMR VEIANDQGNR NELESYAYSLK	828 1299	29.5 37

					TWNDPSVQQDIK SDIDEIVLVGGSTR TFAPEEISAMVLTK ITPSYVAFTPEGER TKPYIQVDIGGGQTK KKELEEIVQPIISK IINEPTAAAIAYGLDK NQLTSNPENTVFDK IINEPTAAAIAYGLDKR VTHAVVTVPAYFNDAQR IEIESFYEGEDFSETLTR IEWLESHQDADIEDFKAK IQQLVK		
P07339	CTSD	Cathepsin D	1.51	nd	VGFAEAAR QVFGAATK VSTLPAILK QPGITFIAAK LSPEDYTLK FDGILGMAYPR LLDIACWIHHK YYTVFDRDNNR LVDQNIFSFYLSR DPDAQPGGELMLGGTDSK ISVNNVLPVFDNLMQQK AIGAVPLIQGEYMIPCEK AYWQVHLDQVEVASGLTLCK EGCEAIVDTGTSLMVGVPVDEVR KAYWQVHLDQVEVASGLTLCK ELQKAIGAVPLIQGEYMIPCEK LVDQNIFSFYLSRDPDAQPGGELMLGGTDS K	606 1284	26.9 46.4

Supplementary Table 2. Downregulated proteins in KGN cells. ²

Protein ID	Gene	Protein	SM/R/RA	Emb/R/RA	Sequence	Protein score	% Sequence coverage
			Average ratio				
P49411	TUFM	Elongation factor Tu, mitochondrial	nd	-2.7	DKPHVNVGTIGHVDHGK FTLRDGNRTIGTGLVTNLTAMTEEEK YEEIVK EVSTYIK QLIVGVNK TIEKFEK QTVAVGVK LPLQDVYK IGGIGTVPVGR STTTGHLIYK EHALLAYTLGVK QTVAVGVKAVDK YYVTIIDAPGHR THINIVVIGHVDSGK VETGVLKPGMVVTFAPVNVTTTEVK NMITGTSQADCAVLIVAAGVGEFEAGISK SGDAAIVDMVPGKPMCVESFSDYPPPLGR DGNASGTTLLEALDCILPPTRPTDKPLR	14 719	14 30.5

² 10 proteins were found to be downregulated by ≥ 1.5 fold after the combined treatment in the KGN cells for 24 hours. Protein ratios from the reciprocal experiments were averaged to calculate the final fold change. nd = not detected. *5 proteins were identified previously but due to a change of personnel for analysis, these were not found in the final list of differentially expressed proteins. These proteins were excluded from GO enrichment analysis.

					KDGNASGTTLLEALDCILPPTRPTDKPLR KIGYNPDTVAFVPISGWNGDNMLEPSANMPWFK DGNASGTTLLEALDCILPPTRPTDKPLRLPLQDVYK KDGNASGTTLLEALDCILPPTRPTDKPLRLPLQDVYK NDPPMEAAGFTAQVIILNHPGQISAGYAPVLDCHTAHIACK		
O94925*	GLSK	Glutaminase	-1.64	nd	QGLLPSLEDLLFYTIAEGQEK	234 234	5.4 5.4
Q16695	HIST3H3	Histone H3.1	nd	-1.99	VTIMPK DIQLAR STELLIR RVTIMPK EIAQDFK YRPGTVALR FQSSAVMALQEACEAYLVGLFEDTNLCAIHAH KLPFQR	289 300	54.4 54.4
Q07021*	C1QBP	Complement component 1Q subcomponent-binding protein, mitochondrial	nd	-1.98	-	- -	14.5 14.5
P35579	MYH9	Myosin-9	nd	-1.81	LSLSTKNMALKK KLEMDLK ASITALEAK VVFQEFR NTNPNFVR QRSMVAAR RGDLPFVVPR ALELDSNLYR THEAQIQEMR YEILTPNSIPK EQADFAIEALAK LDPHLVLDQLR QLEEAEEEEAQR VLQRNCAAYLK KKVEAQLQELQVK	1952 3291	30.1 36.6

				ITDVIIGFQACCR NTDQASMPDNTAAQK NKHEAMITDLEER GFMDGKQACVLMIK QLLQANPILEAFGNAK KQELEEICHDLER IAQLEEQLDNETKER EQLEEEEEAKHNLEK LQVELDNVTGLLSQSDSK LQQELDDLLVDLDHQR HSQAVEELAEQLEQTKR QAQQRDELADEIANSSGK QLVRQVREMEAELEDER INFDVNGYIVGANIETYLLEK DFSALESQIQDTQELLQEENR VEDMAELTCLNEASVLHNLKER VKPLLQVSRQEEEMMAKEEELVK NMDPLNDNIATLLHQSSDKFVSELWK DLGEELEALKTELEDTLSTAAQQELR ALEQQVEEMKTQLEEELEDELQATEDAK GALALEEK CIIPNHEK KLVWVPSDK RQQQLTAMK CIIPNHEKK VKVNKDDIQK DQADKASTRLK VISGVLQLGNIVFK QKLQLEKVTTEAK AGVLAHLEEERDLK VSHLLGINVTDFTK LTEMETLQSQLMAEK GMFRTVGQLYKEQLAK VEDMAELTCLNEASVLHNLK MQQNIQEELEEQLEEEESAR ASITALEAKIAQLEEQLDNETK		
--	--	--	--	---	--	--

P40926*	MDHM	Malate dehydrogenase	nd	-1.76	-	-	13.4
						54	21.6
P05141	SLC25A5	ADP/ATP translocase 2	nd	-1.57	TAVAPIER GNLANVIR GLGDCLVK GAWSNVLR QIFLGGVDK EQGVLSFWR LLLQVQHASK YFPTQALNFAFK GMGGAFVLVLYDEIKK	174 195	29.2 14.8
P62249*	RS16	40S ribosomal protein S16	nd	-1.51	MPSKGPLQSVQVFGRRKKTATAVAHCKRGNGLIKVNGRPL- EMIEPRTLQYKLLPEVLLLKGERFAGVDIRVRVGGGHVAQI- YAIRQSISKALVAYYQKYVDEASKKEIKDILIQYDRTELLVADP- RRCESKKFGGPGARARYQKSYR	- 75	23 23
P62263*	RS14	40S ribosomal protein S14	nd	-1.50	-	-	10.8
						-	10.8
Q16658	FSCN1	Fascin	-1.65	nd	VGKDELFALEQSCAQVVLQAANER KVTGTLDANR YSVQTADHR SSYDVFQLEFNDGAYNIK	277 188	8.5 7.5

Supplementary Table 3. Upregulation of SCD in KGN cells. ³

Sample	Mascot Score	% Sequence Coverage	Peptides Identified		Intensity Ratio (treatment vs DMSO)	Average Intensity Ratio
			All	Unique		
Heavy KGN_SM/RGZ/RA	87	3.6	2	2	5.30	4.50
Light KGN_SM/RGZ/RA	344	8.9	4	4	3.70	
Heavy KGN_Emb/RGZ/RA	45	8.9	4	4	6.14	4.59
Light KGN_Emb/RGZ/RA	179	8.9	4	4	3.03	

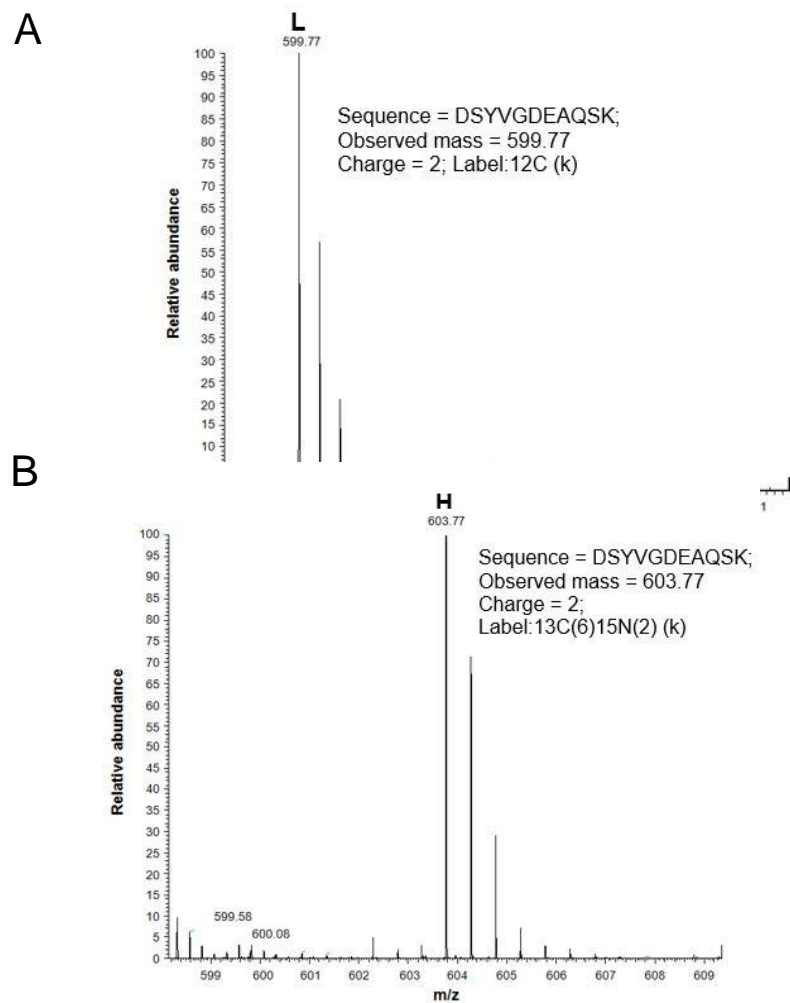
³ Mass spectrometry analysis identified SCD as a protein that is differentially regulated by the combined XIAP inhibition and PPAR γ activation.

Supplementary Table 4. GO enrichment analysis. ⁴

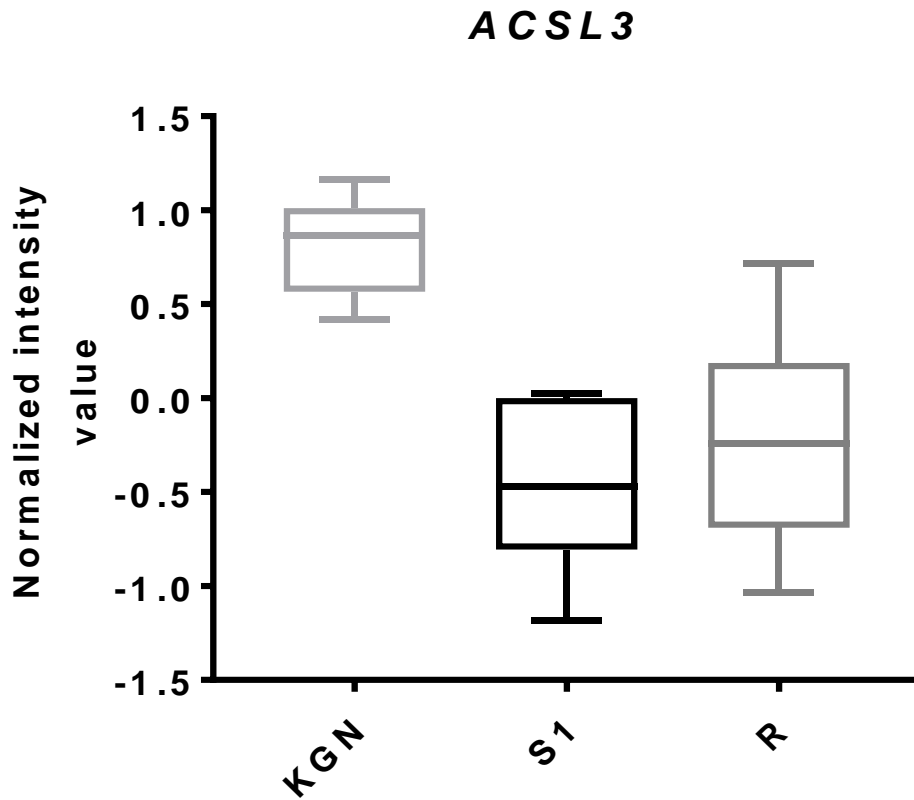
GO biological process	Homo sapiens REF #	#	Expected value	Fold enrichment	<i>P</i> value
Canonical glycolysis	27	3	0.02	>100	0.01
- Glucose catabolic process to pyruvate	27	3	0.02	>100	0.01
- Pyruvate metabolic process	69	4	0.05	75.99	0.00175
- Monocarboxylic acid metabolic process	481	6	0.37	16.35	0.00812
- Carboxylic acid metabolic process	868	8	0.66	12.08	0.000698
- Oxoacid metabolic process	976	8	0.74	10.74	0.00172
- Organic acid metabolic process	993	8	0.76	10.56	0.00196
- Single-organism cellular process	9841	16	7.51	2.13	0.0469
- Single-organism metabolic process	3572	12	2.73	4.40	0.00465
- Glucose catabolic process	30	3	0.02	>100	0.0137
- Single-organism carbohydrate catabolic process	108	4	0.08	48.55	0.0103

⁴ GO enrichment analysis was performed on the genes which encode the 16 upregulated proteins identified from the SILAC study. GO biological processes that are over-represented for this set of genes are listed. Homo sapiens REF # indicates the number of genes in the selected organism (i.e. Homo sapiens) that share the same GO biological process category; total number of genes in the Homo sapiens REF list is 20,972. # refers to number of genes in our data set that are mapped to a particular category. Expected value refers to number of genes one would expect in an analyzed data set for a certain GO biological process. In the case of an over-representation, more genes (#) from the analyzed data set are identified for a biological process than expected ("Expected value"). Fold enrichment of >1 represents that the biological process is overrepresented in the data set. *P* value is the probability of the number of identified genes being annotated in the category by chance.

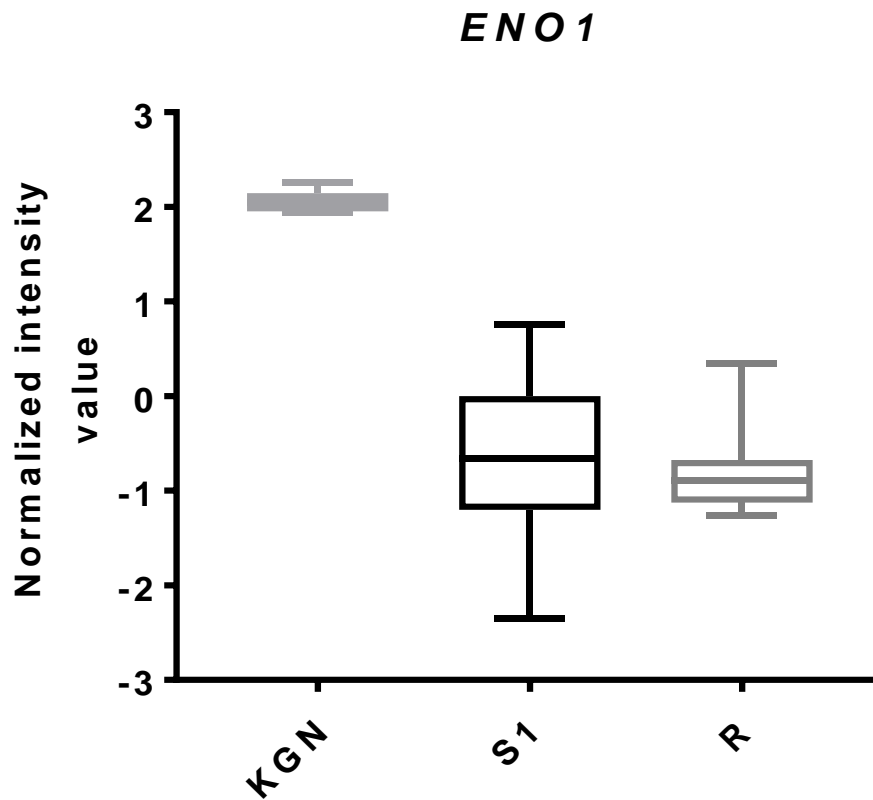
- Carbohydrate catabolic process	115	4	0.09	45.59	0.0133
- Single-organism catabolic process	847	7	0.65	10.83	0.0123
- NADH regeneration	27	3	0.02	>100	0.01
- Oxidation-reduction process	951	7	0.73	9.65	0.0266
- NADH metabolic process	36	3	0.03	>100	0.0237
- NAD metabolic process	70	4	0.05	74.90	0.00186
- Nicotinamide nucleotide metabolic process	112	4	0.09	46.81	0.0119
- Pyridine nucleotide metabolic process	112	4	0.09	46.81	0.0119
- Pyridine-containing compound metabolic process	118	4	0.09	44.43	0.0147
- Oxidoreduction coenzyme metabolic process	128	4	0.10	40.96	0.0202
- Coenzyme metabolic process	289	6	0.22	27.21	0.000414
- Cofactor metabolic process	360	6	0.27	21.85	0.0015
- Glycolytic process through glucose-6-phosphate	28	3	0.02	>100	0.0112
- Glycolytic process through fructose-6-phosphate	28	3	0.02	>100	0.0112
- Glycolytic process	40	4	0.03	>100	0.000201
- ATP generation from ADP	41	4	0.03	>100	0.000222
- ADP metabolic process	47	4	0.04	>100	0.000382
- Purine ribonucleoside diphosphate metabolic process	63	4	0.05	83.22	0.00122
- Purine nucleoside diphosphate metabolic process	65	4	0.05	80.66	0.00138
- Nucleoside diphosphate metabolic process	58	4	0.04	90.40	0.00088
- Ribonucleoside diphosphate metabolic process	64	4	0.05	81.92	0.0013
- Nucleoside diphosphate phosphorylation					
- Nucleoside phosphorylation					
Gluconeogenesis	45	3	0.03	87.38	0.046



Supplementary figure 1. Determination of incorporation efficiency of heavy and light amino acids into the KGN cells by orbitrap mass spectrometer. Peak annotated with L (A) and H (B) is peptide DSYVGDEAQSK of actin, cytoplasmic 1 in untreated KGN cells cultured in SILAC media containing light and heavy amino acids, respectively. The observed mass of peptide DSYVGDEAQSK is 599.75 and 603.77 after incorporation of the $^{12}\text{C}_6$ -lysine (L) and $^{13}\text{C}_6$ - $^{15}\text{N}_2$ -lysine (H), respectively. Incorporation efficiency is calculated by the ratio of the relative abundance of the light and heavy form of actin in the 'heavy' KGN cells (B), which is >99%.



Supplementary figure 2. Microarray analysis of ACSL3 mRNA in the KGN cells, stage 1 and recurrent GCT. Values were averaged and normalized over six stage 1 (S1), six recurrent (R) GCT samples and three replicate samples of the KGN cell line. The box and whiskers plot show the minimum and maximum values of all samples.



Supplementary figure 3. Microarray analysis of *ENO1* mRNA in the KGN cells, stage 1 and recurrent GCT. Values were averaged and normalized over six stage 1 (S1), six recurrent (R) GCT samples and three replicate samples of the KGN cell line. The box and whiskers plot show the minimum and maximum values of all samples.

CHAPTER 5

**REGULATION OF THE CONSTITUTIVE NF- κ B AND AP-1
SIGNALLING IN GCT**

5 Regulation of constitutive NF- κ B and AP-1 signalling in GCT

Our laboratory previously demonstrated that the NF- κ B and AP-1 signalling pathways are constitutively activated in two human GCT-derived cell lines, KGN and COV434 (Chu et al., 2004). Here, I investigated the link between these pathognomonic signalling pathways and the expression of XIAP in the development of GCT.

5.1 Introduction

Both downstream of the TGF β signalling pathway, the NF- κ B and AP-1 activities are under the regulation of the TAK-TAB complex (Hofer-Warbinek et al., 2000). The classical TGF β signalling pathway is governed by a complex of type I (TGFRI) and type II (TGFRII) transmembrane receptors. Upon transphosphorylation of TGFRI by TGFRII, activation of the Smad proteins triggers a series of signalling cascades that are directly or indirectly regulated by Smad (Mao et al., 2011).

TAK1 is a member of the MAP kinase kinase kinase (MAP3K) family. Activation of TAK1 is induced by the autophosphorylation of TAK1 following its interaction with its binding partner, TAB1. TAB1 dimerises with the BIR1 domain of XIAP to induce autophosphorylation of TAK1 and thereby activates TAK1 (Lu et al., 2007, Kim et al., 2009). It is important to note that both TAK1 and TAB1 lack a ubiquitin-binding domain, which had led Zhang et al. (2017a) to suggest the need of a ubiquitin chain-generating/recruiting protein such as the TNF receptor associated factor (TRAF) 6, a process which is required to activate the TAK1-TAB heterodimer (Figure 5.1). TRAF6

is activated by interleukin (IL)-1 and TLR recruitment of MyD88-IRAK1/4 complex (TLR = toll-like receptor; IRAK = IL-1 receptor-associated kinase; Figure 5.1) (Verstak et al., 2014). TRAF6 is a E3 ubiquitin ligase which catalyses the lysine (K) 63-linked polyubiquitylation. Studies have shown that an intact K158 on the TAB1-bound TAK1 is indispensable for the TRAF6-induced K63-linked polyubiquitylation (Mao et al., 2011). The involvement of all three components is essential to the activation of endogenous JNK and IKK; this activation is independent of the Smad pathway (Mao et al., 2011).

In addition to TRAF6, the recruitment of ubiquitin chain could alternatively be performed by two other known binding proteins of TAK1, the homologous proteins TAB 2 and 3. Both TAB2 and TAB3 have a highly-conserved zinc finger domain which allows them to preferentially bind to K63-linked polyubiquitin chains (Kanayama et al., 2004). The interaction between TAB2 or TAB3 with the K63-linked polyubiquitin chains prolongs the period of TAK1-TAB1 association which is required for downstream signalling (Zhang et al., 2017a). It has been speculated that the recruitment of the elongated polyubiquitin chains allows multiple TAK1-TAB2/3 complexes being formed, and subsequently facilitates the activation of TAK1 activity (Kishimoto et al., 2000, Kanayama et al., 2004). NEMO binds to the K63-linked polyubiquitinated TAK1, and then activates IKK which phosphorylates I κ B and releases the I κ B-bound NF- κ B to the nucleus and become activated (Fan et al., 2010b). Similarly, JNK and p38 phosphorylation and subsequent AP-1 activation was also dependent on the ability/presence of the K158 residue of the TAK1 kinase domain to recruit polyubiquitin chains via the binding partners of TAK1 (Fan et al., 2010b).

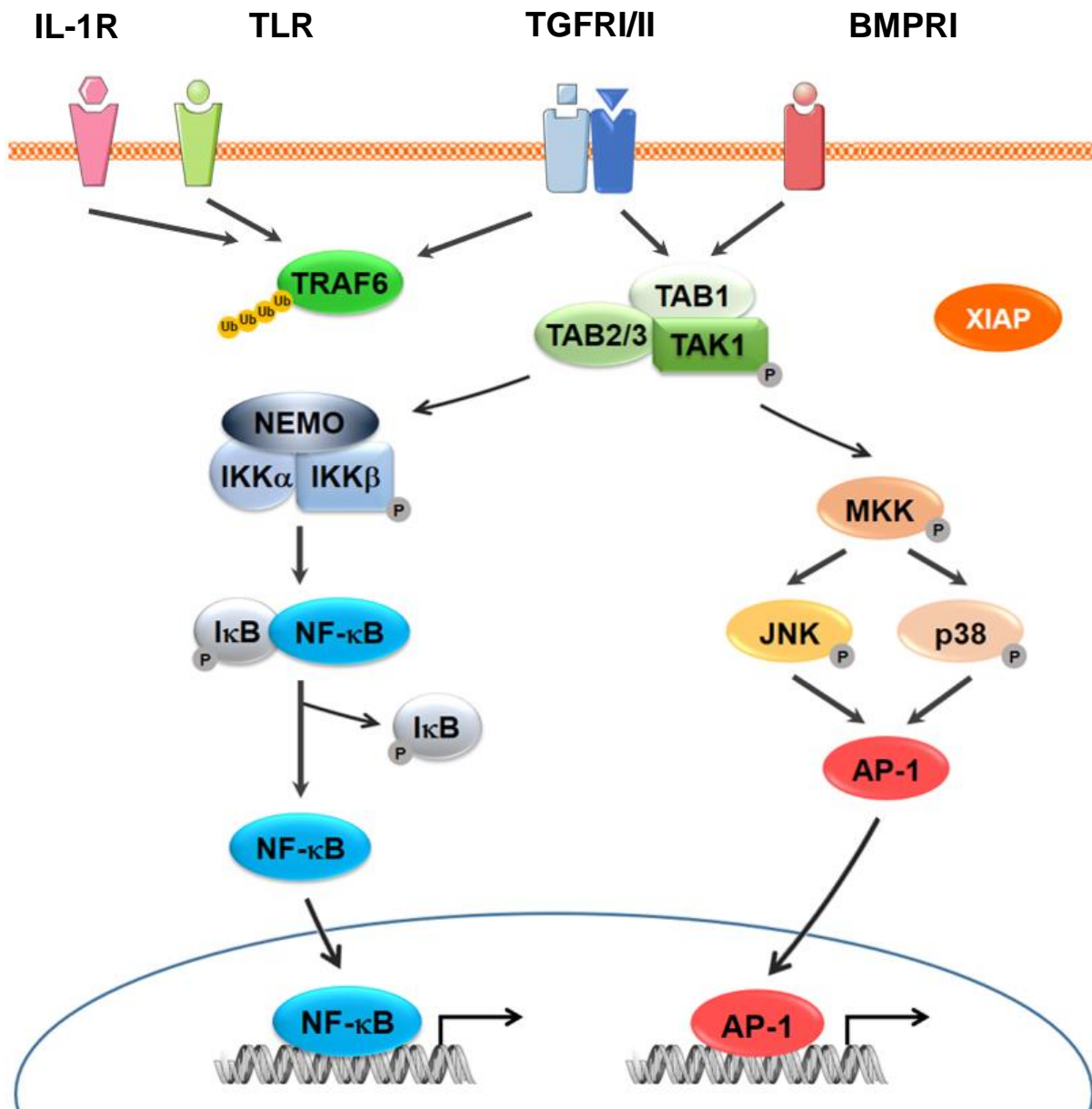


Figure 5.1. Regulation of the TAK-TAB protein complex. TAK1 and its binding partners, TAB1, 2 and 3 form a protein complex to regulate downstream signalling pathways. The activity of the TAK-TAB protein complex is mediated by IL-1, TLR, TGF β and BMP signalling. Activation of the TAK1-TAB complex is achieved by the recruitment of polyubiquitin chains via TRAF6 or XIAP binding to TAB1. Following a series of phosphorylation kinase triggered by the activated TAK1-TAB complex, NF- κ B and AP-1 signalling are activated to regulate their transcriptional targets.

We have produced XIAP-deficient KGN cells using an shRNA system. In this study, in order to study the specific functional domains of XIAP, we have generated expression constructs that contain a mutant XIAP including one that harbors a single point mutation in the BIR1 domain. These constructs are inducible vectors, allowing one to switch on expression of the mutant XIAP with the addition of 4-hydroxy-tamoxifen. The XIAP-deficient KGN cells have been stably transfected with the construct containing the mutant BIR1 domain (referred to as the 'XIAP BIR1 knockdown cells'). My aim is to use a TAK1 inhibitor or the XIAP BIR1 knockdown cells to eliminate the activation of TAK1 via TAB1 binding on XIAP. This will allow us to investigate the effect of TAK1 inhibition on the constitutive NF- κ B and AP-1 signalling and to delineate the source of the constitutive activities of these pro-survival signalling pathways. The experimental design of this study is as follow:

- i) Investigate the effect of TAK1 inhibition using a TAK1 inhibitor, 5Z-7-oxozeaenol;
- ii) Identify by sequencing any activating mutation in the *TAK1* gene; and
- iii) Establish a stable, inducible XIAP knockdown cell line to study the function of the BIR1 domain.

5.2 Methods

5.2.1 Cell lines

5.2.1.1 GCT-derived cell lines

GCT-derived cells, KGN and COV434 were established as previously described (van den Berg-Bakker et al., 1993, Nishi et al., 2001). They were used in this study to investigate the regulation of XIAP and how it regulates other signalling pathways in GCT. The culture conditions are detailed in Chapter 2 Section 2.1.1.1.

5.2.1.2 hGrC1

A human non-luteinised granulosa cell line, hGrC1, was established from GC of a 35-year-old female. The hGrC1 cells express steroidogenesis-related enzymes such as aromatase, the steroidogenic acute regulatory protein (StAR) and the cholesterol side-chain cleavage enzyme (CYP11A). The hGrC1 cells also express LHR and functional FSHR, where stimulation with activin A and FSH stimulates FSHR and aromatase expression, respectively (Bayasula et al., 2012). The hGrC1 were cultured in DMEM supplemented with 10% FBS, 2.4% HEPES buffer, 1% penicillin/streptomycin/amphotericin B and 1% sodium pyruvate. The media and the additives are all purchased from Invitrogen, Thermo Fisher Scientific (Waltham, WA, U.S.A.).

5.2.1.3 Lenti-X HEK293T

In order to produce lentiviral particles, Lenti-X HEK293T cell line was used. The Lenti-X HEK293T cell line is a derivative of the human embryonic kidney cell line,

HEK293 (Graham et al., 1977). The Lenti-X HEK293T cell line is known for having high transfection efficiency as a result of the insertion of the gene encoding SV40 T-antigen and exhibits an epithelioid morphology. The Lenti-X HEK293T cells were cultured in DMEM with 10% FBS, 2.4% HEPES buffer, 1% penicillin/streptomycin/amphotericin B and 1% sodium pyruvate (Invitrogen).

5.2.1.4 Chinese Hamster Ovary (CHO)

The CHO cell line was derived from the ovaries of an adult Chinese hamster (Puck et al., 1958). This cell line was used due to the high efficiency of transfection seen for this cell line and thus serves as a good model to test the robustness of the GEV16-5UAS-XIAP expression vector inducible system. The CHO cells were cultured in DMEM supplemented with 10% FBS, 2.4% HEPES buffer and 1% penicillin/streptomycin/amphotericin B.

5.2.2 *Transactivation assays*

Transactivation assays were performed to assess the effect of TAK1 or XIAP inhibition on AP-1 and NF- κ B mediated transactivation in the KGN and COV434 cells. The protocol for the transactivation assays are described in Chapter 2 Section 2.1.2.

5.2.2.1 Vectors/plasmids

The empty vector pTAL, and the reporter plasmids, pAP1₃-luc and pNF κ B₄-luc, used in this study are described in Chapter 2 Section 2.1.2.1.

5.2.2.2 Drug treatment

The above vectors (Chapter 5 Section 5.2.2.1) are transfected in the KGN and COV434 cells using the transfection reagent, SuperFect (Qiagen, Hilden, Germany) and Trans IT-LT1 (Mirus Bio LLC, Madison, WI, U.S.A.), respectively. The protocol for the transfection is described in Chapter 2 Section 2.3.2.2. Following overnight recovery after the 4-hour incubation with the transfection reagent, the cells were subjected to the following treatment regime for 24 hours (Table 5.1). All drugs were diluted at desired concentration in DMEM for COV434 or DMEM:F12 for KGN; 500 μ l was added to each well. Luciferase assay was conducted at the end of the 24-hour drug treatment as previously described (Chapter 2 Section 2.1.2.3).

Table 5.1. Compounds used in AP-1 and NF- κ B transactivation assay.

Compounds	Effects	Concentrations
Embelin (Emb)	Inhibits XIAP	10 μ M
Smac-mimetic (SM)	Mimics the action of the endogenous XIAP inhibitor	1 μ M
BAY11-7082 (BAY)	Inhibits I κ B phosphorylation, and subsequent NF- κ B translocation to the nucleus	5 μ M for KGN 10 μ M for COV434
PD-98059 (PD)	Inhibits MAP kinase pathway targeting ERK	20 μ M for KGN 30 μ M for COV434
5Z-7-oxozeaenol (5Z-7)	Inhibits TAK1	2.5 μ M

5.2.3 Cell proliferation assay

A cell proliferation assay was performed using the CellTiter 96® AQueous One Solution Cell Proliferation Assay (Promega, Madison, WI, USA) to determine the IC₅₀ of a small molecule inhibitor of TAK1, 5Z-7-oxozeaenol (5Z-7; Sigma Aldrich, St. Louis, MO, USA). 5Z-7 binds to the cysteine residue in the ATP-binding site to compete with ATP and irreversibly inhibit TAK1. The reagent of the proliferation assay contains a tetrazolium compound (MTT) which is reduced by viable cells into a coloured formazan product, hence serves as a colorimetric method for determining the number of viable cells in a proliferation or cytotoxicity assay. Briefly, cells were seeded in a 96-well plate at 4×10^3 KGN cells or 1×10^4 COV434 cells were maintained in 100 µl of respective media in each well. Serial dilution of 5Z-7 was made up in DMEM:F12 for KGN or DMEM for COV434 (Table 5.2). 24-hours post-seeding, cells were washed with PBS and 100 µl of the titrated 5Z-7 was added to each well. The cells were treated for 24 or 48 hours. 20 µl of CellTiter 96® AQueous One Solution Reagent was added into each well containing the cells in 100 µl of medium. The plate was then incubated at 37°C for 4 hours. Absorbance at 490 nm was measured using the EnVision® Multilabel Reader. The absorbance values (y-axis) obtained were plotted against the log concentration of 5Z-7 (x-axis); The IC₅₀ within a 24 or 48-hour period after 5Z-7 treatment was calculated using the variable slope model of the GraphPad Prism version 7.02.

Table 5.2. Serial concentration of 5Z-7 for KGN and COV434 in the MTT assay.

	Serial dilution of 5Z-7 (μM)
KGN	1 x 10 ⁻³ , 2.5 x 10 ⁻³ , 5 x 10 ⁻³ , 1 x 10 ⁻² , 2.5 x 10 ⁻² , 5 x 10 ⁻² , 7.5 x 10 ⁻² , 0.1, 0.25, 0.5, 0.75, 1, 2.5, 5, 10, 25, 50, 75, 100
COV434	

5.2.4 xCELLigence assay

The xCELLigence Real Time Cell Assay (RTCA) system measures electrical impedance across the microelectrodes integrated into the bottom of the tissue culture plates. Continuous impedance measurement is represented as cell index (CI) values. These values provide quantitative information about cell number, viability and morphology in real-time. The RTCA system was utilised to determine the IC₅₀ of a small molecule inhibitor of TAK1, 5Z-7 (Sigma). This allows cross-validation of the data generated from the CellTiter 96® Aqueous One Solution Cell Proliferation Assay (Promega) as well as real-time monitoring of 5Z-7-mediated cytotoxicity. The experimental schedule of the real-time monitoring using xCELLigence is outlined in Table 5.3.

A 96-well plate (E-plate 96) was used for the proliferation assay. It is important to ensure that the connection between the plate and the RTCA system is active and the scan is performed properly. To start, 50 μl of media was first added to each well. This is to 'blank' the impedance measurement and ensure all the activated wells show normal resistance. Next, 50 μl of cell suspension containing 4 x 10³ KGN cells or 1 x 10⁴ COV434 cells in respective media were added into each well. Cells were allowed

4 hours to adhere to the wells.

Table 5.3. Experimental schedule for the xCELLigence assay.

Step	Sweeps	Interval (min)
1. Background measurement	1	1
2. Cell seeding	100	5
	100	15
3. Drug administration	100	15
	999	15
4. Backup	999	15

Serial dilution of 5Z-7 was made up in DMEM:F12 for KGN or DMEM for COV434 (Table 5.4). 100 μ l of the titrated 5Z-7 or 0.1% DMSO was added to the wells in duplicates. Once the drugs were added and plate returned to the machine, step 3 of the experimental schedule commenced. Impedance measurement by the RTCA system was performed for up to 96 hours. Data were analysed using RTCA Software 1.2. Cell index was first normalised to the time of drug addition. A dose-response curve was derived using the 'sigmoidal dose-response equation (variable slope)'. The IC₅₀ within a 24 or 48-hour period after 5Z-7-oxozeaenol treatment was calculated using GraphPad Prism version 7.02.

Table 5.4. Serial concentration of 5Z-7 for KGN and COV434 in the xCELLigence assay.

	Serial dilution of 5Z-7 (μM)
KGN	0.1, 0.25, 0.5, 0.75, 1, 2, 3, 5, 7.5, 10, 25
COV434	0.5, 0.75, 1, 2.5, 5, 7.5, 10, 12.5, 15, 25, 50

5.2.5 Primer design and PCR

Given TAK1 is upstream of the constitutive NF- κ B and AP-1 signalling, we sought to determine if there is an activating mutation in the *TAK1* gene. 5 pairs of primers were designed based on variant B of *TAK1* (NCBI reference sequence: NM_145331.2), which has the longest sequence among the 4 variants, to amplify the *TAK1* gene in the KGN and COV434 cells. The PCR reaction contained 0.5 μl of Pfu DNA polymerase (2.5 U/ μl ; Agilent Technologies), 2.5 μl of Pfu DNA polymerase 10X buffer (Agilent Technologies), 1 μl of dNTP mix (10 mM; Invitrogen), 0.5 μl of 10 μM primers (Table 5.5), 1 μl of cDNA from the KGN and COV434 cells and 19 μl of nuclease-free H₂O to make up a total volume of 25 μl . The PCR conditions were as follow: 95°C for 5 minutes, 1 cycle; 95°C for 30 seconds, primer-specific annealing temperature for 30 seconds and 72°C for 40 seconds, 30 cycles; followed by a final extension at 72°C for 10 minutes. PCR products were examined on a 1.5% agarose gel stained with SYBRTM Safe DNA gel stain (Invitrogen) using gel electrophoresis.

Table 5.5. Primer sequences for the *TAK1* gene.

Nucleotide position	Sequence (5' – 3')	Amplicon length (bp)	Annealing temperature (°C)
409-429; 809-709	Forward: GCGAGGGATCATGTCTACAGC	401	58
	Reverse: TGC GTGGGCAGCAGTATAA		
698-717; 1161-1140	Forward: GGAGCCTGCTTGAATCCAG	464	62
	Reverse: CGAGTACCATTATGAACAGCCC		
1090-1109; 1586-1567	Forward: CGTCGGAAACCCTTTGATG	497	60
	Reverse: CACTCATCCTCTTGCCCTCA		
1483-1502; 1954-1935	Forward: TCAGGCAAAGCAACAGAGT	472	56
	Reverse: CGGTGCTAGAGGCTGTAGTT		
1864-1885; 2265-2243	Forward: CCTGATGATTCCACAGATACC	402	54
	Reverse: TCAAATGTAACGGTCCCAG		

5.2.5.1 DNA extraction from agarose gels

Following amplification, the PCR products of the *TAK1* gene were examined on a 1.5% agarose gel using gel electrophoresis. This ensures no secondary structures or non-specific amplicons are included in the subsequent sequence analysis. DNA extraction was then performed using the QIAquick® gel extraction kit (Qiagen) according to manufacturer's instructions. Under UV light, the DNA fragment was excised from the agarose gel with a sterile, sharp scalpel. The gel slice was weighed in a microcentrifuge tube, after which 3 volumes of Buffer QG was added to 1 volume of the gel slice. It was then incubated at 50°C with vortexing every 2-3 minutes until the gel slice has completely dissolved. 1 gel volume of isopropanol was added to the sample before it is transferred to a QIAquick spin column. The sample was centrifuged for 1 minute at 13,000 rpm; flow-through was discarded. To remove all traces of agarose, 500 µl of Buffer QG was added to the QIAquick spin column and centrifuged for 1 minute at 13,000 rpm; flow-through was discarded. To wash, 750 µl of Buffer PE was added to the QIAquick spin column and centrifuged for 1 minute at 13,000 rpm; flow-through was discarded. To remove residual ethanol from Buffer PE, the QIAquick spin column was placed in a 2 ml collection tube to be centrifuged for 1 minute at 13,000 rpm. 30 µl of Buffer EB was added to the centre of the QIAquick membrane, let stand for a minute, prior to eluting the DNA by centrifugation for 1 minute at 13,000 rpm.

5.2.5.2 Sequencing

The isolated DNA samples were submitted to the Gandel Sequencing Trust Sequencing Facility (Monash Health Translational Precinct, Clayton, Victoria) for

Sanger sequencing. The sequence data were then aligned against the sequence of the human *TAK1* gene using the 'human genomic plus transcript' database on the NCBI BLAST website.

5.2.6 Transcriptome data processing and statistical analyses

We have previously established transcriptome profiles for 6 stage 1 GCT, 6 stage 3 GCT and the KGN cells (Alexiadis et al., 2016), as well as the juvenile GCT-derived COV434 cells and the non-luteinised GC cell line, hGrC1. This dataset enabled us to analyse the mRNA levels of *TAK1* and its binding partners, *TAB1/2/3* and *TRAF6*. Data were analysed using GeneSpring version 14.8 (Agilent) and normalised using the quantile normalisation method. Significant difference between any two sample groups was identified by performing a moderated *t*-test with the $p < 0.05$ computed using the asymptotic method. Genes with a fold change ≥ 2.0 were then subjected to Westfall Young Permutation multiple testing correction. This procedure is applied to avoid false discoveries when multiple testing is performed. This procedure has high detection power and high sensitivity which allows the discovery of statistically significant combination (Westfall and Young, 1993).

5.2.7 Generation of *shRNA-resistant XIAP wildtype and mutant plasmids*

5.2.7.1 Plasmids

5.2.7.1.1 XIAP plasmid constructs

XIAP plasmid constructs, including XIAP wildtype and two mutants (D148A and W310A), were cloned into pF-5UAS (upstream activating sequences)-SV40-puro expression vector (provided by Prof. John Silke, WEHI; Figure 5.2). The XIAP

wildtype construct was generated as a positive control. A single point mutation was introduced to eliminate caspase-3 and -7 binding by BIR2 domain (D148A), or caspase 9 binding by BIR3 domain (W310A) of XIAP. Stable cell lines have been generated with efficient inducible XIAP gene silencing using shRNA. To prevent these XIAP plasmid constructs from being targeted by XIAP gene silencing, each construct has been rendered shRNA-resistant by two silent mutations in the shRNA binding site using site-directed mutagenesis (Chapter 5 Section 5.2.7.2). The shRNA-resistance XIAP plasmid constructs will then be transduced into the XIAP-deficient cell lines. Figure 5.3 shows the map of the expression-empty pF-5UAS-SV40-puro vector.

5.2.7.1.2 GEV16 plasmid

The GEV16 plasmid was used to induce the expression of the XIAP expression constructs in the lentivirus. The GEV16 construct contains the GAL4 DBD lentiviral 5' long terminal repeats (LTR) and 3'-self-inactivating (sin) LTR (Figure 5.4). The construct has a ubiquitin promoter (P_{Ub}) that constitutively drives the expression of the GEV16 transcription factor. In the presence of 4-hydroxy-tamoxifen, GEV16 translocates from cytoplasm to the nucleus and binds to GAL4 upstream activating sequence to upregulate transcription of the gene of interest, in this case, the shRNA-resistant *XIAP* wildtype or mutant gene.

5.2.7.1.3 pTRIPz plasmid

The pTRIPz vector (gift from Dr Julian Quinn, *former* Prince Henry's Institute, Australia) has a tet-on system which allows the regulation of shRNA expression in the presence of doxycycline. The pTRIPz vector consists of a tetracycline response

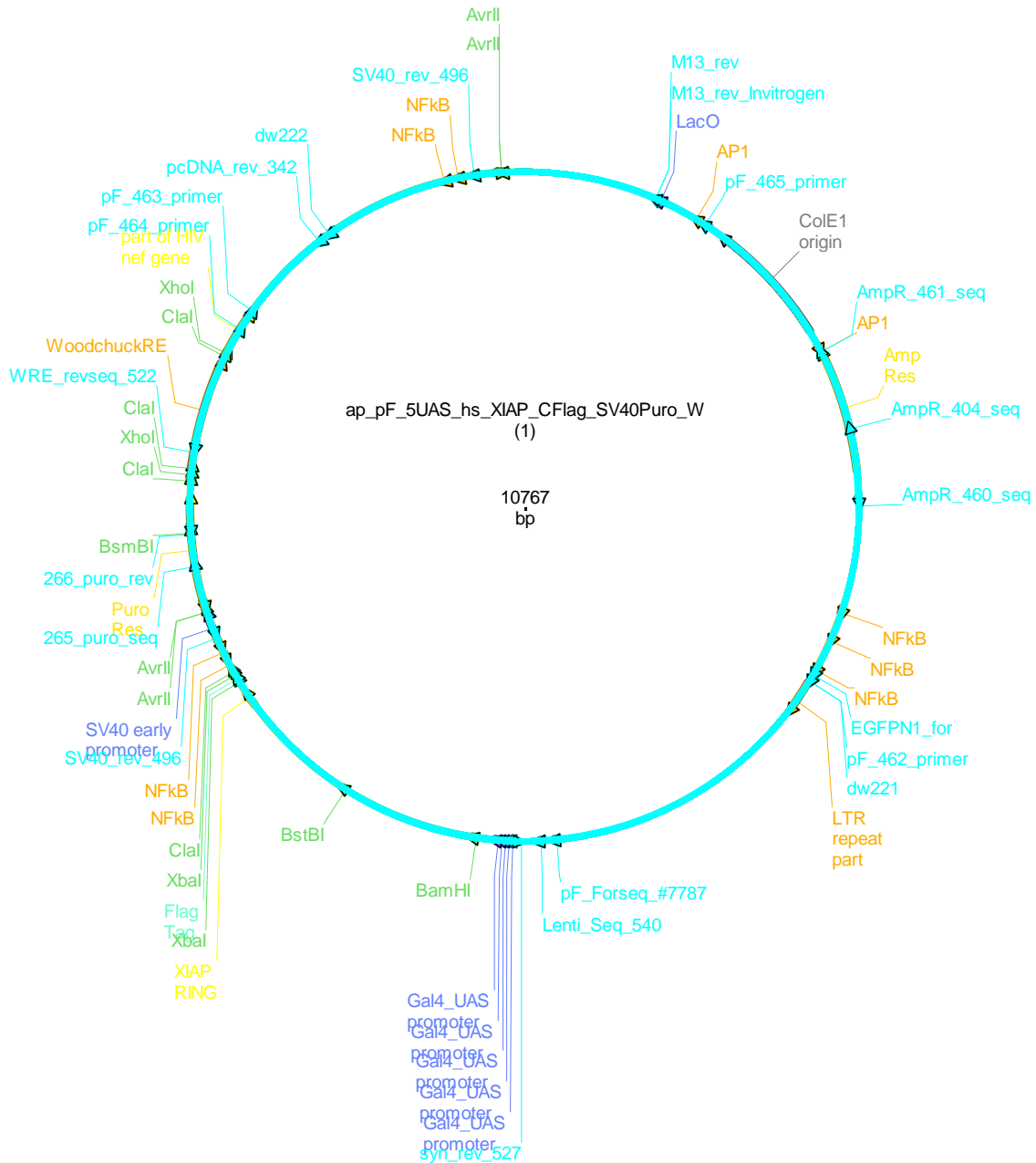


Figure 5.2. Map of the pF-5UAS-SV40-puro expression vector. The pF-5UAS-SV40-puro expression vector carries the puromycin resistance gene as a selection marker. The GAL4/UAS promoter is located upstream of the XIAP wildtype, D148A or W310A mutants to drive the expression of one of these constructs. The vector shown here contains a FLAG-tag but the vector is also available without the tag.

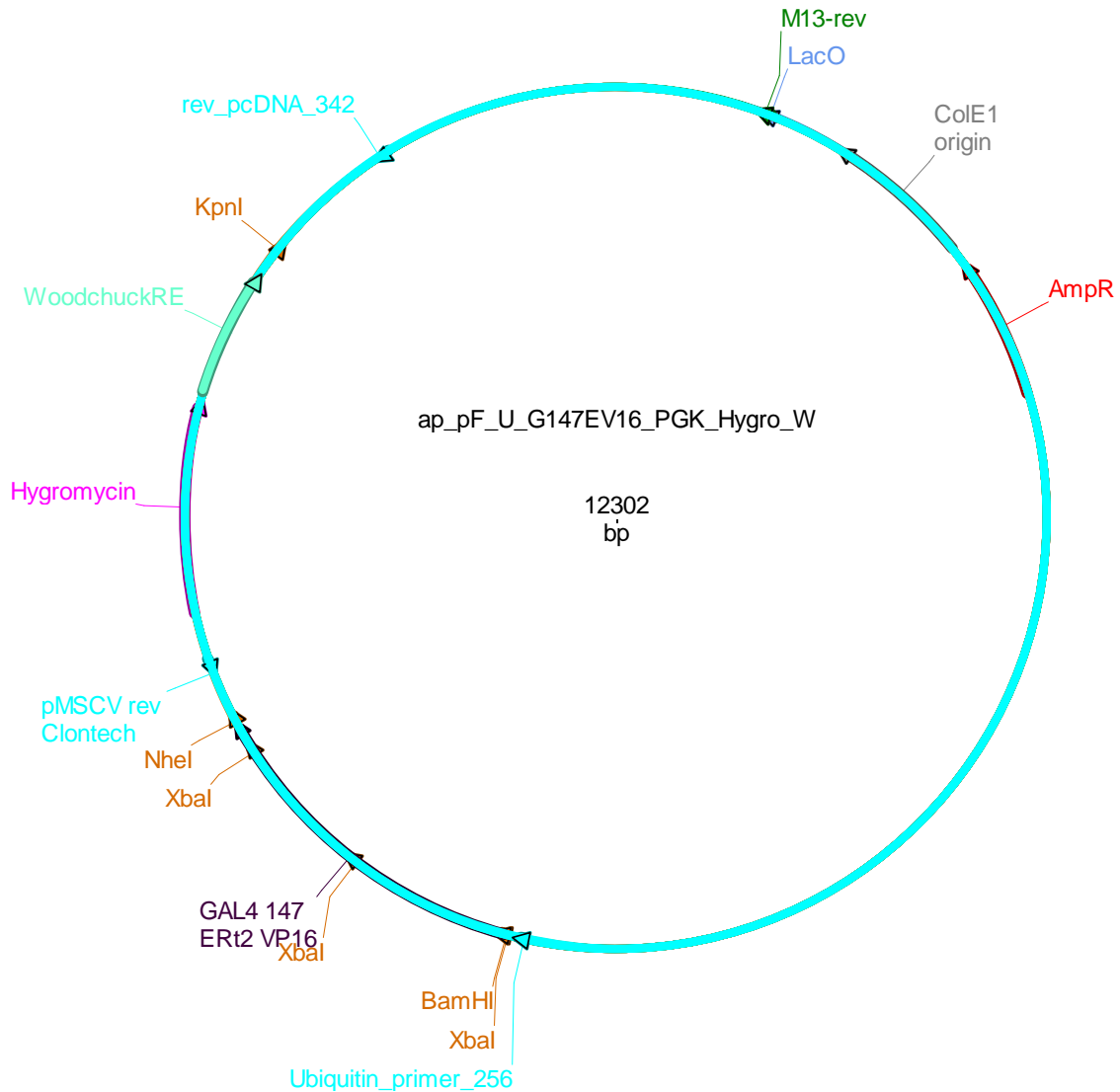


Figure 5.4. Map of the GEV16 plasmid. The GEV16 plasmid is a 4-hydroxy tamoxifen (4HT)-inducible lentiviral expression system which carries a ubiquitin promoter that constitutively drives the expression of the GEV16 transcription factor. Addition of 4HT triggers GEV16 to translocate from the cytoplasm to the nucleus. The nuclear GEV16 then binds to the GAL4 UAS to drive the transcription of the gene of interest.

element (TRE), a transactivator (rtTA 3) and a red fluorescence protein (RFP) reporter. shRNA targeting XIAP (Millennium Science) was cloned into the pTRIPz which underwent restriction digestion using MluI and XhoI. Upon addition of doxycycline, the transactivator binds to and activates expression from the TRE promoter to drive the expression of the XIAP shRNA and RFP. The RFP serves as a visible aid to assess the induction of TRE expression.

5.2.7.2 Site-directed mutagenesis

To introduce a point mutation in the shRNA binding site, the QuikChange II XL Site-Directed Mutagenesis Kit (Agilent Technologies) was used according to the manufacturer's instructions. All materials except the primers, plasmid DNA and dH₂O, were provided with the QuikChange® II XL site-directed mutagenesis kit. PCR was performed to amplify gene products with the desired point mutation. The primer sequences are shown in Table 5.6, incorporating a silent mutation (CAG→CGG) within the shRNA binding site to create shRNA-resistance.

Table 5.6. Primer sequences for site-directed mutagenesis.

shRNA binding site on XIAP	Sequence
302-320	Forward: CAACACTGGCACGAGC G GGGTTTCTTTATACTG
	Reverse: CAGTATAAAGAAACCC C GCTCGTGCCAGTGTTG

*A silent point mutation where A>**G** and T>**C**.

Briefly, PCR reaction mixtures consisted of 125 ng of mutation-specific primers, 65 ng of plasmid DNA, 1 μ l of 10 mM dNTP mix, 5 μ l of 10X reaction buffer, 3 μ l of QuikSolution reagent and dH₂O in a total volume of 50 μ l. 1 μ l of Pfu DNA polymerase (2.5 U/ μ l) was then added to the reaction mixture. Thermal cycling conditions were as follow: 95°C for 1 minute, 1 cycle; 95°C for 50 seconds, 60°C for 50 seconds and 68°C for 12 minutes, 18 cycles; 68°C for 7 minutes, 1 cycle.

After the completion of PCR, 10 μ l of the PCR products was added with 2 μ l of 6X loading dye to load on 1.5% agarose gel stained with ethidium bromide. With the remaining 15 μ l of each PCR product, 1 μ l of Dpn1 restriction enzyme was added prior to incubation at 37°C for 1 hour. For each reaction, 45 μ l of supercompetent cells were added to a pre-chilled 1.5ml microcentrifuge tube. 2 μ l of beta-mercaptoethanol was added into the supercompetent cells 10 minutes prior to transformation. To transform, 3 μ l of Dpn1-treated mixture was added to the supercompetent cells; heat shocked at 42°C for 30 seconds, then put immediately on ice for 2 minutes. Next, 500 μ l of NZY⁺ media (prepared as per manufacturer's protocol), preheated to 42°C, was added into the transformation mixture, shaken at 250 rpm at 37°C for an hour, to allow the cells to recover. Transformed cells were spun down at 13,000 rpm for 3 minutes. 300 μ l of supernatant was drawn out; the pellet was re-suspended in the remaining 250 μ l, and plated on LB-ampicillin plates. The plate was incubated at 37°C overnight. Several colonies were picked from the plate to be inoculated in 5 ml of LB medium containing 75 μ g/ml penicillin. Bacterial cells were harvested for approximately 8 hours at 37°C with vigorous shaking at 250 rpm.

5.2.7.3 Plasmid miniprep

Following overnight culture, the bacterial cells were spun down at 13,000 rpm for 15 minutes using a bench-top microcentrifuge. Plasmid purification was performed using the plasmid miniprep kit (Qiagen), according to manufacturer instructions. All centrifugation steps were performed in a table-top microcentrifuge at 13,000 rpm, unless otherwise specified.

In brief, a single colony was picked from a freshly streaked LB plate and inoculated in 5 ml of LB media with 75 µg/ml of penicillin. The tube was incubated at 37°C overnight with vigorous shaking at 250 rpm. Harvesting of the bacterial cells was by centrifugation for 15 minutes. The supernatant was carefully decanted and the pellet re-suspended in 250 µl of Buffer P1. To lyse the cells, 250 µl of Buffer P2 was added and thoroughly mixed by inverting the sealed tube 4-6 times. Following the addition of 350 µl of neutralisation buffer (Buffer N3), the tube was inverted immediately for 4-6 times to mix, and centrifuged for 10 minutes. The supernatant was applied to a spin column and centrifuged for 30 seconds to allow plasmid DNA to bind to the resin. The spin column with the bound DNA was washed with 500 µl of Buffer PB and centrifuged for 30 seconds. 750 µl of Buffer PE was added to the spin column to remove impurities. The flow-through was discarded upon centrifugation for 30 seconds. An additional 1 minute of centrifugation was carried out to remove residual wash buffer. To elute DNA, 50 µl of dH₂O was added to the centre of the column, which has been placed in a clean 1.5 ml microcentrifuge tube. The tube was let stand for 1 minute, then centrifuged for 1 minute with the supernatant containing the DNA.

NanoDrop Spectrophotometer was used to measure DNA concentration (see Chapter 2 Section 2.1.2). Diluted with dH₂O, 20 ng of plasmid DNA was used as template in DNA amplification using PCR as described in the next section. If needed, 10 ng of diluted plasmid DNA was utilised for a large yield of plasmid production (see Section 5.2.6.4).

5.2.7.4 Plasmid maxiprep

10 ng of the plasmid obtained from the plasmid miniprep was transformed using XL1-blue supercompetent cells as described in Chapter 5 Section 5.2.7.3. 250 ml of LB medium containing 75 µg/ml ampicillin was inoculated with 2 ml of the bacteria transformed with a specific plasmid. The culture was incubated at 37°C with shaking at 250 rpm. After approximately 18 hours, bacterial cells were harvested by centrifugation at 4,255 x g for 15 minutes at 4°C. High yield plasmid purification was performed using the plasmid purification maxiprep kit (Qiagen). 10 ml of Buffer P1 (with RNase A) was added to resuspend the bacterial pellet; complete resuspension was ensured by vortexing until no cell clumps remained. Upon addition of 10 ml of lysis buffer (Buffer P2), the sealed tube was mixed thoroughly by vigorous inversion for 4-6 times. The tube was incubated at room temperature for 5 minutes to ensure complete lysis of bacteria. Subsequently, pre-chilled neutralization buffer (P3) was added, resulting in the precipitation of genomic DNA, protein and cell debris. The tube was mixed again prior to centrifugation at 4,255 x g for 1 hour at 4°C. After centrifugation, the supernatant containing plasmid was removed promptly. The centrifugation step was repeated once more to avoid applying suspended or particulate material to the column. During the centrifugation step, the silica matrix column was equilibrated with 30 ml of equilibration buffer. Once the final

centrifugation step was completed, the supernatant was applied to the column, to allow the plasmid DNA to bind to the silica matrix. Once the plasmid DNA was bound to the resin, 2 washes with buffer QC (10 ml each time) was added to the column to remove contaminants during plasmid DNA preparations. The flow-through was discarded; DNA was eluted in 15 ml of elution buffer (Buffer QF). To precipitate the DNA, 10.5 ml of room-temperature isopropanol was added to the eluate and centrifuged at 4,255 x g for 1 hour at 4°C. Next, the isopropanol/DNA pellet was washed with 5 ml of room-temperature 70% ethanol to remove precipitated salt and centrifuged at 4,700 x g for 1 hour at 4°C. Supernatant was carefully decanted. The DNA pellet was re-dissolved in 100 µl of dH₂O.

5.2.8 Reintroduction of XIAP into XIAP-deficient cell line

5.2.8.1 Generation of lentivirus

Lenti-X HEK293T cells were seeded at 2×10^6 in each of 100-mm plate, maintained in 20 ml of supplemented DMEM and incubated at 37°C with 5% CO₂ overnight. The cells were approximately 80% confluent when transfected. Approximately 24 hours after seeding, existing media was replaced by 10 ml of opti-MEM (Invitrogen) with 1% sodium pyruvate.

Lentiviral particles containing expression vectors of interest were generated using the Lenti-X™ HTX packaging system (Clontech Laboratories), according to the manufacturer's instructions. Plasmid DNA and polymer mixture for each transfection sample were prepared as outlined in Table 5.7.

Table 5.7. Preparation of plasmid DNA and polymer solutions.

Plasmid DNA solution (Tube 1)	Polymer solution (Tube 2)
<ul style="list-style-type: none"> – 7 μg of vector DNA (i.e. shRNA-resistant XIAP WT or mutant); – 36 μl of Lenti-X HTX packaging mix*; – Xfect reaction buffer to make up total volume of 600 μl 	<ul style="list-style-type: none"> – 592.5 μl of Xfect reaction buffer; – 7.5 μl of Xfect polymer

*The Lenti-X HTX packaging mix contains all necessary plasmids encoding packaging elements such as gag, vpr-pro, tet and rev, env (VSV-G) and Tet-Off.

Each tube was vortexed to mix. After combining the two tubes, the DNA-Xfect mixture was vortexed again at a medium speed for 10 seconds. To allow nanoparticle complexes to form, the DNA-Xfect mixture was incubated for 10 minutes at room temperature. The entire 1200 μl of DNA-Xfect mixture was added dropwise to each 100-mm plate of Lenti-X HEK293T cells, during which the plate was gently swirled. The plate was incubated at 37°C overnight.

On day 2, the existing transfection medium was decanted and the plate was washed gently with PBS. 10 ml of fresh opti-MEM and 1% sodium pyruvate were added before returning the plate to 37°C for an overnight incubation.

On day 3, the entire 10 ml of viral supernatant was combined with 3.33 ml of Lenti-X concentrator in a 14 ml Falcon tube. The tube was inverted to mix before incubating at 4°C overnight. The transfection medium was replaced with 10 ml of fresh opti-

MEM, 2% tetracycline-free FBS and 1% sodium pyruvate. The plate was returned to 37°C to incubate overnight.

After an overnight incubation, the viral supernatant with Lenti-X concentrator was centrifuged at 1,500 x g for 45 minutes at 4°C. After centrifugation, supernatant was carefully removed without disturbing the pellet. The pellet was re-suspended in 1 ml of opti-MEM and stored immediately at -70°C.

At 48-hour post-transfection (day 4), the media from the plate was transferred to a sterile container. Using a syringe and a 0.45 µm filter, cellular debris was removed from the viral supernatant prior to storage in 1 ml cryogenic vials at -80°C for future use.

5.2.8.2 Lentiviral titration

Production of lentivirus was confirmed using Lenti-X GoStix. 20 µl of the lentiviral supernatant was applied to the sample well of the GoStix cassette. The viral supernatant produced by Lenti-X HTX Packaging System expressed a ZsGreen1 fluorescent protein. Upon the addition of 4 drops of Chase buffer, a clear band was generated, indicating that viral production was greater than 5×10^5 IFU/ml. This lentiviral titer test was performed on shRNA-resistant XIAP WT and D148A mutant plasmids.

5.2.8.3 Lentiviral transduction of CHO cells

CHO cells were seeded at 5×10^5 per well in a 6-well plate, maintained in 2 ml of supplemented DMEM. A serial dilution was performed on the viral DNA to determine at what concentration the CHO cells would transduce the most efficiently. Using

supplemented DMEM containing 8 $\mu\text{g/ml}$ of polybrene, a serial dilution (range: neat, 1/2, 1/4, 1/8, 1/16 and 0) of the lentiviral pseudoparticles was prepared. Existing media in the wells was removed; cells were washed once with PBS. 1 ml of DMEM containing 8 $\mu\text{g/ml}$ polybrene was added to each well; 200 μl of each of the pseudoparticles containing shRNA-resistant XIAP (wildtype or D148A mutant) and GEV16 was added drop-wise, with gentle swirling of the plate. Next, the plates were centrifuged at 1,500 x g at 22°C for 3 hours. Once the centrifugation was over, the plates were returned to the 37°C incubator.

On day 2, the CHO cells were treated with 4-hydroxy-tamoxifen to activate GEV16 to knockdown XIAP. Existing media was removed then cells were washed once with PBS. 1.5 ml of DMEM containing 1 μM 4-hydroxy-tamoxifen was added to each well. Plates were returned to the 37°C incubator for overnight culture. The CHO cells were lysed to assess the degree of XIAP knockdown using western blot analysis (Chapter 2 Section 2.2.5).

5.2.9 Statistical analyses

All drug treatments and luciferase assays were performed in duplicates and repeated three times. Data are presented as mean \pm SEM. One-way ANOVA was used for statistical analyses where $p < 0.05$ is considered statistically significant.

5.3 Results

Previous studies in our laboratory demonstrated that AP-1 and NF- κ B are constitutively activated in GCT (Chu et al., 2004). This led us to speculate on a potential point of convergence involving the TAK-TAB complex which is upstream of both the AP-1 and NF- κ B signalling pathways (Hofer-Warbinek et al., 2000, Kaur et al., 2005). As mentioned previously in Chapter 1 Section 1.2.2.8, XIAP regulates the activation of the TAK-TAB complex. To test our hypothesis that TAK-TAB is involved in the regulation of AP-1 and NF- κ B signalling in GCT, I transfected the KGN and COV434 cells with the AP-1 and NF- κ B reporter constructs. Cells were subsequently treated with XIAP and TAK1 inhibition to investigate their effects on the constitutive AP-1- or NF- κ B-mediated transactivation.

5.3.1 *IC*₅₀ of 5Z-7-oxozeaenol

The inhibition of TAK1 in the KGN and COV434 cell lines was performed using the compound, 5Z-7-oxozeaenol (5Z-7). 5Z-7 forms a covalent complex with TAK1 and irreversibly inhibits TAK1 activity. The irreversible inhibition abolishes the kinase and the ATPase activity of TAK1.

5.3.1.1 Cell proliferation assay

Cell proliferation assays using the MTT compound was performed to determine the *IC*₅₀ of 5Z-7, which is the dose that exerts 50% inhibitory response on the cells. Figure 5.5 shows the inhibitory dose-response curves of 5Z-7 in the KGN (A and B) and COV434 (C and D) cell lines at 24 and 48 hours. All curves followed the classical sigmoidal shape in a log(inhibitor) vs response curve. As the concentration of 5Z-7

increased, the absorbance, which was derived from the amount of MTT compound being reduced by the viable cells, reduced. The IC₅₀ and Hill slope at 24 and 48 hours are presented in Table 5.8. Hill slope represents the steepness of the curve; the standard hill slope is -1.0.

Table 5.8. IC₅₀ and Hill slope of 5Z-7 in KGN and COV434 at 24 and 48 hours from the MTT assay.

KGN			COV434	
24 hours	48 hours		24 hours	48 hours
5.19	3.68	IC ₅₀ (μM)	12.30	7.90
-1.39	-1.45	Hill slope	-1.48	-0.84

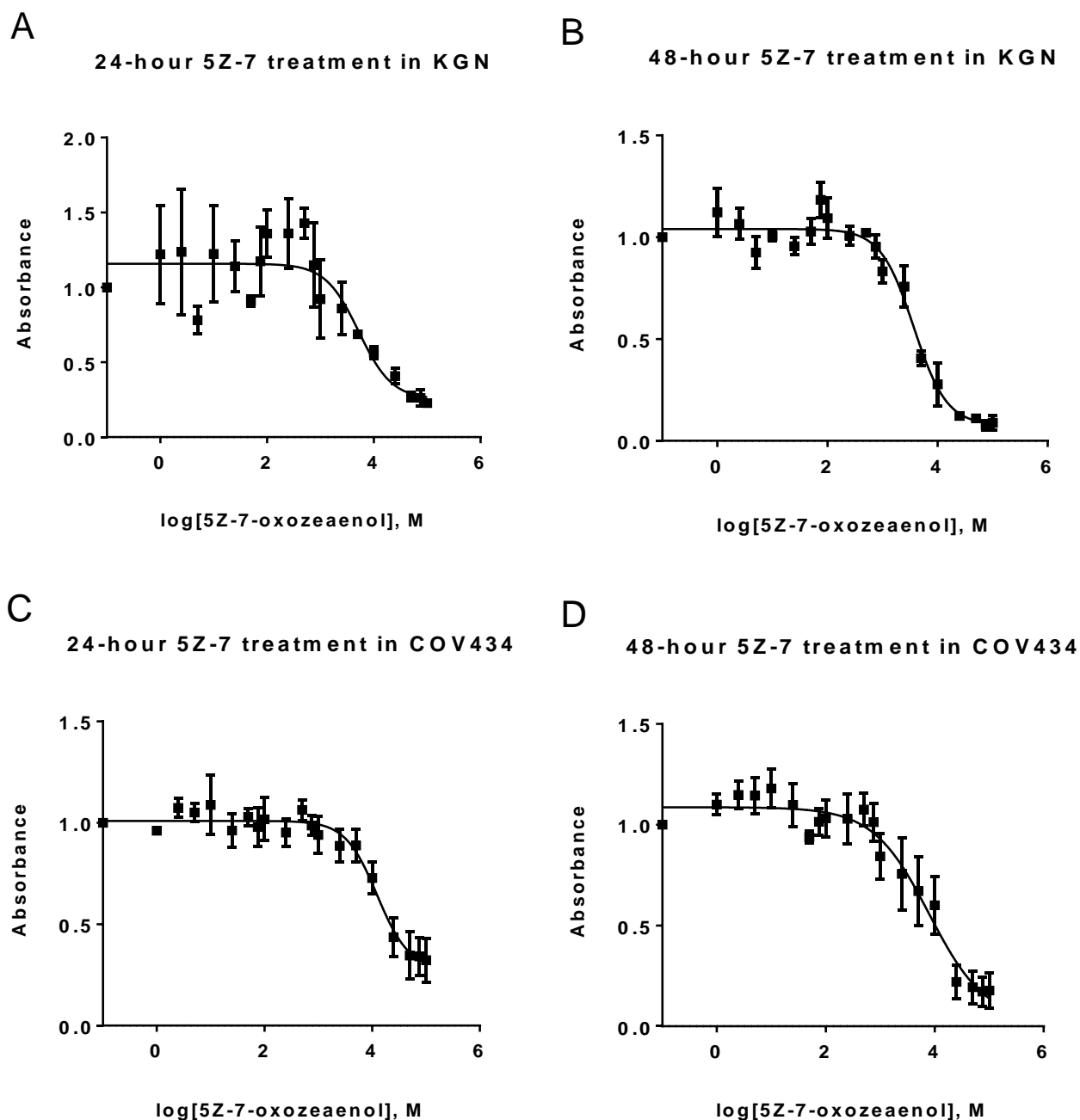


Figure 5.5. IC₅₀ of 5Z-7 from MTT assay. The inhibitory dose-response curve of 5Z-7 in the KGN (A and B) and COV434 (C and D) cells at 24 and 48 hours was determined using the MTT assay. Cell number, represented by absorbance of the MTT compound reduced by viable cells, reduced as the dose of 5Z-7 increased in both cell lines.

5.3.1.2 xCELLigence assay

Unlike the MTT assay which is an end-point cell proliferation assay, the xCELLigence offers real-time monitoring of cell proliferation following addition of 5Z-7 to the KGN and COV434 cells. Cell numbers were normalised to the time of drug addition. The normalised cell indices at 24 and 48 hours were selected to determine the IC₅₀ and hill slope (Table 5.9) to compare to that derived from the MTT assays. The inhibitory dose-response curves are shown in Figure 5.6, which demonstrated a reduced cell index as the concentration of 5Z-7 increased.

Table 5.9. IC₅₀ and Hill slope of 5Z-7 in KGN and COV434 at 24 and 48 hours from the xCELLigence assay.

KGN			COV434	
24 hours	48 hours		24 hours	48 hours
4.06	2.71	IC ₅₀ (μM)	3.66	3.58
-2.81	-3.61	Hill slope	-2.30	-2.58

5.3.2 *AP-1 transactivation is abolished by XIAP and TAK1 inhibition in GCT-derived cell lines*

Similar to previously published data (Chu et al., 2004), I observed a 6- and 7-fold induction of the AP-1-mediated transactivation under basal condition in the KGN and COV434 cells after normalized to the empty vector, pTAL (Figure 5.7), demonstrating

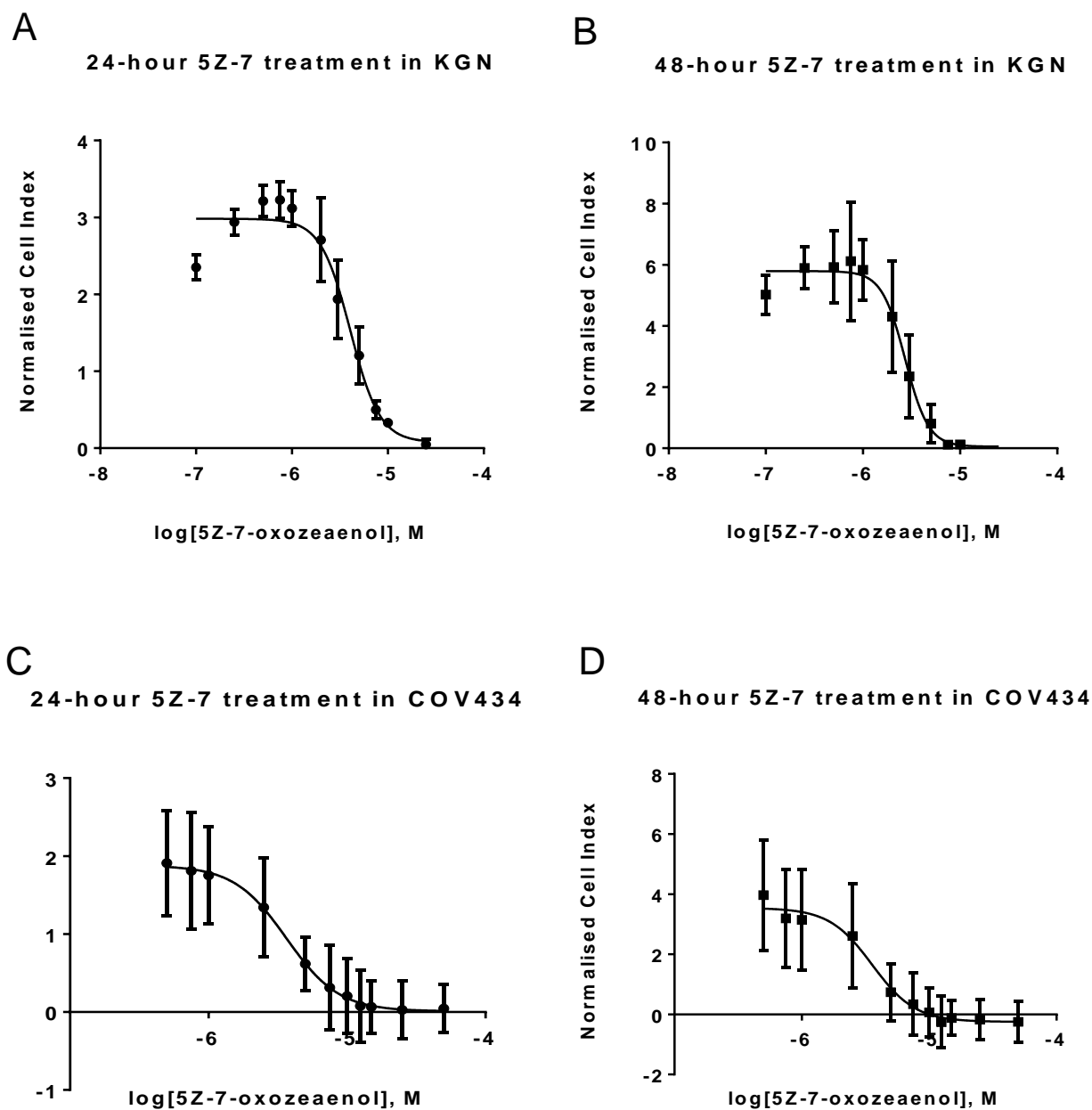


Figure 5.6. IC₅₀ of 5Z-7 from xCELLigence. The inhibitory dose-response curve of 5Z-7 in the KGN (A and B) and COV434 (C and D) cells at 24 and 48 hours was determined using the xCELLigence. As the concentration of 5Z-7 increased, the cell number represented by cell index, decreased. Cell index was normalised to the time of drug addition.

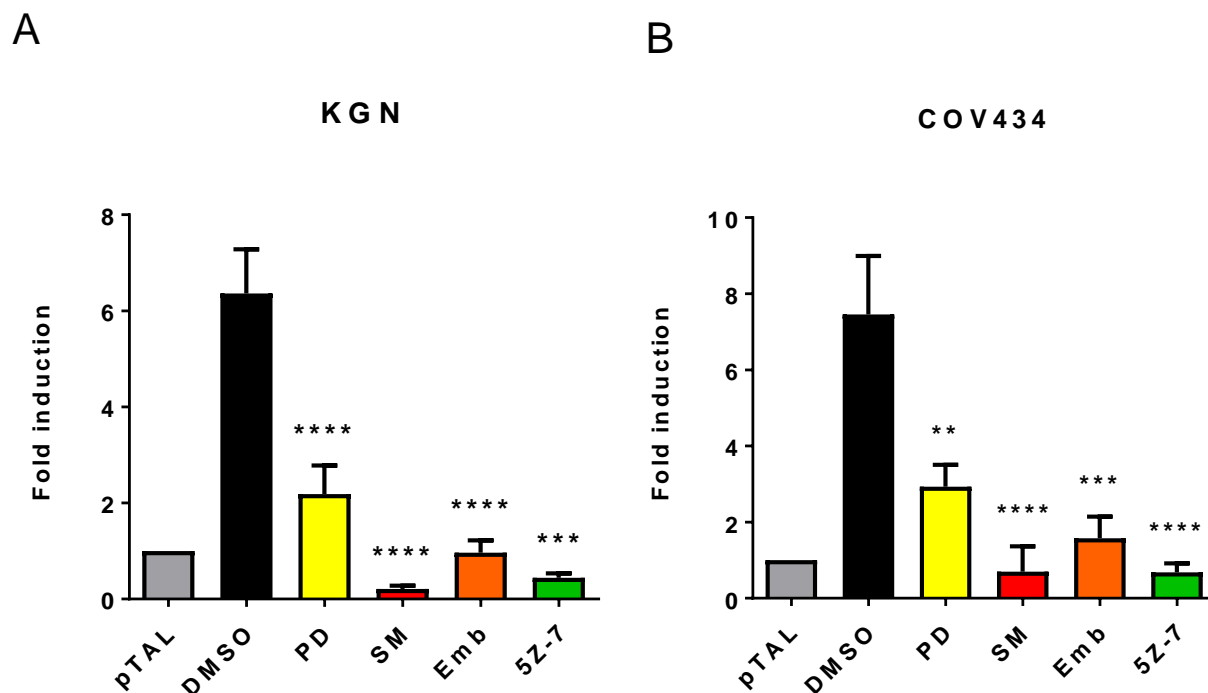


Figure 5.7. AP-1 transactivation assay in GCT-derived cell lines. The KGN (A) and COV434 (B) cells were transiently transfected with AP-1-Luc. 24-hour post transfection, cells were subjected to either vehicle treatment (0.1% DMSO) or inhibition of AP-1, XIAP or TAK1. AP-1-mediated transactivation was induced by 6- and 7-fold following DMSO treatment in the KGN (A) and COV434 (B), respectively, indicating constitutive AP-1 signalling in these cells. This constitutive activity was abolished by the specific AP-1 inhibitor, PD (20 μ M in KGN and 30 μ M in COV434). XIAP inhibition using SM (1 μ M) or Emb (10 μ M), as well as TAK1 inhibition using a suboptimal dose of 5Z-7 (2.5 μ M) significantly reduced AP-1-mediated transactivation to below baseline level in the GCT-derived cell lines. $n = 3$; mean \pm SEM; One-way ANOVA; Bonferroni post-hoc analysis; ** $p < 0.01$, *** $p < 0.001$, **** $p < 0.0001$ when compared to DMSO.

the constitutive activity of AP-1 signalling in these cell lines. The AP-1-mediated signalling was significantly reduced by PD98059 (PD). Inhibiting XIAP using SM ($p < 0.0001$ for KGN; $p < 0.001$ for COV434) or Emb ($p < 0.0001$ for KGN; $p < 0.001$ for COV434) significantly abolished AP-1 transactivation. A sub-optimal dose of 2.5 μ M of 5Z-7 also significantly reduced luciferase activity in both the KGN ($p < 0.0001$) and COV434 ($p < 0.001$) cells.

5.3.3 XIAP and TAK1 regulates NF- κ B signalling in GCT-derived cell lines

Whilst XIAP stimulates TAK1 to activate the TAK-TAB complex which in turn regulates NF- κ B signalling (Lu et al., 2007), I investigated the effects of XIAP and TAK1 inhibition on NF- κ B transactivation. When compared to the empty vector pTAL-luc, I observed a constitutively activated NF- κ B-mediated transactivation of 4- and 2.5-fold induction in the KGN and COV434 cells, respectively. The constitutively activated NF- κ B was abolished by the specific NF- κ B inhibitor, BAY ($***p < 0.001$ for KGN; $****p < 0.0001$ for COV434). The NF- κ B-mediated transactivation in the GCT-derived cells was abrogated to below basal level as a result of XIAP inhibition by SM ($***p < 0.001$ for KGN; $****p < 0.0001$ for COV434) or Emb ($***p < 0.001$ for KGN; $****p < 0.0001$ for COV434). TAK1 inhibition by 5Z-7 also significantly abolished NF- κ B signalling in both KGN and COV434 cell lines ($***p < 0.001$ for KGN; $****p < 0.0001$ for COV434) (Figure 5.8).

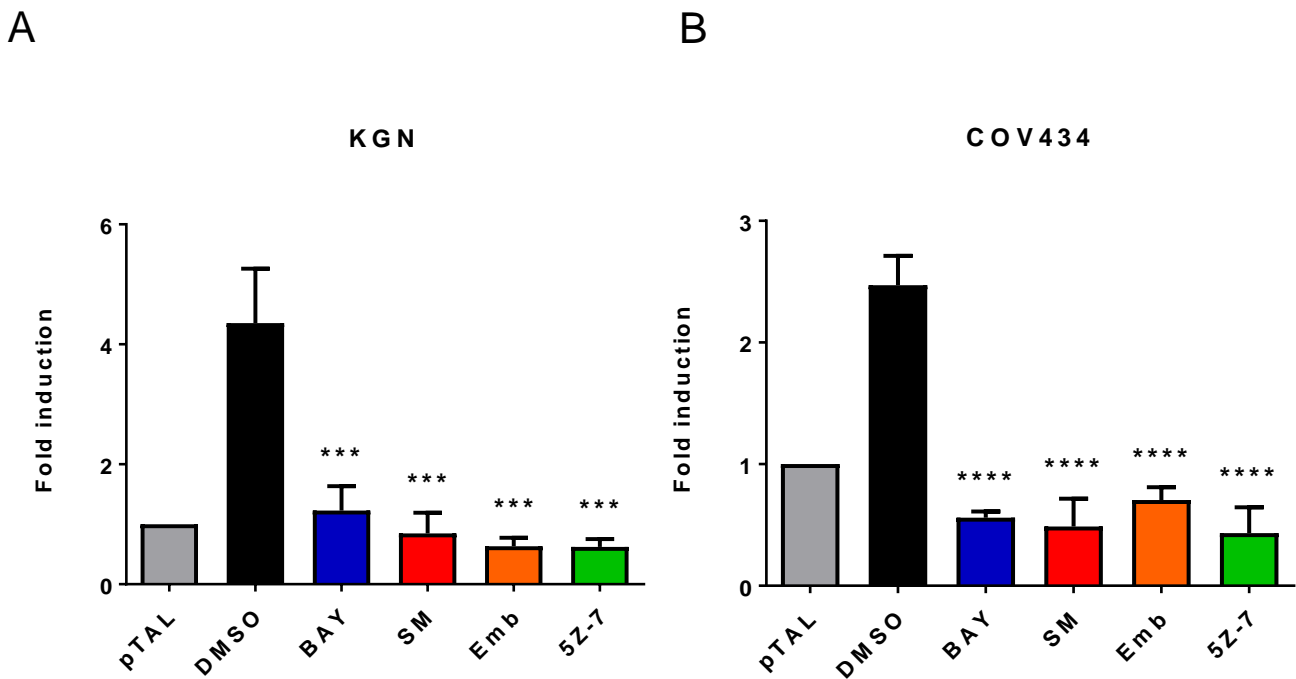


Figure 5.8. NF- κ B transactivation assay in GCT-derived cell lines. The KGN (A) and COV434 (B) cells were transiently transfected with NF- κ B-Luc. Constitutive NF- κ B activity was demonstrated by the 4- and 2.5-fold induction of the NF- κ B-mediated transactivation following vehicle treatment (0.1% DMSO) in the KGN (A) and COV434 (B) cells, respectively. In both cell lines, this constitutive NF- κ B activity was significantly abolished to baseline by the NF- κ B inhibitor, BAY at 10 μ M, XIAP antagonists, SM at 1 μ M or Emb at 10 μ M, or TAK1 inhibitor, 5Z-7 at 2.5 μ M. $n = 3$; mean \pm SEM; One-way ANOVA; Bonferroni post-hoc analysis; *** $p < 0.001$, **** $p < 0.0001$ when compared to DMSO.

5.3.4 Absence of mutations in the *TAK1* coding sequence in KGN and COV434

The *TAK1* cDNA was sequenced using RNA extracted from the KGN and COV434 cells to determine the presence of any activating mutation in the *TAK1* coding sequence that may contribute to the constitutive NF- κ B and AP-1 signalling in these cells. There are 4 splice variants, variant A to D, of *TAK1*. Variant B has the longest sequence and is thus referred to as the 'canonical' sequence. Using Sanger sequencing, I have identified variant A of *TAK1* is the dominant isoform in both KGN and COV434 cell lines. No mutation was identified in the *TAK1* coding sequence in either cell lines.

5.3.5 mRNA levels of the TAK-TAB complex in GCT, KGN, COV434 and hGrC1

We have previously performed a microarray analysis of 12 human GCT and the two GCT-derived cell lines (Alexiadis et al., 2016) which enabled us to analyse the levels of *TAK1*, *TAB1*, *TAB2*, *TAB3* and *TRAF6* mRNA using this data set. The mRNA of all components of the TAK-TAB complex was detected in all samples and in both stage 1 and stage 3 GCT, the stage of the disease does not alter the level of expression of any of these genes.

The COV434 cells which were derived from a juvenile GCT, expressed significantly higher level of *TAK1* mRNA compared to the stage 1 GCT, the KGN cells and the non-luteinised GC cell line, the hGrC1 cells (Figure 5.9A). Conversely, the *TAB2* mRNA level in the COV434 cells was significantly lower than that in the KGN and

hGrC1 cells (Figure 5.9C). Fold changes and p values of significant differences in TAK1 and TAB2 levels are presented in Table 5.10. None of the other groups reach significant difference for *TAK1* and *TAB2*. There were no differences in the mRNA levels of *TAB1*, *TAB3* and *TRAF6* between all cell lines and GCT samples (Figure 5.9B, D and E).

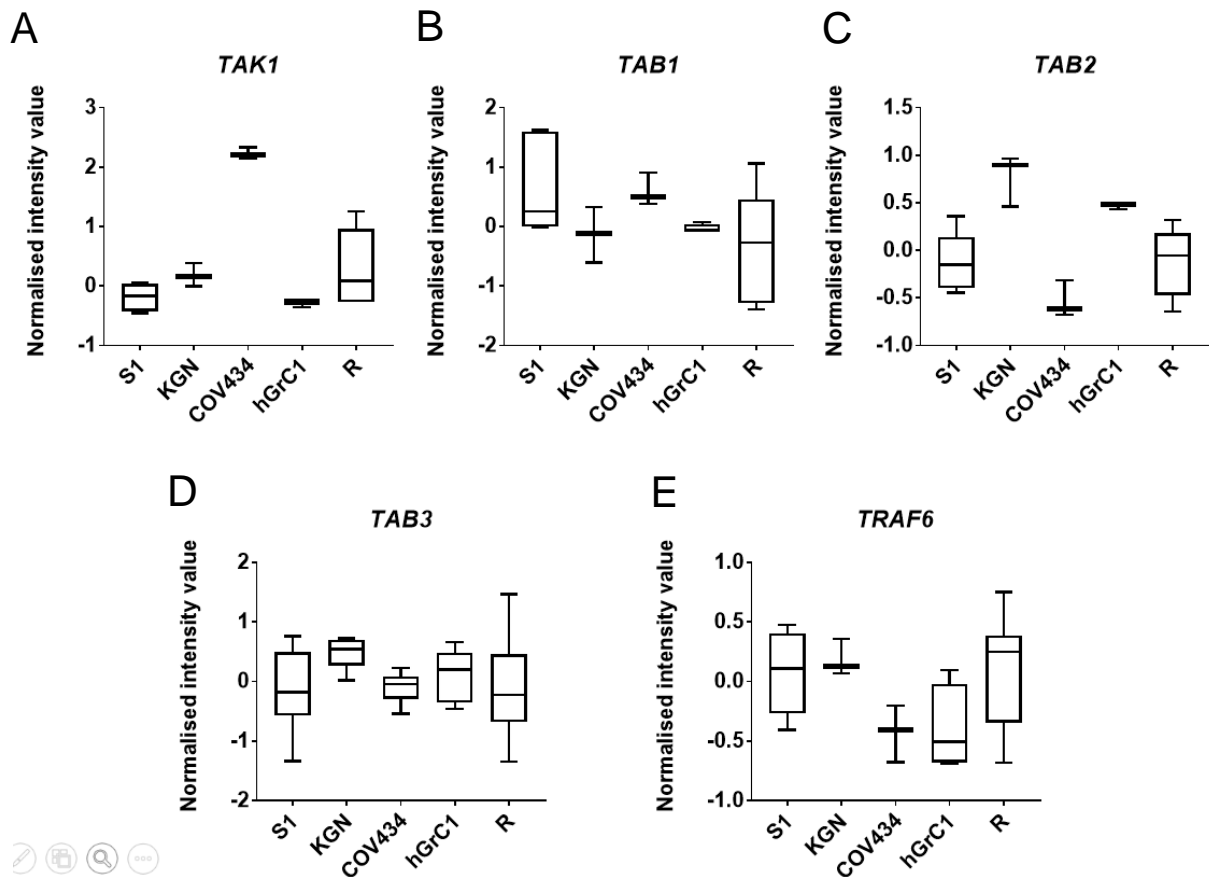


Figure 5.9. Microarray analysis of *TAK1*, *TAB1*, *TAB2*, *TAB3* and *TRAF6* mRNA levels. mRNA of all components of the TAK-TAB complex was detected in all samples and in both stage 1 and stage 3 GCT. Data were analysed using GeneSpring version 14.8 (Agilent) and normalised using the quantile normalisation method. Fold change and *p* values of significant differences are summarised in Table 5.10.

Table 5.10. Fold changes and *p* values of significant differences in *TAK1* and *TAB2* levels.

Between groups	<i>P</i> value	Regulation	Fold change	Log fold change
TAK1 (Probe name: A_23_P500773)				
Sequence: GAGTGATTGGTGGTATATTACGGAAATACGGAACCTTTAGGGATAGTTCCGTGTAAGGGC				
COV434 vs KGN	1.29 x 10 ⁻⁵	Down	-4.13	-2.04
COV434 vs hGrC1	1.57 x 10 ⁻⁷	Down	-5.64	-2.50
COV434 vs S1 GCT	3.65 x 10 ⁻⁶	Down	-5.33	-2.41
TAB2 (Probe name: A_23_P19702)				
Sequence: AGGCCTTGTTTTTCAGCTTCATCTGCAGTTCTATGTGAAGATTGATAAATCAGTTTTTAC				
COV434 vs KGN	4.75 x 10 ⁻⁴	Up	2.50	1.32
COV434 vs hGrC1	1.63 x 10 ⁻⁴	Up	2.03	1.02

5.3.6 Establishment of stable inducible XIAP knockdown cell lines

5.3.6.1 Protein level of XIAP in XIAP knockdown KGN and COV434 cells

The overexpression of XIAP in GCT, as well as highly malignant serous epithelial ovarian cancers (Chapter 3), warrants an investigation of the functional roles of XIAP in these cancers. The two GCT-derived cell lines, KGN and COV434, have also shown high levels of XIAP expression at the message level (Chapter 3). The study of the functional domains of XIAP will improve our knowledge of the caspase-binding activities by providing us with a pre-clinical model for potential therapy that can be utilised in malignancies which overexpress XIAP.

To characterise XIAP function in GCT, we created inducible, stable XIAP-deficient cell lines using the two GCT-derived cell lines, KGN and COV434. We used an expression vector, pTRIPz, that uses the tet-on system to induce the expression of an XIAP shRNA. Upon G418 selection, the pTRIPz-transfected KGN and COV434 cells grew as several colonies. 1 μ g/ml of doxycycline was added to induce the expression of the XIAP shRNA and each colony was then assessed for XIAP knockdown efficiency. Western blot analyses were used to measure the expression of XIAP in doxycycline-treated and untreated cells in the KGN (Figure 5.10A) and COV434 (Figure 5.10A) cells. Densitometric analysis was performed by measuring band intensities using the Image Chemidoc software version 5.2.1 (Bio-Rad), and normalised to the intensity of the β -actin band. We identified two KGN stable lines which had effective XIAP knockdown efficiency. As shown in Figure 5.10B, KGN Δ XIAP#5 showed a 60% knockdown of XIAP in doxycycline-treated cells compared to non-treated cells, while KGN Δ XIAP#6 was even more effective with a

80% knockdown efficiency. The COV434 Δ XIAP clone had a 40% knockdown of XIAP upon doxycycline treatment (Figure 5.11B).

The pTRIPz vector that contains the shRNA against XIAP also contains the red fluorescence protein (RFP) which is expressed upon activation by doxycycline. The RFP thus can be used as a fluorescent marker to determine successful induction of the vector by doxycycline. The untreated COV434 Δ XIAP cells do not express RFP (Figure 5.12A). When the COV434 Δ XIAP were treated with doxycycline (1 μ g/ml), RFP-expressing cells were observed (Figure 5.12B), confirming that these cells had successful integration of the shRNA vector into the cellular genome, and that the inducible system was functional.

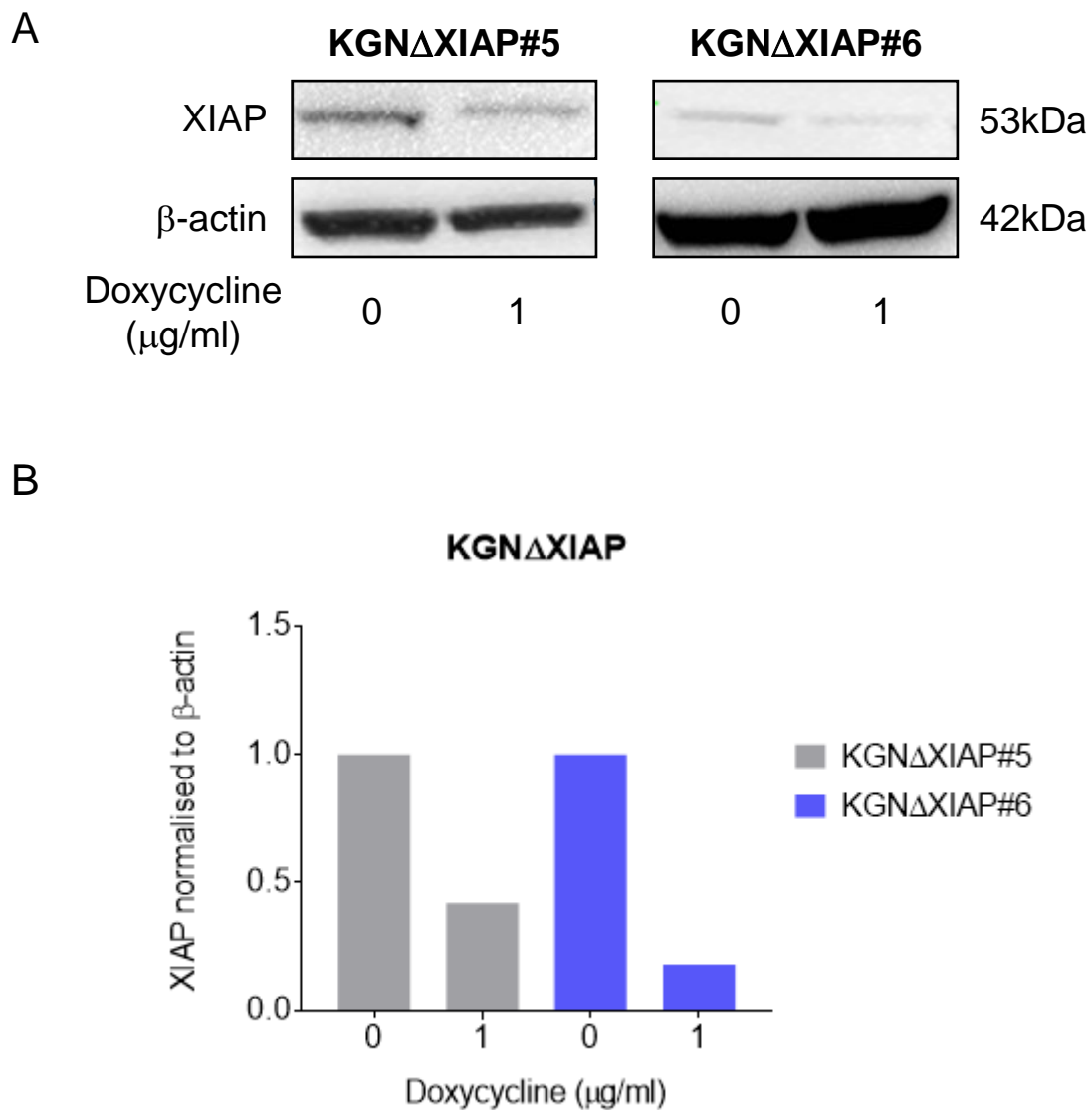


Figure 5.10. Expression of XIAP and β -actin in two KGN Δ XIAP clones. Two KGN clones, Δ XIAP#5 and Δ XIAP#6, showed successful knockdown of XIAP (53 kDa) upon 1 μ g/ml of doxycycline treatment as determined by western blot (A). The densitometric analysis of XIAP normalised to β -actin in KGN Δ XIAP clones #5 and #6 demonstrated a 60% and 80% of XIAP knockdown, respectively.

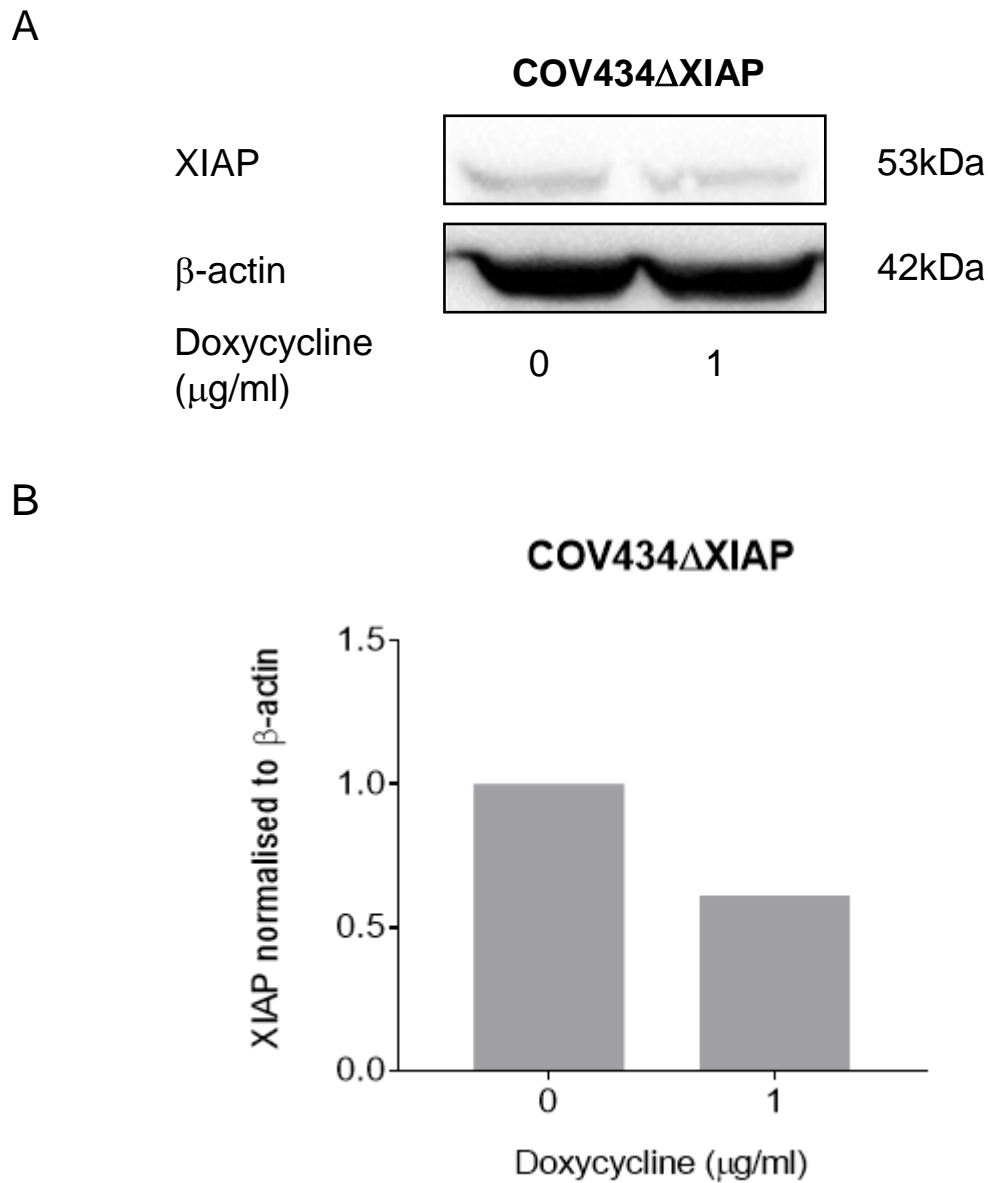


Figure 5.11. Expression of XIAP and β -actin in COV434 Δ XIAP. Western blot (A) showed a small knockdown effect upon treatment with doxycycline (1 μ g/ml) in COV434 Δ XIAP. The densitometric analysis (B) of XIAP normalised to β -actin showed a 40% reduction of XIAP in the COV434 Δ XIAP clone.

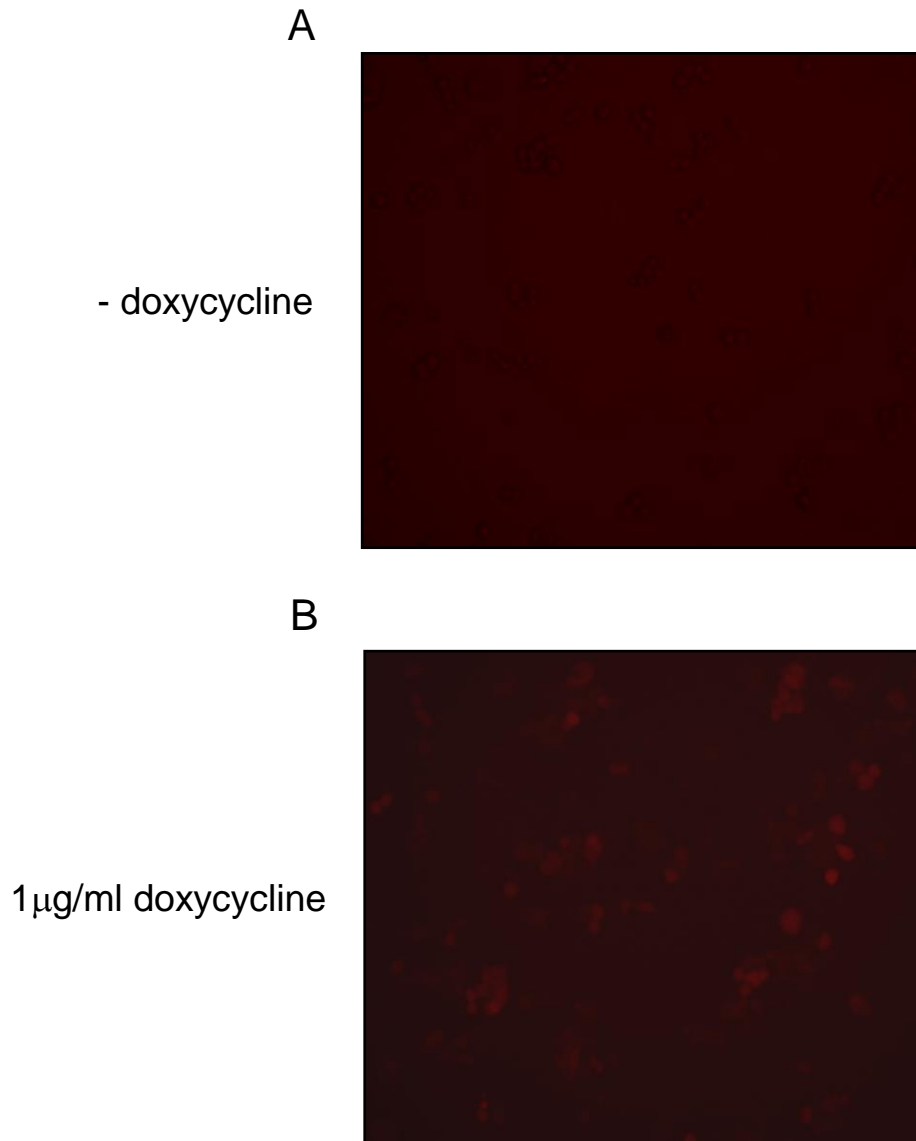


Figure 5.12. COV434 Δ XIAP under fluorescence microscope. The pTRIPz vector that contains the shRNA against XIAP contains RFP was used as a fluorescent marker to determine successful induction of the vector by doxycycline. The untreated COV434 Δ XIAP cells do not express RFP (A). When treated with doxycycline (1 μ g/ml), COV434 Δ XIAP cells expressing RFP were observed (B), confirming the successful integration of the shRNA vector into the COV434 cellular genome.

5.3.6.2 shRNA binding site on XIAP

As discussed previously, we used a shRNA approach to knockdown XIAP in the GCT-derived cell lines. This approach makes it difficult to re-express either XIAP or mutant of XIAP whereby the caspase binding capacity has been eliminated, as the exogenous transcripts would also be targeted for mRNA degradation by the shRNA. The strategy I adopted to circumvent this, was to introduce a silent mutation in the shRNA binding site of the expression vectors for either the wildtype XIAP or the mutant XIAP, thus rendering these vectors resistant to shRNA. I used the Agilent QuikChange® site-directed mutagenesis kit and primers that contained the silent, single point mutation (CAG→CGG) at the shRNA binding site (Figure 5.13). The introduction of this mutation also introduced a unique BsrBI restriction site, thus enabling a simplified way to screen for successfully mutated clones generated through site-directed mutagenesis (Figure 5.13B).

5.3.6.3 Screening successful shRNA-resistant expression vectors using BsrB1 restriction digestion

The BsrBI restriction site that is introduced upon successful mutagenesis serves as a useful screening tool. After performing site-directed mutagenesis for each expression vector (5UAS-XIAPwt, 5UAS-XIAP D148A and 5UAS-XIAP W310A), a 931 bp region of XIAP that encompasses the mutation site was amplified using PCR. The amplicon was then cleaned, and restriction digestion using BsrB1 was performed. Clones where the BsrB1 site was introduced would yield 2 bands 781 and 150 bp. Gel electrophoresis demonstrated successful mutagenesis in all three expression vectors (Figure 5.14). These vectors were then submitted to the Gandel Sequencing Trust Sequencing Facility (Monash Health Translational Precinct) to confirm the mutation

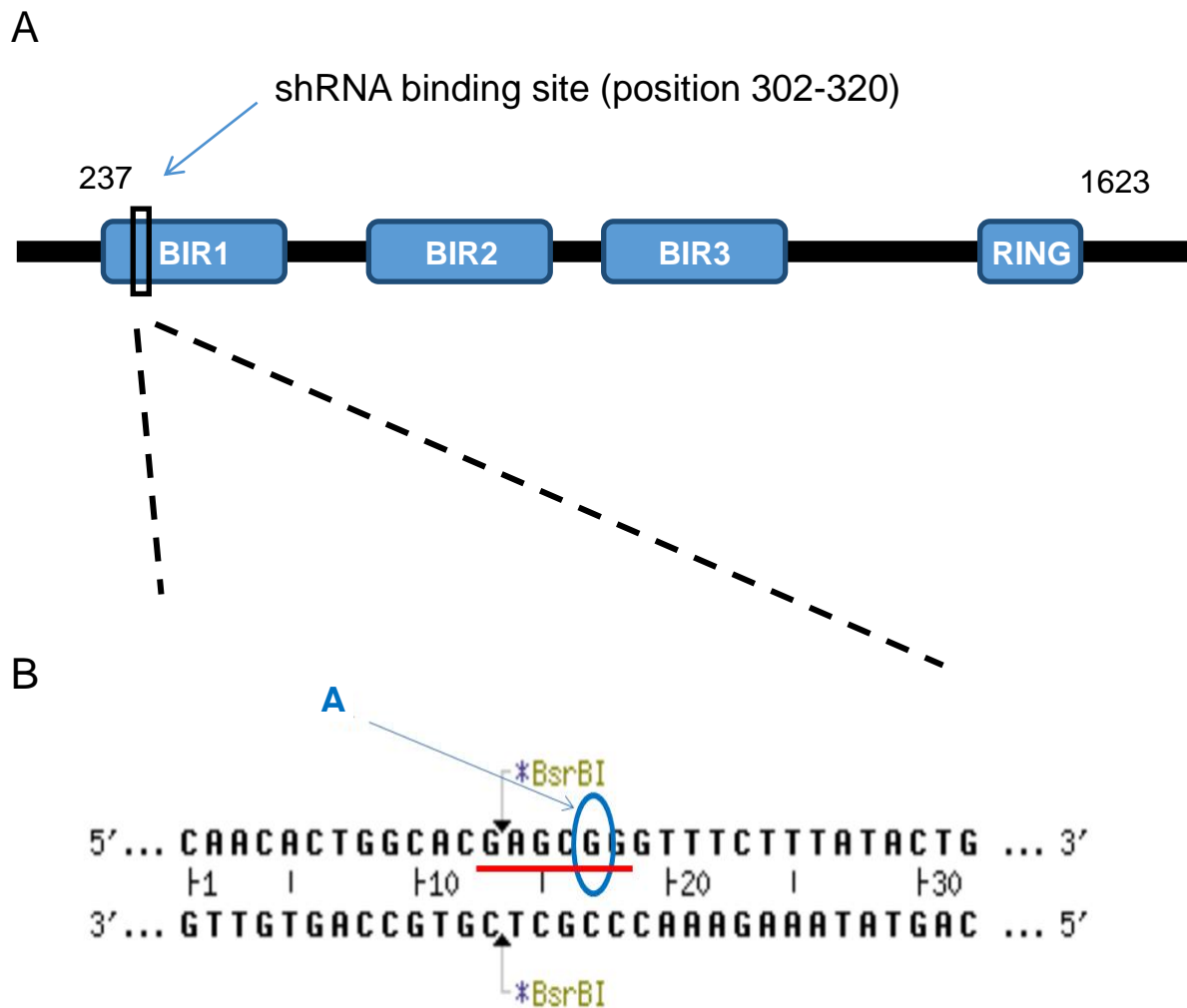


Figure 5.13. The shRNA binding region on the full length *XIAP* gene. The shRNA binding site at position 302-320 is in the coding region of *XIAP* gene (A). The amplified view (B) showed that the primer sequence contains a silent point mutation (G for A) and the introduction of the unique BsrBI restriction site. This primer anneals to position 302–320 of the *XIAP* gene. The incorporation of this mutation will render shRNA resistance and thus allow the re-expression of either the wildtype or mutant *XIAP* proteins in the *XIAP*-deficient cell lines. The silent point mutation is indicated in blue; sequence of BsrBI restriction site is highlighted in red.

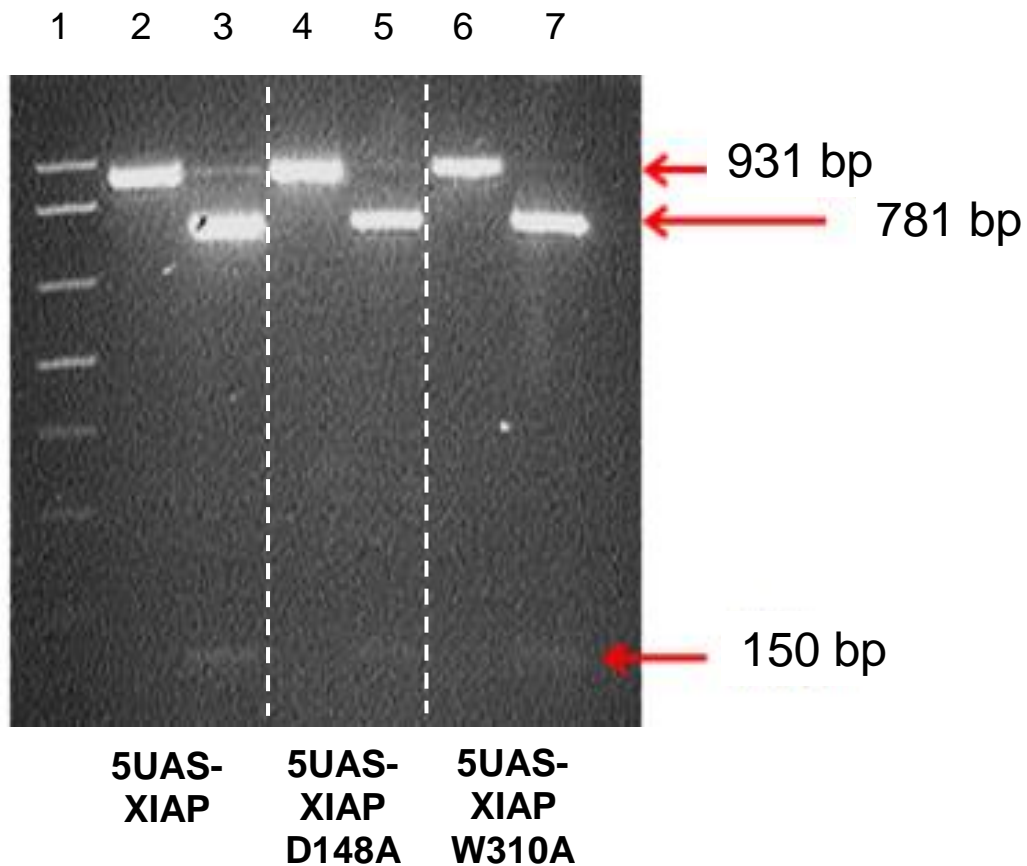


Figure 5.14. Incorporation of a silent mutation of the shRNA binding site of XIAP expression vectors detected by BsrB1 restriction digestion. Gel electrophoresis showing 5UAS-XIAP wt, 5UAS-XIAP D148A and 5UAS-XIAP W310A expression vectors were successfully mutated and thus incorporated a BsrB1 restriction site. Where the BsrB1 site is present, upon digestion, two bands of 781 and 150 bp (lane 3, 5 and 7) were observed. The parental plasmids which do not have the mutation, and thus do not have the BsrB1 restriction site were used as controls (lane 2, 4 and 6), showing an uncut band of 931 bp.

at the desired site and that no further mutations were introduced elsewhere in the vectors.

Sanger sequencing confirmed the mutations following site-directed mutagenesis. To render shRNA resistance, a silent point mutation was inserted in the 5UAS-XIAP wt (Figure 5.15A and B), and the two expression vectors encoding mutant XIAP, 5UAS-XIAP D148A and 5UAS-XIAP W310A (data not shown). The point mutation that abolishes caspase 3 binding (D148A) and caspase 9 activity (W310A) was shown in Figure 5.15C and D, respectively.

5.3.6.4 Generation of lentivirus in CHO cells

The Chinese hamster ovary (CHO) cell line was used to test the robustness of the tamoxifen responsive GEV16 5UAS-XIAP expression vector due to its high transfection efficiency. To optimise the concentration of the viral DNA for efficient transduction in the CHO cells, a serial dilution (range: neat, 1/2, 1/4, 1/8, 1/16 and 0) of the lentiviral pseudoparticles containing shRNA-resistant XIAP vector (wildtype or D148A mutant) and GEV16 plasmid was prepared. Upon addition of 4-hydroxy-tamoxifen, GEV16 is activated and hence, express shRNA-resistant XIAP construct. Compared to the endogenous level of XIAP in the CHO cells, western blot analysis showed that 1/16 dilution of viral DNA is sufficient to induce the expression of the shRNA-resistant XIAP wildtype (Figure 5.16).

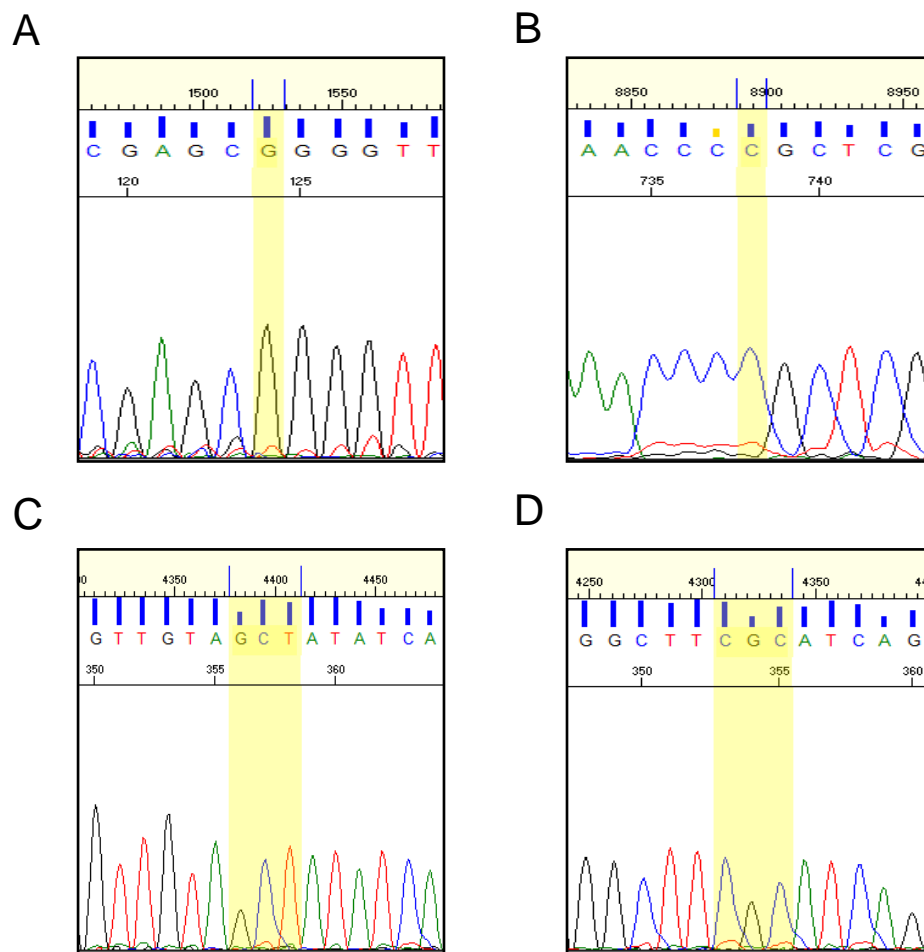


Figure 5.15. Electropherogram of the XIAP sequence following site-directed mutagenesis. To render shRNA resistance, a silent point mutation was inserted in all three XIAP expression vectors, 5UAS-XIAP wt (A, forward sequence; B, reverse sequence), 5UAS-XIAP D148A and 5UAS-XIAP W310A (data not shown). 5UAS-XIAP D148A expression vector contains the point mutation, D148A which abolishes caspase-3 binding at the BIR2 domain (C, forward sequence). 5UAS-XIAP W310A has a W310A mutation which eliminates caspase-9 activity at the BIR3 domain (D, reverse sequence).

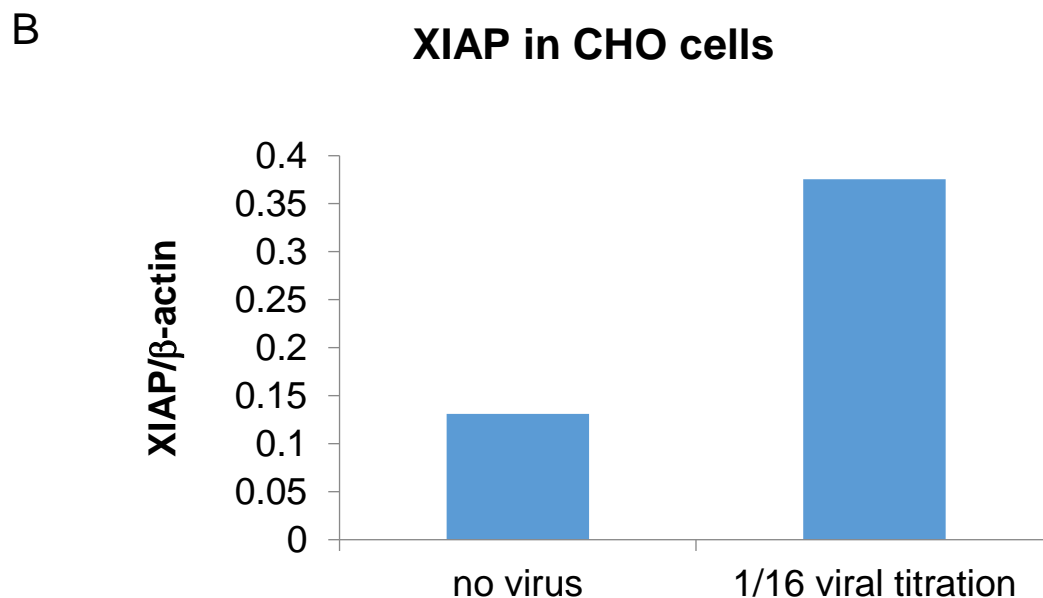
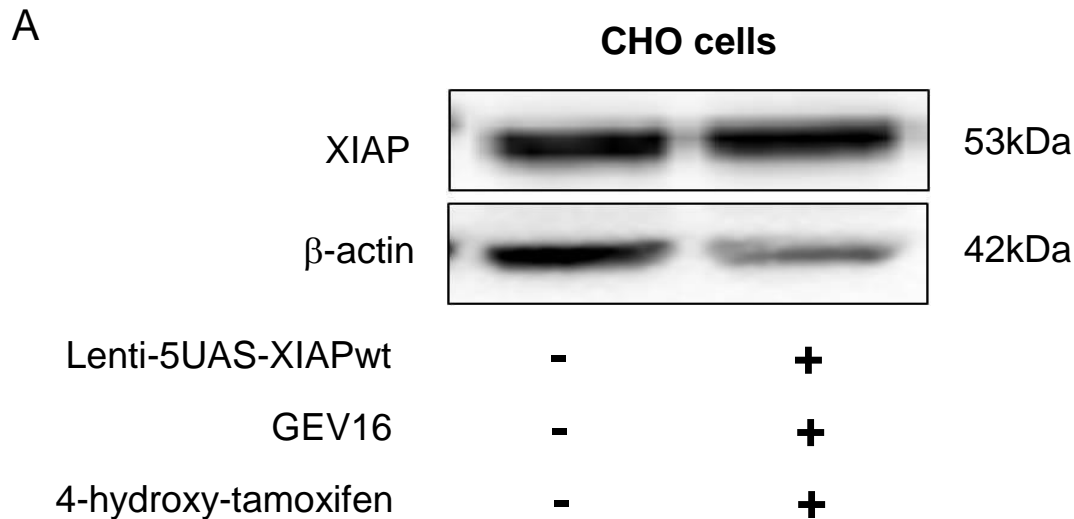


Figure 5.16. Lentiviral transduction of CHO cells. The concentration of the viral DNA for optimal transduction efficiency in the CHO cells was determined by titration of the lentiviral pseudoparticles containing the shRNA-resistant XIAP construct. The endogenous level of XIAP and that upon activation of GEV16 by 4-hydroxy tamoxifen in the CHO cells was measured. Western blot and densitometrical analyses showed that 1/16 dilution of viral DNA is sufficient to induce the expression of the shRNA-resistant XIAP wildtype.

5.4 Discussion

The constitutive NF- κ B and AP-1 signalling pathways have been identified previously by our laboratory in two human GCT-derived cell lines (Chu et al., 2004). This tumorigenic phenotype has also been reported in various cancer types including breast (Ndlovu et al., 2009), pancreatic (Niu et al., 2004) and prostate (Zerbini et al., 2003) cancer. NF- κ B is a transcription factor where upon stimulation, regulates various biological processes such as inflammation, immunity, proliferation and apoptosis. A multiplicity of evidence has illustrated the link between the dysregulated NF- κ B signalling and cancer development (Prasad et al., 2010). NF- κ B responds to various stimuli including TNF α and IL-1 (Drummond and Fuller, 2012). As such, many molecular alterations can impair NF- κ B and thus lead to constitutive activation of this pathway. Activated NF- κ B then mediates oncogenic processes by promoting the transcription of anti-apoptotic genes, the IAP family and Bcl-2 like proteins (Prasad et al., 2010), or pro-proliferation factors such as cyclin D1 (Rinkenbaugh and Baldwin, 2016). A similar pattern is with AP-1, whose constitutive activation by external stimuli promotes tumour progression and metastasis (Shaulian, 2010). Mutations of the NF- κ B and AP-1 components leading to constitutive activity are rare (Shaulian, 2010, DiDonato et al., 2012, Drummond and Fuller, 2012). Various mechanisms involving PI3 kinase (Guo et al., 2008) and cytokines such as IL-1 (Niu et al., 2004) and IL-6 (Zerbini et al., 2003) have been associated with the constitutively activated NF- κ B and AP-1. The specific trigger of the constitutive activation of NF- κ B and AP-1 signalling observed in GCT has not been identified.

In the present study, I replicated the previous findings of Chu *et al.* (2004) that reported constitutive activation of the NF- κ B and AP-1 signalling pathways in the KGN and COV434 cells (Figure 5.7 and 5.8). This constitutive activity was abolished by the inhibition of XIAP. XIAP is an effector of NF- κ B; this finding points to a reciprocal regulatory role of XIAP as part of a feed-forward loop to regulate NF- κ B. Indeed, a previous study has demonstrated that SM does not interact with the BIR1 domain but inhibits the XIAP BIR1:TAK1 interaction (Kaur *et al.*, 2005). NF- κ B and AP-1 are both downstream of the TAK-TAB protein complex of the TGF β signalling pathway. Given the interaction between XIAP and TAK1, one would speculate the possible involvement of the TAK-TAB protein complex as possible mediators of the constitutive activation of NF- κ B and AP-1. Indeed, TAK1 inhibition using a sub-optimal dose of TAK1 inhibitor, 5Z-7, was shown to significantly reduce NF- κ B- and AP-1-mediated transactivation to below basal levels in both the KGN and COV434 cells (Figure 5.7 and 5.8).

If TAK1 is involved in the regulation of the NF- κ B and AP-1 signalling pathways, one possible explanation of the constitutive activity would be a gain-of-function mutation in *TAK1*. However, no mutation in the *TAK1* coding sequence was found in the KGN and COV434 cells. Mutations in *TAK* have been identified in human cancers as listed on the COSMIC (Catalogue of Somatic Mutation in Cancer) database (<http://cancer.sanger.ac.uk/cosmic/gene/analysis?ln=MAP3K7#distribution>) (Forbes *et al.*, 2017). However, none has been reported to be pathognomonic. 5 mutations in *TAK1* have been associated with developmental disorders; 4 of which were found in a subset of patients diagnosed with frontometaphyseal dysplasia (FMD) (Wade *et al.*, 2016). FMD is a genetic disorder characterised by abnormalities in skeletal

development. Two of the 4 mutations in *TAK1* in FMD patients, namely, c.1454C>T (Pro485Leu) and c.502G>C (Gly168Arg), were *de novo* mutations which were found to increase autophosphorylation of *TAK1* and increase NF- κ B-mediated transactivation. MAP kinase pathway effectors including ERK, p38 and JNK are increased by the *TAK1* Pro458Leu mutant but reduced by the Gly168Arg variant. The *TAK1* Pro458Leu mutant also induces phospho-p38 expression *in vitro* (Wade et al., 2016). The other two FMD-causing mutations, c.208G>C (p.Glu70Gln) and c.299T>A (Val100Glu), were germline mutations; neither of these mutations were shown to affect the NF- κ B or MAP kinase pathways (Wade et al., 2016). The *TAK1* c.721T>A (Trp241Arg) mutation is pathognomonic in the cardio-spondylocarpofacial syndrome (CSCF), a developmental disorder featuring growth retardation and various facial malformations (Le Goff et al., 2016). This mutation was found to downregulate phospho-p38 levels following stimulation with TGF β (Le Goff et al., 2016).

Although it has been long recognised that the XIAP:TAB1 interaction is required to induce TGF/BMP-dependent activation of the TAK-TAB complex, a recent study demonstrated this is not the case in the IL-dependent activation of the TAK-TAB heterodimer (Zhang et al., 2017a). Expression of *TAK1* can be regulated by its binding partners such as the TAB proteins and TRAF6. The availability of the data set from previously published transcriptome profiles of 6 stage 1 GCT and 6 stage 3 GCT, and the KGN, COV434 and hGrC1 cell lines allowed us to investigate the mRNA levels of *TAK1* and its binding partners (Alexiadis et al., 2016).

TAB1 was first identified as an activator of *TAK1* for its kinase activity (Shibuya et al., 1996). Following dimerisation with XIAP, TAB1 binds directly to the binding pocket on

the catalytic domain of TAK1 to activate TAK1 by inducing its autophosphorylation (Shibuya et al., 1996, Lu et al., 2007, Kim et al., 2009). Ectopic expression and knockdown studies have concluded that the expression of these two proteins controls the level of kinase activity. Overexpression of either TAK1 or TAB1 does not further increase kinase activity and neither TAK1 or TAB1 demonstrates kinase activity when expressed alone (Shibuya et al., 1996, Kishimoto et al., 2000). TAB2 also forms a complex with TAK1 and TAB1. This occurs upon IL-1 stimulation which accumulates TAB2 in the cytosol to associate with TAK1, TAB1 and TRAF6 (Takaesu et al., 2000). *In vitro* mutational studies have confirmed that, although not a direct activator of TAK1, TAB2 plays important roles in TAK1-mediated downstream signalling. An intact TAB2 achieves this by facilitating the formation of the TRAF6-TAB2-TAK1 complex. Overexpression of TAB2 also increases the kinase activity of TAK1 (Takaesu et al., 2000).

The TAB2 homologue, TAB3, binds to TAK1 at the coiled coil region in the C-terminus in the same manner as TAB2 (Takaesu et al., 2000, Ishitani et al., 2003). Given the high structural similarity, it is not surprising that TAB2 and TAB3 share redundant functions and could compensate the loss of the other protein in signal transduction (Ishitani et al., 2003). Dual inhibition of TAK2 and TAK3 using siRNA however, completely blocks the activation of JNK and p38 in HeLA cells although TAK1 expression remains unaffected (Ishitani et al., 2003). Ubiquitylation of TAB2 and TAB3 can also be induced by overexpressing TRAF6. The effect of this ubiquitylation is similar to IL-1 stimulation, which subsequently leads to the activation of TAK1 (Ishitani et al., 2003).

Our transcriptome profiles showed that the KGN cells have similar levels of *TAK1* and its binding partners, *TAB1/2/3* and *TRAF6* compared to the 6 stage 1 and 6 stage 3 GCT, nor is there any difference compared to the GC cell line, hGrC1. The COV434 cells which were derived from a juvenile GCT however, expressed significantly higher level of *TAK1* compared to stage 1 GCT, the KGN and hGrC1 cells. As mentioned previously, overexpression of TAK1 does not necessarily lead to an induction of TAK1 kinase activity. Indeed, a significantly lower level of *TAB2* in COV434 compared to the KGN and hGrC1 cells might lead to a reduction in the kinase activity of TAK1. However, these preliminary data have yet to be validated by quantitative PCR.

Post-translational modification of TAK1 or its binding partners leading to ubiquitin-mediated inactivation or degradation that results in changes in downstream signalling (reviewed in Hirata et al., 2017). For instance, K48-linked polyubiquitylation at the K72 residue of TAK1 mediates TAK1 proteosomal degradation (Fan et al., 2012). The deubiquitinating enzyme, cylindromatosis (CYLD) forms a complex with TAK1 and inhibits ubiquitylation of TAK1 (Reiley et al., 2007). In contrast, *Cyld*^{-/-} cells showed constitutive activation of JNK and NF-κB as a result of the constitutive polyubiquitylation or, activation of TAK1 (Reiley et al., 2007). Given the involvement of TAK1 in pro-survival signalling, *Cyld*^{-/-} mice injected with lung carcinoma cells demonstrated increased tumour size, more aggressive tumour growth with significant elevation in metastasis compared to wildtype mice (Ahmed et al., 2011). *Cyld* deficiency or mutation has not been reported in GCT.

In this study, we have created an inducible, XIAP knockdown cell line using a lentiviral system. Lentiviral vectors are capable of infecting both dividing and non-

dividing cells (Dykxhoorn and Lieberman, 2005). This method of transducing cells is very efficient, whereby nearly all cells can be transduced, as opposed to lipid-based transfection methods, which at least for GCT-derived cell lines, are inefficient. The ability to transduce close to 100% of cells makes the use of lentiviruses carrying the gene of interest an effective tool for creating stable cell lines, as the vectors are integrated into the genome, thus a long-term, stable expression can be achieved (Dykxhoorn et al., 2003). The high transfection efficiency also makes lentiviral transfer very effective for transient experiments where proliferation, viability and apoptosis are being assessed. Future studies can utilise this system to characterise the functional roles by knocking down one or more XIAP domains.

Collectively, these data provide evidence that the constitutive NF- κ B and AP-1 activity in the GCT-derived cells could be regulated by XIAP or TAK1 inhibition. Levels of the components of the TAK-TAB-TRAF6 protein complex in these cells are also altered. Much effort has to be made to identify the source of the constitutive activity, which is not only applicable to GCT but also other tumours with the same pathognomonic feature. The stable, inducible lentiviral system of XIAP serves as a useful tool for further characterisation of XIAP functional domains. Given the role of XIAP in cancer, this will enable better drug design to maximise anti-apoptotic effects and minimise unwanted off-target complications.

CHAPTER 6
DISCUSSION AND CONCLUSIONS

6.1 Discussion and conclusions

Constitutive activity of the anti-apoptotic transcription factor, NF- κ B, has been commonly reported in solid tumours including pancreatic (Prabhu et al., 2014), colorectal (Sakamoto et al., 2009), prostate (Garg et al., 2012), breast (Kuo et al., 2017), thyroid (Bauerle et al., 2010) and ovarian cancers (Hernandez et al., 2010) as well as haematological malignancies such as lymphoma and leukaemia (Krappmann and Vincendeau, 2016). Aberrant activation of NF- κ B signalling serves several roles in tumorigenesis. Through the regulation of gene transcription, NF- κ B enhances proliferation via cyclin D1 and IL-6 (Arora et al., 2014, Malanga et al., 2015), as well as cell survival via the IAP members (Arora et al., 2014). Other hallmarks of cancer associated with NF- κ B are increased angiogenesis and tumour metastasis which NF- κ B regulates through genes such as VEGF and MMP-2 and -9 (Muscella et al., 2017). Constitutive NF- κ B signalling has also been associated with chemo- or radio-resistance in many cell systems including ovarian cancer cells (Yan et al., 2017). Our laboratory too has shown the constitutively activated NF- κ B signalling in GCT *in vitro* (Chu et al., 2004). Further studies showed that this pathognomonic feature of cancer has, unsurprisingly, molecular impact on important signalling pathways in GCT. The authors demonstrated that the inhibition of NF- κ B using specific NF- κ B antagonist, BAY11-7082, abolished the constitutive NF- κ B activity (Chu et al., 2004). Transactivation assays measuring exogenous ER β -mediated transcription showed no activity of the estrogen response element (ERE)₂-luc reporter when the KGN and COV434 cells with treated with the ER ligand, diethylstilbestrol (DES). However, a combination of NF- κ B inhibition (BAY11-7082) and ER activation (DES) significantly

induced ER β -mediated transactivation (Chu et al., 2004). This demonstrates that NF- κ B transrepresses the transcription of the nuclear receptor, ER β , and that NF- κ B inhibition rescued ER β -mediated transactivation in these cells (Chu et al., 2004).

Similar to what was previously observed with ER β , we also found in this current study that the nuclear receptor, PPAR γ , is transrepressed by the constitutive NF- κ B activity. In the ovary, PPAR γ plays a pro-differentiative role in GC. PPAR γ also modulates lipid and glucose metabolism. PPAR γ agonists, the thiazolidinediones (TZD) such as rosiglitazone (RGZ) and pioglitazone are in clinical use for the treatment of metabolic diseases. We demonstrated using microarray analysis (Alexiadis et al., 2011) and immunohistochemistry on a tissue microarray (TMA) the overexpression of PPAR γ at the mRNA and protein level. 64% of GCT on the TMA were reported to express moderate to high levels of PPAR γ . The paradoxically high expression of PPAR γ in the human GCT and GCT-derived cell lines suggests resistance to PPAR γ activity in this tumour type. Functional analysis of the receptor was then further explored using a PPAR γ transactivation assay. The ligand-dependent PPAR γ -mediated transactivation was induced with the activation of PPAR γ and its heterodimeric partner, RXR α using RGZ and retinoic acid only in the presence of the NF- κ B inhibitor, BAY11-7082. This suggests a repressive effect of NF- κ B on PPAR γ transcription, where it can be reversed by inhibiting NF- κ B in the GCT-derived cell lines.

NF- κ B is a dimeric transcription factor which comprises the Rel family members including p50/p105, p100/p52, p65 (Rel A), Rel B and c-Rel. Members of the Rel family can homo- or heterodimerise with other Rel members; they have the capacity to induce transcriptional regulation where the composition of NF- κ B dimers infers

specificity in the recognition of DNA enhancer motifs (McKay and Cidlowski, 1999). NF- κ B regulates gene transcription upon activation following the release of the inhibitory I κ B and subsequent nuclear translocation. Nuclear receptors such as the glucocorticoid, androgen and estrogen receptors (GR, AR and ER), are examples of known transcriptional targets of NF- κ B. The p65 subunit of NF- κ B is responsible to transrepress GR-mediated transcriptional activity (McKay and Cidlowski, 1998, Kolla and Litwack, 2000). Although these steroid hormone receptors share high structural homology, the mechanism of transrepression varies with the receptors. Some of these receptors such as GR and ER α but not ER β also confer reciprocal transrepression of NF- κ B transactivation (McKay and Cidlowski, 1998, Chu et al., 2004).

Our findings from apoptotic studies using high content screening further suggested that when NF- κ B is inhibited, PPAR γ activation in the GCT cells significantly increases apoptosis. This effect was not seen when the cells were subjected to NF- κ B inhibition or PPAR γ activation alone. Despite being seen as an attractive therapeutic target as an initiator of cancer, therapeutically targeting NF- κ B remains difficult due to its role in normal physiology, particularly in the immune response (Hoesel and Schmid, 2013, Zhang et al., 2017b). One possible avenue is to target one of the effectors of NF- κ B, the X-linked inhibitor of apoptosis protein (XIAP). Downstream of the NF- κ B signalling pathway, the anti-apoptotic XIAP is amongst the 8 members of the Inhibitor of Apoptosis Protein (IAP) family. In the ovarian GC, the expression of XIAP is also under the influence of FSH which stimulates DNA-binding of NF- κ B (Chu et al., 2004). Given the constitutive activity of NF- κ B, we speculated and indeed observed abundant expression of *XIAP* mRNA in human GCT and the

GCT-derived cell lines. Using immunohistochemistry on tissue microarrays, we also demonstrated that close to 70% of GCT showed moderate to high levels of XIAP. The XIAP protein is highly expressed in other malignant ovarian cancers such as serous papillary carcinoma but not in benign ovarian pathologies and post-menopausal ovaries.

Overexpression of XIAP has been associated with chemoresistance and poor prognosis in various malignancies (Yang et al., 2012, Zhao et al., 2017). One of the most promising therapeutic options to overcome this is the inhibition of XIAP using a small molecule inhibitor, Smac-mimetic (SM or CmpdA), a synthetic analogue of the mitochondrial XIAP inhibitor, Smac (Fulda, 2015b). XIAP can also be antagonised by the XIAP BIR3 inhibitor, embelin (Nikolovska-Coleska et al., 2004). The effect of XIAP antagonism in inducing apoptosis and sensitivity to chemotherapy has proven promising in both *in vitro* and *in vivo* studies (Matzinger et al., 2015, Sun et al., 2016). However, SM or embelin alone did not exhibit any anti-tumour effects in the human GCT-derived cell lines. Instead, like NF- κ B inhibition, SM or embelin, in combination with PPAR γ activation significantly reduced cell proliferation and viability in both the KGN and COV434 cells over a period of 24, 48 and 72 hours. This effect was not seen in the normal, non-luteinised GC cell line, hGrC1. High content screening also demonstrated significant induction of apoptosis in the KGN and COV434 cells following the combined treatment. Findings from the KGN cells are accompanied by an induction of other biomarkers of apoptosis such as the pro-apoptotic gene *TNFRSF1B* and *TGM2* at the message level as demonstrated by qRT-PCR. To recapitulate the effect of this combination treatment in a tumour microenvironment, we also generated and treated 3D spheroids of the KGN cells. We observed features of apoptosis such as blebbing and loss of the confined contour of the KGN spheroids

following the combination treatment for 12 days. Viability assays for the KGN spheroids quantified the amount of ATP to determine the number of viable cells present in culture at the end of the 12 day-treatment. These results also replicated the significant reduction in cell viability in the KGN spheroids as we previously saw in the SM/RGZ/RA-treated KGN cells when cultured in a monolayer.

Co-expression of XIAP and PPAR γ has been reported and simultaneously targeted in various cancers (Qiao et al., 2008, Liu et al., 2009). XIAP inhibitors and PPAR γ agonists have demonstrated anti-neoplastic effects by the induction of apoptosis and re-sensitisation to chemo- or radiotherapy (Sasaki et al., 2000). The pro-apoptotic effect was a result of the activation of PARP (Qiao et al., 2008), as well as caspases-3, -7 and -9 (Liu et al., 2009). Once triggered, the cleavage of caspases could not be reversed by the PPAR γ antagonist, GW-9662 (Qiao et al., 2008). To date, these two reagents have been in clinical trials separately for different cancers. Both approaches were reported to be well-tolerated at the clinical stage (Mahadevan et al., 2013, Murakami et al., 2014). Efatutazone, a third generation TZD, has demonstrated effectiveness in disease control with a reduction in tumour size of over 30% (Murakami et al., 2014). Both monovalent and bivalent XIAP inhibitors are evaluated in clinical trials. Birinapant (TL32711), a bivalent small molecule SM, has been investigated as a cancer therapeutics alone or in combination with other chemotherapies (Fulda, 2015a). Birinapant exhibited favourable pharmacokinetics and tolerability which remained unchanged when combined with multiple anti-cancer agents in patients with various advanced malignancies, suggesting that birinapant can be safely administered with other chemotherapeutics (Fetterly et al., 2012). Another phase I study also demonstrated that birinapant increased apoptosis in tumour tissues (Amaravadi et al., 2015). XIAP inhibition using an antisense

oligonucleotide, AEG35156, showed a favourable pharmacokinetic profile in a phase I study. 28 of 38 patients showed significantly induced levels of markers of apoptosis (Dean et al., 2009).

In view of the anti-neoplastic effects that the combination treatment brings about, we sought to explore the molecular consequences of this strategy in the GCT cells. Utilising transactivation assays, we revealed that the inhibition of XIAP abolished the constitutively activated NF κ B₄-luc reporter, and along with PPAR γ activation, restored PPAR γ -mediated transactivation in both KGN and COV434 cells. This implies that XIAP reciprocally regulates NF- κ B and thus can modulate the effect of NF- κ B transrepression of PPAR γ . We also studied changes in gene and protein expression induced by the combination treatment with qRT-PCR and SILAC coupled with mass spectrometry, respectively. Amongst the 32 differentially expressed proteins identified in the SILAC study, stearyl-CoA desaturase (SCD) showed the greatest magnitude of change in the KGN and COV434 cells after the treatment of XIAP inhibition (SM or embelin) and PPAR γ activation (RGZ and RA). SCD is a rate-limiting enzyme which catalyses the synthesis of monosaturated fatty acids, oleate and palmitoleate, from stearyl- and palmitoyl-CoA. The treatment-induced expression of SCD was in line with the increased SCD mRNA levels we observed using digital PCR. We also had 2 GCT available during the course of this study which allowed us to establish an explant model to investigate the effects of the combined treatment. We replicated the *in vitro* finding that SCD levels increase in the explant model after 24 hours of XIAP and PPAR γ treatment. Besides SCD, other proteins associated with metabolism including acyl-CoA synthetase long-chain family member 3 (ACSL3) and α -enolase (ENO1) also showed increased expression in the treated cells. Since PPAR γ has a role in lipid and glucose metabolism, the elevated levels of

these proteins led us to believe that PPAR γ activity is restored by the combined XIAP and PPAR γ treatment. These proteomic changes were in line with the alterations we observed in the mRNA levels. The downregulation of a PPAR γ -regulated gene, *CYP19A1*, further supports the notion that PPAR γ activity is rescued by the combination treatment.

Literature has documented elevated levels of SCD mRNA and protein in the presence of TZD in human adipocytes (Yao-Borengasser et al., 2008). The same phenomenon has also been observed in other cell types and species (Shi et al., 2013, Ikeda et al., 2015). Given the repeated reports showing that SCD is a target of PPAR γ , we decided to pursue the possibility of PPAR γ binding to the SCD promoter region to illicit the transcriptional response. The only existing characterisation of *SCD* gene promoter only covered 500 bases upstream of the *SCD* transcriptional start site (Bene et al., 2001). In the search for a PPAR γ binding site, I extended the screening to 10 kb of the promoter region upstream of the *SCD* transcriptional start site using the Ensembl website (www.ensembl.org/index.html) and the JASPAR dataset (<http://jaspar.genereg.net/>). Two putative PPAR γ binding sites were identified within the 10kb *SCD* promoter region. Subsequent ChIP-PCR analyses confirmed that the expression of one of the putative PPAR γ binding sites showed significant induction after SM/RGZ/RA combined treatment in the KGN cells. This is the first demonstration of the mechanism by which PPAR γ regulates *SCD* gene transcription. It is widely accepted that an altered metabolic profile is a hallmark of cancer. The elevated levels of proteins associated with metabolism alerted us to a potential risk of an increased metabolism in these cells. For instance, fatty acids produced in the presence of SCD can be oxidised by the mitochondria to produce ATP via β -

oxidation, with the by-product, acetyl CoA, being fed into the citric acid cycle and oxidative phosphorylation (OXPHOS; or electron transport chain) to generate more ATP. In light of this concern, we utilised the Seahorse mito-stress test to examine the metabolic profile of the KGN cells. The Warburg effect states that cancer cells favour anaerobic glycolysis even in the presence of oxygen (Warburg et al., 1927). In the mito-stress assay, as cells are metabolically challenged by oligomycin (ATP synthase inhibitor) and FCCP (depolarises mitochondrial membrane), it triggers either an increase in aerobic or anaerobic respiration in the cells in response to an increased energy demand. The ability to meet a heightened ATP demand, or the spare respiratory capacity, reduces in cells with mitochondrial dysfunction. Comparing the control and the SM/RGZ/RA-treated KGN cells, the latter has a significantly lower spare respiratory capacity. Further, we did not observe changes in overall ATP production between the control and RGZ/RA- or SM/RGZ/RA-treated KGN cells. Consistently and significantly lower rates of OXPHOS, as indicated by the oxygen consumption rate (OCR), was also seen in the SM/RGZ/RA-treated KGN cells throughout the experiment. However, there were no differences in anaerobic respiration, expressed as extracellular acidification rate (ECAR), between the control and treatment group, nor with the addition of metabolic stressors. A shift in the ratio of OCR/ECAR usually suggests a change in preference for aerobic versus anaerobic respiration. Cancer cells with robust glycolytic and OXPHOS activity are perceived as highly metabolic and proliferative (Zhang et al., 2012). A reduced OCR to ECAR ratio could suggest an increase in anaerobic glycolysis, or a switch to a more “cancer-like”, glycolytic phenotype. However, the reduction in OCR/ECAR we observed in the SM/RGZ/RA-treated KGN cells is due to a reduction in OCR with no change in ECAR. This suggests the diminished ability of the cells to respond to an increase in energy

demand, with a specific impairment in their ability to utilise aerobic respiration. This led us to rule out the possibility of increased metabolism resulting from the treatment-induced expression of metabolic proteins and we conclude that the combination treatment has compromised the cells metabolically.

When GCT metastasise, patients have limited options since adjuvant treatments such as hormonal therapies, chemo- or radio-therapies have not been shown to improve survival rates (Seagle et al., 2017). We therefore investigated the effects of the combined treatment on metastasis of GCT *in vitro* in real-time using the xCELLigence RTCA system. The KGN cells in the upper chamber of the plate were allowed to invade through a layer of matrix (Matrigel®) to the lower chamber with serum-containing media as the chemoattractant. In comparison to the control KGN cells, the SM/RGZ/RA-treated KGN cells showed significantly delayed onset of invasion by 8 hours. The overall lower cell index measured at the lower chamber also indicates the treated cells were less invasive. The cell index of the SM/RGZ/RA-treated KGN cells plateaued 4 hours after the onset of invasion, suggesting that the treatment prevented further proliferation after these cells invaded into the lower chamber. The impact of the treatment on invasion is in line with the identification of the treatment-reduced expression of fascin from my SILAC study (data not shown). Fascin (FCSN) is an actin-bundling protein which plays a role in cell motility, tumour cell migration, invasion and metastasis (Tan et al., 2013). mRNA level of *FCSN* was also downregulated following the combination treatment (data not shown). We have purchased a fascin inhibitor which will allow us to investigate its impact alone or in combination with XIAP inhibition and PPAR γ activation on the GCT cells in the future. To further characterise the relationship between XIAP and NF- κ B, we identified from the literature a possible mechanism by which XIAP can reciprocally regulates its

effector, NF- κ B, via the TAK-TAB complex (Sakurai et al., 2002). The BIR1 domain of XIAP dimerises with TAB1 to trigger TAK1 autophosphorylation and subsequently, activation of the TAK-TAB complex (Lu et al., 2007). Interestingly, one of the downstream signalling pathways of the TAK-TAB complex is AP-1 (Sakurai et al., 2002), another pathway that is constitutively activated in the GCT cells (Chu et al., 2004). As with NF- κ B, constitutive activity of AP-1 has also been reported in a wide variety of cancers (Ndlovu et al., 2009, Mishra et al., 2010, Tyagi et al., 2017). AP-1 is a protein complex formed from the homo-dimerisation of Jun (c-Jun, JunB and JunD) subunits, or hetero-dimerisation with Fos (c-Fos, FosB, Fra-1 and Fra-2) proteins or ATF subfamilies (Shaulian and Karin, 2002). Hyperactivity of AP-1 with selective participation of some subunits have been individually or collectively associated with chemo- or radio-resistance, as well as cancer growth and survival (Yang et al., 2014, Gupta et al., 2015, Tyagi et al., 2017). The constitutive activity of both NF- κ B and AP-1 in GCT cells, as well as the role of XIAP in the activation of the TAK-TAB complex provides a strong rationale to investigate this protein complex.

To test the involvement of the TAK-TAB complex and the effect of XIAP inhibition on these constitutively activated pathways, we performed transactivation assays using the NF- κ B- and AP-1-luc reporters in the KGN and COV434 cells. Inhibition of TAK1 using a suboptimal dose of the TAK1 inhibitor, 5Z-7 oxozeaenol (5Z-7), significantly abolished the constitutive activity of NF- κ B and AP-1 in these cells. This finding indicates the involvement of TAK-TAB complex in regulating the two constitutively activated pathways. Moreover, a significant reduction of NF- κ B- and AP-1-mediated transactivation was also observed with XIAP inhibition using SM or embelin. These inhibitory effects were comparable or greater than that with the use of NF- κ B or AP-1 inhibitors, BAY11-7082 or PD-98059, respectively. Given the role of XIAP in TAK1

activation, these effects suggest that XIAP can modulate the constitutive activity of NF- κ B and AP-1 in the KGN and COV434 cells, likely via the TAK-TAB complex.

Little is known about the source of the NF- κ B and AP-1 constitutive activity in GCT *in vitro*. Mutations of the NF- κ B and AP-1 components of these pathways lead to constitutive activity are rare (Shaulian, 2010, DiDonato et al., 2012, Drummond and Fuller, 2012). In a panel of human GCT and the two human GCT-derived cell lines, KGN and COV434, our laboratory performed mutation analysis on the *IKK α* , *IKK β* or *IKK γ* (or NEMO) genes and identified no mutations (Jamieson and Fuller, 2013). To elucidate the role, if any, of mutation in the *TAK1* gene, I sequenced the coding region of *TAK1* using RNA extracted from the KGN and COV434 cells. Variant A of the *TAK1* gene is the predominant splice variant in these two cell lines. However, no mutation was found in the *TAK1* gene in the KGN or COV434 cells.

In the absence of genetic mutations, we turned to our recently published microarray analysis (Alexiadis et al., 2016) in the hope of identifying alterations in mRNA levels that may explain the constitutive activity. Using this data set from a panel of 12 human GCT (6 advanced and 6 stage 1 disease), the two GCT-derived cell lines, KGN and COV434, as well as a non-luteinised GC cell line, hGrC1, we were able to examine the mRNA levels of the components of the TAK-TAB complex. Of the 5 genes, *TAK1*, *TAB1/2/3* and *TRAF6*, that we examined, the levels in the advanced tumours showed no difference compared to that in the stage 1 GCT or the cell line counterpart, the KGN cells. The KGN cells were established from a recurrent GCT; this finding reassured us that the molecular profile of these cells is indeed representative of the advanced stage GCT. However, the levels of these genes in the tumours did not appear to deviate from the hGrC1 cells. The only significant difference was observed in *TAK1* and *TAB2* in the COV434 cells. The level of *TAK1*

is significantly higher in the COV434 than in the KGN and hGrC1 cells, and the S1 GCT. On the contrary, the COV434 cells exhibited a significantly lower level of *TAB2* compared to the KGN and hGrC1 cells; no difference was seen between other sample groups.

I have not explored post-translational modifications which could also alter protein expression of TAK1 and its binding partners. Levels of TAK1 and its binding partners have been reported to impact TAK1 kinase activity in a cooperative manner (Shibuya et al., 1996, Kishimoto et al., 2000, Takaesu et al., 2000, Ishitani et al., 2003). Previous studies have shown that TAK1 overexpression alone does not increase TAK1 activity (Kishimoto et al., 2000). Induction of TAK1 kinase activity requires TAB1 or TAB2 overexpression to increase XIAP BIR1:TAB1 dimerisation or the formation of the TRAF6-TAB2-TAK1 complex (Takaesu et al., 2000, Lu et al., 2007). Based on the findings from the digital PCR and SILAC study, SM or embelin/RGZ/RA-treated KGN and COV434 cells did not appear to regulate mRNA or protein expression of TAK1 or its binding partners. As mentioned, we demonstrated a significant reduction of the constitutive activation of NF- κ B and AP-1 with XIAP or TAK1 inhibition. When combined with PPAR γ activation, XIAP antagonism exhibited anti-neoplastic effects in the KGN and COV434 cells. In light of these effects, the unaffected expression of the TAK-TAB complex arguably suggests that it is not the source of the pathognomonic constitutive activation of NF- κ B and AP-1 in the GCT cells.

Collectively, our results demonstrated that the XIAP inhibitor, SM, can remove NF- κ B transrepression on PPAR γ and modulate the constitutive activation of NF- κ B and AP-1 in GCT-derived cell lines. Although we have not identified the source of the constitutive activities, we demonstrated that inhibiting XIAP or TAK1 could abolish

the hyperactivated transcription of NF- κ B and AP-1. With the addition of PPAR γ /RXR α activation, RGZ/RA, apoptosis was significantly induced in the KGN cells in monolayers and in spheroid form. This combined treatment also substantially reduced cell viability and proliferation, and also compromised metabolism such that the treated cells failed to respond to an increased energy demand. Importantly, these anti-neoplastic effects were only seen with the combined XIAP and PPAR γ treatment but not when cells were treated singularly. Given the overexpression of XIAP and PPAR γ in GCT, these two proteins warrant further investigation as promising therapeutic target in this tumour type, as well as other cancers that exhibit the same aberrant protein expression.

A challenge in GCT research is the lack of animal models that adequately recapitulate this FOXL2 mutation-dependent disease and the very limited number of cell lines that adequately reflect these cancers. Given the infrequency of the disease, primary tumours are difficult to obtain. The two GCT explants in this study thus offered a valuable tool to studying these tumours. Indeed the KGN cell line utilised in this study is really the only cell line/model currently available that contains the FOXL2 C134W mutation. The KGN cells are derived from a lymph node metastasis (Nishi et al., 2001) which defines the original tumour as being of an advanced stage with aggressive behaviour. Like adult GCT, the KGN cells have a molecular profile similar to that of granulosa cells of a hormonally-active, late pre-ovulatory follicle. We provided strong proof of the anti-neoplastic effects of the combined PPAR γ and XIAP treatment. Induction of apoptosis, reduction in cell viability and proliferation was observed in not only the monolayer KGN but also KGN in 3D spheroids. The KGN spheroids replicates the

phenotype of the original GCT and better mimics the tumour microenvironment. Furthermore, molecular changes such as the induction of *SCD* following restoration of PPAR γ activity was also replicated in GCT explant models. Nonetheless, our recent transcriptomic analysis indeed showed significant differences across the 10 adult GCT included in that study (Alexiadis et al., 2016). There is therefore a need to correlate findings in these lines with markers in the actual tumours as we have done and where possible, obtain primary tissues to confirm the findings in the KGN cells.

6.2 Future directions

We have created a stable, inducible lentiviral system of XIAP knockdown in this study. The next step will be to utilise this to study the functional domains of XIAP by re-introducing either wildtype or mutant XIAP plasmid into the XIAP-deficient cell lines. The characterisation study can be performed at the message level using RNA-seq analysis or at the proteomic level utilising SILAC and mass spectrometry. Cells with wildtype XIAP will be compared with XIAP mutant cells with knockdown of one or more functional domains. This will enable the identification of the domain-specific XIAP-regulated genes. Given that than one of the XIAP domains possess anti-apoptotic effects, we will likely see changes in genes/proteins associated with proliferation and apoptosis. Pathway analyses of the domain-specific XIAP-regulated genes will provide insights which might aid the designs of new XIAP inhibitors. Anti-apoptotic activity or potential unwanted side effects of the mono- or bi-valent XIAP antagonists targeting one or two domains can be better predicted at the pre-clinical stage. XIAP BIR1 domain knockdown cells will be compared with XIAP wildtype cells treated with TAK1 inhibition. This will allow the evaluation of the levels the TAK-TAB protein complex, as well as the effects on the NF- κ B and AP-1 constitutive activity. Levels of regulators upstream of the TAK-TAB protein complex should be investigated as this may shed light upon the source of the constitutive activity which is potentially applicable to other tumours exhibiting the same pathological feature.

Future studies should also further explore the impact of the combined treatment on invasion. We have in our laboratory a commercial fascin inhibitor which could be tested alone or in combination with the combined PPAR γ and XIAP treatment. Invasion assays using the xCELLigence RTCA system will be extended using 3D

cultures of the KGN cells. The 3D culture better mimics the tumour microenvironment and the findings will illustrate the effectiveness of the proposed treatment in relation to cancer cell growth and their metastatic potential. These studies will provide important pre-clinical data prior to embarking on animal studies and clinical trials.

BIBLIOGRAPHY

- Ahmed, N., Zeng, M., Sinha, I., Polin, L., Wei, W. Z., Rathinam, C., Flavell, R., Massoumi, R. & Venuprasad, K. 2011. The E3 ligase Itch and deubiquitinase Cyl5 act together to regulate Tak1 and inflammation. *Nat Immunol*, 12, 1176-83.
- Al-Alem, L., Southard, R. C., Kilgore, M. W. & Curry, T. E. 2011. Specific thiazolidinediones inhibit ovarian cancer cell line proliferation and cause cell cycle arrest in a PPAR gamma independent manner. *PLoS One*, 6.
- Alexiadis, M., Chu, S., Leung, D., Gould, J. A., Jobling, T. & Fuller, P. J. 2016. Transcriptomic analysis of stage 1 versus advanced adult granulosa cell tumors. *Oncotarget*, 7, 14207-19.
- Alexiadis, M., Eriksson, N., Jamieson, S., Davis, M., Drummond, A. E., Chu, S., Clyne, C. D., Muscat, G. E. & Fuller, P. J. 2011. Nuclear receptor profiling of ovarian granulosa cell tumors. *Horm Cancer*, 2, 157-69.
- Ali, S., Gattuso, P., Howard, A., Mosunjac, M. B. & Siddiqui, M. T. 2008. Adult granulosa cell tumor of the ovary: fine-needle-aspiration cytology of 10 cases and review of literature. *Diagn Cytopathol*, 36, 297-302.
- Amaravadi, R. K., Schilder, R. J., Martin, L. P., Levin, M., Graham, M. A., Weng, D. E. & Adjei, A. A. 2015. A Phase I Study of the SMAC-Mimetic Birinapant in Adults with Refractory Solid Tumors or Lymphoma. *Mol Cancer Ther*, 14, 2569-75.
- Armstrong, D. T., Xia, P., de Gannes, G., Tekpetey, F. R. & Khamsi, F. 1996. Differential effects of insulin-like growth factor-I and follicle-stimulating hormone on proliferation and differentiation of bovine cumulus cells and granulosa cells. *Biol Reprod*, 54, 331-8.
- Arora, R., Yates, C., Gary, B. D., McClellan, S., Tan, M., Xi, Y., Reed, E., Piazza, G. A., Owen, L. B. & Dean-Colomb, W. 2014. Panepoxydone targets NF-kB and FOXM1 to inhibit proliferation, induce apoptosis and reverse epithelial to mesenchymal transition in breast cancer. *PLoS One*, 9, e98370.
- Bai, L., Smith, D. C. & Wang, S. 2014. Small-molecule SMAC mimetics as new cancer therapeutics. *Pharmacol Ther*, 144, 82-95.
- Bauerle, K. T., Schweppe, R. E. & Haugen, B. R. 2010. Inhibition of nuclear factor-kappa B differentially affects thyroid cancer cell growth, apoptosis, and invasion. *Mol Cancer*, 9, 117.
- Bayasula, Iwase, A., Kiyono, T., Takikawa, S., Goto, M., Nakamura, T., Nagatomo, Y., Nakahara, T., Kotani, T., Kobayashi, H., Kondo, M., Manabe, S. & Kikkawa, F. 2012. Establishment of a human nonluteinized granulosa cell line that transitions from the gonadotropin-independent to the gonadotropin-dependent status. *Endocrinology*, 153, 2851-60.
- Bene, H., Lasky, D. & Ntambi, J. M. 2001. Cloning and characterization of the human stearoyl-CoA desaturase gene promoter: transcriptional activation by sterol regulatory element binding protein and repression by polyunsaturated fatty acids and cholesterol. *Biochem Biophys Res Commun*, 284, 1194-8.
- Benedet, J. L., Bender, H., Jones III, H., Ngan, H. Y. S. & Pecorelli, S. 2000. FIGO staging classification and clinical practice guidelines in the management of gynaecologic cancers. *International Journal of Gynecology & Obstetrics*, 70, 54.

- Besse, A., Lamothe, B., Campos, A. D., Webster, W. K., Maddineni, U., Lin, S. C., Wu, H. & Darnay, B. G. 2007. TAK1-dependent signaling requires functional interaction with TAB2/TAB3. *J Biol Chem*, 282, 3918-28.
- Burgermeister, E. & Seger, R. 2007. MAPK kinases as nucleo-cytoplasmic shuttles for PPAR gamma. *Cell Cycle* 6.
- Burstein, H. J., Demetri, G. D., Mueller, E., Sarraf, P., Spiegelman, B. M. & Winer, E. P. 2003. Use of the peroxisome proliferator-activated receptor (PPAR) gamma ligand troglitazone as treatment for refractory breast cancer: a phase II study. *Breast Cancer Res Treat*, 79, 391-7.
- Carter, B. Z., Mak, D. H., Morris, S. J., Borthakud, G., Estey, E. & Byrd, A. L. 2011. XIAP antisense oligonucleotide (AEG35156) achieves target knockdown and induces apoptosis preferentially in CD34+38-cells in a phase 1/2 study of patients with relapsed/refractory AML. *Apoptosis*, 16, 8.
- Chai, J., Shiozaki, E., Srinivasula, S. M., Wu, Q., Datta, P., Alnemri, E. S. & Shi, Y. 2001. Structural basis of caspase-7 inhibition by XIAP. *Cell*, 104, 769-80.
- Chou, F. S., Wang, P. S., Kulp, S. & Pinzone, J. J. 2007. Effects of thiazolidinediones on differentiation, proliferation, and apoptosis. *Mol Cancer Res*, 5, 523-30.
- Chu, S., Alexiadis, M. & Fuller, P. J. 2009. Proteasome inhibition by bortezomib decreases proliferation and increases apoptosis in ovarian granulosa cell tumors. *Reprod Sci*, 16, 397-407.
- Chu, S., Nishi, Y., Yanase, T., Nawata, H. & Fuller, P. J. 2004. Transrepression of estrogen receptor beta signaling by nuclear factor-kappab in ovarian granulosa cells. *Mol Endocrinol*, 18, 1919-28.
- Chu, S., Rushdi, S., Zumpe, E. T., Mamers, P., Healy, D. L., Jobling, T., Burger, H. G. & Fuller, P. J. 2002. FSH-regulated gene expression profiles in ovarian tumours and normal ovaries. *Mol Hum Reprod*, 8, 426-33.
- Couse, J. F., Yates, M. M., Deroo, B. J. & Korach, K. S. 2005. Estrogen receptor-beta is critical to granulosa cell differentiation and the ovulatory response to gonadotropins. *Endocrinology*, 146, 3247-62.
- Couse, J. F., Yates, M. M., Walker, V. R. & Korach, K. S. 2003. Characterization of the hypothalamic-pituitary-gonadal axis in estrogen receptor (ER) Null mice reveals hypergonadism and endocrine sex reversal in females lacking ERalpha but not ERbeta. *Mol Endocrinol*, 17, 1039-53.
- Dai, Y., Qiao, L., Chan, K. W., Zou, B., Ma, J., Lan, H. Y., Gu, Q., Li, Z., Wang, Y., Wong, B. L. & Wong, B. C. 2008. Loss of XIAP sensitizes rosiglitazone-induced growth inhibition of colon cancer in vivo. *Int J Cancer*, 122, 2858-63.
- Dean, E., Jodrell, D., Connolly, K., Danson, S., Jolivet, J., Durkin, J., Morris, S., Jowle, D., Ward, T., Cummings, J., Dickinson, G., Aarons, L., Lacasse, E., Robson, L., Dive, C. & Ranson, M. 2009. Phase I trial of AEG35156 administered as a 7-day and 3-day continuous intravenous infusion in patients with advanced refractory cancer. *J Clin Oncol*, 27, 1660-6.
- Dean, E. J., Ranson, M., Blackhall, F. & Dive, C. 2007. X-linked inhibitor of apoptosis protein as a therapeutic target. *Expert Opin. Ther. Targets*, 11, 14.

- DiDonato, J. A., Mercurio, F. & Karin, M. 2012. NF-kappaB and the link between inflammation and cancer. *Immunol Rev*, 246, 379-400.
- Drummond, A. E. & Fuller, P. J. 2010. The importance of ERbeta signalling in the ovary. *J Endocrinol*, 205, 15-23.
- Drummond, A. E. & Fuller, P. J. 2012. Activin and inhibin, estrogens and NFkappaB, play roles in ovarian tumourigenesis is there crosstalk? *Mol Cell Endocrinol*, 359, 85-91.
- Du, C., Fang, M., Li, Y., Li, L. & Wang, X. 2000. Smac, a mitochondrial protein that promotes cytochrome c-dependent caspase activation by eliminating IAP inhibition. *Cell*, 102, 33-42.
- Dupont, J., Reverchon, M., Cloix, L., Froment, P. & Rame, C. 2012. Involvement of adipokines, AMPK, PI3K and the PPAR signaling pathways in ovarian follicle development and cancer. *Int J Dev Biol*, 56, 959-67.
- Dykxhoorn, D. M. & Lieberman, J. 2005. The silent revolution: RNA interference as basic biology, research tool, and therapeutic. *Annu Rev Med*, 56, 401-23.
- Dykxhoorn, D. M., Novina, C. D. & Sharp, P. A. 2003. Killing the messenger: short RNAs that silence gene expression. *Nat Rev Mol Cell Biol*, 4, 457-67.
- Ehdaivand, S. 2016. Ovary tumor [Online]. Available: <http://www.pathologyoutlines.com/topic/ovarytumorgctadult.html> [Accessed].
- Eppig, J. J. 2001. Oocyte control of ovarian follicular development and function in mammals. *Reproduction*, 122, 10.
- Esheba, G. E. 2015. Granulosa cell tumor group [Online]. Medscape. Available: <http://emedicine.medscape.com/article/1627984-overview#a2> [Accessed].
- Fan, X., Gabbi, C., Kim, H. J., Cheng, G., Andersson, L. C., Warner, M. & Gustafsson, J. A. 2010a. Gonadotropin-positive pituitary tumors accompanied by ovarian tumors in aging female ERbeta^{-/-} mice. *Proc Natl Acad Sci U S A*, 107, 6453-8.
- Fan, Y., Shi, Y., Liu, S., Mao, R., An, L., Zhao, Y., Zhang, H., Zhang, F., Xu, G., Qin, J. & Yang, J. 2012. Lys48-linked TAK1 polyubiquitination at lysine-72 downregulates TNFalpha-induced NF-kappaB activation via mediating TAK1 degradation. *Cell Signal*, 24, 1381-9.
- Fan, Y., Yu, Y., Shi, Y., Sun, W., Xie, M., Ge, N., Mao, R., Chang, A., Xu, G., Schneider, M. D., Zhang, H., Fu, S., Qin, J. & Yang, J. 2010b. Lysine 63-linked polyubiquitination of TAK1 at lysine 158 is required for tumor necrosis factor alpha- and interleukin-1beta-induced IKK/NF-kappaB and JNK/AP-1 activation. *J Biol Chem*, 285, 5347-60.
- Ferlay, J., Shin, H. R., Bray, F., Forman, D., Mathers, C. & Parkin, D. M. 2010. GLOBOCAN 2008 v2.0, Cancer Incidence and Mortality Worldwide: IARC CancerBase No. 10 [Online]. Lyon, France: International Agency for Research on Cancer. Available: <http://globocan.iarc.fr> [Accessed].
- Ferlay, J., Soerjomataram, I., Ervik, M., Dikshit, R., Eser, S., Mathers, C., Rebelo, M., Parkin, D. M., Forman, D. & Bray, F. 2013. GLOBOCAN 2012 v1.0, Cancer Incidence and Mortality Worldwide: IARC CancerBase No. 11.
- Fernandes, K. 2008. Human development. Queen Mary University of London.

- Ferrari, S. M., Materazzi, G., Baldini, E., Ulisse, S., Miccoli, P., Antonelli, A. & Fallahi, P. 2016. Antineoplastic Effects of PPARgamma Agonists, with a Special Focus on Thyroid Cancer. *Curr Med Chem*, 23, 636-49.
- Fetterly, G. J., Liu, B., Senzer, N. N., Amaravadi, R. K., Schilder, R. J., Martin, L. P., LoRusso, P., Papadopoulos, K. P., Adjei, A. A., Zagst, P. D., McKinlay, M. A., Weng, D. E. & Graham, M. A. 2012. Clinical pharmacokinetics of the Smac-mimetic birinapant (TL32711) as a single agent and in combination with multiple chemotherapy regimens. *J Clin Oncol*, 30.
- Fiandalo, M. V. & Kyprianou, N. 2012. Caspase control: protagonists of cancer cell apoptosis. *Exp Oncol*, 34, 165-75.
- Forbes, S. A., Beare, D., Boutselakis, H., Bamford, S., Bindal, N., Tate, J., Cole, C. G., Ward, S., Dawson, E., Ponting, L., Stefancsik, R., Harsha, B., Kok, C. Y., Jia, M., Jubb, H., Sondka, Z., Thompson, S., De, T. & Campbell, P. J. 2017. COSMIC: somatic cancer genetics at high-resolution. *Nucleic Acids Res*, 45, D777-D783.
- Froment, P., Gizard, F., Defever, D., Staels, B., Dupont, J. & Monget, P. 2006. Peroxisome proliferator-activated receptors in reproductive tissues: from gametogenesis to parturition. *J Endocrinol*, 189, 199-209.
- Fulda, S. 2007. Inhibitor of apoptosis proteins as targets for anticancer therapy. *Expert Rev Anticancer Ther*, 7, 1255-64.
- Fulda, S. 2015a. Promises and Challenges of Smac Mimetics as Cancer Therapeutics. *Clin Cancer Res*, 21, 5030-6.
- Fulda, S. 2015b. Targeting IAP proteins in combination with radiotherapy. *Radiat Oncol*, 10, 105.
- Fulda, S. & Vucic, D. 2012. Targeting IAP proteins for therapeutic intervention in cancer. *Nat Rev Drug Discov*, 11, 109-24.
- Fuller, P. J. & Chu, S. 2004. Signalling pathways in the molecular pathogenesis of ovarian granulosa cell tumours. *Trends Endocrinol Metab*, 15, 122-8.
- Fuller, P. J., Leung, D. & Chu, S. 2017. Genetics and genomics of ovarian sex cord-stromal tumors. *Clin Genet*, 91, 285-291.
- Fuller, P. J., Verity, K., Shen, Y., Mamers, P., Jobling, T. & Burger, H. G. 1998. No evidence of a role for mutations or polymorphisms of the follicle-stimulating hormone receptor in ovarian granulosa cell tumors. *Journal of Clinical Endocrinology & Metabolism*, 83, 6.
- Garg, R., Blando, J., Perez, C. J., Wang, H., Benavides, F. J. & Kazanietz, M. G. 2012. Activation of nuclear factor kappaB (NF-kappaB) in prostate cancer is mediated by protein kinase C epsilon (PKCepsilon). *J Biol Chem*, 287, 37570-82.
- Gelman, L., Michalik, L., Desvergne, B. & Wahli, W. 2005. Kinase signaling cascades that modulate peroxisome proliferator-activated receptors. *Curr Opin Cell Biol*, 17, 216-22.
- Graham, F. L., Smiley, J., Russell, W. C. & Nairn, R. 1977. Characteristics of a human cell line transformed by DNA from human adenovirus type 5. *J Gen Virol*, 36, 59-74.

- Guo, R. X., Qiao, Y. H., Zhou, Y., Li, L. X., Shi, H. R. & Chen, K. S. 2008. Increased staining for phosphorylated AKT and nuclear factor-kappaB p65 and their relationship with prognosis in epithelial ovarian cancer. *Pathol Int*, 58, 749-56.
- Gupta, S., Kumar, P., Kaur, H., Sharma, N., Saluja, D., Bharti, A. C. & Das, B. C. 2015. Selective participation of c-Jun with Fra-2/c-Fos promotes aggressive tumor phenotypes and poor prognosis in tongue cancer. *Sci Rep*, 5, 16811.
- Gurumurthy, M., Bryant, A. & Shanbhag, S. 2014. Effectiveness of different treatment modalities for the management of adult-onset granulosa cell tumours of the ovary (primary and recurrent). *Cochrane Database Syst Rev*, 4, CD006912.
- Hau, P., Kunz-Schughart, L., Bogdahn, U., Baumgart, U., Hirschmann, B., Weimann, E., Muhleisen, H., Ruemmele, P., Steinbrecher, A. & Reichle, A. 2007. Low-dose chemotherapy in combination with COX-2 inhibitors and PPAR-gamma agonists in recurrent high-grade gliomas - a phase II study. *Oncology*, 73, 21-5.
- Hauser, S., Adelmant, G., Sarraf, P., Wright, H. M., Mueller, E. & Spiegelman, B. M. 2000. Degradation of the peroxisome proliferator-activated receptor gamma is linked to ligand-dependent activation. *J Biol Chem*, 275, 18527-33.
- Hernandez, L., Hsu, S. C., Davidson, B., Birrer, M. J., Kohn, E. C. & Annunziata, C. M. 2010. Activation of NF-kappaB signaling by inhibitor of NF-kappaB kinase beta increases aggressiveness of ovarian cancer. *Cancer Res*, 70, 4005-14.
- Hirata, Y., Takahashi, M., Morishita, T., Noguchi, T. & Matsuzawa, A. 2017. Post-Translational Modifications of the TAK1-TAB Complex. *Int J Mol Sci*, 18.
- Hoesel, B. & Schmid, J. A. 2013. The complexity of NF-kappaB signaling in inflammation and cancer. *Mol Cancer*, 12, 86.
- Hofer-Warbinek, R., Schmid, J. A., Stehlik, C., Binder, B. R., Lipp, J. & de Martin, R. 2000. Activation of NF-kappa B by XIAP, the X chromosome-linked inhibitor of apoptosis, in endothelial cells involves TAK1. *J Biol Chem*, 275, 22064-8.
- Huang, Y., Park, Y. C., Rich, R. L., Segal, D., Myszka, D. G. & Wu, H. 2001. Structural basis of caspase inhibition by XIAP: differential roles of the linker versus the BIR domain. *Cell*, 104, 781-90.
- Huang, Y., Rich, R. L., Myszka, D. G. & Wu, H. 2003. Requirement of both the second and third BIR domains for the relief of X-linked inhibitor of apoptosis protein (XIAP)-mediated caspase inhibition by Smac. *J Biol Chem*, 278, 49517-22.
- Ikeda, J., Ichiki, T., Takahara, Y., Kojima, H., Sankoda, C., Kitamoto, S., Tokunou, T. & Sunagawa, K. 2015. PPARgamma Agonists Attenuate Palmitate-Induced ER Stress through Up-Regulation of SCD-1 in Macrophages. *PLoS One*, 10, e0128546.
- Imbert, V. & Peyron, J. F. 2017. NF-kappaB in Hematological Malignancies. *Biomedicines*, 5.
- Ishitani, T., Takaesu, G., Ninomiya-Tsuji, J., Shibuya, H., Gaynor, R. B. & Matsumoto, K. 2003. Role of the TAB2-related protein TAB3 in IL-1 and TNF signaling. *EMBO J*, 22, 6277-88.
- Jamieson, S., Butzow, R., Andersson, N., Alexiadis, M., Unkila-Kallio, L., Heikinheimo, M., Fuller, P. J. & Anttonen, M. 2010. The FOXL2 C134W mutation is characteristic of adult granulosa cell tumors of the ovary. *Mod Pathol*, 23, 1477-85.

Jamieson, S. & Fuller, P. J. 2012. Molecular pathogenesis of granulosa cell tumors of the ovary. *Endocr Rev*, 33, 109-44.

Jamieson, S. & Fuller, P. J. 2013. Characterization of the inhibitor of kappaB kinase (IKK) complex in granulosa cell tumors of the ovary and granulosa cell tumor-derived cell lines. *Horm Cancer*, 4, 277-92.

Jiang, C., Yi, X. P., Shen, H. & Li, Y. X. 2012. Targeting x-linked inhibitor of apoptosis protein inhibits pancreatic cancer cell growth through p-Akt depletion. *World J Gastroenterol*, 18, 10.

Kanayama, A., Seth, R. B., Sun, L., Ea, C. K., Hong, M., Shaito, A., Chiu, Y. H., Deng, L. & Chen, Z. J. 2004. TAB2 and TAB3 activate the NF-kappaB pathway through binding to polyubiquitin chains. *Mol Cell*, 15, 535-48.

Karin, M. S., E. 2002. AP-1 as a regulator of cell life and death. *Nature Cell Biology*, 4, 6.

Kaur, S., Wang, F., Venkatraman, M. & Arsur, M. 2005. X-linked inhibitor of apoptosis (XIAP) inhibits c-Jun N-terminal kinase 1 (JNK1) activation by transforming growth factor beta1 (TGF-beta1) through ubiquitin-mediated proteosomal degradation of the TGF-beta1-activated kinase 1 (TAK1). *J Biol Chem*, 280, 38599-608.

Khorasanizadeh, S. & Rastinejad, F. 2016. Visualizing the Architectures and Interactions of Nuclear Receptors. *Endocrinology*, 157, 4212-4221.

Kim, J., Sato, M., Li, Q., Lydon, J. P., Demayo, F. J., Bagchi, I. C. & Bagchi, M. K. 2008. Peroxisome proliferator-activated receptor gamma is a target of progesterone regulation in the preovulatory follicles and controls ovulation in mice. *Mol Cell Biol*, 28, 1770-82.

Kim, S. I., Kwak, J. H., Na, H. J., Kim, J. K., Ding, Y. & Choi, M. E. 2009. Transforming growth factor-beta (TGF-beta1) activates TAK1 via TAB1-mediated autophosphorylation, independent of TGF-beta receptor kinase activity in mesangial cells. *J Biol Chem*, 284, 22285-96.

Kim, S. Y., Shim, J. H., Chun, E. & Lee, K. Y. 2012. Reciprocal inhibition between the transforming growth factor-beta-activated kinase 1 (TAK1) and apoptosis signal-regulating kinase 1 (ASK1) mitogen-activated protein kinase kinases and its suppression by TAK1-binding protein 2 (TAB2), an adapter protein for TAK1. *J Biol Chem*, 287, 3381-91.

Kishimoto, K., Matsumoto, K. & Ninomiya-Tsuji, J. 2000. TAK1 mitogen-activated protein kinase kinase is activated by autophosphorylation within its activation loop. *J Biol Chem*, 275, 7359-64.

Kobel, M., Gilks, C. B. & Huntsman, D. G. 2009. Adult-type granulosa cell tumors and FOXL2 mutation. *Cancer Res*, 69, 9160-2.

Kolla, V. & Litwack, G. 2000. Inhibition of mineralocorticoid-mediated transcription by NF-kappaB. *Arch Biochem Biophys*, 383, 38-45.

Komatsu, Y., Yoshino, T., Yamazaki, K., Yuki, S., Machida, N., Sasaki, T., Hyodo, I., Yachi, Y., Onuma, H. & Ohtsu, A. 2014. Phase 1 study of efatutazone, a novel oral peroxisome proliferator-activated receptor gamma agonist, in combination with

FOLFIRI as second-line therapy in patients with metastatic colorectal cancer. *Invest New Drugs*, 32, 473-80.

Krappmann, D. & Vincendeau, M. 2016. Mechanisms of NF-kappaB deregulation in lymphoid malignancies. *Semin Cancer Biol*, 39, 3-14.

Kuo, W. Y., Hwu, L., Wu, C. Y., Lee, J. S., Chang, C. W. & Liu, R. S. 2017. STAT3/NF-kappaB-Regulated Lentiviral TK/GCV Suicide Gene Therapy for Cisplatin-Resistant Triple-Negative Breast Cancer. *Theranostics*, 7, 647-663.

Le Goff, C., Rogers, C., Le Goff, W., Pinto, G., Bonnet, D., Chrabieh, M., Alibeu, O., Nistchke, P., Munnich, A., Picard, C. & Cormier-Daire, V. 2016. Heterozygous Mutations in MAP3K7, Encoding TGF-beta-Activated Kinase 1, Cause Cardiospondylocarpofacial Syndrome. *Am J Hum Genet*, 99, 407-13.

Leaner, V. D., Donniger, H. & Birrer, M. J. 2007. Transcription factors as targets for cancer therapy: AP-1 a potential therapeutic target. *Current Cancer Therapy Reviews*, 3, 6.

Lee, Y. K., Park, N. H., Kim, J. W., Song, Y. S., Kang, S. B. & Lee, H. P. 2008. Characteristics of recurrence in adult-type granulosa cell tumor. *Int J Gynecol Cancer*, 18, 642-7.

Levkau, B., Garton, K. J., Ferri, N., Kloke, K., Nofer, J. R., Baba, H. A., Raines, E. W. & Breithardt, G. 2001. XIAP induces cell-cycle arrest and activates nuclear factor-kappaB : new survival pathways disabled by caspase-mediated cleavage during apoptosis of human endothelial cells. *Circ Res*, 88, 282-90.

Li, W., Srinivasula, S. M., Chai, J., Li, P., Wu, J. W., Zhang, Z., Alnemri, E. S. & Shi, Y. 2002. Structural insights into the pro-apoptotic function of mitochondrial serine protease HtrA2/Omi. *Nat Struct Biol*, 9, 436-41.

Lin, S. C., Huang, Y., Lo, Y. C., Lu, M. & Wu, H. 2007. Crystal structure of the BIR1 domain of XIAP in two crystal forms. *J Mol Biol*, 372, 847-54.

Liston, P., Fong, W. G., Kelly, N. L., Toji, S., Miyazaki, T., Conte, D., Tamai, K., Craig, C. G., McBurney, M. W. & Korneluk, R. G. 2001. Identification of XAF1 as an antagonist of XIAP anti-Caspase activity. *Nat Cell Biol*, 3, 128-33.

Liu, J. J., Guo, Y. W., Fang, Z. G., Si, X. N., Wu, X. Y., Liu, P. Q., Lin, D. J., Xiao, R. Z., Xu, Y., Wang, C. Z., Li, X. D., He, Y. & Huang, R. W. 2009. Activation of peroxisome proliferator-activated receptor-gamma induces apoptosis on acute promyelocytic leukemia cells via downregulation of XIAP. *Int J Mol Med*, 24, 623-32.

Long, M. J., Sairam, M. R. & Komar, C. M. 2009. Initiation of the expression of peroxisome proliferator-activated receptor gamma (PPAR gamma) in the rat ovary and the role of FSH. *Reprod Biol Endocrinol*, 7, 145.

Lovekamp-Swan, T., Jetten, A. M. & Davis, B. J. 2003. Dual activation of PPARalpha and PPARgamma by mono-(2-ethylhexyl) phthalate in rat ovarian granulosa cells. *Mol Cell Endocrinol*, 201, 133-41.

Lu, M., Lin, S. C., Huang, Y., Kang, Y. J., Rich, R., Lo, Y. C., Myszkka, D., Han, J. & Wu, H. 2007. XIAP induces NF-kappaB activation via the BIR1/TAB1 interaction and BIR1 dimerization. *Mol Cell*, 26, 689-702.

Lunardi, A., Ala, U., Epping, M. T., Salmena, L., Clohessy, J. G., Webster, K. A., Wang, G., Mazzucchelli, R., Bianconi, M., Stack, E. C., Lis, R., Patnaik, A., Cantley,

- L. C., Bublely, G., Cordon-Cardo, C., Gerald, W. L., Montironi, R., Signoretti, S., Loda, M., Nardella, C. & Pandolfi, P. P. 2013. A co-clinical approach identifies mechanisms and potential therapies for androgen deprivation resistance in prostate cancer. *Nat Genet*, 45, 747-55.
- Ma, J. J., Chen, B. L. & Xin, X. Y. 2009. XIAP gene downregulation by small interfering RNA inhibits proliferation, induces apoptosis, and reverses the cisplatin resistance of ovarian carcinoma. *Eur J Obstet Gynecol Reprod Biol*, 146, 222-6.
- Mahadevan, D., Chalasani, P., Rensvold, D., Kurtin, S., Pretzinger, C., Jolivet, J., Ramanathan, R. K., Von Hoff, D. D. & Weiss, G. J. 2013. Phase I trial of AEG35156 an antisense oligonucleotide to XIAP plus gemcitabine in patients with metastatic pancreatic ductal adenocarcinoma. *Am J Clin Oncol*, 36, 239-43.
- Malanga, D., De Marco, C., Guerriero, I., Colelli, F., Rinaldo, N., Scrima, M., Mirante, T., De Vitis, C., Zoppoli, P., Ceccarelli, M., Riccardi, M., Ravo, M., Weisz, A., Federico, A., Franco, R., Rocco, G., Mancini, R., Rizzuto, A., Gulletta, E., Ciliberto, G. & Viglietto, G. 2015. The Akt1/IL-6/STAT3 pathway regulates growth of lung tumor initiating cells. *Oncotarget*, 6, 42667-86.
- Malladi, S., Challa-Malladi, M. & Bratton, S. B. 2010. Apoptosis. *In*: CA, M. (ed.) *Comprehensive toxicology*. 2nd ed. UK: Elsevier Ltd.
- Mao, R., Fan, Y., Mou, Y., Zhang, H., Fu, S. & Yang, J. 2011. TAK1 lysine 158 is required for TGF-beta-induced TRAF6-mediated Smad-independent IKK/NF-kappaB and JNK/AP-1 activation. *Cell Signal*, 23, 222-7.
- Matthews, C. P., Colburn, N. H. & Young, M. R. 2007. AP-1 a target for cancer prevention. *Current Cancer Drug Targets*, 7, 8.
- Matzinger, O., Viertl, D., Tsoutsou, P., Kadi, L., Rigotti, S., Zanna, C., Wiedemann, N., Vozenin, M. C., Vuagniaux, G. & Bourhis, J. 2015. The radiosensitizing activity of the SMAC-mimetic, Debio 1143, is TNFalpha-mediated in head and neck squamous cell carcinoma. *Radiother Oncol*, 116, 495-503.
- McKay, L. I. & Cidlowski, J. A. 1998. Cross-talk between nuclear factor-kappa B and the steroid hormone receptors: mechanisms of mutual antagonism. *Mol Endocrinol*, 12, 45-56.
- McKay, L. I. & Cidlowski, J. A. 1999. Molecular control of immune/inflammatory responses: interactions between nuclear factor-kappa B and steroid receptor-signaling pathways. *Endocr Rev*, 20, 435-59.
- Mehta, R. G., Peng, X., Roy, S., Hawthorne, M., Kalra, A., Alimirah, F., Mehta, R. R. & Kopelovich, L. 2013. PPARgamma antagonist GW9662 induces functional estrogen receptor in mouse mammary organ culture: potential translational significance. *Mol Cell Biochem*, 372, 249-56.
- Mihaly, S. R., Ninomiya-Tsuji, J. & Morioka, S. 2014. TAK1 control of cell death. *Cell Death Differ*, 21, 1667-1676.
- Mishra, A., Bharti, A. C., Saluja, D. & Das, B. C. 2010. Transactivation and expression patterns of Jun and Fos/AP-1 super-family proteins in human oral cancer. *Int J Cancer*, 126, 819-29.

- Morizane, Y., Honda, R., Fukami, K. & Yasuda, H. 2005. X-linked inhibitor of apoptosis functions as ubiquitin ligase toward mature caspase-9 and cytosolic Smac/DIABLO. *J Biochem*, 137, 125-32.
- Murakami, H., Ono, A., Takahashi, T., Onozawa, Y., Tsushima, T., Yamazaki, K., Jikoh, T., Boku, N. & Yamamoto, N. 2014. Phase I study of Efatutazone, an oral PPAR γ agonist, in patients with metastatic solid tumors. *Anticancer Res*, 34, 5133-41.
- Muscella, A., Vetrugno, C. & Marsigliante, S. 2017. CCL20 promotes migration and invasiveness of human cancerous breast epithelial cells in primary culture. *Mol Carcinog*.
- Nakatani, Y., Kleffmann, T., Linke, K., Condon, S. M., Hinds, M. G. & Day, C. L. 2013. Regulation of ubiquitin transfer by XIAP, a dimeric RING E3 ligase. *Biochem J*, 450, 629-38.
- Ndlovu, M. N., Van Lint, C., Van Wesemael, K., Callebert, P., Chalbos, D., Haegeman, G. & Vanden Berghe, W. 2009. Hyperactivated NF- κ B and AP-1 transcription factors promote highly accessible chromatin and constitutive transcription across the interleukin-6 gene promoter in metastatic breast cancer cells. *Mol Cell Biol*, 29, 5488-504.
- Nikolovska-Coleska, Z., Xu, L., Hu, Z., Tomita, Y., Li, P., Roller, P. P., Wang, R., Fang, X., Guo, R., Zhang, M., Lippman, M. E., Yang, D. & Wang, S. 2004. Discovery of embelin as a cell-permeable, small-molecular weight inhibitor of XIAP through structure-based computational screening of a traditional herbal medicine three-dimensional structure database. *J Med Chem*, 47, 2430-40.
- Nishi, Y., Yanase, T., Mu, Y., Oba, K., Ichino, I., Saito, M., Nomura, M., Mukasa, C., Okabe, T., Goto, K., Takayanagi, R., Kashimura, Y., Haji, M. & Nawata, H. 2001. Establishment and characterization of a steroidogenic human granulosa-like tumor cell line, KGN, that expresses functional follicle-stimulating hormone receptor. *Endocrinology*, 142, 437-45.
- Niu, J., Li, Z., Peng, B. & Chiao, P. J. 2004. Identification of an autoregulatory feedback pathway involving interleukin-1 α in induction of constitutive NF- κ B activation in pancreatic cancer cells. *J Biol Chem*, 279, 16452-62.
- Ondrey, F. 2009. Peroxisome proliferator-activated receptor gamma pathway targeting in carcinogenesis: implications for chemoprevention. *Clin Cancer Res*, 15, 2-8.
- Palermo, R. 2007. Differential actions of FSH and LH during folliculogenesis. *Reproductive BioMedicine Online*, 15, 12.
- Park, J. Y., Jin, K. L., Kim, D. Y., Kim, J. H., Kim, Y. M., Kim, K. R., Kim, Y. T. & Nam, J. H. 2012. Surgical staging and adjuvant chemotherapy in the management of patients with adult granulosa cell tumors of the ovary. *Gynecol Oncol*, 125, 80-6.
- Parodo, G., Gerosa, C. & Soddu, S. 2013. *Ovarian neoplasm imaging*, Springer.
- Peng, J., Li, Q., Wigglesworth, K., Rangarajan, A., Kattamuri, C., Peterson, R. T., Eppig, J. J., Thompson, T. B. & Matzuk, M. M. 2013. Growth differentiation factor 9:bone morphogenetic protein 15 heterodimers are potent regulators of ovarian functions. *Proc Natl Acad Sci U S A*, 110, E776-85.

- Prabhu, L., Mundade, R., Korc, M., Loehrer, P. J. & Lu, T. 2014. Critical role of NF-kappaB in pancreatic cancer. *Oncotarget*, 5, 10969-75.
- Prasad, S., Ravindran, J. & Aggarwal, B. B. 2010. NF-kappaB and cancer: how intimate is this relationship. *Mol Cell Biochem*, 336, 25-37.
- Puck, T. T., Cieciora, S. J. & Robinson, A. 1958. Genetics of somatic mammalian cells. III. Long-term cultivation of euploid cells from human and animal subjects. *J Exp Med*, 108, 945-56.
- Puttabyatappa, M., Vandervoort, C. A. & Chaffin, C. L. 2010. hCG-induced down-regulation of PPARgamma and liver X receptors promotes periovulatory progesterone synthesis by macaque granulosa cells. *Endocrinology*, 151, 5865-72.
- Qiao, L., Dai, Y., Gu, Q., Chan, K. W., Ma, J., Lan, H. Y., Zou, B., Rocken, C., Ebert, M. P. & Wong, B. C. 2008. Loss of XIAP sensitizes colon cancer cells to PPARgamma independent antitumor effects of troglitazone and 15-PGJ2. *Cancer Lett*, 268, 260-71.
- Reiley, W. W., Jin, W., Lee, A. J., Wright, A., Wu, X., Tewalt, E. F., Leonard, T. O., Norbury, C. C., Fitzpatrick, L., Zhang, M. & Sun, S. C. 2007. Deubiquitinating enzyme CYLD negatively regulates the ubiquitin-dependent kinase Tak1 and prevents abnormal T cell responses. *J Exp Med*, 204, 1475-85.
- Ricci, C. G., Silveira, R. L., Rivalta, I., Batista, V. S. & Skaf, M. S. 2016. Allosteric Pathways in the PPARgamma-RXRalpha nuclear receptor complex. *Sci Rep*, 6, 19940.
- Richards, J. S. 1994. Hormonal control of gene expression in the ovary. *Endocrine reviews*, 15, 27.
- Richards, M. A., Russell, D. L., Ochsner, S., Hsieh, M., Doyle, K. H., Falender, A. E., Lo, Y. K. & Sharma, C. G. 2002. Novel signaling pathways that control ovarian follicular development, ovulation and luteinization. *The Endocrine Society*, 26.
- Rinkenbaugh, A. L. & Baldwin, A. S. 2016. The NF-kappaB Pathway and Cancer Stem Cells. *Cells*, 5.
- Robker, R. L. & Richards, J. S. 1998. Hormone-induced proliferation and differentiation of granulosa cells: a coordinated balance of the cell cycle regulators cyclin D2 and p27^{Kip1}. *Molecular Endocrinology*, 12, 17.
- Roett, M. A. & Evans, P. 2009. Ovarian cancer: an overview. *American Family Physician*, 80, 8.
- Rusovici, R. & LaVoie, H. A. 2003. Expression and distribution of AP-1 transcription factors in the porcine ovary. *Biol Reprod*, 69, 64-74.
- Sakamoto, K., Maeda, S., Hikiba, Y., Nakagawa, H., Hayakawa, Y., Shibata, W., Yanai, A., Ogura, K. & Omata, M. 2009. Constitutive NF-kappaB activation in colorectal carcinoma plays a key role in angiogenesis, promoting tumor growth. *Clin Cancer Res*, 15, 2248-58.
- Sakurai, H., Nishi, A., Sato, N., Mizukami, J., Miyoshi, H. & Sugita, T. 2002. TAK1-TAB1 fusion protein: a novel constitutively active mitogen-activated protein kinase kinase kinase that stimulates AP-1 and NF-kappaB signaling pathways. *Biochem Biophys Res Commun*, 297, 1277-81.
- Saladin, K. S. 2007. *Anatomy and physiology: the unit of form and function*.

- Sarraj, M. A. & Drummond, A. E. 2012. Mammalian foetal ovarian development: consequences for health and disease. *Reproduction*, 143, 151-63.
- Sasaki, H., Sheng, Y., Kotsuji, F. & Tsang, B. K. 2000. Down-regulation of X-linked inhibitor of apoptosis protein induces apoptosis in chemoresistant human ovarian cancer cells. *Cancer Res*, 60, 5659-66.
- Schimmer, A. D., Dalili, S., Batey, R. A. & Riedl, S. J. 2006. Targeting XIAP for the treatment of malignancy. *Cell Death Differ*, 13, 179-88.
- Schmidt, D., Ovitt, C. E., Anlag, K., Fehsenfeld, S., Gredsted, L., Treier, A. C. & Treier, M. 2004. The murine winged-helix transcription factor Foxl2 is required for granulosa cell differentiation and ovary maintenance. *Development*, 131, 933-42.
- Schumer, S. T. 2003. Granulosa Cell Tumor of the Ovary. *Journal of Clinical Oncology*, 21, 1180-1189.
- Seagle, B. L., Ann, P., Butler, S. & Shahabi, S. 2017. Ovarian granulosa cell tumor: A National Cancer Database study. *Gynecol Oncol*.
- Seger, R., Hanoch, T., Rosenberg, R., Dantes, A., Merz, W. E., Strauss, J. F., 3rd & Amsterdam, A. 2001. The ERK signaling cascade inhibits gonadotropin-stimulated steroidogenesis. *J Biol Chem*, 276, 13957-64.
- Servier 2012. Reproduction.
- Shah, S. P., Kobel, M., Senz, J., Morin, R. D., Clarke, B. A. & Wiegand, K. C. 2009. Mutation of FOXL2 in granulosa-cell tumors of the ovary. *the New England Journal of Medicine*, 360, 2719.
- Sharma, S. C. & Richards, J. S. 2000. Regulation of AP1 (Jun/Fos) factor expression and activation in ovarian granulosa cells. Relation of JunD and Fra2 to terminal differentiation. *J Biol Chem*, 275, 33718-28.
- Shaulian, E. 2010. AP-1--The Jun proteins: Oncogenes or tumor suppressors in disguise? *Cell Signal*, 22, 894-9.
- Shaulian, E. & Karin, M. 2002. AP-1 as a regulator of cell life and death. *Nat Cell Biol*, 4, E131-6.
- Shi, H., Luo, J., Zhu, J., Li, J., Sun, Y., Lin, X., Zhang, L., Yao, D. & Shi, H. 2013. PPAR gamma Regulates Genes Involved in Triacylglycerol Synthesis and Secretion in Mammary Gland Epithelial Cells of Dairy Goats. *PPAR Res*, 2013, 310948.
- Shi, Y. 2002. Mechanisms of caspase activation and inhibition during apoptosis. *Mol Cell*, 9, 459-70.
- Shibuya, A., Wada, K., Nakajima, A., Saeki, M., Katayama, K., Mayumi, T., Kadowaki, T., Niwa, H. & Kamisaki, Y. 2002. Nitration of PPARgamma inhibits ligand-dependent translocation into the nucleus in a macrophage-like cell line, RAW 264. *FEBS Lett*, 525, 43-7.
- Shibuya, H., Yamaguchi, K., Shirakabe, K., Tonegawa, A., Gotoh, Y., Ueno, N., Irie, K., Nishida, E. & Matsumoto, K. 1996. TAB1: an activator of the TAK1 MAPKKK in TGF-beta signal transduction. *Science*, 272, 1179-82.
- Shimazaki, N., Togashi, N., Hanai, M., Isoyama, T., Wada, K., Fujita, T., Fujiwara, K. & Kurakata, S. 2008. Anti-tumour activity of CS-7017, a selective peroxisome proliferator-activated receptor gamma agonist of thiazolidinedione class, in human

tumour xenografts and a syngeneic tumour implant model. *Eur J Cancer*, 44, 1734-43.

Shiozaki, E. N., Chai, J., Rigotti, D. J., Riedl, S. J., Li, P., Srinivasula, S. M., Alnemri, E. S., Fairman, R. & Shi, Y. 2003. Mechanism of XIAP-mediated inhibition of caspase-9. *Mol Cell*, 11, 519-27.

Silke, J., Ekert, P. G., Day, C. L., Hawkins, C. J., Baca, M., Chew, J., Pakusch, M., Verhagen, A. M. & Vaux, D. L. 2001. Direct inhibition of caspase 3 is dispensable for the anti-apoptotic activity of XIAP. *EMBO J*, 20, 3114-23.

Smallridge, R. C., Copland, J. A., Brose, M. S., Wadsworth, J. T., Houvras, Y., Menefee, M. E., Bible, K. C., Shah, M. H., Gramza, A. W., Klopper, J. P., Marlow, L. A., Heckman, M. G. & Von Roemeling, R. 2013. Efatutazone, an oral PPAR-gamma agonist, in combination with paclitaxel in anaplastic thyroid cancer: results of a multicenter phase 1 trial. *J Clin Endocrinol Metab*, 98, 2392-400.

Smith, M. R., Manola, J., Kaufman, D. S., George, D., Oh, W. K. & Mueller, E. 2004. Rosiglitazone versus placebo for men with prostate carcinoma and a rising serum prostate-specific antigen level after radical prostatectomy and/or radiation therapy. *Cancer*, 101, 6.

Stenwig, J. T., Hazekamp, J. T. & Beecham, J. B. 1979. Granulosa cell tumors of the ovary. A clinicopathological study of 118 cases with long-term follow-up. *Gynecol Oncol*, 7, 136-52.

Sun, C., Cai, M., Gunasekera, A. H., Meadows, R. P., Wang, H., Chen, J., Zhang, H., Wu, W., Xu, N., Ng, S. C. & Fesik, S. W. 1999. NMR structure and mutagenesis of the inhibitor-of-apoptosis protein XIAP. *Nature*, 401, 818-22.

Sun, Y., He, N., Dong, Y. & Jiang, C. 2016. MiR-24-BIM-Smac/DIABLO axis controls the sensitivity to doxorubicin treatment in osteosarcoma. *Sci Rep*, 6, 34238.

Suzuki, Y., Nakabayashi, Y. & Takahashi, R. 2001. Ubiquitin-protein ligase activity of X-linked inhibitor of apoptosis protein promotes proteasomal degradation of caspase-3 and enhances its anti-apoptotic effect in Fas-induced cell death. *Proc Natl Acad Sci U S A*, 98, 8662-7.

Takaesu, G., Kishida, S., Hiyama, A., Yamaguchi, K., Shibuya, H., Irie, K., Ninomiya-Tsuji, J. & Matsumoto, K. 2000. TAB2, a novel adaptor protein, mediates activation of TAK1 MAPKKK by linking TAK1 to TRAF6 in the IL-1 signal transduction pathway. *Mol Cell*, 5, 649-58.

Tan, V. Y., Lewis, S. J., Adams, J. C. & Martin, R. M. 2013. Association of fascin-1 with mortality, disease progression and metastasis in carcinomas: a systematic review and meta-analysis. *BMC Med*, 11, 52.

Tsukahara, T. & Haniu, H. 2012. Peroxisome proliferator-activated receptor gamma overexpression suppresses proliferation of human colon cancer cells. *Biochem Biophys Res Commun*, 424, 524-9.

Tyagi, A., Vishnoi, K., Kaur, H., Srivastava, Y., Roy, B. G., Das, B. C. & Bharti, A. C. 2017. Cervical cancer stem cells manifest radioresistance: Association with upregulated AP-1 activity. *Sci Rep*, 7, 4781.

van den Berg-Bakker, C. A., Hagemeyer, A., Franken-Postma, E. M., Smit, V. T., Kuppen, P. J., van Ravenswaay Claasen, H. H., Cornelisse, C. J. & Schrier, P. I.

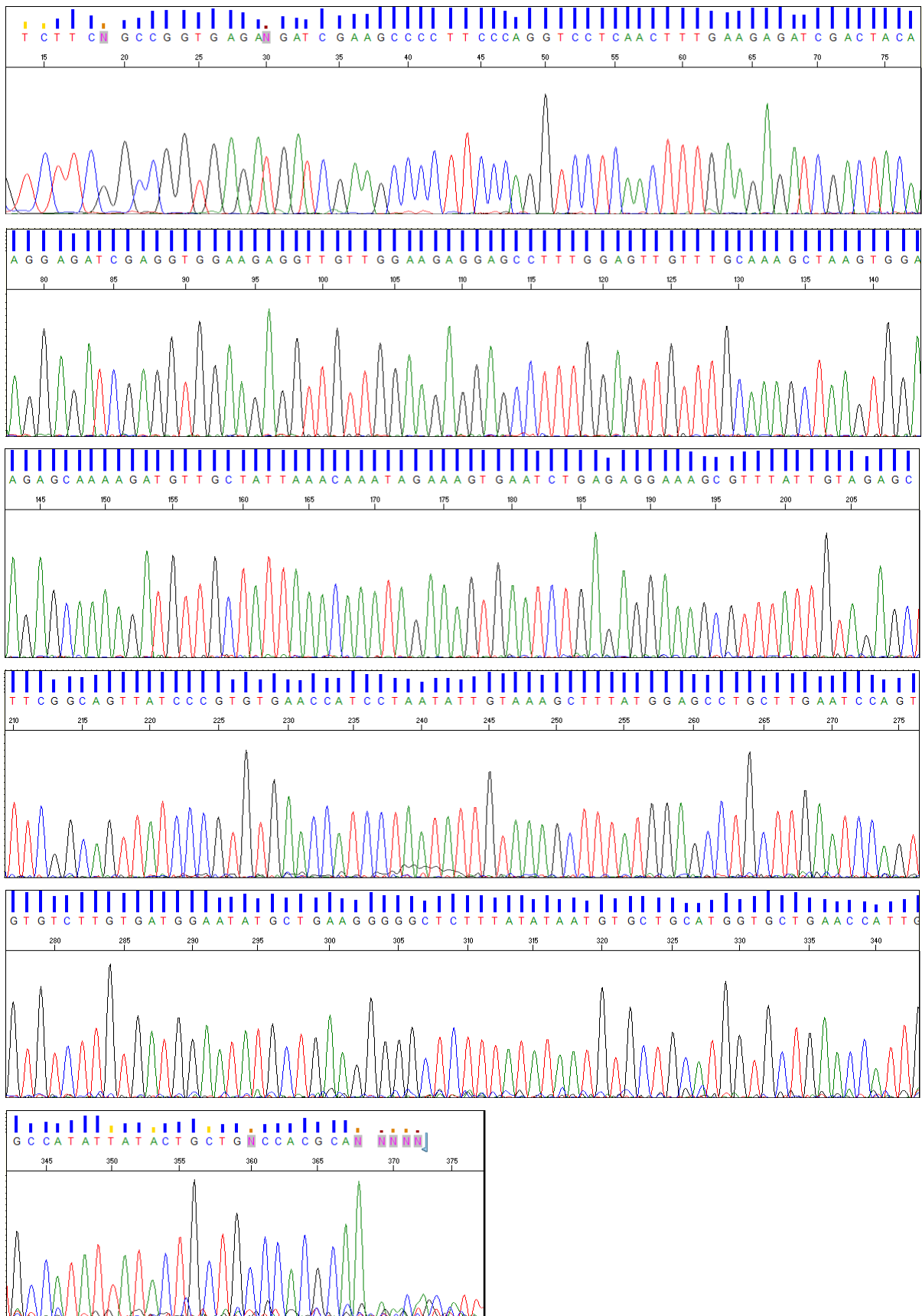
1993. Establishment and characterization of 7 ovarian carcinoma cell lines and one granulosa tumor cell line: growth features and cytogenetics. *Int J Cancer*, 53, 613-20.
- van Meurs, H. S., van Lonkhuijzen, L. R., Limpens, J., van der Velden, J. & Buist, M. R. 2014. Hormone therapy in ovarian granulosa cell tumors: a systematic review. *Gynecol Oncol*, 134, 196-205.
- Vegetti, W. 2006. FSH and folliculogenesis: from physiology to ovarian stimulation. *Reproductive BioMedicine Online*, 12, 11.
- Verstak, B., Stack, J., Ve, T., Mangan, M., Hjerrild, K., Jeon, J., Stahl, R., Latz, E., Gay, N., Kobe, B., Bowie, A. G. & Mansell, A. 2014. The TLR signaling adaptor TRAM interacts with TRAF6 to mediate activation of the inflammatory response by TLR4. *J Leukoc Biol*, 96, 427-36.
- Vignati, S., Albertini, V., Rinaldi, A., Kwee, I., Riva, C., Oldrini, R., Capella, C., Bertoni, F., Carbone, G. M. & Catapano, C. V. 2006. Cellular and molecular consequences of peroxisome proliferator-activated receptor-gamma activation in ovarian cancer cells. *Neoplasia*, 8, 851-61.
- Vogler, M., Walczak, H., Stadel, D., Haas, T. L., Genze, F., Jovanovic, M., Gschwend, J. E., Simmet, T., Debatin, K. M. & Fulda, S. 2008. Targeting XIAP bypasses Bcl-2-mediated resistance to TRAIL and cooperates with TRAIL to suppress pancreatic cancer growth in vitro and in vivo. *Cancer Res*, 68, 7956-65.
- Wade, E. M., Daniel, P. B., Jenkins, Z. A., McInerney-Leo, A., Leo, P., Morgan, T., Addor, M. C., Ades, L. C., Bertola, D., Bohring, A., Carter, E., Cho, T. J., Duba, H. C., Fletcher, E., Kim, C. A., Krakow, D., Morava, E., Neuhann, T., Superti-Furga, A., Veenstra-Knol, I., Wieczorek, D., Wilson, L. C., Hennekam, R. C., Sutherland-Smith, A. J., Strom, T. M., Wilkie, A. O., Brown, M. A., Duncan, E. L., Markie, D. M. & Robertson, S. P. 2016. Mutations in MAP3K7 that Alter the Activity of the TAK1 Signaling Complex Cause Frontometaphyseal Dysplasia. *Am J Hum Genet*, 99, 392-406.
- Wang, Y. 2002. Role and Gonadotrophic Regulation of X-Linked Inhibitor of Apoptosis Protein Expression During Rat Ovarian Follicular Development In Vitro. *Biology of Reproduction*, 68, 610-619.
- Warburg, O., Wind, F. & Negelein, E. 1927. The Metabolism of Tumors in the Body. *J Gen Physiol*, 8, 519-30.
- Westfall, P. H. & Young, S. S. 1993. *Resampling-Based Multiple Testing: Examples and Methods for P-value Adjustment*, New York, Wiley.
- Westwick, J. K., Schwamborn, K. & Mercurio, F. 2009. NF-kB: a key integrator of cell signaling *Handbook of Cell Signaling*. 2nd ed.: Elsevier Inc.
- Wong, R. S. Y. 2011. Apoptosis in cancer: from pathogenesis to treatment. *J Exp Clin Cancer Res*, 30, 14.
- Wu, G., Chai, J., Suber, T. L., Wu, J. W., Du, C., Wang, X. & Shi, Y. 2000. Structural basis of IAP recognition by Smac/DIABLO. *Nature*, 408, 1008-12.
- Yan, X. Y., Zhang, Y., Zhang, J. J., Zhang, L. C., Liu, Y. N., Wu, Y., Xue, Y. N., Lu, S. Y., Su, J. & Sun, L. K. 2017. p62/SQSTM1 as an oncotarget mediates cisplatin resistance through activating RIP1-NF-kappaB pathway in human ovarian cancer cells. *Cancer Sci*, 108, 1405-1413.

- Yang, F., Nam, S., Brown, C. E., Zhao, R., Starr, R., Ma, Y., Xie, J., Horne, D. A., Malkas, L. H., Jove, R. & Hickey, R. J. 2014. A novel berbamine derivative inhibits cell viability and induces apoptosis in cancer stem-like cells of human glioblastoma, via up-regulation of miRNA-4284 and JNK/AP-1 signaling. *PLoS One*, 9, e94443.
- Yang, X. H., Feng, Z. E., Yan, M., Hanada, S., Zuo, H., Yang, C. Z., Han, Z. G., Guo, W., Chen, W. T. & Zhang, P. 2012. XIAP is a predictor of cisplatin-based chemotherapy response and prognosis for patients with advanced head and neck cancer. *PLoS One*, 7, e31601.
- Yao-Borengasser, A., Rassouli, N., Varma, V., Bodles, A. M., Rasouli, N., Unal, R., Phanavanh, B., Ranganathan, G., McGehee, R. E., Jr. & Kern, P. A. 2008. Stearoyl-coenzyme A desaturase 1 gene expression increases after pioglitazone treatment and is associated with peroxisomal proliferator-activated receptor-gamma responsiveness. *J Clin Endocrinol Metab*, 93, 4431-9.
- Zerbini, L. F., Wang, Y., Cho, J. Y. & Libermann, T. A. 2003. Constitutive activation of nuclear factor kappaB p50/p65 and Fra-1 and JunD is essential for deregulated interleukin 6 expression in prostate cancer. *Cancer Res*, 63, 2206-15.
- Zhang, H., Vollmer, M., De Geyter, M., Litzistorf, Y., Ladewig, A., Durrenberger, M., Guggenheim, R., Miny, P., Holzgreve, W. & De Geyter, C. 2000. Characterization of an immortalized human granulosa cell line (COV434). *Mol Hum Reprod*, 6, 146-53.
- Zhang, J., Macartney, T., Pegg, M. & Cohen, P. 2017a. Interleukin-1 and TRAF6-dependent activation of TAK1 in the absence of TAB2 and TAB3. *Biochem J*, 474, 2235-2248.
- Zhang, J., Nuebel, E., Wisidagama, D. R., Setoguchi, K., Hong, J. S., Van Horn, C. M., Imam, S. S., Vergnes, L., Malone, C. S., Koehler, C. M. & Teitell, M. A. 2012. Measuring energy metabolism in cultured cells, including human pluripotent stem cells and differentiated cells. *Nat Protoc*, 7, 1068-85.
- Zhang, Q., Lenardo, M. J. & Baltimore, D. 2017b. 30 Years of NF-kappaB: A Blossoming of Relevance to Human Pathobiology. *Cell*, 168, 37-57.
- Zhao, C., Zhao, Q., Zhang, C., Wang, G., Yao, Y., Huang, X., Zhan, F., Zhu, Y., Shi, J., Chen, J., Yan, F. & Zhang, Y. 2017. miR-15b-5p resensitizes colon cancer cells to 5-fluorouracil by promoting apoptosis via the NF-kappaB/XIAP axis. *Sci Rep*, 7, 4194.
- Zhou, P., Baumgarten, S. C., Wu, Y., Bennett, J., Winston, N., Hirshfeld-Cytron, J. & Stocco, C. 2013. IGF-I signaling is essential for FSH stimulation of AKT and steroidogenic genes in granulosa cells. *Mol Endocrinol*, 27, 511-23.
- Zuccotti, M., Merico, V., Cecconi, S., Redi, C. A. & Garagna, S. 2011. What does it take to make a developmentally competent mammalian egg? *Hum Reprod Update*, 17, 525-40.

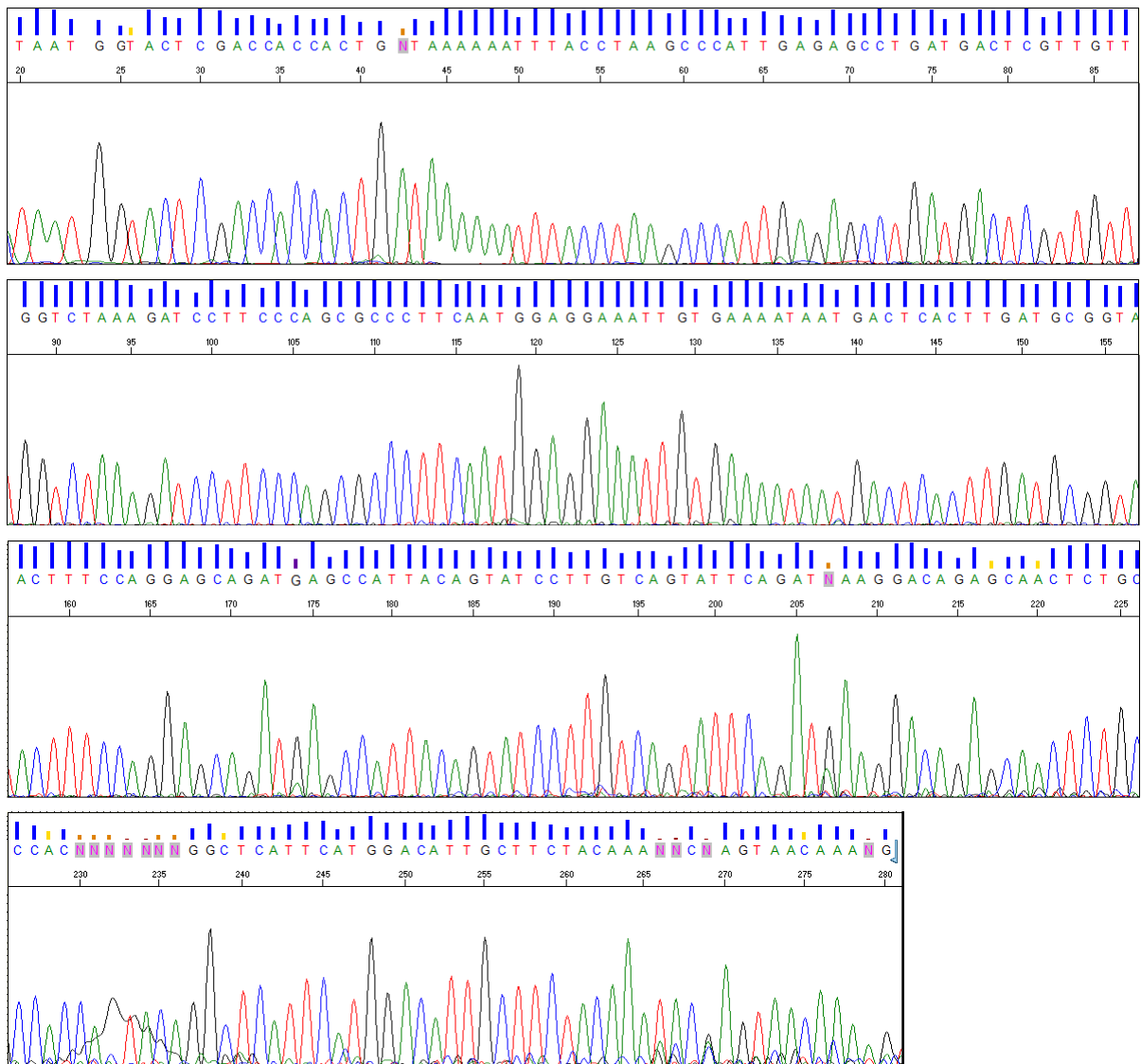
APPENDIX A

ELECTROPHEROGRAM OF TAK1 CODING SEQUENCE

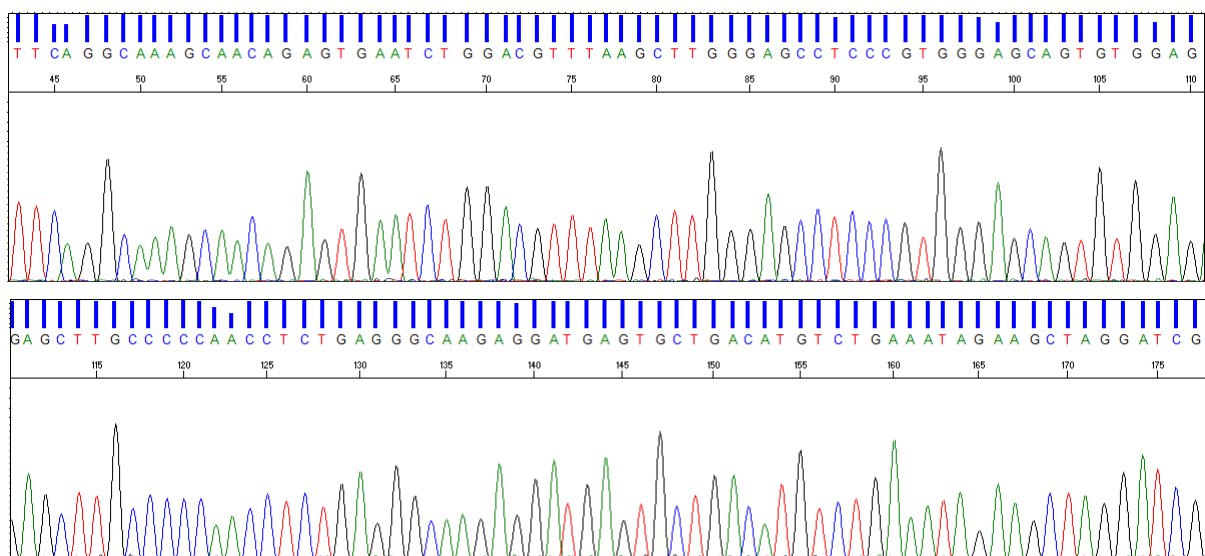
KGN TAK1 FWD 455-807

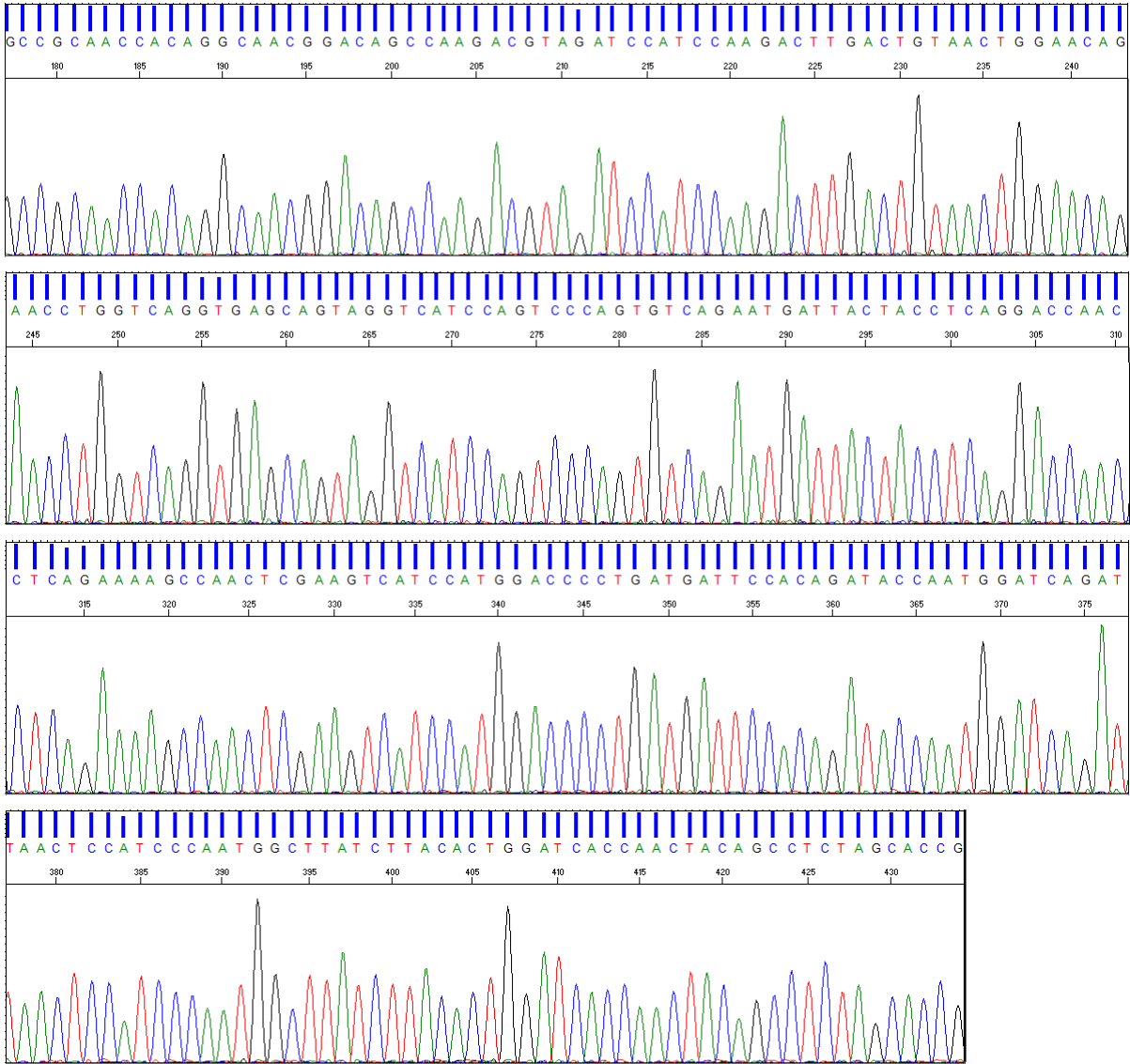


KGN TAK1 FWD 1150-1408

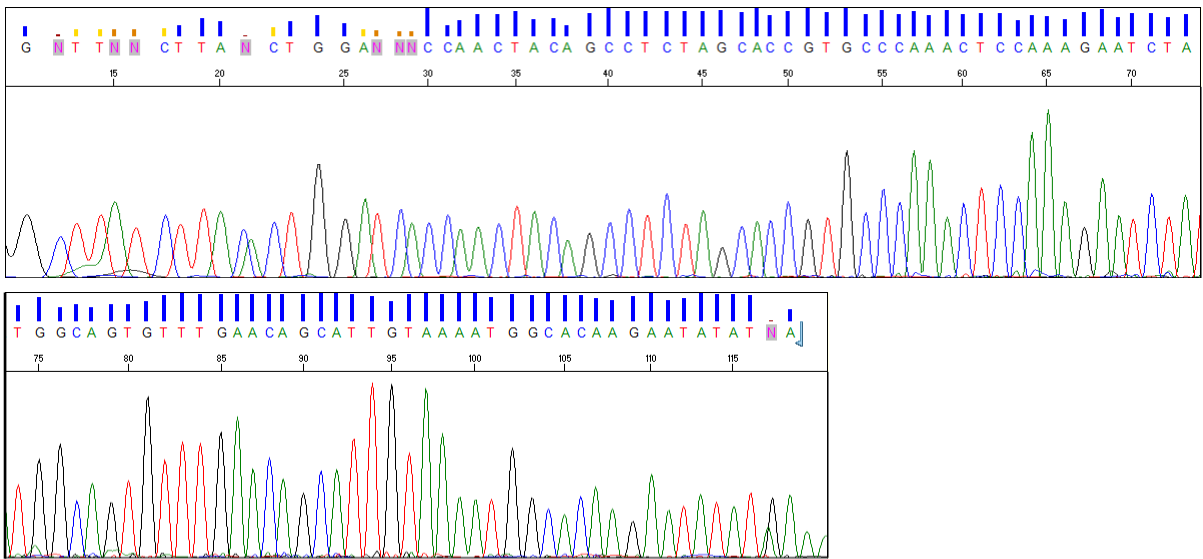


KGN TAK1 FWD 1483-1873

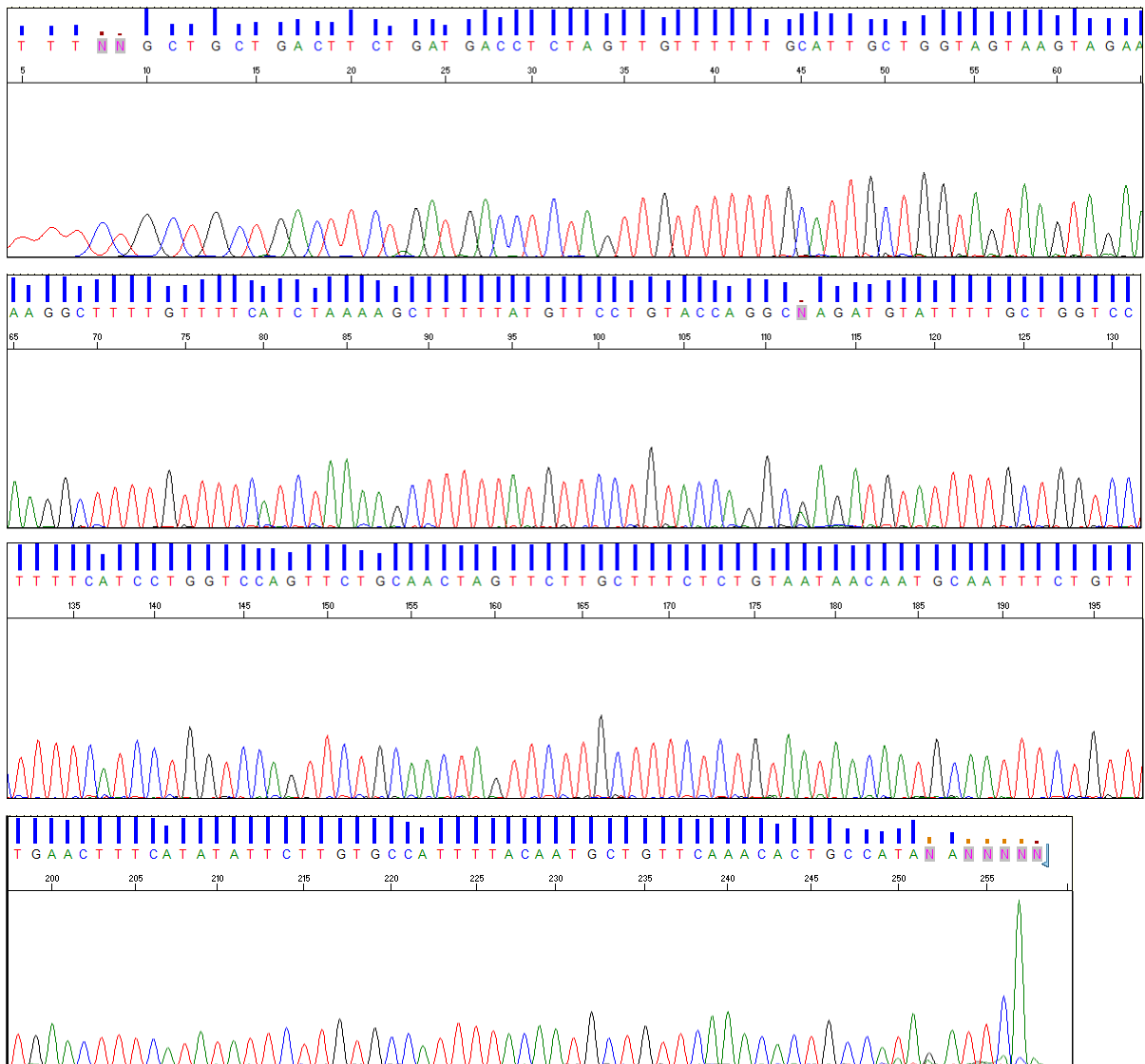




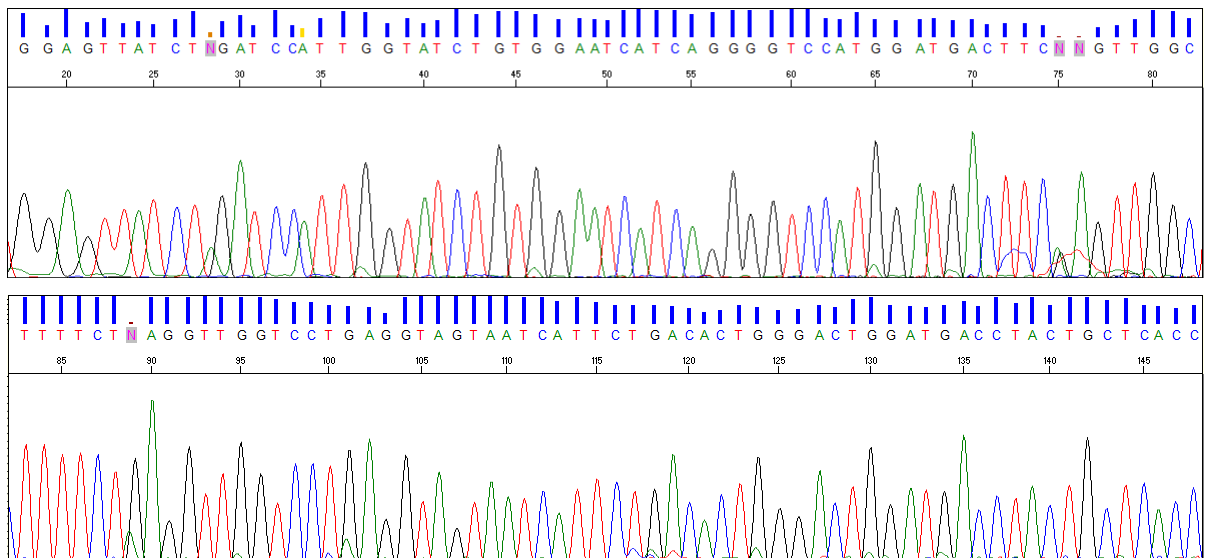
KGN TAK1 FWD 1832-1938

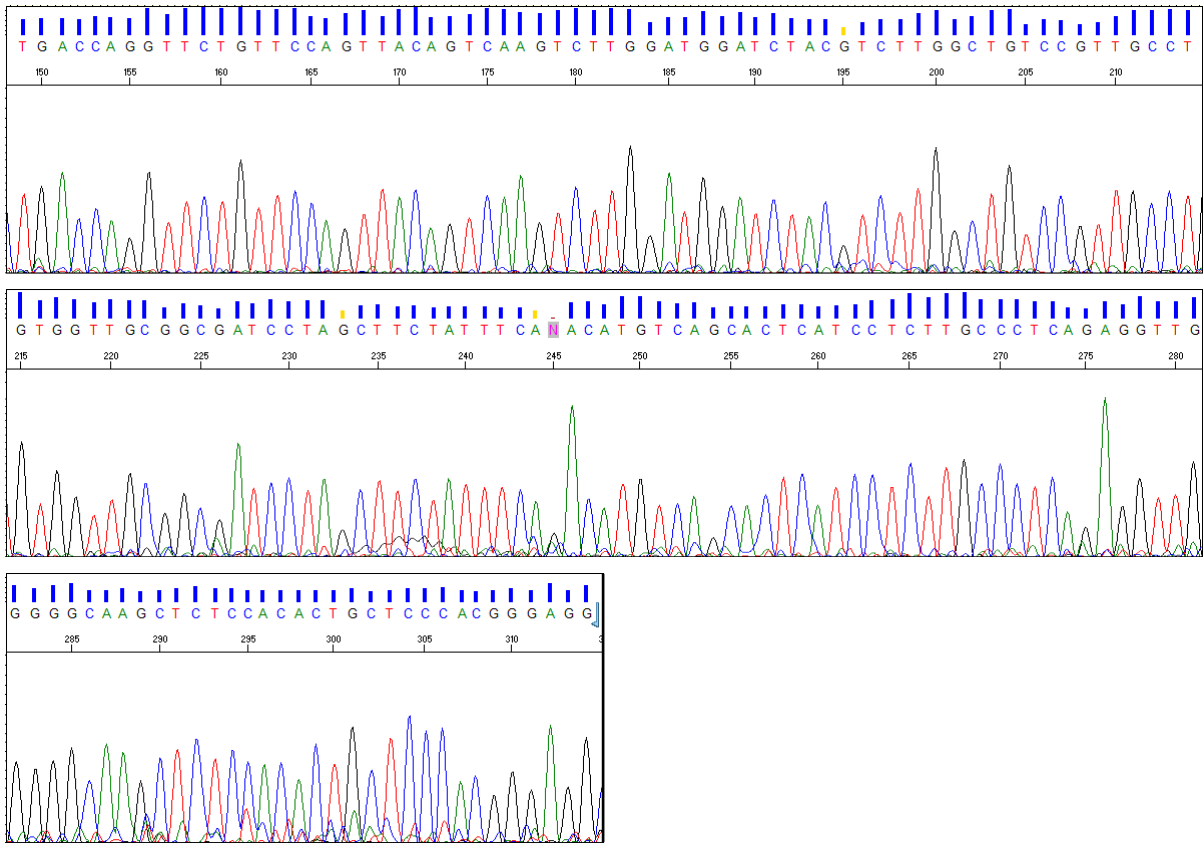


KGN TAK1 REV 2140-1889

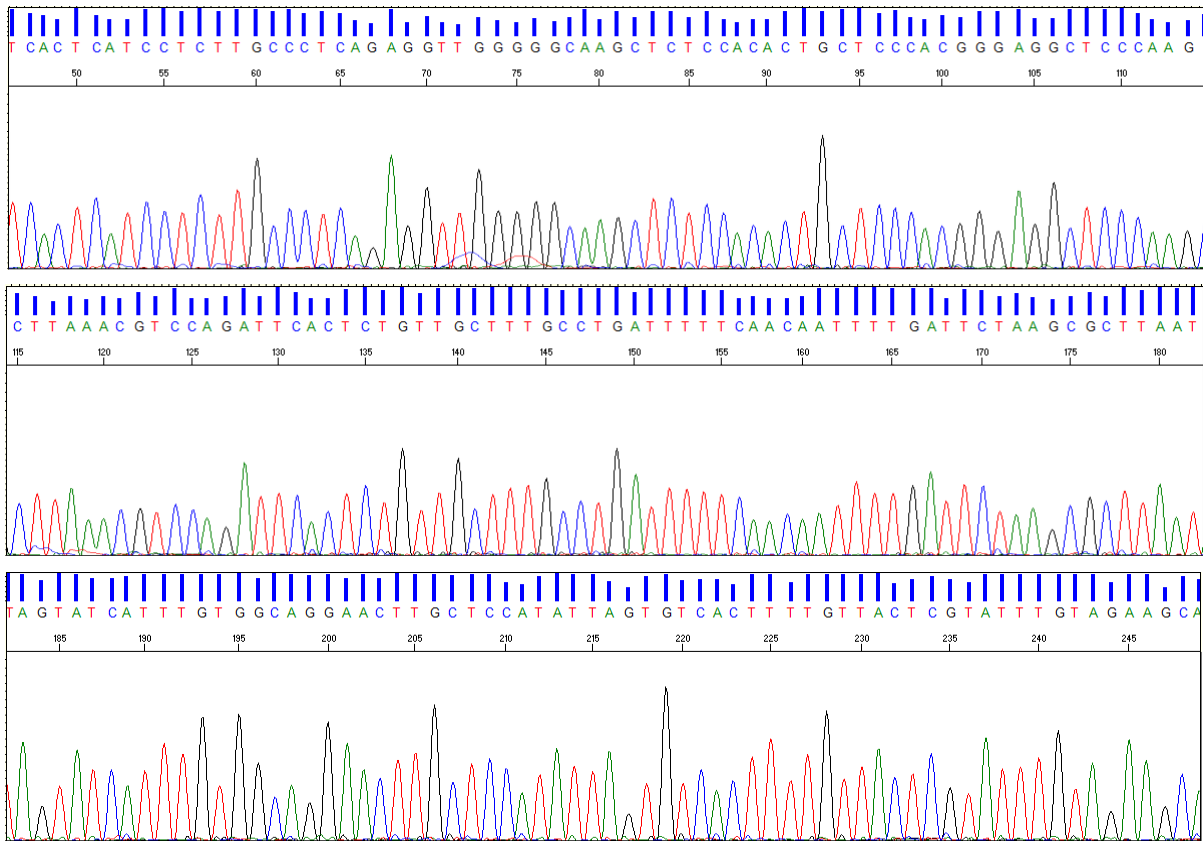


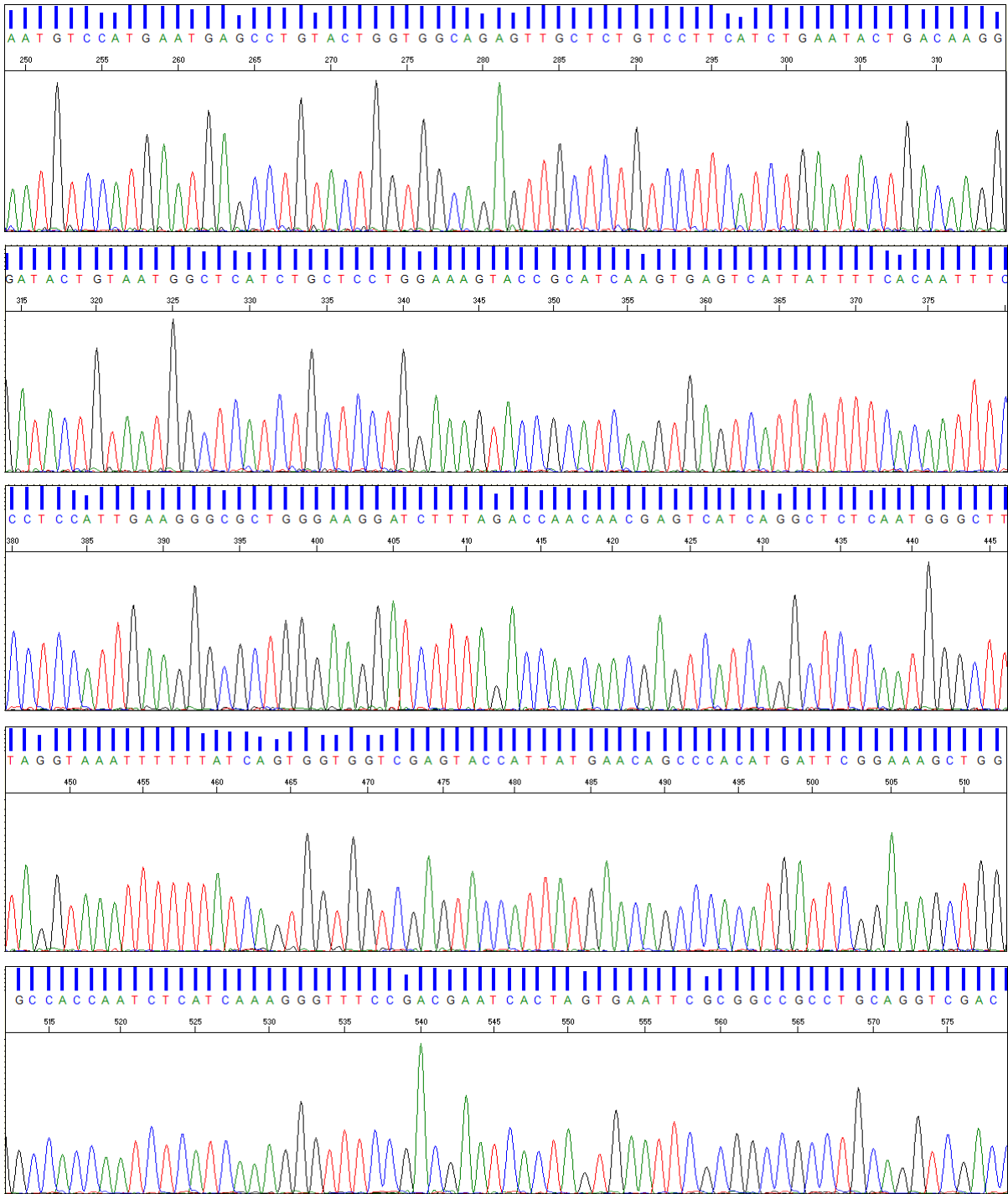
KGN TAK1 REV 1903-1527



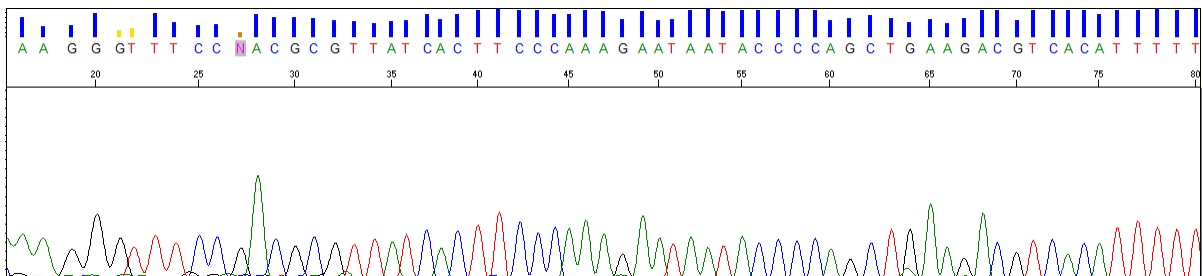


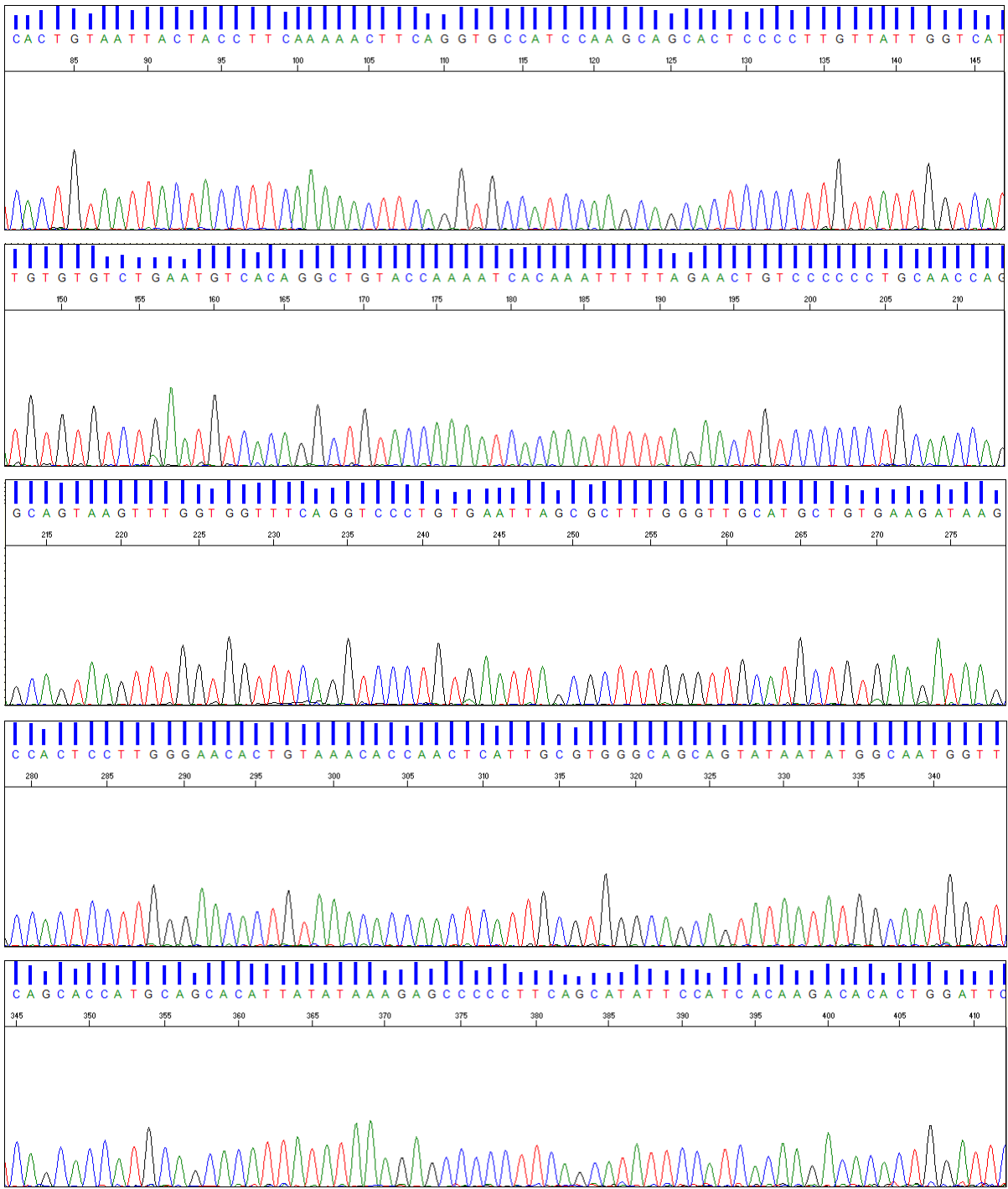
KGN TAK1 REV 1586-1091



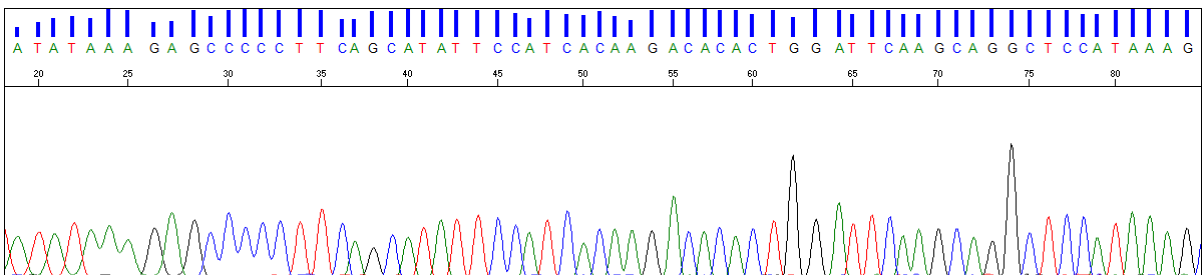


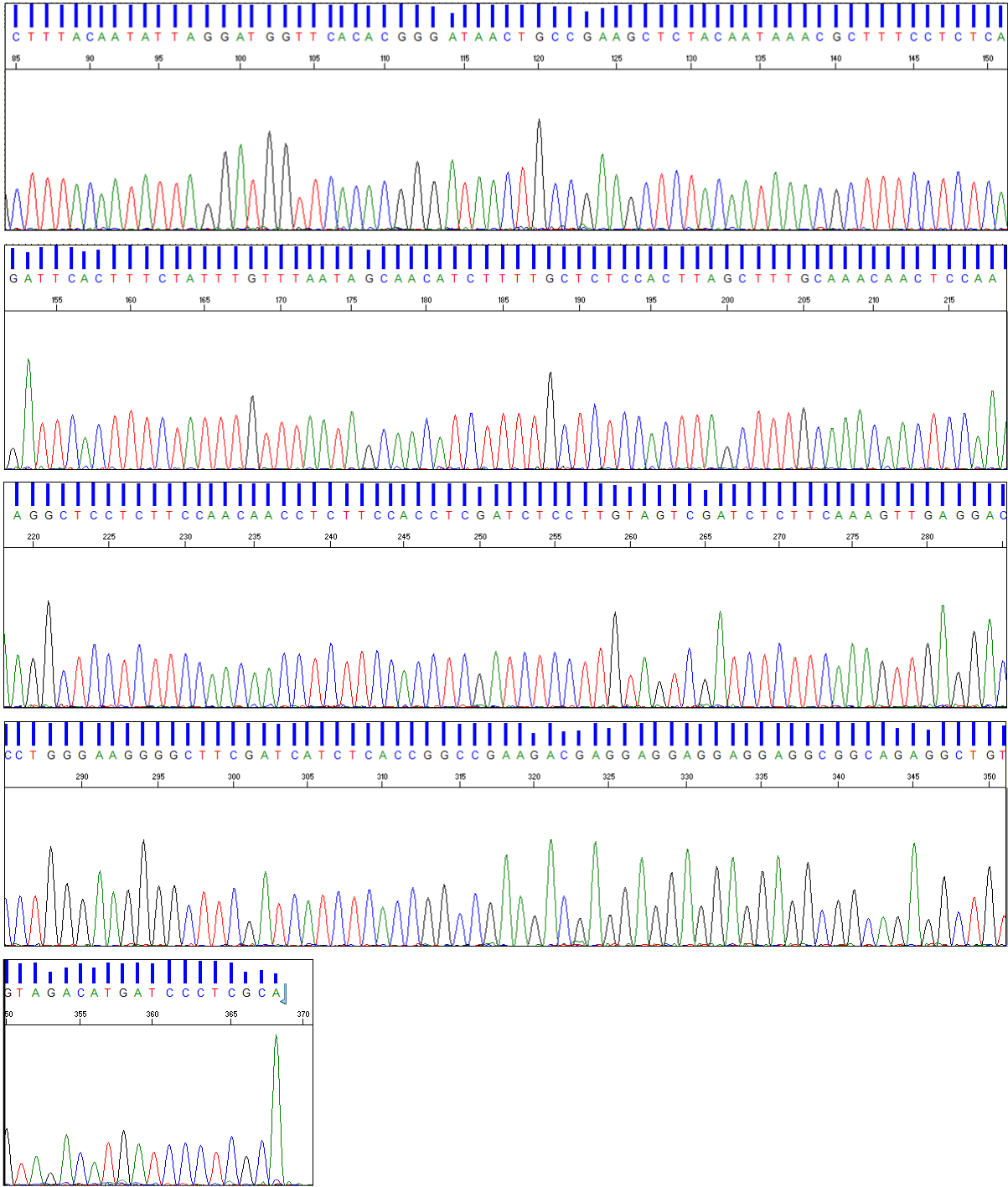
KGN TAK1 REV 1104-692





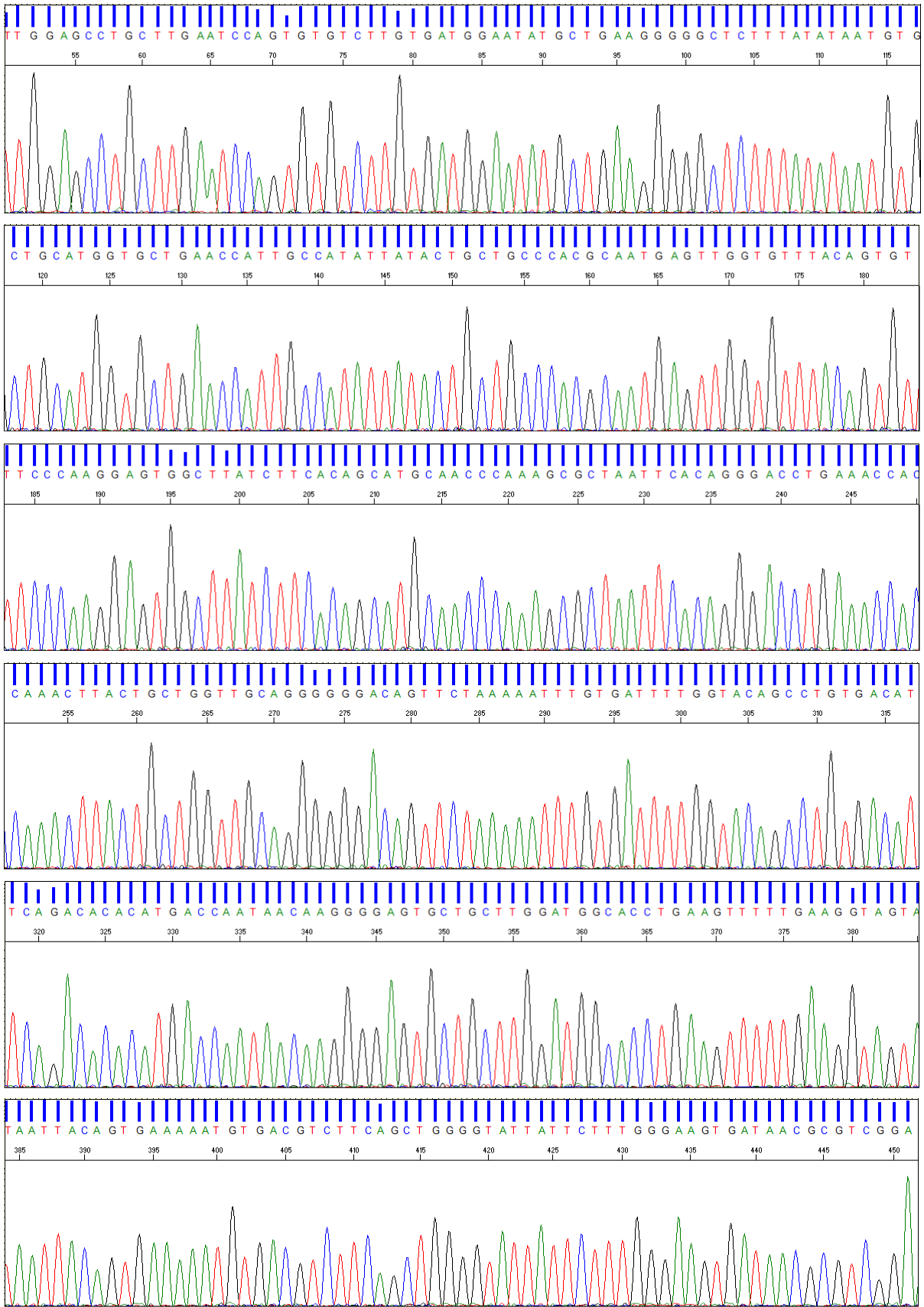
KGN TAK1 REV 757-409

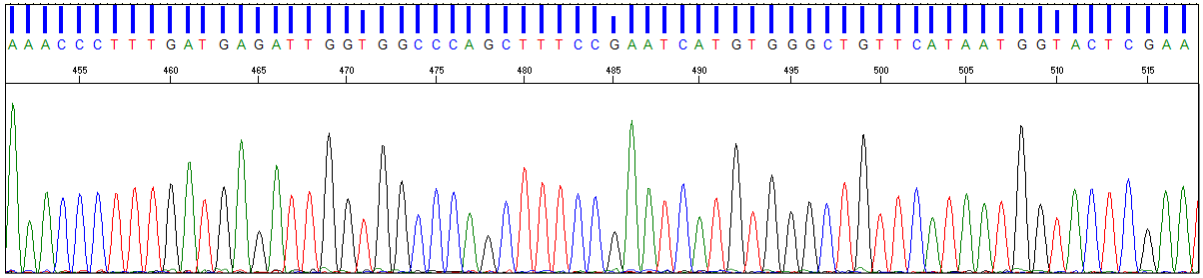




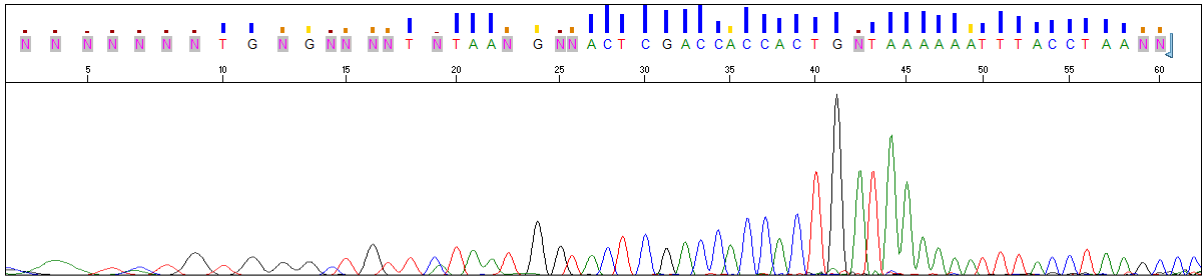
COV434 TAK1 FWD 409-802



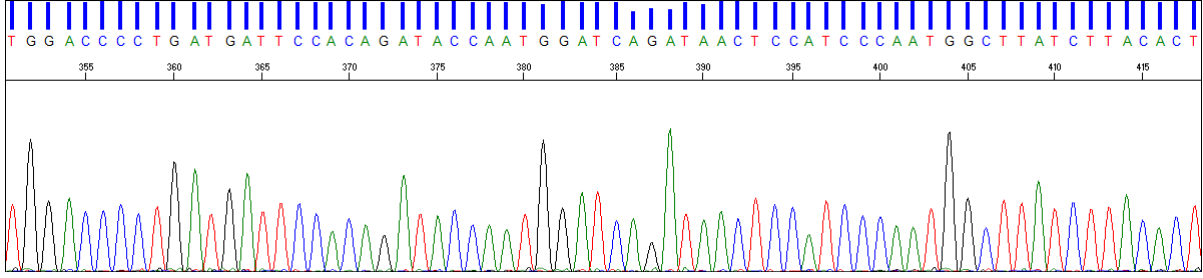
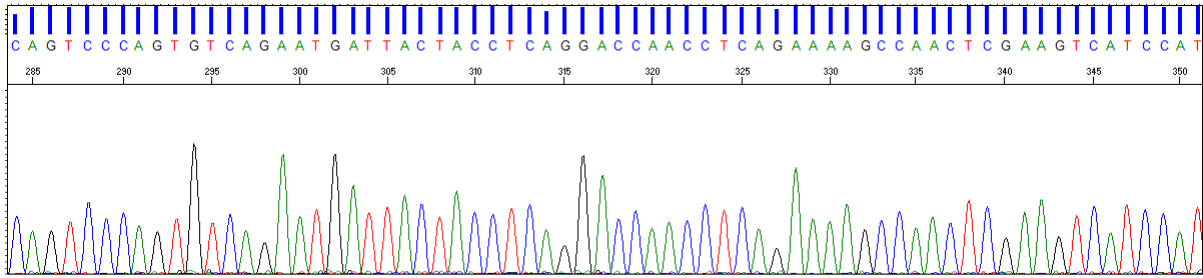
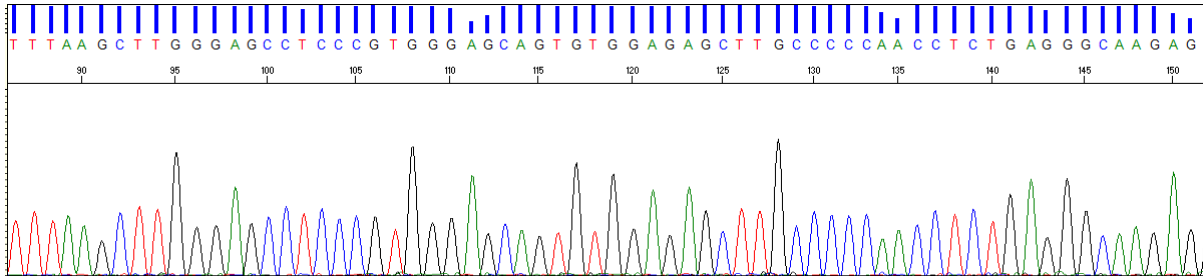
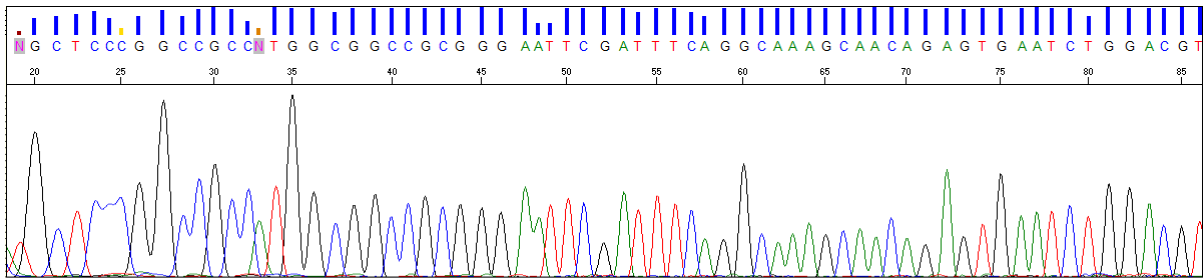




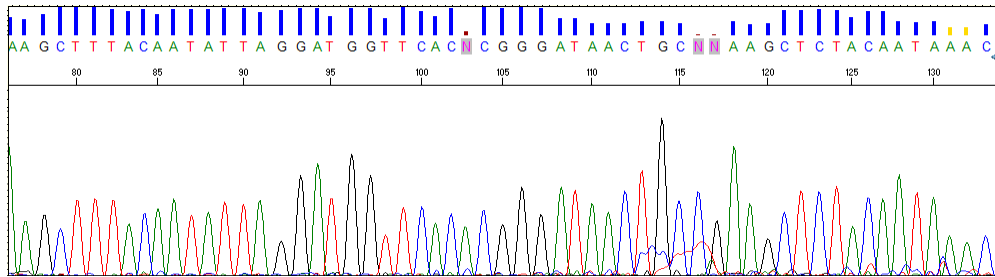
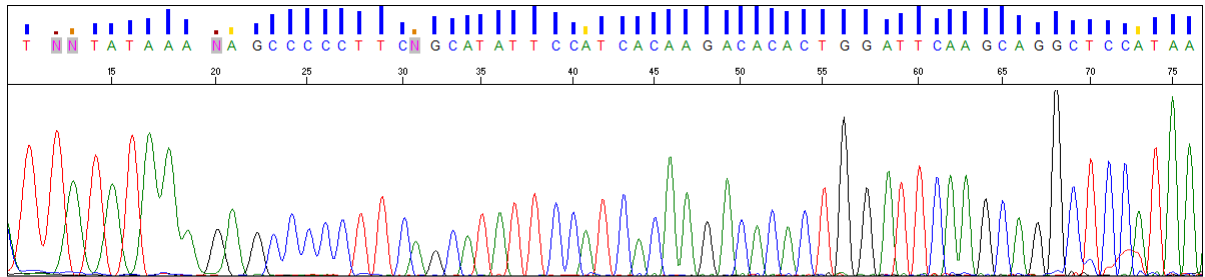
COV434 TAK1 FWD 1192-1139



COV434 TAK1 FWD 1483-1873



COV434 TAK1 REV 758-637



APPENDIX B
PUBLICATIONS



Signalling networks in focus

Impact of FOXL2 mutations on signaling in ovarian granulosa cell tumors

Dilys T.H. Leung^{a,b}, Peter J. Fuller^a, Simon Chu^{a,*}^a Hudson Institute of Medical Research, 27-31 Wright Street, Clayton, VIC 3168, Australia^b Department of Biochemistry and Molecular Biology, Faculty of Medicine, Nursing and Health Sciences, Monash University, Bldg. 77, 23 Innovation Walk, Clayton, VIC 3168, Australia

ARTICLE INFO

Article history:

Received 6 November 2015

Received in revised form 8 January 2016

Accepted 8 January 2016

Available online 11 January 2016

Keywords:

FOXL2

Ovary

Ovarian cancer

Granulosa cell tumor

ABSTRACT

Granulosa cell tumors (GCT) are unique sex-cord stromal tumors which account for ~8% of all ovarian malignancies. They exhibit morphological, biochemical and hormonal features similar to proliferating granulosa cells of the preovulatory follicle, including estrogen and inhibin synthesis. A somatic missense mutation in the forkhead box L2 (FOXL2) gene (C134W) is unique to adult GCT, and absent in other ovarian cancers. FOXL2 is a transcription factor that plays a critical role in ovarian function, in particular, proliferation and differentiation of granulosa cells. The molecular mechanisms underlying the pathogenicity of the mutant FOXL2 remain unresolved. Here we review the molecular alterations known to be associated with mutant FOXL2 and the potential signaling implications. Several studies suggest that dysregulated FOXL2 function may alter cell cycle progression and apoptosis. Further insights into the molecular mechanism of GCT pathophysiology may identify therapeutic targets for the treatment of these tumors.

© 2016 Elsevier Ltd. All rights reserved.

1. Introduction

Forkhead box (FOX) proteins are a family of evolutionarily conserved transcription factors. The characteristic, highly conserved 80–100 amino acid DNA binding domain, known as the ‘forkhead’ domain, binds to a consensus DNA sequence to regulate transcription. It was first described in *Drosophila* in 1990 and since then more than 170 FOX genes have been identified in 14 species, including 50 in the human genome. The FOX genes are categorized into 19 subfamilies, from FOXA to FOXS, based on the degree of sequence conservation (Jackson et al., 2010). Their modes of action as pioneer factors, transcription factors, or both, are quite diverse. They participate in a wide spectrum of physiological processes including development, stem cell differentiation, metabolism and immunity. This review focuses on the forkhead box protein L2 (FOXL2), a critical transcription factor in sex determination. FOXL2 is expressed in the ovary (Schmidt et al., 2004), endometrium (Governini et al., 2014), pituitary (Schmidt et al., 2004) and the developing eyelid (Crisponi et al., 2001). In addition to the forkhead domain, FOXL2 contains an alanine/proline-rich domain in the C-terminus which is responsible for transcriptional regulation (Crisponi et al., 2001).

Here we review the function of FOXL2 in ovarian development and the molecular alterations associated with mutant FOXL2 in a subset of ovarian cancer, the granulosa cell tumors (GCT). The adult form of GCT is characterized by a somatic missense mutation in the FOXL2 gene which has been shown to potentially impact FOXL2 signaling.

2. Functions, cascades and key molecules

2.1. FOXL2 in sex determination and early ovarian development

FOXL2 is the earliest marker of ovarian development. In mice, it is detected from 12.5 days post-coitum, and its expression is sustained in the granulosa cells (GC) and stromal cells of ovarian follicles throughout female reproductive life (Schmidt et al., 2004). The sexually dimorphic pattern of gene expression of FOXL2 in the ovaries, or SRY and SOX9 in the testes, determines the fate of the bi-potential gonad in development. The importance of FOXL2 expression extends beyond this initial sex determination stage. It is required to maintain the ovarian phenotype. Ablation of FOXL2 alone in sexually mature female mice leads to structural changes suggesting sex-reversal, including oocyte degeneration and the occurrence of cells morphologically similar to Sertoli cells (Uhlenhaut et al., 2009) (Fig. 1). In addition, SOX9 expression and other Sertoli cell markers were markedly increased.

In the postnatal ovary, FOXL2 regulates GC differentiation and supports follicular growth. In FOXL2^{-/-} mice, GC failed to complete

* Corresponding author.

E-mail addresses: dilys.leung@hudson.org.au (D.T.H. Leung), peter.fuller@hudson.org.au (P.J. Fuller), simon.chu@hudson.org.au (S. Chu).

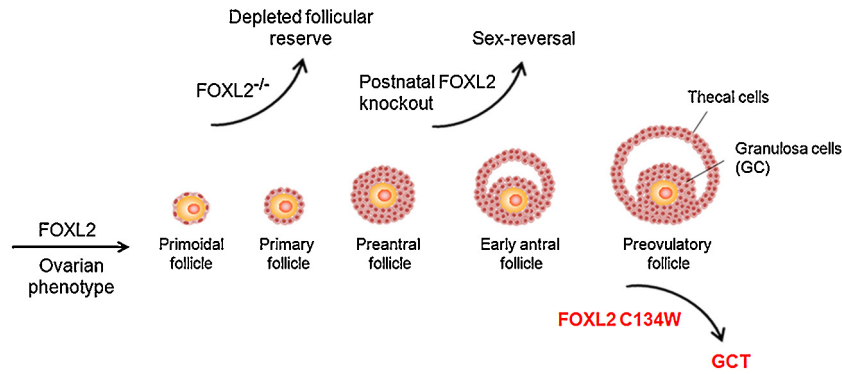


Fig. 1. Roles of FOXL2 in ovarian biology. Expression of FOXL2 is required to drive ovarian development and maintain ovarian phenotype. In the postnatal ovary, FOXL2 regulates differentiation of squamous to cuboidal GC and support follicular growth. In $FOXL2^{-/-}$ mice, lack of cuboidal GC blocks follicular growth, oocytes undergo atresia and follicular reserve is depleted. In postnatal female mice, ablation of FOXL2 alone is sufficient to induce sex-reversal phenotypes. The $FOXL2^{C134W}$ mutation is unique to aGCT and is arguably pathognomonic for these cancers.

the squamous-to-cuboidal transition which represents as a gateway to GC proliferation (Schmidt et al., 2004) (Fig. 1). Without the support of cuboidal GC, follicular growth was blocked. Atresia was observed in most of the oocytes, with no maturation into secondary follicles.

2.2. FOXL2 in the hypothalamic–pituitary–gonadal axis

The hypothalamic–pituitary–gonadal axis is a critical pathway in development and reproduction. Major components include gonadotropin-releasing hormone (GnRH) which is secreted by the hypothalamus, luteinizing hormone (LH) and follicle-stimulating hormone (FSH) that are produced by the anterior pituitary upon GnRH stimulation. The regulation of FSH production is multifactorial. In particular, FOXL2 and the homolog of *Drosophila* Small Mothers Against Decapentaplegic 3 (SMAD3) synergistically induce transcription of the *FSH β* gene in response to the transforming growth factor (TGF)- β superfamily member, activin (Roybal et al., 2014). Transcriptional regulation of *FSH β* requires physical interaction of both transcription factors. In line with this process, FOXL2 expression has been described in the adult mouse pituitary, where

it co-localizes with FSH in the gonadotropes and thyrotropes. Activin induces the phosphorylation of SMAD3, which then translocates to the nucleus to stimulate transcription of *FSH β* , which is rate-limiting for the formation of the dimeric biologically active FSH molecule. The FOXL2-SMAD3-activin-induced FSH promotes GC differentiation, induces LH receptors and stimulates aromatization; all of which are essential to foster follicular development.

SMAD3 is also essential in FOXL2-induced follistatin transcription in GC (Nonis et al., 2013) (Fig. 2). The FOXL2-SMAD3 complex acts in synergy with growth differentiation factor-9 (GDF-9) to increase follistatin transcription. Follistatin is predominantly expressed in the ovary, especially GC of the developing follicles. It binds to activin to attenuate activin-induced GC proliferation (Cheng et al., 2014).

3. FOXL2 as determinant of folliculogenesis

Overexpression of FOXL2 induces apoptosis in normal rat GC, an essential mechanism in folliculogenesis. The anti-proliferative function of FOXL2 involves the regulation of activin and follistatin in TGF- β signaling. It does so by promoting cleavage of

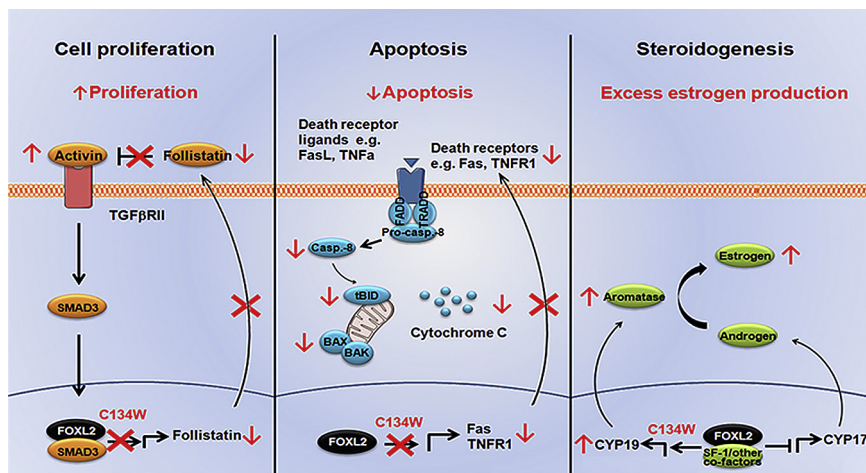


Fig. 2. FOXL2 in cell proliferation, apoptosis and steroidogenesis. FOXL2 is a transcription factor that plays a critical role in ovarian function, in particular, proliferation, apoptosis and steroidogenesis. The potential impact of the $FOXL2^{C134W}$ mutation is indicated in red. The FOXL2-SMAD3 complex stimulates follistatin gene transcription, and subsequently modulates activin-induced proliferation. Mutant $FOXL2^{C134W}$ suppresses follistatin gene transcription and subsequently reduces the inhibitory effect of follistatin on activin, leading to an increase in activin-induced proliferation. The anti-proliferative function of FOXL2 involves the transcriptional regulation of death receptors e.g. Fas and TNFR1. Cells expressing $FOXL2^{C134W}$ showed reduced transcription of death receptors, diminished activation of caspases, BID, BAX, BAK and cytochrome C production and as a result, a decrease in apoptosis. In steroidogenesis, the FOXL2-SF-1 complex regulates *CYP17* and *CYP19* gene transcription. FOXL2-SF-1-regulated *CYP19* and *CYP17* gene transcription is disrupted by the $C134W$ mutation. *CYP19* transcription is upregulated while repression of *CYP17* transcription is lost. These events increase aromatization and consequently, excess estrogen production.

caspace-8, followed by a cascade of BID cleavage and translocation, BAK and/or BAX oligomerization and subsequently, cytochrome C release which elicits apoptosis via activation of caspace-9 (Kim et al., 2011) (Fig. 2). Additionally, FOXL2 induces transcription of p21 to increase apoptosis (Kim et al., 2014).

3.1. FOXL2 in steroidogenesis

FOXL2 transcriptionally represses the steroidogenic acute regulatory protein (StAR). In the ovary, StAR is predominantly localized in the thecal layer. It is a marker of GC differentiation and its expression in human GC is confined to that of the preovulatory follicles (Pollack et al., 1997). The human StAR contains multiple forkhead-responsive consensus sites for FOXL2 binding. Cotransfection studies have revealed that the alanine/proline-rich C-terminus of FOXL2 binds to and suppresses the promoter activity of StAR (Pisarska et al., 2004). In support of these findings, reciprocal expression of StAR and FOXL2 was noted during follicular development.

It has been reported in human and rat GC that FOXL2 binds to the DNA-binding domain of steroidogenic factor-1 (SF-1) to negatively regulate the transcriptional activity of SF-1, and inhibit SF-1-induced CYP17 transcription (Park et al., 2010) (Fig. 2). CYP17 is the key steroidogenic enzyme involved in androgen production. Conversely, the FOXL2-SF-1 complex mediates CYP19 transcription (P450 aromatase) to regulate androgen to estrogen conversion (Uhlenhaut et al., 2009). The development of ovarian follicles depends on the sequential effects of the gonadotropins in conjunction with normal steroidogenesis.

3.2. Regulation of FOXL2 by post-translational modifications

FOXL2 activity is modulated by post-translational modifications such as SUMOylation, phosphorylation and ubiquitylation. UBC-9-induced SUMO conjugation of FOXL2 inhibits ubiquitylation causing protein stabilization (Kim et al., 2014). Phosphorylation at serine 33 by GSK3 β diminishes FOXL2 activity, inducing MDM2-mediated ubiquitylation. Alternatively, phosphorylation by the serine/threonine kinase LATS1 at a serine residue stimulates FOXL2 transcription activity (Pisarska et al., 2010).

4. Associated pathologies and therapeutic implications

4.1. Blepharophimosis–Ptosis–Epicanthus inversus syndrome (BPES)

As aforementioned, FOXL2 is expressed in the developing eyelid. Mutations in FOXL2 lead to a rare condition, BPES, which may be autosomal dominant and sporadic. The mutation usually involves expansion of the polyalanine domain, creating a premature stop codon or frameshift, resulting in a truncated protein. This germline loss-of-function mutation leads to eyelid and craniofacial malformation, with (BPES type I) or without (BPES type II) premature ovarian insufficiency (Crisponi et al., 2001).

4.2. Ovarian granulosa cell tumors (GCT)

Consistent with its role in ovarian development, dysregulated FOXL2 expression has been associated with tumorigenesis of the ovary, in particular, adult GCT (aGCT). GCT are ovarian sex-cord stromal tumors which make up approximately 8% of all ovarian cancers (Jamieson and Fuller, 2012). The landmark study by Shah et al. identified a single somatic missense mutation in the FOXL2 gene in 4 aGCT using whole-transcriptome paired-end RNA sequencing (Shah et al., 2009). This mutation results in a single amino acid substitution of tryptophan for cysteine at position 134 (C134W).

Our laboratory and other groups have consistently reported a high prevalence (90–97%) of this FOXL2^{C134W} mutation in aGCT (Shah et al., 2009; Kobel et al., 2009; Jamieson et al., 2010). The mutation is not observed in the rarer juvenile subtype which has either low or absent FOXL2 protein expression (Jamieson and Fuller, 2012), nor in other ovarian cancers including the more common epithelial ovarian cancers or stromal-derived ovarian tumors. Although the molecular consequences of this mutation are still unclear, it is regarded as a specific marker for differential diagnosis for sex cord-stromal tumors and is indeed arguably pathognomonic for aGCT (Jamieson and Fuller, 2012; Shah et al., 2009; Kobel et al., 2009).

aGCT exhibit a molecular profile similar to FSH-primed proliferating GC of the preovulatory follicle, including expression of functional FSH receptors (Chu et al., 2002; Fuller et al., 1998) with FSH binding (Graves et al., 1985) and synthesis of estrogen (Amsterdam and Selvaraj, 1997). However, little is known about the mechanism by which the FOXL2^{C134W} mutation drives tumorigenesis. The molecular switches that trigger the progression from a Stage I to advanced aggressive disease also remain unresolved. Studies of GCT have been aided by two human GCT-derived cell lines, KGN (Nishi et al., 2001) and COV434 (van Den Berg-Bakker et al., 1993). KGN cells, like aGCT, are heterozygous for the FOXL2^{C134W} mutation and show abundant FOXL2 expression. In contrast, COV434 cells resemble juvenile GCT being wildtype for FOXL2, with no detectable FOXL2 expression (Jamieson and Fuller, 2012). Unlike the FOXL2 mutants associated with BPES where protein mislocalization or aggregation is often observed, the FOXL2^{C134W} mutant remains nuclear and fully diffusible, demonstrating no signs of perturbation in reaching its target promoters (Benayoun et al., 2010).

In both KGN and COV434 cells, the transcriptional repression of FOXL2 on the StAR promoter is lost (Fleming et al., 2010). In addition, KGN cells with FOXL2^{C134W} showed increased stimulation of CYP19/aromatase (Fig. 2). Fleming et al. postulated that FOXL2^{C134W} likely binds to putative forkhead elements in the aromatase promoter, recruiting as yet unknown cofactors to stimulate aromatase production (Fleming et al., 2010). Alteration in steroidogenesis as a result of the mutation may contribute to the pathogenesis of these tumors.

Hallmarks of cancer such as heightened proliferation and abated apoptotic activity have been associated with the FOXL2^{C134W} mutation. Anttonen et al. reported that GATA4 attenuates the pro-apoptotic effect of overexpression of FOXL2^{WT} in KGN cells, an effect not observed when FOXL2^{C134W} is overexpressed (Anttonen et al., 2014). Unlike FOXL2^{WT} overexpression, FOXL2^{C134W} overexpression has little effect on inducing caspase-3/7 activity. FOXL2^{C134W} also suppresses GDF-9-induced follistatin gene transcription (Nonis et al., 2013). As a consequence of FOXL2-stimulated follistatin production, KGN cells overexpressing FOXL2^{C134W} but not FOXL2^{WT} demonstrated an upregulation of activin-induced cell proliferation. This observation mimicked the pro-proliferative effects of activin treated KGN cells (Cheng et al., 2014). The same group has also reported that FOXL2^{WT} ectopically expressed in KGN could modulate GnRH-induced apoptosis by increasing GnRH receptor (GnRHR) protein and mRNA expression (Cheng et al., 2013). This increased expression coincides with increased caspase-3 levels and reduced cell viability. The effect was abolished with GnRHR knock down, consolidating its involvement in the apoptotic process. Caution should be taken when interpreting these findings, as endogenous FOXL2^{C134W} is still present. Benayoun et al. reported increased transactivation capability of FOXL2^{C134W} on luciferase reporters containing the GnRHR activating sequence or FOXL2 promoter sequence in KGN cells (Benayoun et al., 2010). Although the authors did allude to the assumption that the endogenous FOXL2^{C134W} should be outweighed by the overexpression of

FOXL2 variants, the findings from the luciferase assays were by in large unremarkable.

The relationship between FOXL2^{C134W} and the unique genetic profile of aGCT has been explored using transcriptome analysis (Benayoun et al., 2013). Echoing the high prevalence of FOXL2^{C134W} in aGCT, 960 known FOXL2 target genes were found to be differentially expressed across 10 human aGCT samples versus 2 GC controls derived from an IVF program. Functional annotation revealed that 377 downregulated FOXL2 target genes were significantly enriched for gene ontology (GO) terms associated with apoptosis and cell cycle arrest. Conversely, 583 upregulated FOXL2 target genes were associated with GO terms linked to proliferation. It is important to note that the GC controls were exposed to FSH stimulation as part of IVF protocol, which likely impacts on their gene expression patterns.

A retrospective study using archival GCT tissues reported no significant correlation between the FOXL2 mutation status and clinicopathological variables including tumor size and disease stage in 26 patients (Rosario et al., 2013). However, patients hemizygous/homozygous for the FOXL2 mutation had significantly higher relapse rates.

A better understanding of the tumorigenic properties of the FOXL2^{C134W} mutation will help identify specific therapeutic strategies for aGCT. To date, whilst surgical resection is the standard management for early-stage diseases, optimal treatment has yet to be established for advanced or recurrent aGCT. Non-surgical treatment regimens include the traditional platinum-based chemotherapies and hormonal therapies developed for treating epithelial ovarian cancer show limited efficacy (Jamieson and Fuller, 2012). Without effective treatment beyond surgery, approximately 80% of patients with aggressive or recurrent aGCT succumb to the disease, indicating a need to develop a more targeted therapy for this cancer. Despite the fundamental role of the FOXL2^{C134W} mutation in the pathogenesis of aGCT, achieving specificity when targeting mutant FOXL2 may be a challenge given the high homology amongst the FOX family members (Jamieson and Fuller, 2012).

Many questions remain to be answered regarding the impact of this mutation on FOXL2 conformation/structure, its interaction partners and associated signaling pathways. Deciphering these aspects will likely yield potential therapeutic targets to treat aGCT.

5. Conclusion

In conclusion, the FOXL2^{C134W} mutation is present in virtually all aGCT and hence serves as a diagnostic marker. The mutation has been reported to alter steroidogenic and apoptotic process *in vitro* which may have implications in the progression of the disease. However, further insights into the function and molecular consequences of this mutation should allow the identification of targetable alterations in GCT.

Acknowledgements

We thank Dr Ann Drummond for critically reviewing this manuscript and Ms Sue Panckridge for assistance in preparing the figures.

This work is supported by grants-in-aid from the Cancer Council Victoria; S.C. is supported by the Ovarian Cancer Research Foundation, the Granulosa Cell Tumor of the Ovary Foundation and the National Health & Medical Research Council of Australia through a Project Grant (#1058334) and a Senior Principal Research Fellowship to P.J.F. (#1002559). The Hudson Institute is supported by the Victorian Government's Operational Infrastructure Scheme.

References

- Amsterdam, A., Selvaraj, N., 1997. Control of differentiation, transformation, and apoptosis in granulosa cells by oncogenes, oncoviruses, and tumor suppressor genes. *Endocr. Rev.* 18 (4), 435–461.
- Anttonen, M., et al., 2014. FOXL2, GATA4, and SMAD3 co-operatively modulate gene expression, cell viability and apoptosis in ovarian granulosa cell tumor cells. *PLoS ONE* 9 (1), pe85545.
- Benayoun, B.A., et al., 2010. Functional exploration of the adult ovarian granulosa cell tumor-associated somatic FOXL2 mutation p.Cys134Trp (c.402C>G). *PLoS ONE* 5 (1), pe8789.
- Benayoun, B.A., et al., 2013. Adult ovarian granulosa cell tumor transcriptomics: prevalence of FOXL2 target genes misregulation gives insights into the pathogenic mechanism of the p.Cys134Trp somatic mutation. *Oncogene* 32 (22), 2739–2746.
- Cheng, J.C., Klausen, C., Leung, P.C., 2013. Overexpression of wild-type but not C134W mutant FOXL2 enhances GnRH-induced cell apoptosis by increasing GnRH receptor expression in human granulosa cell tumors. *PLoS ONE* 8 (1), pe55099.
- Cheng, J.C., et al., 2014. FOXL2-induced follistatin attenuates activin A-stimulated cell proliferation in human granulosa cell tumors. *Biochem. Biophys. Res. Commun.* 443 (2), 537–542.
- Chu, S., et al., 2002. FSH-regulated gene expression profiles in ovarian tumours and normal ovaries. *Mol. Hum. Reprod.* 8 (5), p8.
- Crisponi, L., et al., 2001. The putative forkhead transcription factor FOXL2 is mutated in blepharophimosis/ptosis/epicanthus inversus syndrome. *Nat. Genet.* 27 (2), 159–166.
- Fleming, N.I., et al., 2010. Aromatase is a direct target of FOXL2: C134W in granulosa cell tumors via a single highly conserved binding site in the ovarian specific promoter. *PLoS ONE* 5 (12), pe14389.
- Fuller, P.J., et al., 1998. No evidence of a role for mutations or polymorphisms of the follicle-stimulating hormone receptor in ovarian granulosa cell tumors. *J. Clin. Endocrinol. Metab.* 83 (1), p6.
- Governini, L., et al., 2014. FOXL2 in human endometrium: hyperexpressed in endometriosis. *Reprod. Sci.* 21 (10), 1249–1255.
- Graves, P.E., et al., 1985. Adenylate cyclase in human ovarian cancers: sensitivity to gonadotropins and nonhormonal activators. *Am. J. Obstet. Gynecol.* 153 (8), 877–882.
- Jackson, B.C., et al., 2010. Update of human and mouse forkhead box (FOX) gene families. *Hum. Genomics* 4 (5), 345–352.
- Jamieson, S., Fuller, P.J., 2012. Molecular pathogenesis of granulosa cell tumors of the ovary. *Endocr. Rev.* 33 (1), p35.
- Jamieson, S., et al., 2010. The FOXL2 C134W mutation is characteristic of adult granulosa cell tumors of the ovary. *Mod. Pathol.* 23 (11), 1477–1485.
- Kim, J.H., et al., 2011. Differential apoptotic activities of wild-type FOXL2 and the adult-type granulosa cell tumor-associated mutant FOXL2 (C134W). *Oncogene* 30 (14), 1653–1663.
- Kim, J.H., et al., 2014. FOXL2 posttranslational modifications mediated by GSK3beta determine the growth of granulosa cell tumours. *Nat. Commun.* 5, p2936.
- Kobel, M., Gilks, C.B., Huntsman, D.G., 2009. Adult-type granulosa cell tumors and FOXL2 mutation. *Cancer Res.* 69 (24), 9160–9162.
- Nishi, Y., et al., 2001. Establishment and characterization of a steroidogenic human granulosa-like tumor cell line, KGN, that expresses functional follicle-stimulating hormone receptor. *Endocrinology* 142 (1), p9.
- Nonis, D., McTavish, K.J., Shimasaki, S., 2013. Essential but differential role of FOXL2 wt and FOXL2C134W in GDF-9 stimulation of follistatin transcription in co-operation with Smad3 in the human granulosa cell line COV434. *Mol. Cell. Endocrinol.* 372 (1–2), 42–48.
- Park, M., et al., 2010. FOXL2 interacts with steroidogenic factor-1 (SF-1) and represses SF-1-induced CYP17 transcription in granulosa cells. *Mol. Endocrinol.* 24 (5), 1024–1036.
- Pisarska, M.D., et al., 2004. Forkhead l2 is expressed in the ovary and represses the promoter activity of the steroidogenic acute regulatory gene. *Endocrinology* 145 (7), 3424–3433.
- Pisarska, M.D., et al., 2010. LATS1 phosphorylates forkhead l2 and regulates its transcriptional activity. *Am. J. Physiol. Endocrinol. Metab.* 299 (1), E101–E109.
- Pollack, S.E., et al., 1997. Localization of the steroidogenic acute regulatory protein in human tissues. *J. Clin. Endocrinol. Metab.* 82 (12), 4243–4251.
- Rosario, R., et al., 2013. Adult granulosa cell tumours (GCT): clinicopathological outcomes including FOXL2 mutational status and expression. *Gynecol. Oncol.* 131 (2), 325–329.
- Roybal, L.L., et al., 2014. Roles of binding elements, FOXL2 domains, and interactions with cJUN and SMADs in regulation of FSHbeta. *Mol. Endocrinol.* 28 (10), 1640–1655.
- Schmidt, D., et al., 2004. The murine winged-helix transcription factor Foxl2 is required for granulosa cell differentiation and ovary maintenance. *Development* 131 (4), 933–942.
- Shah, S.P., et al., 2009. Mutation of FOXL2 in granulosa-cell tumors of the ovary. *N. Engl. J. Med.* 360 (11), p2719.
- Uhlenhaut, N.H., et al., 2009. Somatic sex reprogramming of adult ovaries to testes by FOXL2 ablation. *Cell* 139 (6), 1130–1142.
- van Den Berg-Bakker, C.A., et al., 1993. Establishment and characterization of 7 ovarian carcinoma cell lines and one granulosa tumor cell line: growth features and cytogenetics. *Int. J. Cancer* 20 (53(4)), p8.

Transcriptomic analysis of stage 1 versus advanced adult granulosa cell tumors*

Maria Alexiadis^{1,*}, Simon Chu^{1,2,*}, Dilys Leung^{1,2}, Jodee A. Gould^{1,3}, Tom Jobling⁴, Peter J. Fuller^{1,2}

¹Hudson Institute of Medical Research (formerly Prince Henry's Institute of Medical Research) Monash Health, Clayton, Victoria 3168, Australia

²Monash University Department of Biochemistry and Molecular Biology Monash Health, Clayton, Victoria 3168, Australia

³MHTP Medical Genomics Facility, Clayton, Victoria 3168, Australia

⁴Department of Gynecology Oncology, Monash Health, Clayton, Victoria 3168, Australia

*These authors have contributed equally to this work

Correspondence to: Peter J. Fuller, **e-mail:** peter.fuller@hudson.org.au

Keywords: granulosa cells, FOXL2, ovary, transcriptome, stromal tumors

Received: September 03, 2015

Accepted: January 29, 2016

Published: February 16, 2016

ABSTRACT

Ovarian granulosa cell tumors (GCT) are hormonally-active neoplasms characterized, in the adult-subtype, by a mutation in the FOXL2 gene (C134W). They exhibit an indolent course with an unexplained propensity for late recurrence; ~80% of patients with aggressive, advanced stage tumors die from their disease; aside from surgery, therapeutic options are limited. To identify the molecular basis of advanced stage disease we have used whole transcriptome analysis of FOXL2 C134W mutation positive adult (a)GCT to identify genes that are differentially expressed between early (stage 1) and advanced (stage 3) aGCT. Transcriptome profiles for early ($n=6$) and stage 3 ($n=6$) aGCT, and for the aGCT-derived KGN, cell line identified 24 genes whose expression significantly differs between the early and stage 3 aGCT. Of these, 16 were more abundantly expressed in the stage 3 aGCT and 8 were higher in the stage 1 tumors. These changes were further examined for the genes which showed the greatest fold change: the cytokine CXCL14, microfibrillar-associated protein 5, insulin-like 3 and desmin. Gene Set Enrichment Analysis identified overexpression of genes on chromosome 7p15 which includes the homeobox A gene locus. The analysis therefore identifies a small number of genes with clearly discriminate patterns of expression arguing that the clinicopathological-derived distinction of the tumor stage is robust, whilst confirming the relative homogeneity of expression for many genes across the cohort and hence of aGCT. The expression profiles do however identify several overexpressed genes in both stage 1 and/or stage 3 aGCT which warrant further study as possible therapeutic targets.

INTRODUCTION

Granulosa cell tumors of the ovary (GCT), the major form of ovarian stromal tumors, arise from proliferating granulosa cells of the ovarian follicle [1]. They exhibit features of granulosa cells that include estrogen biosynthesis as well as the production of gonadal peptides including inhibin and anti-Müllerian hormone (AMH). GCT are classified as adult (95% of GCT) or juvenile, based on histopathological and clinical criteria. The identification of a specific somatic missense

mutation in the FOXL2 gene (c.402 C→G; pC134W) in ~97% of aGCT [2, 3] argues strongly that this mutation both defines the disease and indeed is etiologic in the disease. A striking feature of aGCT is their propensity for late recurrence, sometimes decades after their initial identification. Although the majority of aGCT are stage 1 and are cured by surgery, approximately 80% of the patients with aggressive disease at diagnosis and/or recurrence will succumb to their disease [1]. All aGCT, whether stage 1 or advanced stage, contain the FOXL2 mutation so other genetic changes in the tumor are

likely to be responsible for these differing stages and/or behaviour. The identification of molecular markers that predict recurrence and/or aggressive behaviour would be a great asset in the management of aGCT. Additionally, understanding the pathogenesis of advanced stage disease might aid the development of targeted therapies. Currently treatment options, once surgery is no longer relevant, are limited [1]. Although there have been a number of studies which explore the role of various mitogenic signaling pathways in aGCT [4–7] the specific question of what differentiates stage 1 disease from advanced stage disease has not been explored.

One approach to defining the molecular difference between stage 1 disease and advanced stage disease is to analyse their pattern of gene expression seeking critical differences and gene signatures of prognostic or therapeutic significance. There have been, until recently, relatively few whole transcriptome gene expression studies for aGCT [8]. Benayoun et al [9] used gene expression microarrays to compare 10 GCT of mixed stage (9 × stage 1 and 1 × advanced) with two granulosa cell samples collected during IVF. In a subsequent study they correlated these findings with the results of comparative genomic hybridization (CGH) in these tumors [10]. Rosairo et al [11] have explored gene expression in two human GCT-derived cell lines, COV434 and KGN. In the present study we have sought to identify changes in gene expression in aGCT (defined by the presence of the FOXL2 C134W mutation) that reflect the transition from stage 1 disease restricted to the ovary and therefore hopefully cured by surgery to stage 3 disease with transcoelomic spread to distant sites in the peritoneal cavity. We present the analysis of the transcription profiles for 6 stage 1 and 6 stage 3 aGCT and identify 24 genes whose expression significantly differs between the stage 1 and stage 3 GCT.

RESULTS

The aGCT samples were obtained as previously described [3, 6]; their clinical details are in Table 1. All cases are heterozygous for the FOXL2 C134W mutation [3]. Transcription profiles for the 12 tumors and also for the KGN cell line, which is also heterozygous for the FOXL2 C134W mutation and thus derived from an aGCT [3] were obtained.

Of ~9,000 expressed genes in both stage 1 and stage 3 aGCT, we identified 24 genes whose expression differed between the two groups. The analysis is presented as a volcano plot with the 24 genes that differ by ≥ 2 -fold at a p -value of ≤ 0.05 and passed a Westfall Young Permutative multiple correction test represented by the 26 red points (Figure 1): 2 of the genes are represented by two independent probes on the array (Table 2). 16 genes were expressed at 2-fold higher levels in the stage 3 aGCT

when compared to the stage 1 aGCT while the expression of 8 genes was down regulated in the advanced aGCT at a significance of $p < 0.05$. The full list of 26 gene probes is shown in Supplementary Table 1.

Unsupervised hierarchical clustering of the 24 genes is presented as a Heat Map which shows clear discrimination of the two groups (Figure 2). The observed changes were assessed for 4 genes, selected on the basis of their fold change and p -value, by quantitative RT-PCR (Figure 3) using an overlapping but non-identical group of tumors (Table 1): microfibrillar-associated protein 5 (MFAP5) which was significantly more highly expressed in the stage 3 group; and insulin-like 3 (INSL3) and desmin (DES) which were significantly more abundant in the stage 1 aGCT. For the orphan cytokine CXCL14, the grouped data did not achieve significance reflecting the heterogeneity in the observed levels within each group. The results are presented as a scatterplot; the levels observed in the KGN cell line are also indicated (Figure 3).

The expression of 3 of these genes, (INSL3, CXCL14 and MFAP5) was examined at the protein level using immunohistochemistry (Figure 4); the results, although semi-quantitative are consistent with the relative abundances observed at a RNA level: stage 1 vs stage 3 aGCT. Of more importance however, is that the immunohistochemistry confirms that these genes are indeed expressed in the tumor cells *per se*.

The transcriptome from the KGN cells when compared with the stage 3 aGCT showed substantial differences. In an analysis of all 12 aGCT compared to the KGN cells, 3674 entities differed by ≥ 2 -fold at a p -value of ≤ 0.05 and passed a Westfall Young Permutative multiple correction test. Of the 24 genes that differ between the stage 1 and advanced aGCT, only 5 differed: SIX1 (SIX homeobox 1), BDKRB1 (bradykinin receptor B1), FMO3 (flavin-containing monooxygenases 3) and GINS1(GINS subunit 1) were increased in the KGN cells when compared to all of the aGCT, whereas MCF2L was significantly lower in the KGN cells. In that the KGN cell line is derived from a very aggressive aGCT [3], a comparison with the transcriptome of the stage 3 aGCT alone may be seen as more appropriate. That comparison again shows a substantial differential expression with 4369 entities (≥ 2 -fold; p -value of ≤ 0.05 , after a Westfall Young Permutative multiple correction test). Of the 24 genes that differ by stage, 15 differed when the stage 3 aGCT and KGN transcriptomes are compared. PLCD1 (a member of the phospholipase C family), EMID1 (EMI domain containing 1), CSTA (cystatin A) and INSL3 (Figure 3), which are down in the stage 3 when compared to the stage 1 aGCT, are further significantly down in the KGN cells. Curiously, of the genes that are increased in the stage 3 aGCT and therefore might be expected to be further increased in the KGN cells, CXCL14 (Figure 3), MFAP5 (Figure 3), CYP2C8 (cytochrome P450 2C8), IGF2

Table 1: Clinical information for the aGCT studied

Sample	Stage	Surgery	Menopausal Status	Age at Surgery
1*^	1	Primary	Pre	53
2*^	1	Primary	Pre	54
3*^	1c	Primary	Post	50
4*	1	Primary	Post	79
5*^	1	Primary	Pre	31
6*	1a	Primary	Pre	43
7^	1a	Primary	Post	61
8^	1	Primary	Pre	29
9*^	3	Secondary	Post	58
10*^	3	Secondary	Pre	45
11*^	3	Secondary	Post	56
12*	3	Secondary	Post	54
13*^	3	Secondary	Pre	48
14*^	3	Secondary	Post	84
15^	3	Secondary	NA	47
16^	3	Secondary	Post	70

*Microarray; ^qRT-PCR

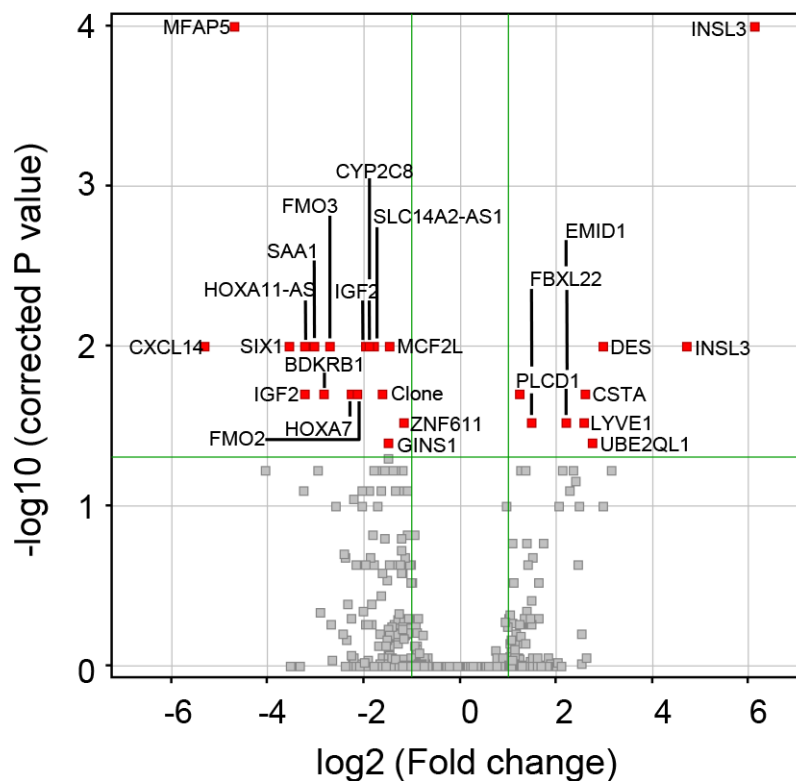


Figure 1: Volcano plot revealing the 26 statistically significant probes between stage 1 GCT and stage 3 aGCT representing 24 genes. A moderated *t*-test was performed; the 26 probes with a *p*-value of ≤ 0.05 and ≥ 2 fold change that passed a Westfall Young Permutative multiple correction test can be seen in red with gene symbols (Table 2) indicated.

Table 2: Differentially expressed genes

GeneSymbol	Gene Name	FC (abs)	p (Corr)
CXCL14	Chemokine (C-X-C motif) ligand 14	39.933685	0.01010101
MFAP5	Microfibrillar associated protein 5, transcript variant 1	26.172625	0
SIX1	SIX homeobox 1	11.79884	0.01010101
HOXA11-AS	HOXA11 antisense RNA	9.483171	0.01010101
IGF2	Insulin-like growth factor 2, transcript variant 1	9.4279175	0.02020202
SAA1	Serum amyloid A1, transcript variant 1	8.28538	0.01010101
BDKRB1	Bradykinin receptor B1	7.1152983	0.02020202
FMO3	Flavin containing monooxygenase 3, transcript variant 2	6.5978975	0.01010101
HOXA7	Homeobox A7	4.861581	0.02020202
FMO2	Flavin containing monooxygenase 2 (non-functional), transcript variant 1	4.451478	0.02020202
CYP2C8	Cytochrome P450, family 2, subfamily C, polypeptide 8, transcript variant 1	3.8967078	0.01010101
IGF2	Insulin-like growth factor 2, transcript variant 1	3.6979346	0.01010101
SLC14A2-AS1	SLC14A2 antisense RNA 1, long non-coding RNA	3.484851	0.01010101
Clone- BU567832	AGENCOURT_10399047 NIH_MGC_82 cDNA clone IMAGE:6614537 5'	3.0842583	0.02020202
GINS1	GINS complex subunit 1 (Psf1 homolog)	2.826527	0.04040404
MCF2L	cDNA FLJ12122 fis, clone MAMMA1000129	2.80219	0.01010101
ZNF611	zinc finger protein 611	2.2500026	0.030303031
PLCD1	Phospholipase C, delta 1, transcript variant 2	-2.3632836	0.02020202
FBXL22	F-box and leucine-rich repeat protein 22	-2.7893722	0.030303031
EMID1	EMI domain containing 1, transcript variant 1	-4.5672774	0.030303031
LYVE1	Lymphatic vessel endothelial hyaluronan receptor 1	-5.93999	0.030303031
CSTA	Cystatin A (stefin A)	-6.0303144	0.02020202
UBE2QL1	Ubiquitin-conjugating enzyme E2Q family-like 1	-6.751078	0.04040404
DES	Desmin	-7.8715506	0.01010101
INSL3	Insulin-like 3 (Leydig cell), transcript variant 2	-25.868898	0.01010101
INSL3	Insulin-like 3 (Leydig cell), transcript variant 2	-69.227425	0

FC(abs) – absolute fold change, advanced vs stage 1 aGCT;
p(Corr) – corrected p value.

(insulin-like growth factor 2), MCF2L (MCF.2 cell-line -derived transforming sequence-like) and ZNF611 (zinc finger protein 611) are lower in the KGN cells than the aGCT, whereas SIX1, BDKRB1, FMO3 and GINS1 expression is further increased in the KGN cells.

Two other methods were used to interrogate the microarray data. The ontogeny of the genes identified as differing between the two groups of genes was examined using the MetaCore™ software analysis suite, however no pathways or processes were identified that achieved significance. The microarray data was also analysed using the Gene Set Enrichment Analysis (GSEA) method [12]. The GSEA software also performs an unsupervised hierarchical Heat Map that validated many of the genes identified using the Genespring software, and also similarly shows clear discrimination of the two groups when grouping the top 50 features for each tumor type (Supplementary Figure 1). The microarray datasets for stage 1 and stage 3 aGCT were analysed against the curated MSigDB v4.1 genesets in order to determine whether an *a priori* defined set of genes show statistically significant, concordant differences between stage 1 and stage 3 aGCT. Using this method, we identified a significant enrichment of genes located on chromosome 7p15 (Figure 5, Supplementary Table 2), with an

enrichment score (ES) of -0.557 ($p = 0.025$) in stage 1 aGCT vs stage 3 aGCT (Figure 5A). This region includes the homeobox A (HOXA) gene locus. A graphical view of the over-represented and overexpressed genes located on chromosome 7p15 in stage 3 aGCT compared to stage 1 aGCT is shown in Figure 5B.

DISCUSSION

Comparison of the gene expression profiles revealed a relatively small number of genes that differ between the stage 1 and the advanced, stage 3 aGCT. This relative homogeneity across stage in part reflects the presumption of shared aetiology with respect to cell type of origin and a shared initiating event, the FOXL2 C134W mutation. This homogeneity is consistent with observations in other studies of expression of specific genes in aGCT [13–17] and indeed also with the observations that aGCT exhibit relative genomic stability when compared to epithelial ovarian cancers [2]. Although the tumor classification is robust with respect to aGCT, i.e. all contain the FOXL2 C134W mutation, the designation of stage could potentially be problematic in that a stage 1 aGCT could, for instance, be an advanced tumor caught early. The robust distinction between the groups reflected in the 24

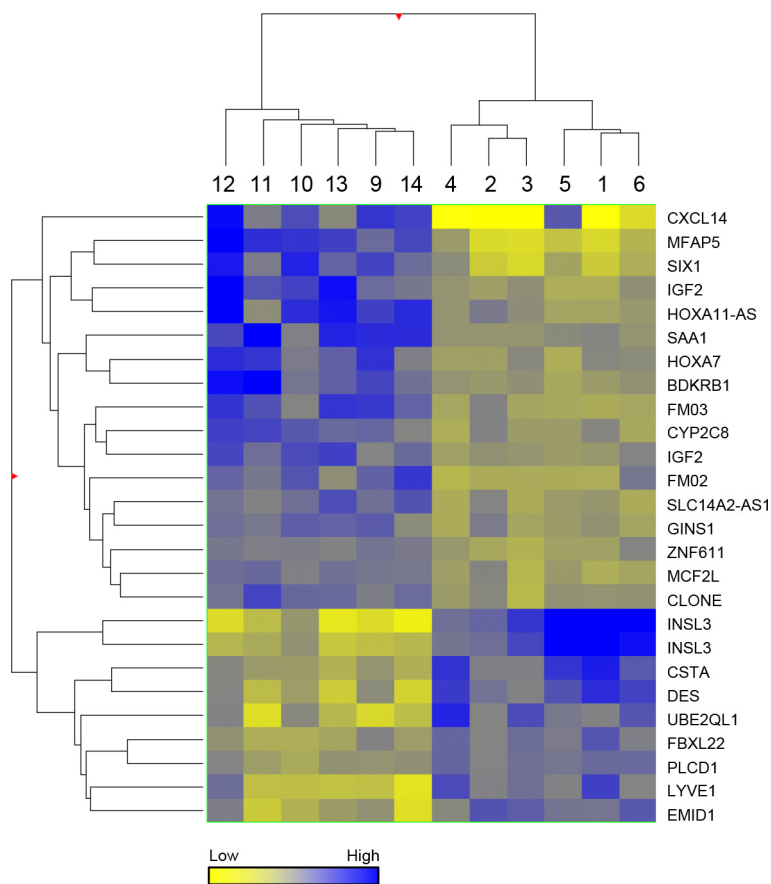


Figure 2: Heat map. Hierarchical analysis clustered by normalised intensity values of the 26 statistically significant probes between stage 1 and stage 3 aGCT, using a Euclidean similarity measure and Ward's linkage rule.

genes identified (Figure 2) however argues strongly for the validity of the prospective classification used. Attempts to segregate the data using other comparisons, e.g. age, menopausal status, did not reveal distinct patterns of expression.

Of the 8 genes whose expression is significantly diminished in the stage 3 aGCT, INSL3 stands out as a robust discriminator being ~70-fold higher in stage 1 disease with no overlap between groups (Figure 3). INSL3 is a member of the insulin-like hormone superfamily that is predominantly expressed in gonadal tissues. Its actions are mediated by the relaxin-insulin-like family peptide receptor 2 (RXFP2). Although RXFP2 expression appears higher in the stage 1 aGCT this was not significant (data not shown). INSL3 is expressed in the adult ovary primarily in theca and luteal granulosa cells where it is thought to have a role in maintenance of steroidogenesis [18]. INSL3 expression has recently been shown to be regulated in Leydig cells by COUP-TFII [19] which is abundantly expressed in aGCT [17]. INSL3 expression is inhibited by the bone morphogenetic proteins [18]; this diminished expression with stage 3 disease may be a bystander effect or perhaps reflect activation of the BMP-SMAD signalling pathway in advanced aGCT.

Desmin expression is also significantly reduced in the stage 3 aGCT being 7-fold higher in stage 1 disease.

Desmin is a class III intermediate filament usually associated with muscle, however it has been observed to be expressed strongly in a range of tumors unrelated to muscle [20]; the significance of the decrease in expression in aGCT with advanced disease is not clear. Similarly UBE2QL1 – ubiquitin-conjugating enzyme E2Q family-like 1 is down-regulated in the stage 3 aGCT. There is a very limited literature for UBE2QL1 in malignancy; however one study [21] ascribes a tumor suppressor function to UBE2QL1 which could be seen as consistent with its down-regulation in the context of more aggressive malignancy. Similarly, PLCD1, which encodes a member of the phospholipase C family, has higher expression in the stage 1 tumors consistent with reports in several tumor types that it is a tumor suppressor gene [22]. EMID1 is decreased in the stage 3 aGCT but information about its function is limited.

Other genes whose expression was higher in the stage 1 aGCT exhibited more modest differences. F-box and leucine-rich repeat protein 22 (FBXL22) is a member of the F-box gene family. It interacts with S-phase kinase associated protein 1A and cullin to form a complex with ubiquitin-ligase activity [23]. LYVE1 (lymphatic vessel hyaluronon receptor-1) expression is ~ 6-fold higher in the stage 1 aGCT. LYVE1 is a type 1 integral membrane glycoprotein predominantly expressed in lymphatic

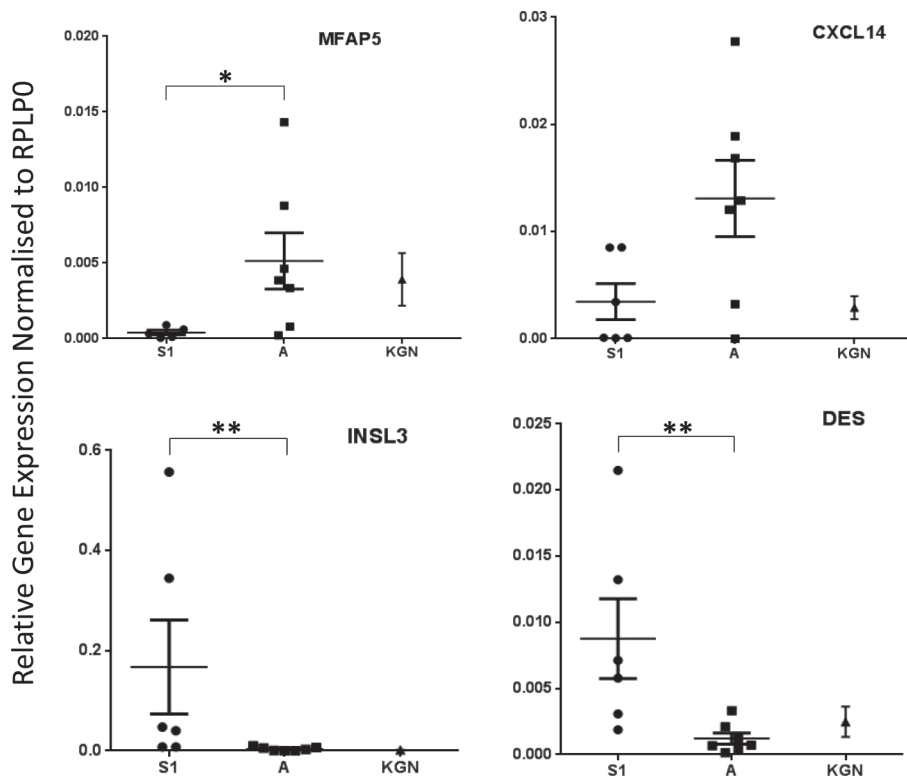


Figure 3: Scatter plots representing relative gene expression of MFAP5 ($p = 0.0303$), CXCL14 ($p = 0.1014$), INSL3 ($p = 0.0047$) and DES ($p = 0.0082$) in stage 1 vs stage 3 aGCT samples. The mean \pm standard error of the mean from 3 independent experiments is shown. Samples were normalised to RPLP0 gene expression and the non-parametric Mann-Whitney test was performed. KGN data is also shown.

vessels [24]; indeed it has been extensively used as an immunohistochemical marker of lymphatics [25]. The decreased levels may be consistent with a less organised tissue structure with advancing malignancy. The CSTA (cystatin A) gene is also ~6-fold more abundant in the stage 1 tumors. This gene encodes stefin A, a cysteine protease inhibitor which is thought to primarily inhibit cathepsin B [26]. Cathepsin B expression, although abundant from the microarray analyses, does not differ between the two stages. Loss of CSTA expression is associated with progression of ductal breast cancer *in situ* to invasive breast cancer [26], presumptively via increased cathepsin B activity which raises the possibility that cathepsin B may be a relevant therapeutic target in aGCT.

Of the 16 genes whose expression was increased with advanced disease, CXCL14 shows the greatest increase. CXCL14 is an orphan member of the Cys-x-Cys subfamily of cytokines which, although chemotactic for cells of the monocyte/macrophage lineage, appears not to be required for their normal function [27]. CXCL14 expression is markedly up-regulated (~40-fold) in the stage 3 aGCT in the microarray analysis but not significant in the RT-PCR (Figure 3) reflecting a striking heterogeneity of expression, particularly in the stage 3 aGCT. CXCL14

has been associated with both favourable and unfavourable outcomes depending on tumor type [28]. Augsten et al [27] argue that pro-tumoral effects of CXCL14 reflect overexpression in cancer-associated fibroblasts however immunohistochemical staining of the aGCT (Figure 4) shows clear expression in the tumor cells. A possible explanation of this apparent dichotomy may lie with the stromal origin of granulosa cells. Riesten et al [29] have recently identified CXCL14 as a key element in a gene expression signature that predicts outcome in advanced epithelial ovarian cancer. Fibroblast activating protein (FAP) which is abundantly expressed in both groups of aGCT is also part of that signature. Like CXCL14, FAP expression has been associated with cancer-associated fibroblasts. FAP shows ~4 fold increase in the stage 3 aGCT but this is not significant after correction for FDR (false discovery rate). It is however of interest, being an emerging therapeutic target with considerable specificity [30]. FAP is a cell surface glycoprotein with dipeptidyl peptidase activity whose expression is normally restricted to fibroblasts in healing wounds [31]. Some years ago we were surprised to find that it was also expressed by the normal human ovary [32]. Whilst its expression in normal ovary may reflect the “wound healing response”

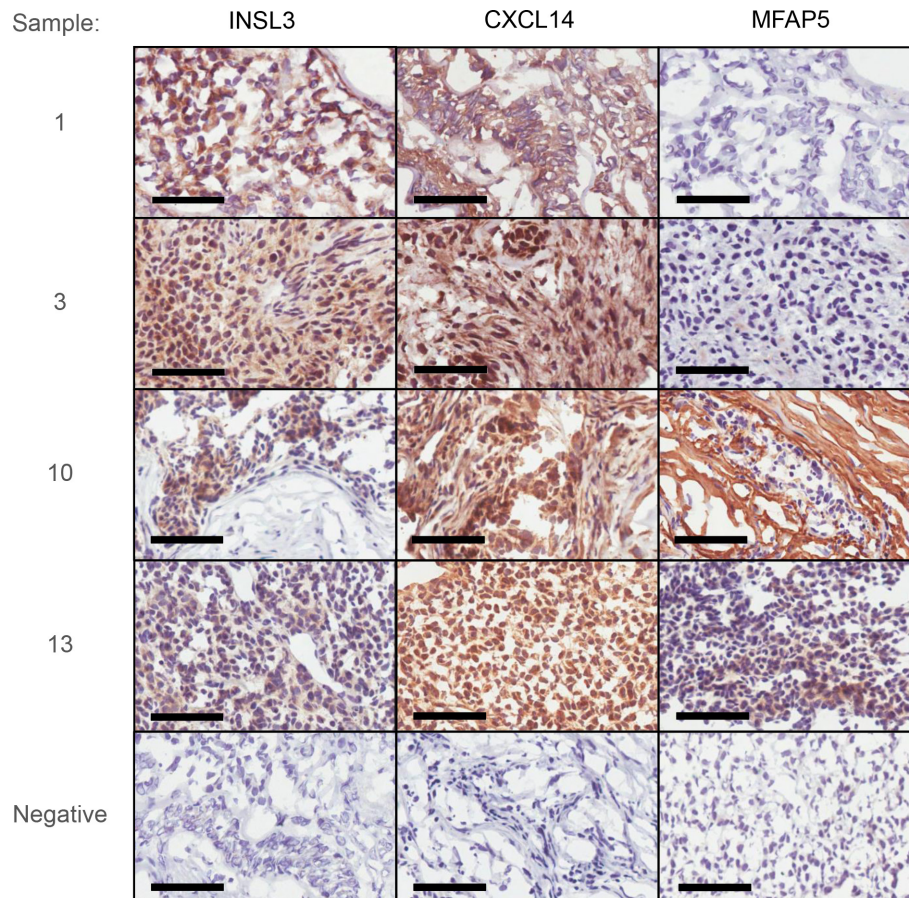


Figure 4: Immunohistochemical examination of INSL3, CXCL14 and MFAP5 in two stage 1 (1 and 3) and two stage 3 aGCT (10 and 13). Negative controls are shown as inserts for each sample. Bars correspond to 60 μ .

associated with ovulation, it raises the possibility that FAP is a product of GC, which as noted are stromal in origin. Conversely, FAP expression is not observed in the KGN cells which may argue that it is not a feature of advanced aGCT per se. Secretion by activated stromal fibroblasts of FAP has also been associated with epithelial ovarian cancer cell proliferation, migration and invasion [33].

MFAP5 showed the second greatest (~26)-fold increase. MFAP5 is a microfibril-associated glycoprotein which predicts poor survival and chemoresistance in patients with advanced high-grade serous epithelial ovarian cancer [34]. Of the other genes that are significantly upregulated with advanced disease, SAA1 (serum amyloid A1) is part of the family of highly homologous acute-phase proteins that have been associated with tumor progression and reduced survival in a range of cancers [35]. Of the other members of this family, SAA2, S100P (serum 100 calcium binding protein P), S100B, S100A7, S100A3, S100A1, S100A3 and S100BPB

(S100P binding protein) were identified on the microarray but did not differ between groups.

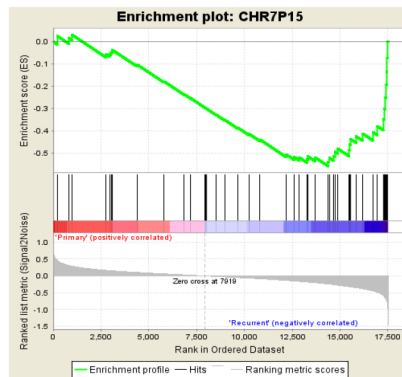
SIX1 is a homeobox gene which has a well characterised role in development [36]; it has also been found to be upregulated in a number of solid tumors which correlates with a worse prognosis. SIX1 expression was further increased in the KGN cells suggesting an association with increasing malignancy. SIX1 increases cyclin D1 expression in solid tumors [36], however cyclin D1 levels as determined from the microarray data did not differ by stage in the aGCT. Cyclin D2 plays a critical role in granulosa cell proliferation and has increased expression in GCT [13, 37]; however, although abundantly expressed being ~10 fold higher than cyclin D1, cyclin D2 expression also did not differ by stage.

FMO2 and FMO3 encode flavin-containing monooxygenases whose expression was also increased in advanced disease. They are found in a cluster with the other FMO genes: FMO1, and FMO4, although neither

A

Chromosome 7p15 Gene Set
Enrichment Plot
Primary vs Recurrent

ES	-0.557
NES	-1.85
Nominal p-Value	0.025
FDR q-Value	0.25



B

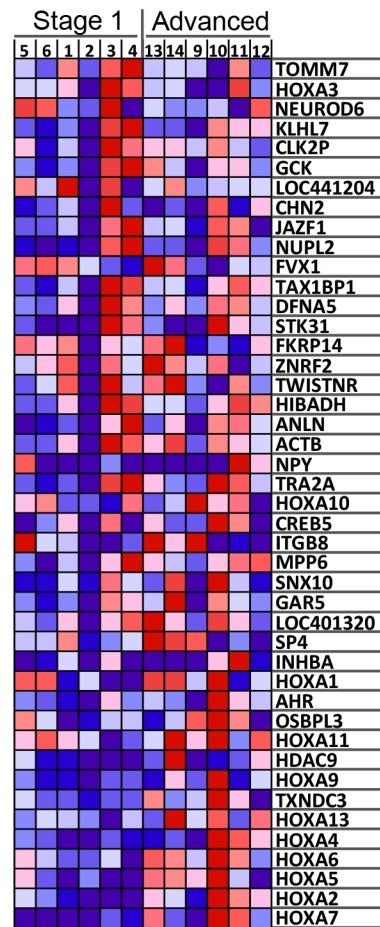


Figure 5: Gene set enrichment analysis (GSEA) from the microarray data comparing stage 1 with stage 3 aGCT showing enrichment of genes clustered on chromosome 7p15. (A) GSEA Enrichment plot shows values for the Enrichment Score (ES), Normalized Enrichment Score (NES), nominal *P*-value and False Discovery Rate *q*-Value (FDR-*q* value). (B) GSEA generated heatmap for highly enriched genes on Chromosome 7p15 in stage 1 compared to stage 3 aGCT.

of these genes differ by stage. These NADPH-dependent flavoenzymes catalyse the oxidation of numerous drugs and xenobiotics. FMO3 is predominately expressed in the liver where it plays a role in the metabolism of xenobiotics including a number of anti-cancer drugs [38]. Aside from hepatic tumors, there is little work on the role of FMO3 in other tissues or tumors. Curiously, it is expressed in the Fallopian tubal epithelium [39]. One might speculate that FMO3 upregulation might be associated with resistance to chemotherapy. FMO3, but not FMO2, is one of the 4 genes whose expression is further increased in the KGN cells. CYP2C8 whose expression is also increased in the stage 3 aGCT, is a cytochrome P450, known to metabolise many xenobiotics including paclitaxel [40]. SLC14A2 (solute family 14, member A) is a urea transporter normally expressed in the renal epithelium has not previously been associated with malignancy but may have a role in the efflux of toxic metabolites from the tumor cells.

HOXA11-AS1 is a non-coding anti-sense transcript directed at the homeotic HOXA11 gene whose biology has been described in the human endometrium [41]. Epigenetic silencing of HOXA11 has been observed in a number of tumors including ovarian cancer [42]; it is associated with a worse prognosis and/or chemotherapy resistance. HOXA11 expression appeared low but did not differ between groups. This contrasts with the HOXA7 homeobox gene whose expression is increased with advanced disease. We observed a significant enrichment of genes located on chromosome 7p15 using GSEA. Significantly, this locus contains many of the HOX genes, including HOXA7. HOXA7 expression has previously been reported in normal granulosa cells and in KGN cells where it regulates expression of the epidermal growth factor receptor [43], however there was no evidence of a change in the expression of this receptor. Knock-down of HOXA7 expression in KGN cells has been reported to decrease cell proliferation, again arguing for an active role for HOXA7 in GCT tumorigenesis [43].

MCF2L, which encodes a guanine nucleotide exchange factor, is expressed in articular chondrocytes [44]; the significance of its increased expression in stage 3 aGCT is unclear. BDKRB1 is synthesised *de novo* following tissue injury. Its expression has been reported to be upregulated in a range of tumors including another stromal tumor, chondrosarcoma [45], but its role in malignancy is unclear. The ligands for this receptor, bradykinin and kallidin, are known to induce angiogenesis, cell migration and metastasis [46] so the increased expression could relate to cells other than the tumor cells (e.g. inflammatory cells, the vasculature), however expression in the KGN cells supports a tumoral origin. The GINS complex is associated with the initiation of DNA replication in yeast and *Xenopus*. GINS1, also known as PSF1, has been associated with high proliferative activity [47] and indeed its expression is also further increased in the KGN cell line.

Increased expression of IGF2 is seen in the stage 3 aGCT, as in a broad range of tumors, where it is associated with increasing malignancy [48]; its mitogenic properties have been extensively characterised. We have previously described IGF1 and 2 expression in a mixed group of GCT which was heterogenous but we did not analyse this by stage or type [15]. The increased expression in the stage 3 aGCT of ZNF611, a member of the large family of zinc finger containing transcription factors located on chromosome 19, and the clone BU567832, is of uncertain significance, neither having previously been associated with malignancy. The clone BU567832 localises to an intragenic region of chromosome 18; whilst transcripts have been reported in other tissues, the nature of the RNA detected remains to be determined.

The previous aGCT transcriptomic study by Benayoun et al [9] using predominantly stage 1 tumors (9 of 10 aGCT) compared to two granulosa cell samples obtained at IVF identified changes in the expression of FOXL2 regulated genes consistent with the presence of the FOXL2 p.Cys134Trp mutation. In the current study, all tumors have this mutation so this same pattern of enrichment, as expected, was not observed. Rosario et al [11] applied transcriptomic analysis to the KGN cells and another human GCT-derived cell line, COV434, which in contrast to the KGN cells neither expresses FOXL2 nor contains the p.Cys134Trp mutation, consistent with it having been derived from a juvenile GCT [3]. They identified a number of differences between the two but the genes were not amongst those identified in the current study. The marked difference between the aGCT transcriptome and that of the KGN cells argues for some caution in extrapolating findings *in vitro* using KGN cells to aGCT.

Of the genes decreased in advanced disease, several may reflect a loss of the differentiated state eg INSL3, desmin; the others do not clearly reflect specific pathways relevant to the advanced malignancy. Similarly, of the genes upregulated in advanced disease many have been associated previously with advanced malignancy in other tumor types; those that are further increased in the KGN cells, particularly SIX1 and GNS1 which have established associations with malignancy and proliferation, respectively, may represent drivers of the neoplastic process.

In seeking to understand the changes in gene expression we applied pathway and process analyses but this was not revealing, likely reflecting the relatively small number of genes that differed by stage. Gene set enrichment analysis highlighted over expression of genes on chromosome 7p15 in stage 3 aGCT. This finding is consistent with a report investigating the prognostic significance of chromosomal imbalances detected using CGH for GCT [49] which reported gain of 7p15-p21 to be a feature in some GCT samples. Other studies using cytogenetics or CGH have variably identified trisomy

of chromosomes 12 and 14 in approximately one third of cases [10, 50] with a lesser frequency in several other chromosomes/loci. Increased HOX gene mRNA levels may also simply reflect co-ordinate increased expression of this locus as can be observed at certain stages of development. Our analysis demonstrates a rather compelling association of the HOXA locus on 7p15 with stage in that the relative expression of the locus taken as a whole clearly segregates with stage. One might argue that an amplification of the HOX gene locus represents a strong candidate marker for advanced disease; whether this has prognostic value i.e. can predict recurrent or aggressive disease will require a prospective study.

Although the majority of stage 1 aGCT are cured with surgery, advanced disease represents a significant therapeutic challenge. These studies identifies a panel of genes that differ between stage 1 and stage 3 aGCT; in some cases they robustly discriminate the stages (Figure 3). It remains to be established whether these differences can be used to establish prognosis. Thus confirmation in an independent cohort and a prospective study will ultimately be required. The molecular basis of these changes in gene expression remains to be determined; although a large number of known and putative oncogenes have been examined in aGCT [1], an unbiased mutation screen, aside from the study of Shah et al [2] in which 4 aGCT were examined, has not been reported. The expression profiles do however identify several overexpressed genes in both stage 1 and stage 3 aGCT, or just the stage 3 aGCT, which warrant further study as potential therapeutic targets. Some, such as FAP appear relatively stromal cell specific, whilst others are emerging targets in other tumor types.

METHODS

RNA was isolated from 6 stage 1 aGCT and 6 stage 3 aGCT collected sequentially and predominantly at our institution [3, 6]. Stage is defined according to the FIGO (International Federation of Gynecology and Obstetrics) criteria used for ovarian cancer [51]. The stage 3 aGCT were all collected at a surgery subsequent to their initial surgery and may thus be interpreted as either a recurrence or progression of a known aGCT. The GCT-derived cell line, KGN which is heterozygous for the FOXL2 mutation has been described previously [3, 52].

Transcriptome profiles

We established transcriptome profiles for the aGCT using the Agilent Whole Human Genome 4 × 44K Expression Microarrays (Agilent Technologies, Santa Clara, CA). Cyanine-3 (Cy3) labeled cRNA was prepared from 200 ng total RNA using the One Color Low Input Quick Amp Labeling Kit (Agilent) followed by RNeasy column purification (Qiagen, Hilden, Germany). Dye incorporation and cRNA yield were checked using

the NanoDrop ND-1000 Spectrophotometer (Thermo Scientific, MA). 600 ng of cRNA for each sample was then hybridized onto a separate array for 17 h at 65°C and washed following the manufacturer's instructions. Slides were scanned using an Agilent DNA Microarray Scanner (G5205B) (Agilent) using the one-color scan setting for '4 × 44K' slides. The scanned images were analysed with Feature Extraction Software 9.5.3.1 (Agilent) using default parameters to obtain background-subtracted and spatially detrended processed signal intensities. Data from feature extraction were imported into GeneSpring GX13.1 (Agilent) for analysis. Data was normalised using the quantile normalisation method and tested for significant differences between stage 1 and stage 3 aGCT by performing a moderated *t*-test with the *P* value (≤ 0.05 deemed significant) computed using the asymptotic method. Genes which also had a fold change ≥ 2.0 were then subjected to Westfall Young Permutative multiple testing correction. All data produced was MIAME-compliant.

Pathway analysis

Of the 17,847 entities identified as expressed in the microarray, 50 of them were found to pass the Moderated *T*-test with a Westfall-Young Permutation method for False Discovery Rate and threshold settings of 1.5 fold and *p*-value of 0. They were then subjected to a pathway analysis with the MetaCore™ software analysis suite (Thomson Reuters, New York, NY).

Gene set enrichment analysis (GSEA)

In addition, the normalised microarray data was analysed using the Gene Set Enrichment Analysis (GSEA) method [12]. The microarray datasets were stratified and assigned phenotypes as stage 1 and stage 3 aGCT. GSEA was then performed for each of the samples using the gene permutation algorithm. Enrichment analysis was performed using the default parameter settings. We compared the gene expression levels from the stage 1 versus the stage 3 aGCT groups and identified the genes that had significantly different expression in the GSEA by using the gene sets from the Molecular Signatures Database (MSigDB v4.1) (www.broadinstitute.org/gsea). The enrichment score (ES) was calculated for each gene set reflecting if the genes in the particular gene set appeared in the top (positive score), in the bottom (negative score), or were randomly distributed (close to zero score). The ranking metric used was the signal-to-noise ratio. Scores were compared with scores calculated from 1,000 randomly permuted gene lists, in order to calculate false discovery rates (FDR) (cut-off at FDR = 0.05). The ES, normalized ES (NES), *p* value, and FDR *q*-value were then used to rank the gene sets. Definitions of these output variables can be found in [12].

RT-PCR

The comparative Ct ($\Delta\Delta C_t$) method was used to validate four genes. FAM labeled TaqMan Gene Expression assays for CXCL14, MFAP5, INSL3 and DES were purchased along with a FAM labeled RPLP0 probe which was used as an endogenous control. A 10 μ l reaction was prepared with 1 \times TaqMan universal PCR master mix (Applied Biosystems, Foster City, CA) and diluted cDNA. All PCR reactions were carried out in triplicate in MicroAmp optical 384-well reaction plates (Applied Biosystems). The cycling parameters were initiated by by 2 min at 50°C and 10 min at 95°C, followed by 40 cycles of 15 s at 95°C and 60°C for 1min using the 7900HT fast real-time PCR system (Applied Biosystems).

Immunohistochemistry

Frozen GCT were blocked with OCT and 4 μ m sections were prepared using the cryostat. All incubations and washes were performed at room temperature unless stated otherwise. Frozen GCT sections were fixed in 4% paraformaldehyde for 30 min followed by quenching of endogenous peroxidase using 0.3% hydrogen peroxide/PBS for 30 min. For membrane permeation, slides were incubated in 0.1% triton X-100/PBS for 10 min. Nonspecific binding was blocked by 10% goat serum in 3% BSA for an hour. Incubations with primary antibody, rabbit polyclonal INSL3 (Abcam ab 65981; 1:250), CXCL14 (Abcam ab46010; 1:400) or MFAP5 (Sigma abHPA010552; 1:500) was performed at 4°C overnight. Goat serum was used as a negative control. After PBS washes, slides were incubated with biotinylated goat anti-rabbit secondary antibody (Dako; 1:200) for an hour. VECTORSTAIN® avidin/biotinylated enzyme complex was made up as per manufacturer's instructions, added to sections and incubated for an hour. Staining was visualised by incubation of DAB solution (Dako) for 3 min. Sections were counterstained with hematoxylin, dehydrated with ethanol (70% and 100%) and mounted with DPX. Validation of the antibodies using a positive control tissue is shown in Supplementary Figure 2.

ACKNOWLEDGMENTS

The authors wish to thank Nicole Fairweather, Professor Martin Oehler and Zdenka Prodanovic (Victorian Cancer Biobank) for assistance with collection of the tissue samples and clinical information; Ross Chapman for advice on the microarray analyses, Claudette Thiedeman for preparation of the manuscript and Sue Panckridge for preparation of the figures.

GRANT SUPPORT

This work is supported by grants-in-aid from the Cancer Council Victoria; S.C. is supported by the Ovarian Cancer Research Foundation, the Granulosa Cell Tumor of the Ovary Foundation and the National Health & Medical Research Council of Australia through a Project Grant (#1058334) and a Senior Principal Research Fellowship to P.J.F. (#1002559). The Hudson Institute is supported by the Victorian Government's Operational Infrastructure Scheme.

CONFLICTS OF INTEREST

The authors declare no potential conflicts of interest.

REFERENCES

1. Jamieson S, Fuller PJ. Molecular pathogenesis of granulosa cell tumors of the ovary. *Endoc Rev.* 2012; 33:109–144.
2. Shah SP, Köbel M, Senz J, Morin RD, Clarke BA, Wiegand KC, Leung G, Zayed A, Mehl E, Kalloger SE, Sun M, Giuliany R, Yorida E, et al. Mutation of FOXL2 in granulosa-cell tumors of the ovary. *N Engl J Med.* 2009; 360: 2719–2729.
3. Jamieson S, Butzow R, Andersson N, Alexiadis M, Unkila-Kallio L, Heikinheimo M, Fuller PJ, Anttonen M. The FOXL2 C134W mutation is characteristic of adult granulosa cell tumors of the ovary. *Mod Pathol.* 2010; 23:1477–1485.
4. Chu S, Alexiadis M, Fuller PJ. Expression, mutational analysis and *in vitro* response of imatinib mesylate and nilotinib target genes in ovarian granulosa cell tumors. *Gynecol Oncol.* 2008; 108:182–190.
5. Färkkilä A, Anttonen M, Pociuviene J, Leminen A, Butzow R, Heikinheimo M, Unkila-Kallio L. Vascular endothelial growth factor (VEGF) and its receptor VEGFR-2 are highly expressed in ovarian granulosa cell tumors. *Eur J Endocrinol.* 2011; 164:115–122.
6. Jamieson S, Fuller PJ. Characterization of the inhibitor of kappaB kinase (IKK) complex in granulosa cell tumors of the ovary and granulosa cell tumor-derived cell lines. *Horm Cancer.* 2013; 4:277–292.
7. Jamieson S, Fuller PJ. Tyrosine kinase inhibitors as potential therapeutic agents in the treatment of granulosa cell tumors of the ovary. *Int J Gynecol Cancer.* 2015; 25:1224–31.
8. Colombo N, Parma G, Zanagnolo V, Insinga A. Management of ovarian stromal cell tumors. *J Clin Oncol.* 2007; 25:2944–2951.
9. Benayoun BA, Anttonen M, L'Hôte D, Bailly-Bechet M, Andersson N, Heikinheimo M, Veitia RA. Adult ovarian granulosa cell tumor transcriptomics: prevalence of FOXL2 target genes misregulation gives insights into the pathogenic

- mechanism of the p.Cys134Trp somatic mutation. *Oncogene*. 2013; 32:2739–2746.
10. Caburet S, Anttonen M, Todeschini AL, Unkila-Kallio L, Mestivier D, Butzow R, Veitia RA. Combined comparative genomic hybridization and transcriptomic analyses of ovarian granulosa cell tumors point to novel candidate driver genes. *BMC Cancer*. 2015; 15:251.
 11. Rosairo R, Araki H, Print CG, Shelling AN. The transcriptional targets of mutant FOXL2 in granulosa cell tumors. *PLoS One*. 2012; 7:e46270.
 12. Subramanian A, Tamayo P, Mootha VK, Mukherjee S, Ebert BL, Gillette MA, Paulovich A, Pomeroy SL, Golub TR, Lander ES, Mesirov JP. Gene set enrichment analysis: a knowledge-based approach for interpreting genome-wide expression profiles. *Proc Natl Acad Sci USA*. 2005; 102:15545–15550.
 13. Chu S, Rushdi S, Zumpe ET, Mamers P, Healy DL, Jobling T, Burger HG, Fuller PJ. FSH-regulated gene expression profiles in ovarian tumours and normal ovaries. *Mol Hum Reprod*. 2002; 8:426–433.
 14. Jamieson S, Alexiadis M, Fuller PJ. Expression status and mutational analysis of the ras and B-raf genes in granulosa cell and epithelial tumors of the ovary. *Gynecol Oncol*. 2004; 95:603–609.
 15. Alexiadis M, Mamers P, Chu S, Fuller PJ. Insulin-like growth factor, insulin-like growth factor-binding protein-4, and pregnancy-associated plasma protein-A gene expression in human granulosa cell tumors. *Int J Gynecol Cancer*. 2006; 16:1973–1979.
 16. Bittinger, S, Alexiadis, M, Fuller, P.J. Expression status and mutational analysis of the PTEN and P13K subunit genes in ovarian granulosa cell tumors. *Int J Gynecol Cancer*. 2008; 19:339–342.
 17. Alexiadis M, Eriksson N, Jamieson S, Davis M, Drummond AE, Chu S, Clyne CD, Muscat GE, Fuller PJ. Nuclear receptor profiling of ovarian granulosa cell tumors. *Horm. Cancer*. 2011; 2:157–169.
 18. Glister C, Satchell L, Bathgate RAD, Wade JD, Dai Y, Ivell R, Anand-Ivell R, Rodgers RJ, Knight PG. Functional link between bone morphogenetic proteins and insulin-like peptide 3 signaling in modulating ovarian androgen production. *Proc Natl Acad Sci USA*. 2013; 110:E1426–E1435.
 19. Mendoza-Villarreal REI, Di-Luoffo M, Camiré E, Giner XC, Brousseau C, Tremblay JJ. The *Insl3* gene is a direct target for the orphan nuclear receptor COUP-TFII in Leydig cells. *J Mol Endocrinol*. 2014; 53:43–55.
 20. Miettinen M. Immunohistochemistry of soft tissue tumours: review with emphasis on 10 markers. *Histopath*. 2014; 64:101–118.
 21. Wake NC, Ricketts CJ, Morris MR, Prigmore E, Gribble SM, Skytte AB, Brown M, Clarke N, Banks RE, Hodgson S, Turnell AS, Maher ER, Woodward ER. *UBE2QL1* is disrupted by a constitutional translocation associated with renal tuor predisposition and is a novel candidate renal tumor suppressor gene. *Hum Mutat*. 2013; 34:1650–1661.
 22. Danielsen SA, Cekaite L, Agesen TH, Sveen A, Nesbakken A, Thilis-Evensen E, Skotheim RI, Lind GE, Lothe RA. Phospholipase C isozymes are deregulated in colorectal cancer – insights gained from gene set enrichment analysis of the transcriptome. *PLoS One*. 2011; 6:e24419.
 23. Spaich S, Will RD, Just S, Spaich S, Kuhn C, Frank D, Berger IM, Wiemann S, Korn B, Koegl M, Backs J, Katus HA, Rottbauer W, et al. F-Box and leucine-rich protein 22 is a cardiac-enriched F-Box protein that regulates sarcomeric protein turnover and is essential for maintenance of contractile function *in vivo*. *Circ Res*. 2012; 111:1504–1516.
 24. Platonava N, Miquel G, Regenfuss B, Taouji S, Cursiefen C, Chevet E, Bikfalvi A. Evidence for the interaction of fibroblast growth factor-2 with the lymphatic endothelial cell marker LYVE-1. *Blood*. 2013; 121:1229–1237.
 25. Vainionpää N, Bützow R, Hukkanen M, Jackson DG, Pihlajaniemi T, Sakai LY et al. Basement membrane protein distribution in LYVE-1-immunoreactive lymphatic vessels of normal tissues and ovarian carcinomas. *Cell Tissue Res*. 2007; 328:317–328.
 26. Lee S, Stewart S, Nagtegaal I, Luo J, Wu Y, Colditz G, Medina D, Allred DC. Differentially expressed genes regulating the progression of ductal carcinoma *in situ* to invasive breast cancer. *Cancer Res*. 2012; 72:4574–4586.
 27. Augsten M, Sjöberg E, Frings O, Vorrink SU, Frijhoff J, Olsson E, Borg Å, Östman A. The pro-tumorigenic effect of CXCL14-expressing fibroblasts depends on Nos1-derived nitric oxide signaling. *Cancer Res*. 2014; 74:2999–3010.
 28. Hara T, Tanegashima K. Pleiotropic functions of the CXCL-type chemokine CXCL14 in mammals. *J Biochem*. 2012; 151:469–476.
 29. Riester M, Wei W, Waldron L, Culhane AC, Trippa L, Oliva E, Kim SH, Michor F, Huttenhower C, Parmigiani G, Birrer MJ. Risk prediction for late-stage ovarian cancer by meta-analysis of 1525 patient samples. *J Natl Cancer Inst*. 2014; 106:dju 048.
 30. Brennen WN, Isaacs JT, Denmeade SR. Rationale behind targeting fibroblast activation protein-expressing carcinoma-associated fibroblasts as a novel chemotherapeutic strategy. *Mol Cancer Ther*. 2012; 11:257–266.
 31. Cheng JD, Weiner LM. Tumors and their micro environments: tilling the soil. *Clin Cancer Res*. 2003; 9:1639–1647.
 32. McNeilage J, Alexiadis M, Susil BJ, Mamers P, Jobling T, Laslett G, Trajstman A, Fuller PJ. Molecular characterization of sarcomatous change in a granulosa cell tumor. *Int J Gynecol Cancer*. 2007; 17:398–406.
 33. Yang W, Han W, Ye S, Liu D, Wu J, Liu H, Li C, Chen H. Fibroblast activation protein-a promotes ovarian cancer cell

- proliferation and invasion via extracellular and intracellular signaling mechanisms. *Exp Mol Pathol.* 2013; 95:105–110.
34. Spivey KA, Banyard J. A prognostic signature in advanced ovarian cancer reveals a microfibril-associated protein (MAGP2) as a promoter of tumor cell survival and angiogenesis. *Cell Adh Migr.* 2010; 4:169–171.
 35. Hansen MT, Forst B, Cremers N, Quagliata L, Ambartsumian N, Grum-Schwensen B, Klingelhöfer J, Abdul-AI A, Herrmann P, Osterland M, Stein U, Nielsen GH, Scherer PE, et al. A link between inflammation and metastasis: serum amyloid A1 and A3 induce metastasis, and are targets of metastasis-inducing S100A4. *Oncogene.* 2015; 34:424–35.
 36. Wu W, Ren Z, Li P, Yu D, Chen J, Huang R, Liu H. Six1: a critical transcription factor in tumorigenesis. *Int J Cancer.* 2015; 136:1245–53.
 37. Sicinski P, Donaher JL, Geng Y, Parker SB, Gardner H, Park MY, Robker RL, Richards JS, McGinnis LK, Biggers JD, Eppig JJ, Bronson RT, Elledge SJ, et al. Cyclin D2 is an FSH-responsive gene involved in gonadal cell proliferation and oncogenesis. *Nature.* 1996; 384:470–474.
 38. Phillips IE, Shephard EA. Flavin-containing mono oxygenases: mutations, disease and drug response. *Trends Pharmacol Sci.* 2008; 29:294–301.
 39. Yuan Z, Wang L, Wang Y, Zhang T, Li L, Cragun JM, Chambers SK, Kong B, Zheng W. Tubal origin of ovarian endometriosis. *Mod Pathol.* 2014; 27:1154–1162.
 40. de Weger VA, Beijnen JH, Schellens JH. Cellular and clinical pharmacology of the taxanes docetaxel and paclitaxel – a review. *Anticancer Drugs.* 2014; 25:488–494.
 41. Chau YM, Pando S, Taylor HS. HOXA11 silencing and endogenous HOXA11 antisense ribonucleic acid in the uterine endometrium. *J Clin Endocrinol Metab.* 2002; 87:2674–2680.
 42. Matei D, Fang F, Changyu S, Schilder J, Arnold A, Zeng Y, Berry WA, Huang T, Nephew KP. Epigenetic resensitization to platinum in ovarian cancer. *Cancer Res.* 2012; 72:2197–2205.
 43. Zhang Y, Huang Q, Cheng J-C, Nishi Y, Yanase T, Huang H-F et al. Homeobox A7 increases cell proliferation by up-regulation of epidermal growth factor receptor expression in human granulosa cells. *Reprod Biol Endocrinol.* 2010; 8:61.
 44. Day-Williams AG, Southam L, Panoutsopoulou K, Rayner NW, Esko T, Estrada K, Helgadottir HT, Hofman A, Ingvarsson T, Jonsson H, Keis A, Kerkhof HJ, Thorleifsson G, et al. A variant in MCF2L is associated with osteoarthritis. *Am J Hum Genetics.* 2011; 89:446–450.
 45. Yang WH, Chang JT, Hsu SF, Li TM, Cho DY, Huang CY, Fong YC, Tang CH. Bradykinin enhances cell migration in human chondrosarcoma cells through BK receptor signaling pathways. *J Cell Biochem.* 2010; 109:82–92.
 46. Lu DY, Leung YM, Huang SM, Wong KL. Bradykinin-induced cell migration and COX-2 production mediated by the bradykinin B1 receptor in glioma cells. *J Cell Biochem.* 2010; 110:141–150.
 47. Nagahama Y, Ueno M, Miyamoto S, Morii E, Minami T, Mochizuki N, Saya H, Takakura N. PSF1, a DNA replication factor expressed widely in stem and progenitor cells, drives tumorigenic and metastatic properties. *Cancer Res.* 2010; 70:1215–1224.
 48. Livingstone C. IGF2 and cancer. *Endocr Rel Cancer.* 2013; 20:R321–R339.
 49. Lin YS, Eng HL, Jan YJ, Lee HS, Ho WL, Liou CP, Lee WY, Tzeng CC. Molecular cytogenetics of ovarian granulosa cell tumors by comparative genomic hybridization. *Gynecol Oncol.* 2005; 97:68–73.
 50. Van den Berghe I, Dal Cin P, De Groef K, Michielssen P, Van den Berghe H. Monosomy 22 and trisomy 14 may be early events in the tumorigenesis of adult granulosa cell tumor. *Cancer Genet Cytogenet.* 1999; 112:46–48.
 51. Prat J, Belhadj H, Berek J, Bermudez A, Bhatla N, Cain J, Denny L, Fujiwara K, Hacker N, Avall-Lundqvist E, Mutch D, Odicino F, Pecorelli S, et al. Abridged republication of FIGO's staging classification for cancer of the ovary, fallopian tube, and peritoneum. FIGO Committee on Gynecologic Oncology. *Eur J Gynaecol Oncol.* 2015; 36:367–369.
 52. Nishi Y, Yanase T, Mu Y, Oba K, Ichino I, Saito M, Nomura M, Mukasa C, Okabe T, Goto K, Takayanagi R, Kashimura Y, Haji M, et al. Establishment and characterization of a steroidogenic human granulosa-like tumor cell line, KGN, that expresses functional follicle-stimulating hormone receptor. *Endocrinol.* 2001; 142:437–445.

Review

Genetics and genomics of ovarian sex cord-stromal tumors

Fuller P.J., Leung D.T., Chu S.. Genetics and genomics of ovarian sex cord-stromal tumors.

Clin Genet 2016. © John Wiley & Sons A/S. Published by John Wiley & Sons Ltd, 2016

Ovarian sex cord-stromal tumors (SCST) represent approximately 8% of malignant ovarian tumors. The most common are granulosa cell tumors (GCT) which account for approximately 90% of malignant SCST. Recent studies have unraveled the key genomic and genetic events contributing to their pathogenesis. SCST are found in the hereditary syndromes: Peutz-Jeghers syndrome, Ollier disease and Maffucci syndrome, and DICER1 syndrome. Genomic studies have largely been limited to GCT where a number of recurring chromosomal abnormalities (monosomy and trisomy) have been identified although their contribution to pathogenesis remains unclear. In addition to the recurrent DICER1 mutations reported in non-hereditary cases of Sertoli cell and Sertoli–Leydig cell tumors, recurrent somatic mutations in both the juvenile (j) and adult (a) forms of GCT have been reported. Approximately 30% of jGCT contain a somatic mutation, the *gsp* oncogene, while a further 60% have an activating mutation in the *AKT* gene. In the case of aGCT, a well characterized mutation in the FOXL2 transcription factor (FOXL2 C134W) is found in almost all cases, which arguably defines the disease, although the molecular events that determine the stage, behavior and prognosis of aGCT remain to be determined.

Conflict of interest

The authors declare that they have no conflict of interest.

**P.J. Fuller^a, D.T. Leung^a
and S. Chu^a**

^aCentre for Endocrinology and Metabolism, Hudson Institute of Medical Research, Clayton, Australia and

^bDepartment of Molecular and Translational Science, Monash University, Clayton, Australia

Key words: FOXL2 – granulosa cells – ovarian cancer – ovary – stromal tumors

Corresponding author: Prof Peter J. Fuller, Hudson Institute of Medical

Received 18 August 2016, revised and accepted for publication 24 October 2016

Ovarian sex cord-stromal tumors (SCST) represent approximately 8% of ovarian cancers. They are thought to arise primarily from the sex-cord and/or stromal cells of the ovarian follicles and/or their precursor cells (1). Malignant ovarian tumors should be viewed not as a single entity, but as a group of histologically, genetically and functionally distinct diseases, associated with the same organ, the ovary. Epithelial ovarian cancers (EOC) represent the majority of ovarian tumors, the other two primary classifications are germ cell tumors and SCST (2). Ovarian SCST are classified histologically as granulosa cell tumors (GCT), theca-fibroma, Sertoli stromal tumors and SCST of mixed or unclassified cell type, with the sub-classifications of these groups shown in Table 1. The most common of the malignant tumors are GCT which account for approximately 90% of malignant SCST. The clinical and molecular features

of GCT have previously been reviewed by Jamieson and Fuller (2). Although recurrent and advanced stage GCT are associated with approximately 80% mortality (2), they remain a relatively neglected subset of tumors. The high mortality rate of advanced disease is not helped by the tendency to simply group all ovarian cancers with EOC and to apply treatment regimens, based on therapeutic approaches for EOC, rather than tailored to SCST (2). The need to understand the genetics and hence the biology of these distinct tumors therefore has an immediacy beyond just understanding the tumor biology, with targeted therapeutics urgently needed for women with SCST. In this review we will explore recent studies that provide further insights into the genetics and genomics of these tumors, and seek to identify key unanswered questions.

Table 1. Histological classification of ovarian sex cord-stromal tumors^a

A. Granulosa-stromal cell tumors
1. Granulosa cell tumor
2. Tumors in the thecoma-fibroma group
a. Thecoma
b. Fibroma
c. Unclassified
B. Sertoli–Leydig cell tumors
1. Well-differentiated
a. Sertoli cell tumor
b. Sertoli cell tumor with lipid storage
c. Sertoli–Leydig cell tumor (tubular adenoma with Leydig cells)
2. Of intermediate differentiation
3. Poorly differentiated (sarcomatoid)
4. With heterologous elements
C. Gynandroblastoma
D. Unclassified

^aAdapted from Scully (1) and the 2014 WHO classification (66).

Ovarian SCST: clinical, histology and functional aspects

Granulosa cell tumors

As the name implies, they arise from the granulosa cells (GC) of the ovarian follicle, which is reflected in both a response to endocrine stimuli and the synthesis of both estrogen and gonadal peptides. The former may result in inappropriate pre-pubertal or post-menopausal estrogenization while gonadal peptides such as inhibin and anti-Mullerian hormone (AMH) can be used in diagnosis and more specifically as tumor markers. The relative clinical merits of these markers has been extensively canvassed (2). Studies from our and other laboratories examining gene expression and signaling pathways have provided compelling support that GC are indeed the cell type of origin for GCT with features consistent with proliferating GC of the early antral follicle (3). GCT are sub-classified into juvenile (jGCT) and adult (aGCT) forms; jGCT represent approximately 5% of all GCT.

Fibromas

They are benign tumors, composed almost entirely of fibroblasts forming collagen and are the most common benign SCST, accounting for 4% of all ovarian tumors (1).

Thecomas

As the name implies, they have the appearance of theca cells or occasionally of lutein cells; they may secrete gonadal steroids.

Sertoli–Leydig cell tumors

Sertoli–Leydig cell tumors (SLCT) exhibit cellular and molecular markers consistent with a dysgenesis of the ovarian stromal cells, reminiscent of disorders of

gonadal dysgenesis reviewed elsewhere in this issue of the journal.

Gynandroblastomas

They are very uncommon tumors which exhibit bidirectional differentiation, typically consisting of cells with both ovarian (GC and/or theca) and testicular (Sertoli and or Leydig) features.

The other histological types (Table 1) are very uncommon with the classification being almost exclusively histological, i.e. descriptive.

Hereditary syndromes associated with ovarian SCST

Peutz-Jeghers syndrome

Peutz-Jeghers syndrome (PJS) is associated with ovarian SCST having a histological type that is intermediate between GCT and Sertoli cell tumors (4). In the majority of cases, PJS is caused by autosomal dominant germ line mutations in the *STK11/LKB1* (serine/threonine kinase 11/liver kinase B1) gene on chromosome 19p13.3 (5, 6). *LKB1* activates AMP kinase and is commonly thought of as a tumor suppressor gene. Patients with PJS have pigmentation of the lips, buccal mucosa and digits, together with gastrointestinal hamartomata, polyposis and both benign and malignant tumors of various organs (7). Mutations in the *LKB1* gene and loss of heterozygosity (LOH) at chromosome 19p13.3 have not been found in sporadic ovarian SCST (8, 9).

Ollier disease and Maffucci syndrome

They are rare inherited disorders characterized by enchondroma, a benign cartilaginous tumor. Juvenile GCT have been reported in association with both conditions (10–16). While Ollier disease is associated with multiple enchondromas at multiple sites, in Maffucci syndrome these are found in association with multiple soft tissue hemangiomas (17). Mutations in the isocitrate dehydrogenase (*IDH*) 1 and 2 genes have been identified in enchondroma in both Ollier disease and Maffucci syndrome (18, 19). The mutant *IDH* gene produces the potential ‘oncometabolite’ 2-hydroxyglutarate (2-HG) which induces hypermethylation of histones in DNA (20). The role of either the mutant *IDH* gene or 2-HG in the pathogenesis of jGCT is not known, but they may represent an early post-zygotic event which accounts for the initiation of the disease process (21).

DICER1 syndrome

It results from germ-line mutations in the *DICER1* gene. Dicer plays a fundamental role in processing micro(mi)RNA to their mature forms. Both germ line and somatic mutations in the *DICER1* gene have been associated with ovarian SCST, predominantly SLCT. Initially reported to cause familial pleuro-pulmonary blastoma, *DICER1* mutations were subsequently found in a variety of tumors, including ovarian SLCT and in association

with benign thyroid pathologies (22). Approximately 60% of ovarian Sertoli cell and SLCT harbor a DICER1 mutation which in 80% is the p.E1705K mutation (22, 23). DICER1 mutations were also found in gynadroblastomas but they have not been associated with GCT or indeed, testicular stromal tumors (22–24). This DICER1 mutation induces a selective reduction in RNaseIIIb activity but RNaseIIIa activity is retained which may bias the mutated DICER1 toward processing of the RNaseIIIa strand of the miRNA duplex (23, 25).

Genomic changes in ovarian SCST

Studies of changes at a genomic level in ovarian SCST have largely been restricted to aGCT. In contrast to EOC, GCT have a relatively stable karyotype (26). Cytogenetic (27) and comparative genomic hybridization (CGH) (28) studies have reported trisomy of chromosomes 12 and 14 in approximately one third of cases and monosomy of chromosome 22 in a similar percentage (27, 28). Although between 5% and 20% of GCT are aneuploid, neither the karyotype nor ploidy provides prognostic information (27, 29–31). A lesser frequency of mutations has been observed at other loci.

Caburet et al. (32) have recently applied CGH to a panel of aGCT. They also collated data from a total of 94 aGCT from previous studies. A total of 64 had large-scale chromosomal changes. They report supernumerary chromosomes 8, 9, 12 and 14; the latter being very common (25 of 64). They also report partial or complete loss of chromosomes 1p, 13p, 16, 11 and 22, with monosomy 22 being very common (36 of 64). They found co-occurrence of chromosomal alterations but only a statistically significant non-random association for +14 with -22 and +7 with -16q. Caburet et al. (32) also combined transcriptomic data from a previous study (33) to seek to identify gene copy number changes that may reflect putative driver changes in the pathogenesis of these tumors. They identified 20 genes from the regions of chromosomal imbalance with a plausible, pathological role, across nine chromosomes (1, 5, 11, 12, 14–17, 22) with the *AKT1* gene being the most frequently amplified (6 of 10 tumors) and the nuclear receptor, *rev-erbA α* being the second most frequent (5 of 10 GCT). The later is consistent with the findings of a previous study of nuclear receptor gene expression in aGCT (34). They also sought recurrent ‘broken’ genes as defined by the presence of a mapping breakpoint within the genes in two or more tumors. Five genes were identified on five different chromosomes. The authors (32) highlight the potential of these genes to drive the pathogenesis of GCT, while noting the limitation that the correlation set comprised only 10 aGCT, 9 of which were stage one.

Somatic genetics of jGCT

jGCT, as with aGCT, macroscopically exhibit a mixture of solid and cystic components with hemorrhagic areas. However, their histology differs from aGCT with a follicular or diffuse pattern of larger luteinized cells. The cells contain hyperchromatic or markedly bizarre

nuclei which lack the nuclear grooving characteristic of aGCT (2). Although the histologic appearances are therefore more ‘aggressive’ than for aGCT, the prognosis is generally better. The distinction, aGCT vs jGCT, is therefore primarily based on the histology. This has created diagnostic dilemmas which are increasingly being resolved by the use of the molecular markers discussed below (24, 35, 36). FSH stimulation of GC growth is mediated by the FSH receptor, a G-protein-coupled, seven-transmembrane domain receptor. We and others postulated that activation of these pathways, perhaps through mutations in these signaling molecules, may play a role in the pathogenesis of GCT as is seen in other endocrine tumors (2). Despite extensive investigations, this does not appear to be the case for aGCT. However, the *gsp* oncogene has been observed in approximately 30% of jGCT (37). This activating mutation of the stimulatory alpha-subunit of the heterotrimeric G-protein ($G\alpha_s$) that couples to the seven-transmembrane domain receptors, has been reported as a somatic mutation in pituitary, thyroid and adrenal tumors as well as being the inherited mutation in the McCune–Albright syndrome (38). In jGCT the mutation is either R201C or R201H. Kalfa et al. (37) reported that the *gsp* mutation was associated with a poorer prognosis. Recently Bessiere et al. (39) pursued the hypothesis that since the FSH receptor also signals through the oncoprotein AKT, mutations in this signaling pathway may be involved in the pathogenesis of jGCT. They found that >60% of jGCT have an inframe duplication that involves the plekstrin-homology domains leading to activation of AKT1; jGCT also contain AKT1 point mutations of uncertain significance. The mechanism by which this mutation activates AKT1 appears to relate to increased membrane association of the AKT1 with resulting constitutive FOXO3 repression. A subsequent study using transcriptomic analyses by the same group found that the changes in gene expression in these tumors may reflect a limited set of transcription factors altered by AKT1 activation (40).

Somatic genetics of aGCT

In 2009 Shah et al. (26) reported that >97% of aGCT contained a specific missense mutation in the *FOXL2* gene. Their approach involved a transcriptome analysis of four aGCT using massive parallel sequencing or ‘RNA-Seq’. They identified a single somatic missense mutation in codon 134 (402C→G) resulting in the substitution of a highly conserved cysteine residue by tryptophan. Subsequent studies from a number of groups, including our own, (reviewed in Ref. 2) confirmed this finding. In the expanded cohort component of the study of Shah et al. (26) and in subsequent studies, both heterozygosity and hemi-homozygosity were observed. The mutation appears unique to aGCT in that it is found in neither jGCT nor in other tumor types (2). The otherwise rare exceptions to this rule appear either to be mixed tumors in which elements are in fact of GC origin or the occasional tumor which truly is ‘the exception to the rule’. In the characterization of our cohort (35), we found

exceptionally high FOXL2 mRNA levels in a GCT (from an elderly women) with wild-type FOXL2 but otherwise, by all traditional clinical and histopathological criteria, an aGCT.

The presence of the FOXL2 C134W mutation provides a clear distinction between jGCT and aGCT, indeed in jGCT FOXL2 expression maybe low or absent, (35, 41) whereas in aGCT expression levels in tumors bearing the mutation are generally consistent with levels in the normal ovary (35) with expression in heterozygous tumors being equivalent for the wild-type and mutant FOXL2 alleles. In jGCT low or absent expression of FOXL2 is a feature of aggressive disease and carries a poor prognosis. The presence of the FOXL2 C134W mutation provides a molecular diagnosis of aGCT which is helpful in resolving the diagnosis of aGCT in histologically ambiguous or problematic cases (24, 35, 36).

FOXL2 is a member of the forkhead box (FOX) family of evolutionarily conserved transcription factors. The C134W mutation is predicted to lie close to but not in the DNA-binding domain (26). FOXL2 plays a fundamental and essential role in ovarian development; its biology has been extensively studied (42–44). Conversely, despite an extensive understanding of the biology of FOXL2, the mechanisms of the tumorigenesis mediated by the FOXL2 C134W mutation in aGCT remain to be clearly established. There is *in vitro* evidence that it impacts both steroidogenesis and apoptosis in GC (44). It is likely that post-translational modifications (sumoylation, phosphorylation, acetylation and ubiquitinylation) play a critical role in the modulation of FOXL2 function (42, 44). Kim et al. (45) reported increased phosphorylation of FOXL2 as a result of the C134W mutation leading to ubiquitinylation and degradation. The biology is likely to reflect an impact of the mutation on critical protein–protein interactions of FOXL2 but these also remain to be clearly elucidated. Caburet et al. (42) in a detailed review of FOXL2 function and the C134W mutation argued that FOXL2 is a tumor suppressor gene with loss-of-function being associated with malignancy as is seen in jGCT and therefore that the C134W mutation compromised function rather than being associated with activation or indeed a gain of function. Conversely, others have argued that FOXL2 may be a tumor suppressor gene in jGCT but that FOXL2 C134W may be oncogenic in aGCT (43). It is likely to be more complex than a simple loss-of-function, otherwise aGCT would surely have been identified containing other inactivating mutations of FOXL2 (2). It is perhaps reminiscent of the situation with the DICER1 mutation in SLCT where one aspect of DICER function is selectively lost (25). It is also of course curious that aGCT express the wild-type FOXL2 allele at equivalent levels to the mutant allele, a scenario which arguably demands that the mutant FOXL2 must be ‘dominant negative’ if there is suppression of function.

Although the majority of aGCT are stage 1 tumors and therefore cured by surgical resection, those that present at a more advanced stage or recur, sometimes many years later, carry a poor prognosis (2). As the FOXL2 C134W mutation is present in essentially all aGCT, it cannot explain differences in stage or behavior.

It may be, as with certain inherited mutations, e.g. the ret proto-oncogene in medullary thyroid cancer (46), that the transition from ‘hyperplasia’ induced by the etiologic mutation to frank malignancy requires a second independent hit; this second event may be less specific than the first. In the case of aGCT, the genomic changes described above may for instance reflect the ‘second hit’ that results in aggressive clonal expansion. The subsequent somatic mutations that presumably drive tumorigenesis, recurrence, aggressive behavior, transcoelomic spread and metastatic disease remain to be elucidated.

Currently the only published study of unbiased mutation detection for aGCT is the Shah et al. (26) study and that involved only four GCT. The approach taken by The Cancer Genome Atlas project (TCGA) where a defined cohort of tumors is subjected to the full gamut of genomic and genetic technologies (47) has yet to be applied to aGCT or indeed to other ovarian SCST. There have been many studies which sequence candidate genes and known oncogenes in GCT (2); these have served to exclude changes in genes commonly affected in other malignancies such as p53, PI3K, RAS and BRAF but specific, putatively ‘second-hit’ mutations remain to be identified.

The GCT transcriptome

Several transcriptomic studies have recently been published which identified genes whose expression has been altered; in some cases these may reflect genomic rearrangements. Benayoun et al. (33) used gene expression microarrays to compare the aforementioned 10 aGCT with two GC samples obtained during *in vitro* fertilisation (IVF) egg retrieval. In principal IVF should provide a ready source of ‘normal’ tissue to use as a control in these studies; the caveat, however, is that most IVF cycles involve a hyperstimulation regime with gonadotropin which means that at the time of retrieval the GC are partially luteinized, which is a limitation of their use as a control, because as noted earlier, aGCT appear to arise from GC in the proliferative phase (3). Benayoun et al. (33) identified upregulation of genes linked to cell proliferation and described decreased expression of genes that promote apoptosis. They also found clear evidence of regulation of genes known to be FOXL2 targets. They emphasized that genes normally down-regulated by FOXL2 but increased in this context were those associated with malignancy whereas those normally increased by FOXL2, which are associated with apoptosis, were down-regulated. They argue that the FOXL2 C134W mutation therefore causes a partial loss-of-function as seen in a tumor suppressive gene which they view as being consistent with the finding of the loss of FOXL2 expression in jGCT as discussed above (42).

We have explored the transcriptomic profile of six stage 1 and six stage 3 aGCT to identify differences in gene expression that may contribute to advanced stage disease using a gene microarray approach (48). As in the study of Benayoun et al. (33), all of the aGCT studied were heterozygous for the FOXL2 C134W mutation. A total of 16 genes were identified that were more abundant in

the advanced aGCT and 8 were found to be more highly expressed in the stage 1 aGCT as defined by a p value of <0.05 and more than twofold change after appropriate statistical testing to exclude false discovery. The two most prominently expressed genes in the advanced stage aGCT, CXCL14 (chemokine C-X-C-motif ligand 14), an orphan member of the CYS-X-CYS subfamily of cytokines and MFAP5 (microfibrillar-associated protein 5 transcript variant 1) were 40- and 26-fold higher, respectively. Both have been associated with malignancy. Of the genes whose expression was high in the stage 1 aGCT, INSL3 (insulin-like 3 transcript variant 2) stood out by being 75-fold higher and provided robust discrimination of the two groups. Whether it inhibits tumorigenesis or whether the diminished expression with advanced stage disease is simply a marker of de-differentiation of the tumor remains to be determined.

Gene Set Enrichment Analysis (GSEA) of these data sets (48) identified increased expression of genes on chromosome 7p15 in the stage 3 aGCT consistent with the report of Lin et al. (28) who in a study of GCT using CGH identified gain of chromosome region 7p15-p21 in some samples. This region contains the HOXA locus providing evidence that the increased expression at this locus may be a feature of advanced disease.

The 'miRNA-ome' and other non-coding RNAs

The identification of a pathogenetic role for aberrant miRNA processing in SLCT and gynandroblastomas argues for a more general role for miRNA in SCST. Studies of the 'miRNA-ome' have, however been limited. Rosario et al. (49) have profiled miRNA expression and regulation in two human GCT-derived cell lines; they found that COV434 cells preferentially expressed miR-17 family members whereas the KGN cells preferentially expressed members of the let-7 miRNA gene family. There have not, however, been systematic studies in GCT or, to our knowledge, in other SCST.

Long non-coding (lnc) RNA's have also been implicated in oncogenesis (50). There is a growing body of evidence that lncRNA can produce short peptides from small open reading frames (smORFs) to regulate biological processes (51). The status of both lncRNA, and indeed, smORFs remains to be investigated in SCST.

GCT-derived cell lines

The two human GCT-derived cell lines KGN and COV434 have been used extensively in studies of GCT and indeed of GC. Both exhibit some features of normal proliferating GC including a functional follicle stimulating hormone (FSH) receptor and aromatase activity. Jamieson et al. (35) analyzed the FOXL2 status of both lines: COV434 cells lack the FOXL2C134W mutation in their DNA and do not express FOXL2 providing compelling evidence that they are derived from a jGCT (35). Conversely, the KGN cell line, which was established from a metastatic GCT, both expresses FOXL2 and is heterozygous for the FOXL2

mutation, consistent with it being derived from an aGCT (35). Both are derived from advanced aggressive disease.

Both lines are notable for constitutive activation of the NFkB and Braf/ERK signaling pathways (52–55).

Rosario et al. (56) used a transcriptomic approach with these cell lines to identify potential targets of FOXL2. They found many of the genes regulated by wild-type FOXL2 to be also regulated by the mutant FOXL2. Using pathway analysis they found genes in the transforming growth factor-beta (TGF- β) signaling pathway to be regulated by FOXL2 and mutant FOXL2. Their analysis also highlighted the significant differences between the jGCT-derived COV434 and the aGCT-derived KGN cells gene-expression profiles (56). In our transcriptomic analysis of aGCT (48) we found that greater 3000 entities differed by more than twofold at a p value of <0.05 when the 12 aGCT were compared with the KGN cells which is in stark contrast to when the stages 1 and 3 aGCT were compared with only 24 genes being identified. The two cell lines therefore, while valuable tools in the analysis of signaling pathways in the context of both GCT and indeed GC, do not greatly help in the genomic and/or genetic analysis of aGCT.

Animal models of ovarian SCST

There are a number of mouse models in which GCT arise but none truly recapitulate the human situation (2, 57). Liu et al. (57) have described the development of GCT in mice with FOXO1/3 inactivated selectively in GC; the appearance of these tumors was accelerated by PTEN deletion. They also examined five human aGCT for PTEN and FOXO1/3 expression, all of which they found to be low. They conclude that this mouse model in contrast to others shares some characteristics with aGCT. Involvement of PTEN in the model, however, is more consistent with activation of PI3K/AKT as is seen in the jGCT. It should be noted that neither mutation, over-expression of PIK3CA or PIK3R1, nor loss of expression of PTEN, has been reported in aGCT (58). Work from Lague et al. (59) has provided evidence in mouse models for a synergistic effect of the Wnt/ β -catenin and PI3K/AKT pathways in the formation of GCT which is of interest in the context of recent studies which identify a role for AKT1 mutations in jGCT. The Wnt/ β -catenin signaling pathway has well established roles in ovarian development and in GC function (2). Although dysregulation of Wnt/ β -catenin signaling has been identified in many human cancers, studies in human GCT (60, 61) did not identify activation of this signaling pathway in contrast to equine GCT which have clear evidence of activation of Wnt/ β -catenin signaling (60). Increased ovarian R-spondin1 signaling, which will modulate Wnt signaling is associated with GC-like tumors (62). Gao et al. (63) targeted expression of a constitutively activated TGF- β receptor to GC and found GCT that were associated with elevated inhibin and estrogen levels as is seen in human GCT which

perhaps more closely recapitulates the clinical situation than earlier models in which inhibin gene deletion resulted in GCT (64). One of the downstream consequences of this activation is again, increased AKT signaling.

Conclusions

It is often said that rare tumors can be prismatic in the identification of molecular mechanisms in oncogenesis and the ovarian SCST are no exception. A series of recent genetic discoveries has provided profound insights into the molecular pathogenesis of ovarian SCST. The DICER1 mutation in SLCT highlights both the asymmetry and complexity of miRNA processing while also highlighting the potential for so-called ‘non-coding’ RNA’s to play a critical role in neoplasia. The presence of the recurring *gsp* oncogene and the unique AKT1 mutation observed in jGCT, highlights the critical role of the cyclic AMP/protein kinase A and PI3kinase/AKT signaling pathways respectively, in hormone-mediated cell proliferation and, when constitutively activated, in malignancy. Although the FOXL2 C134W mutation would appear pathognomic for aGCT, the precise mechanism of this effect remains somewhat controversial. Other mutations, however, appear restricted to their syndromic context.

These findings have provided insights into the biology of these genes and to the role they play in sex-cord stromal cell development and biology. Of critical interest to those women afflicted with these malignancies is whether this information can be translated into both prognostic information and indeed into therapeutic options; the current treatments have recently been reviewed by Foulkes et al. (65). It is very clear that these tumors are not the same as EOC and in the age of ‘precision’ medicine each must be treated with a tumor-, and perhaps, mutation-specific approach. In the case of aGCT which are the most common and when advanced, carry a poor prognosis, options beyond the FOXL2 mutation are needed. The later is likely to be difficult to target and it is clear that other genetic or genomic changes must determine late recurrence and an advanced stage. We can anticipate that with the application of whole-exome sequencing, RNA-seq and perhaps interrogation of the miRNA-ome that critical driver mutations will be found for GCT and indeed the other SCST that are ‘actionable mutations’.

Acknowledgements

This work is supported by grants-in-aid from the Cancer Council Victoria; the Ovarian Cancer Research Foundation (S.C.); the Granulosa Cell Tumor of the Ovary Foundation; the National Health & Medical Research Council of Australia through a Project Grant (#1058334) and a Senior Principal Research Fellowship to P.J.F. (#1002559); and the Endocrine Society of Australia through a Research Higher Degree Scholarship to D. L. The Hudson Institute is supported by the Victorian Government’s Operational Infrastructure Scheme.

The authors wish to thank Jeana Thomas and Karen O’Keefe for preparation of the manuscript; and Maria Alexiadis for discussion and technical support.

References

1. Scully RE. Classification of human ovarian tumors. *Environ Health Perspect* 1987; 73: 15–25.
2. Jamieson S, Fuller PJ. Molecular pathogenesis of granulosa cell tumors of the ovary. *Endocr Rev* 2012; 33 (1): 109–144.
3. Chu S, Rushdi S, Zumpe ET et al. FSH-regulated gene expression profiles in ovarian tumours and normal ovaries. *Mol Hum Reprod* 2002; 8: 426–433.
4. Young RH, Welch WR, Dickersin GR, Scully RE. Ovarian sex cord tumor with annular tubules: review of 74 cases including 27 with Peutz-Jeghers syndrome and four with adenoma malignum of the cervix. *Cancer* 1982; 50: 1384–1402.
5. Hemminki A, Tomlinson I, Markie D et al. Localization of a susceptibility locus for Peutz-Jeghers syndrome to 19p using comparative genomic hybridization and targeted linkage analysis. *Nat Genet* 1997; 15: 87–90.
6. Hemminki A, Markie D, Tomlinson I et al. A serine/threonine kinase gene defective in Peutz-Jeghers syndrome. *Nature* 1998; 391: 184–187.
7. Yoo LI, Chung DC, Yuan J, LKB1 – a master tumour suppressor of the small intestine and beyond. *Nat Rev Cancer* 2002; 2: 529–535.
8. Kato N, Romero M, Catusus L, Prat J. The STK11/LKB1 Peutz-Jegher gene is not involved in the pathogenesis of sporadic sex cord-stromal tumors, although loss of heterozygosity at 19p13.3 indicates other gene alteration in these tumors. *Hum Pathol* 2004; 35: 1101–1104.
9. Wang ZJ, Churchman M, Campbell IG et al. Allele loss and mutation screen at the Peutz-Jeghers (LKB1) locus (19p13.3) in sporadic ovarian tumours. *Br J Cancer* 1999; 80: 70–72.
10. Young RH, Dickersin GR, Scully RE. Juvenile granulosa cell tumor of the ovary. A clinicopathological analysis of 125 cases. *Am J Surg Pathol* 1984; 8: 575–596.
11. Tamimi HK, Bolen JW. Enchondromatosis (Ollier’s disease) and ovarian juvenile granulosa cell tumor. *Cancer* 1984; 53: 1605–1608.
12. Clement PB, Young RH, Scully RE. Clinical syndromes associated with tumors of the female genital tract. *Semin Diagn Pathol* 1991; 8: 204–233.
13. Tanaka Y, Sasaki Y, Nishihira H, Izawa T, Nishi T. Ovarian juvenile granulosa cell tumor associated with Maffucci’s syndrome. *Am J Clin Pathol* 1992; 97: 523–527.
14. Gell JS, Stannard MW, Ramnani DM, Bradshaw KD. Juvenile granulosa cell tumor in a 13-year-old girl with enchondromatosis (Ollier’s disease): a case report. *J Pediatr Adolesc Gynecol* 1998; 11: 147–150.
15. Leyva-Carmona M, Vazquez-Lopez MA, Lendinez-Molinos F. Ovarian juvenile granulosa cell tumors in infants. *J Pediatr Hematol Oncol* 2009; 31: 304–306.
16. Rietveld L, Nieboer TE, Kluivers KB, Schreuder HW, Bulten J, Malsuger LF. First case of juvenile granulosa cell tumor in an adult with Ollier disease. *Int J Gynecol Pathol* 2009; 28: 464–467.
17. Pansuriya TC, Kroon HM, Bovee JV. Enchondromatosis: insights on the different subtypes. *Int J Clin Exp Pathol* 2010; 3: 557–569.
18. Amary MF, Damato S, Halaï D et al. Ollier disease and Maffucci syndrome are caused by somatic mosaic mutations of IDH1 and IDH2. *Nat Genet* 2011; 43 (12): 1262–1265.
19. Pansuriya TC, van Eijk R, d’Adamo P et al. Somatic mosaic IDH1 and IDH2 mutations are associated with enchondroma and spindle cell hemangioma in Ollier disease and Maffucci syndrome. *Nat Genet* 2011; 43 (12): 1256–1261.
20. Jin Y, Elalaf H, Watanabe M et al. Mutant IDH1 dysregulates the differentiation of mesenchymal stem cells in association with gene-specific histone modifications to cartilage- and bone-related genes. *PLoS One* 2015; 10 (7): e0131998.
21. Verdegaal SH, Bovée JV, Pansuriya TC et al. Incidence, predictive factors, and prognosis of chondrosarcoma in patients with Ollier disease and Maffucci syndrome: an international multicenter study of 161 patients. *Oncologist* 2011; 16 (12): 1771–1779.
22. Heravi-Moussavi A, Anglesio MS, Cheng SW et al. Recurrent somatic DICER1 mutations in nonepithelial ovarian cancers. *N Engl J Med* 2012; 366 (3): 234–242.

23. Conlon N, Schultheis AM, Piscuoglio S et al. A survey of DICER1 hotspot mutations in ovarian and testicular sex cord-stromal tumors. *Mod Pathol* 2015; 28 (12): 1603–1612.
24. Stewart CJ, Alexiadis M, Crook ML, Fuller PJ. An immunohistochemical and molecular analysis of problematic and unclassified ovarian sex cord-stromal tumors. *Hum Pathol* 2013; 44 (12): 2774–2781.
25. Wang Y, Chen J, Yang W et al. The oncogenic roles of DICER1 RNase IIIb domain mutations in ovarian Sertoli-Leydig cell tumors. *Neoplasia* 2015; 17 (8): 650–660.
26. Shah SP, Kobel M, Senz J et al. Mutation of FOXL2 in granulosa-cell tumors of the ovary. *N Engl J Med* 2009; 360: 2719–2729.
27. Mayr D, Kaltz-Wittmer C, Arbogast S, Amann G, Aust DE, Diebold J. Characteristic pattern of genetic aberrations in ovarian granulosa cell tumors. *Mod Pathol* 2002; 15: 951–957.
28. Lin YS, Eng HL, Jan YJ et al. Molecular cytogenetics of ovarian granulosa cell tumors by comparative genomic hybridization. *Gynecol Oncol* 2005; 97 (1): 68–73.
29. King LA, Okagaki T, Gallup DG, Twigg LB, Messing MJ, Carson LF. Mitotic count, nuclear atypia, and immunohistochemical determination of Ki-67, c-myc, p21-ras, c-erbB2, and p53 expression in granulosa cell tumors of the ovary: mitotic count and Ki-67 are indicators of poor prognosis. *Gynecol Oncol* 1996; 61: 227–232.
30. Miller BE, Barron BA, Dockter ME, Delmore JE, Silva EG, Gershenson DM. Parameters of differentiation and proliferation in adult granulosa cell tumors of the ovary. *Cancer Detect Prev* 2001; 25: 48–54.
31. Villella J, Herrmann FR, Kaul S et al. Clinical and pathological predictive factors in women with adult-type granulosa cell tumor of the ovary. *Int J Gynecol Pathol* 2007; 26: 154–159.
32. Caburet S, Anttonen M, Todeschini AL et al. Combined comparative genomic hybridization and transcriptomic analyses of ovarian granulosa cell tumors point to novel candidate driver genes. *BMC Cancer* 2015; 15: 251.
33. Benayoun BA, Anttonen M, L'Hôte D et al. Adult ovarian granulosa cell tumor transcriptomics: prevalence of FOXL2 target genes misregulation gives insights into the pathogenic mechanism of the p.Cys134Trp somatic mutation. *Oncogene* 2013; 32 (22): 2739–2746.
34. Alexiadis M, Eriksson N, Jamieson S et al. Nuclear receptor profiling of ovarian granulosa cell tumors. *Horm Cancer* 2011; 2 (3): 157–169.
35. Jamieson S, Butzow R, Andersson N et al. The FOXL2 C134W mutation is characteristic of adult granulosa cell tumors of the ovary. *Mod Pathol* 2010; 23 (11): 1477–1485.
36. Rosario R, Wilson M, Cheng WT et al. Adult granulosa cell tumours (GCT): clinicopathological outcomes including FOXL2 mutational status and expression. *Gynecol Oncol* 2013; 131 (2): 325–329.
37. Kalfa N, Ecochard A, Patte C et al. Activating mutations of the stimulatory g protein in juvenile ovarian granulosa cell tumors: a new prognostic factor? *J Clin Endocrinol Metab* 2006; 91: 1842–1847.
38. Salpea P, Stratakis CA. Carney complex and McCune Albright syndrome: an overview of clinical manifestations and human molecular genetics. *Mol Cell Endocrinol* 2014; 386 (1-2): 85–91.
39. Bessière L, Todeschini AL, Auguste A et al. A hot-spot of in-frame duplications activates the oncoprotein AKT1 in juvenile granulosa cell tumors. *EBioMedicine* 2015; 2 (5): 421–431.
40. Auguste A, Bessière L, Todeschini AL et al. Molecular analyses of juvenile granulosa cell tumors bearing AKT1 mutations provide insights into tumor biology and therapeutic leads. *Hum Mol Genet* 2015; 24 (23): 6687–6698.
41. Kalfa N, Philibert P, Patte C et al. Extinction of FOXL2 expression in aggressive ovarian granulosa cell tumors in children. *Fertil Steril* 2007; 87: 896–901.
42. Caburet S, Georges A, L'Hôte D, Todeschini AL, Benayoun BA, Veitia RA. The transcription factor FOXL2: at the crossroads of ovarian physiology and pathology. *Mol Cell Endocrinol* 2012; 356 (1-2): 55–64.
43. Rosario R, Cohen PA, Shelling AN. The role of FOXL2 in the pathogenesis of adult ovarian granulosa cell tumours. *Gynecol Oncol* 2014; 133 (2): 382–387.
44. Leung DT, Fuller PJ, Chu S. Impact of FOXL2 mutations on signaling in ovarian granulosa cell tumors. *Int J Biochem Cell Biol* 2016; 72: 51–54.
45. Kim JH, Kim YH, Kim HM et al. FOXL2 posttranslational modifications mediated by GSK3 β determine the growth of granulosa cell tumours. *Nat Commun* 2014; 5: 2936.
46. Wells SA Jr, Asa SL, Dralle H et al. American Thyroid Association Guidelines Task Force on medullary thyroid carcinoma. revised American Thyroid Association guidelines for the management of medullary thyroid carcinoma. *Thyroid* 2015; 25 (6): 567–610.
47. Cancer Genome Atlas Research Network. Integrated genomic analyses of ovarian carcinoma. *Nature* 2011; 474 (7353): 609–615.
48. Alexiadis M, Chu S, Leung D, Gould JA, Jobling T, Fuller PJ. Transcriptomic analysis of stage I versus advanced adult granulosa cell tumors. *Oncotarget* 2016; 7 (12): 14207–14219.
49. Rosario R, Blenkiron C, Shelling AN. Comparative study of microRNA regulation on FOXL2 between adult-type and juvenile-type granulosa cell tumours in vitro. *Gynecol Oncol* 2013; 129 (1): 209–215.
50. McClelland ML, Mesh K, Lorenzana E et al. CCAT1 is an enhancer-templated RNA that predicts BET sensitivity in colorectal cancer. *J Clin Invest* 2016; 126 (2): 639–652.
51. Saghatelian A, Couso JP. Discovery and characterization of smORF-encoded bioactive polypeptides. *Nat Chem Biol* 2015; 11 (12): 909–916.
52. Chu S, Nishi Y, Yanase T, Nawata H, Fuller PJ. Transrepression of estrogen receptor beta signaling by nuclear factor- κ B in ovarian granulosa cells. *Mol Endocrinol* 2004; 18: 1919–1928.
53. Steinmetz R, Wagoner HA, Zeng P et al. Mechanisms regulating the constitutive activation of the extracellular signal-regulated kinase (ERK) signaling pathway in ovarian cancer and the effect of ribonucleic acid interference for ERK1/2 on cancer cell proliferation. *Mol Endocrinol* 2004; 18: 2570–2582.
54. Jamieson S, Fuller PJ. Characterization of the inhibitor of kappaB kinase (IKK) complex in granulosa cell tumors of the ovary and granulosa cell tumor-derived cell lines. *Horm Cancer* 2013; 4 (5): 277–292.
55. Jamieson S, Fuller PJ. Tyrosine kinase inhibitors as potential therapeutic agents in the treatment of granulosa cell tumors of the ovary. *Int J Gynecol Cancer* 2015; 25 (7): 1224–1231.
56. Rosario R, Araki H, Print CG, Shelling AN. The transcriptional targets of mutant FOXL2 in granulosa cell tumours. *PLoS One* 2012; 7 (9): e46270.
57. Liu Z, Ren YA, Pangas SA et al. FOXO1/3 and PTEN depletion in granulosa cells promotes ovarian granulosa cell tumor development. *Mol Endocrinol* 2015; 29 (7): 1006–1024.
58. Bittinger S, Alexiadis M, Fuller PJ. Expression status and mutational analysis of the PTEN and P13K subunit genes in ovarian granulosa cell tumors. *Int J Gynecol Cancer* 2009; 19: 339–342.
59. Lague MN, Paquet M, Fan HY et al. Synergistic effects of Pten loss and WNT/CTNNB1 signaling pathway activation in ovarian granulosa cell tumor development and progression. *Carcinogenesis* 2008; 29: 2062–2072.
60. Boerboom D, Paquet M, Hsieh M et al. Misregulated Wnt/ β -catenin signaling leads to ovarian granulosa cell tumor development. *Cancer Res* 2005; 65: 9206–9215.
61. Ohishi Y, Oda Y, Kurihara S et al. Nuclear localization of E-cadherin but not beta-catenin in human ovarian granulosa cell tumours and normal ovarian follicles and ovarian stroma. *Histopathology* 2011; 58: 423–432.
62. De Cian MC, Pauper E, Bandiera R et al. Amplification of R-spondin1 signaling induces granulosa cell fate defects and cancers in mouse adult ovary. *Oncogene* 2016 Epub ahead of print.
63. Gao Y, Vincent DF, Davis AJ, Sansom OJ, Bartholin L, Li Q. Constitutively active transforming growth factor β receptor 1 in the mouse ovary promotes tumorigenesis. *Oncotarget* 2016 Epub ahead of print.
64. Matzuk MM, Finegold MJ, Su JG, Hsueh AJ, Bradley A. Alpha-inhibin is a tumour-suppressor gene with gonadal specificity in mice. *Nature* 1992; 360: 313–319.
65. Foulkes WD, Gore M, McCluggage WG. Rare non-epithelial ovarian neoplasms: pathology, genetics and treatment. *Gynecol Oncol* 2016; 142: 190–198.
66. Kurman RJ, Carcangiu ML, Herrington CS, Young RH. WHO classification of tumours of female reproductive organs. In: WHO classification of tumours, 4 edn. Lyon: WHO Press, 2014.

Graphical Abstract

- Ovarian sex cord-stromal tumors (SCST) represent ~8% of malignant ovarian tumors.
- SCST are found in the hereditary syndromes: Peutz-Jeghers Syndrome, Ollier disease and Maffucci syndrome, and DICER1 syndrome.
- DICER1 mutations are in non-hereditary cases of Sertoli cell and Sertoli-Leydig cell tumors.
- Juvenile granulosa cell tumors (GCT) contain a somatic mutation, the *gsp* oncogene, in ~30%, while a further 60% have an activating mutation in the AKT gene.
- In adult GCT, a mutation in the FOXL2 transcription factor (FOXL2 C134W) is found in almost all cases.